University of Cape Town

Faculty of Engineering and The Built Environment

Influence of Symmetry on the Stability Behaviour of Plane and Space Frames

Chisanga Kaluba

Supervisor

Professor Alphose Zingoni

Thesis Presented for the Degree of

DOCTOR OF PHILOSOPHY

in the Department of Civil Engineering

UNIVERSITY OF CAPE TOWN

August 2023

DECLARATION

This thesis is submitted for the degree of Doctor of Philosophy in the Faculty of Engineering & the Built Environment at the University of Cape Town. I hereby declare that the research project reported herein is my own unaided work, unless otherwise stated. The study was carried out within the Structural Engineering and Mechanics Research Group, University of Cape Town between February 2018 and August 2023. No part of this thesis has been submitted in support of an application for a degree in this University or any other educational establishment.

Full Name: Chisanga KALUBA

Signature: Signed by candidate

This thesis is dedicated to my wife.

Abstract

Symmetry refers to a property of an object or a system that remains unchanged or invariant under a transformation, such as reflection, rotation, or scaling. This study sought to investigate how symmetry influences the buckling behaviour of open frames as well as closed polygonal and prismatic frames. This was achieved by employing analytical methods developed in this study and the finite element method to study plane and space frames. The analytical results were used to validate the finite element models developed in Abaqus. The finite element models were then used to carry out more detailed studies on the influence of symmetry on the stability behaviour of plane frames. In addition, the study also proposed an alternative method for tracing the post buckling paths of lattice domes.

Two group theoretic approaches to the buckling analysis of plane frames were developed based on the matrix stiffness method, and slope deflection method respectively. This was achieved by using group theory to decompose an n-dimensional problem into smaller independent problems of much smaller dimensions. The buckling loads and mode shapes are then computed with much less computational effort and numerical problems of ill conditioning are avoided. This was very useful for the group theoretic slope deflection approach developed in this study. The group theoretic slope deflection approach was used to obtain analytical results for the buckling loads and modes of plane frames. Another advantage of the group theoretic approach developed was that insights on the symmetry of the buckling modes were obtained even before detailed computations for eigenvalues are carried out.

The analytical results obtained from the group theoretic slope deflection method were used to validate Finite element models created in Abaqus of the C_{nv} plane and space frames, and D_{nh} space frames. These finite element models were then used to conduct more detailed investigations of the influence of symmetry on the stability behaviour of plane and space frames.

This study found that for plane frames symmetric to a C_{nv} group in terms of stiffness and loading, the lowest buckling load had an eigenmode with the symmetry of a subgroup of C_{nv} with the highest order of elements. The study found that the order of emergence of symmetries for eigenmodes of higher eigenvalues was from the subgroups of C_{nv} with the highest order of elements to those with the lowest order of elements and this order of emergence repeats every $2n$

eigenvalue. The study also found that when eigenvalues are categorised by the symmetry group of their eigenmodes, eigenvalues whose eigenmodes have the symmetries of subgroup of C_{nv} with the highest order of elements, formed the lower bound eigenvalues; and the eigenvalues whose eigenmodes have the C_n symmetries formed the higher bound eigenvalues. Further, this study found that when the group index of an eigenmode is greater than two, the respective eigenvalue is a repeating eigenvalue; and that when the group index is equal to two, then the respective eigenvalue is non-repeating. This study also found that space frames that are C_{nv} symmetric in terms of stiffness and subjected to a loading arrangement symmetric to a subgroup of C_{nv}, display the buckling behaviour of a frame that is symmetric to that particular subgroup in terms of stiffness and loading. Lastly this study found that, plane frames that are C_{nv} symmetric in terms of loading and subjected to $C_{nv/2}$ loading display the buckling behaviour of a plane frame symmetric to C_{nv} with respect to loading and stiffness for the case where $n/2$ is even. Some of the findings of these two approaches (matrix formulation and slope-deflection) have already been reported in a publication of the American Society of Civil Engineers, and presented at an international conference.

For laterally unrestrained C_{nv} symmetric space frames, this study found that for $n>2$: the buckling mode for the lowest buckling value is C_{1v} symmetric and the frame sways along one line of symmetry; and the lowest buckling value is a repeating buckling value.

For D_{nh} symmetric space frames in terms of stiffness and loading, the post-buckling behaviour was investigated in addition to the buckling behaviour. Such space frames were found to display the following stability behaviour: the symmetries of the buckling modes are subgroups of D_{nh}; the order of emergence of symmetries of buckling modes repeats every $4n$ buckling value; the buckling values whose buckling modes have the C_n symmetries form the higher bound buckling values when all buckling values are arranged by buckling mode symmetry. This study also found that space frames that are D_{nh} symmetric in terms of stiffness and subjected to a loading arrangement symmetric to a subgroup of D_{nh}, display the buckling behaviour of a frame that is symmetric to that particular subgroup in terms of stiffness and loading. Lastly, this study found that the post-buckling behaviour of space frames is stable and is independent of the beam to column stiffness.

This study also demonstrated how the post buckling equilibrium paths of lattice space domes can be traced using a load excitation method, without having to use special path switching algorithms. In this method, the pattern of the applied load arrangement to excite a particular bifurcation path is based on the symmetry of the deformation pattern of the dome on that particular bifurcation path. Thus, the post buckling equilibrium paths can be traced by simply using geometric non-linear analysis in a Finite element software such as Abaqus.

Acknowledgements

I extend my sincere gratitude to my PhD supervisor, Prof. Alphose Zingoni, at the University of Cape Town, for his invaluable constructive criticisms, patience, and unwavering support throughout this research endeavor. His guidance has significantly contributed to my development as a researcher and deepened my comprehension of structural engineering.

Additionally, I wish to express my appreciation for the financial support extended through the Bathe SEMC PhD and Professor Zingoni. Their generous assistance has been instrumental in making this study possible, and I am truly grateful for their contributions.

Table of Contents

List of tables

List of figures:

Blank page

Nomenclature

e	Identity element
FEM	Finite Element Model
P_{cr}	Critical buckling load
E	Modulus of elasticity for the material
I	Second area moment
L	length
β	Beam to column stiffness ratio
Ψ	Subspace eigenvector
σ	Reflection symmetry element
C_n	Rotation of $2\pi/n$ about an axis of symmetry
S_n	Rotation through an angle $2\pi/n$, combined with a reflection in the plane perpendicular to axis of rotation
G	Symmetry group
$P^{(i)}$	Idempotents of the group algebra
$\boldsymbol{\lambda}$	Eigenvalue
K	Stiffness matrix
Δ	Lateral deflection
ϕ	Conventional basis vector
Φ	Symmetry adapted basis vector
γ	Load imperfection parameter
m/n	Group index
i	Inversion

Chapter 1

1. Introduction

1.1 General introduction

Symmetry is a concept that describes the similarity between different parts of an object, shape, pattern, or system. There are several types of symmetry, and these are: reflectional symmetry, rotational symmetry, and translational symmetry.

Reflectional symmetry is the most common type of symmetry. In this type of symmetry, an object or shape is mirror symmetric if there is a line (vertical plane) through which one side is the mirror image of the other side. The plane frame shown in Figure *1.1 (a)*, for example, has reflection symmetry about two vertical planes marked by the *x* and *y* axes, respectively.

A shape possesses rotational symmetry if looks the same when rotated about a point at certain angles. For example, the plane frame shown in Figure *1.1 (a)*, can be rotated about the centre of symmetry *O* by *180* degrees clockwise or counterclockwise and the rectangular frame will still appear the same. The plane frame shown in Figure *1.1 (c)* on the other hand, can be rotated by either *90* or *180* degrees clockwise or counterclockwise about the centre of symmetry *O* and the square frame will still look the same.

Reflectional symmetry and rotational symmetry are the two types of symmetry that were considered in this study. Translational symmetry, which involves shifting an object or pattern along a straight line without changing its appearance was not considered in this study.

Symmetry is a fundamental principle in various fields, including mathematics, art, biology, and physics. In physics, for example, the concept of symmetry plays a crucial role in understanding the fundamental laws of the universe. In mathematics, group theory is a field that studies symmetry and its various properties.

Symmetry is often employed in engineering structures to enhance aesthetics, functionality, and overall structural efficiency. While employing symmetry in structures can improve structural efficiency by evenly distributing loads among the members of the structure, it can also make the structure more prone to failure caused by buckling. This is because symmetric structures display

multiple bifurcation paths that emerge at critical points that appear on the equilibrium paths of symmetric structures such as lattice domes (Ikeda et al., 1986b; Ikeda & Torii, 1987b; Healey, 1988; Ikeda & Murota, 1991; Wohlever & Healey, 1995). The multiplicity of critical points and the unstable nature of the post buckling paths make symmetric structures such as lattice domes and shells especially sensitive to imperfections (Britvec, 1960; Hoff, 1966; Koiter, 1970; Thompson, 1963). Such structures are known to fail at loads that are much lower than the computed theoretical values. To aid the understanding of the stability behaviour of lattice domes, a framework was designed from the results of heuristic case studies, to describe the bifurcation hierarchy of lattice domes symmetric to the C_{nv} symmetry groups in terms of geometry, loading and stiffness. The equilibrium paths of the lattice domes were traced, and it was found that on the fundamental equilibrium paths the deformation patterns of the domes were C_{nv} symmetric, while the deformation patterns on the bifurcated paths were symmetric to subgroups of the particular C_{nv} symmetry group of the problem and this is described as the bifurcation hierarchy (Ikeda et al., 1986b; Ikeda et al., 1986a; Ikeda & Torii, 1987a; Ikeda & Torii, 1987b; Ikeda et al., 1991). This framework of describing the stability behaviour of lattice domes in terms of a hierarchy of bifurcations provides a priori knowledge of the stability behaviour of lattice domes, which is useful for validating Finite Element Models (*FEM*) of lattice domes and the stability design of lattice domes. A similar approach has been used to study the stability behaviour of shells.

Symmetry has not only been employed to explain the stability behaviour of symmetric structures, but it has also been used to reduce the computational effort required to analyse symmetric structures. In stability analysis, symmetry has been extensively utilised in the stability analysis of lattice domes (Healey, 1988; Ikeda & Murota, 1991; Wohlever & Healey, 1995). Other researchers have also used similar techniques for the buckling of plane frames (Kaveh & Nikbakht, 2006; Kaveh & Nikbakht, 2008; Kaveh et al., 2010). When symmetry is employed, the numerical challenges of ill conditioning associated with double critical points common in symmetric structures are avoided. Further, the computational effort required for the analysis is reduced by decomposing the problem into independent problems of lower orders of symmetry.

It is worth noting that symmetry has been employed in other types of structural analysis such as in vibrations, and this will be discussed in Chapter two.

1.2 Motivation of study

Studies on the influence of symmetry on the stability behaviour of plane and space frames do not appear to be as extensive as that for lattice domes. Mises & Ratzersdorfer (1926), investigated the lowest buckling load of C_{nv} symmetric plane frames in terms of geometry, loading, and stiffness. However, they did not report on the buckling modes associated with the buckling loads. Further, they did not investigate the effect of applying different combinations of symmetry of geometry, loading, and stiffness (Mises & Ratzersdorfer, 1926).

From the few studies that have addressed the stability behaviour of space frames, the bifurcation behaviour of space frames has been found to be characterised by three types of buckling modes: sway buckling; torsional buckling; and combined sway-torsional buckling (LeRoy, 1961; Shosuke, 1970). The sway buckling mode was found to have the lowest buckling load both numerically and experimentally. These studies did not investigate the nature of the post-buckling paths of the C_{nv} frames considered in these studies. Further, the studies did not investigate the stability behaviour of D_{nh} space frames. This study, therefore, sought to further investigate the influence of symmetry on the stability behaviour of space frames.

Further, this study also served as a continuation of previous work at the University of Cape Town, which sought to better understand the *vibration* behaviour of C_{nv} and D_{nh} space grids and cable nets (Zingoni, 1996; Zingoni, 2005b; Zingoni, 2014; Zingoni, 2018).

1.3 The scope of the research work

Space frames of different symmetrical configurations are applied in construction of buildings, research outposts and mechanical components. Engineering structures can fail due to buckling at loads much lower than the design strength load of the structure. This is especially the case for highly symmetric structures. The scope of this research included the following:

- Investigation of the influence of symmetry on the global stability behaviour of plane and space frames, which are symmetric to the C_{nv} and D_{nh} symmetry groups (Figure 1.1, 1.2 and 1.3);
- development of a symmetry adapted stiffness method to determine the buckling loads and buckling modes of symmetric plane frames;

- development of a symmetry adapted slope deflection method to determine the buckling loads of plane frames;
- development of a framework for describing the bifurcation behaviour of plane and space frames; and
- investigation of the stability of post buckling paths of D_{nh} symmetric space frames.

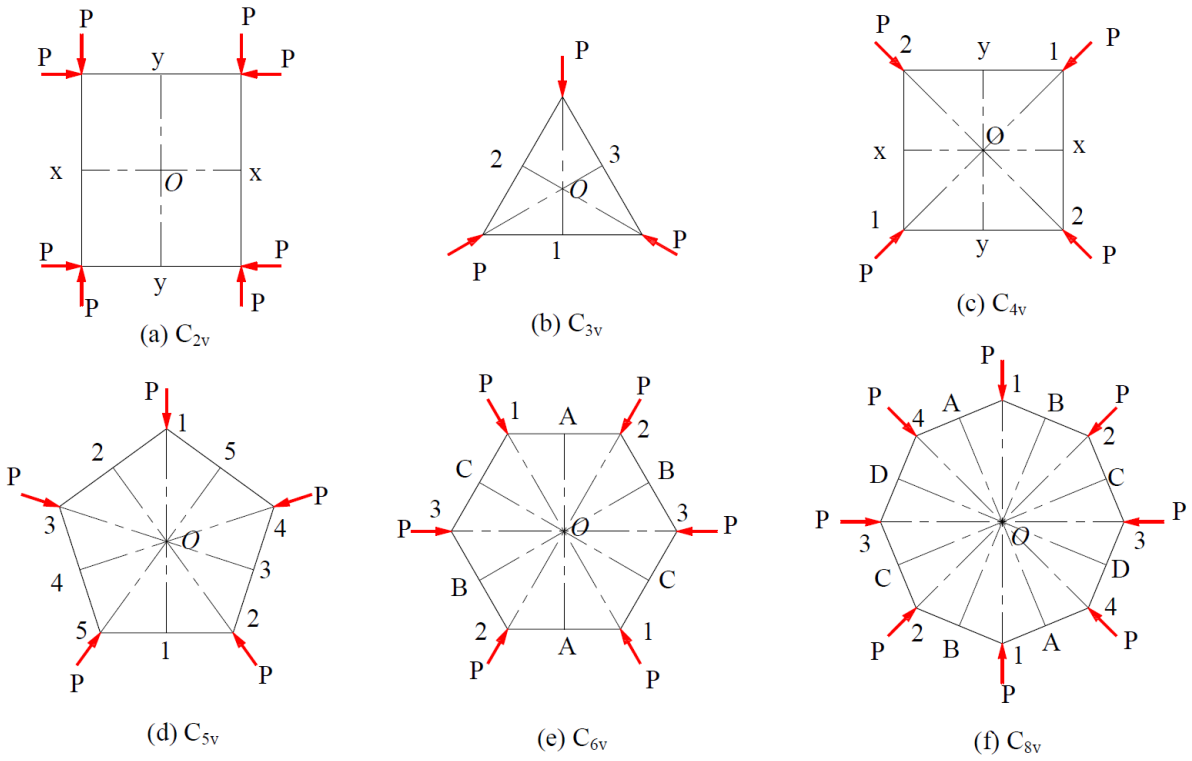

Figure 1.1: C_{nv} Plane Frames

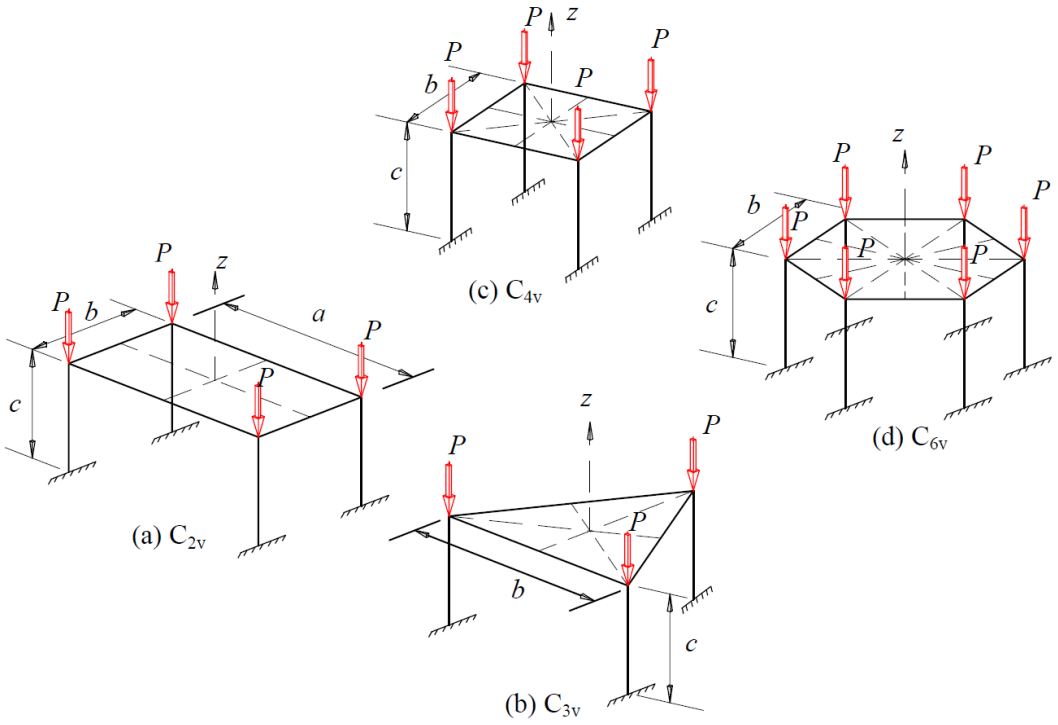

Figure 1.2: C_{nv} Space Frames

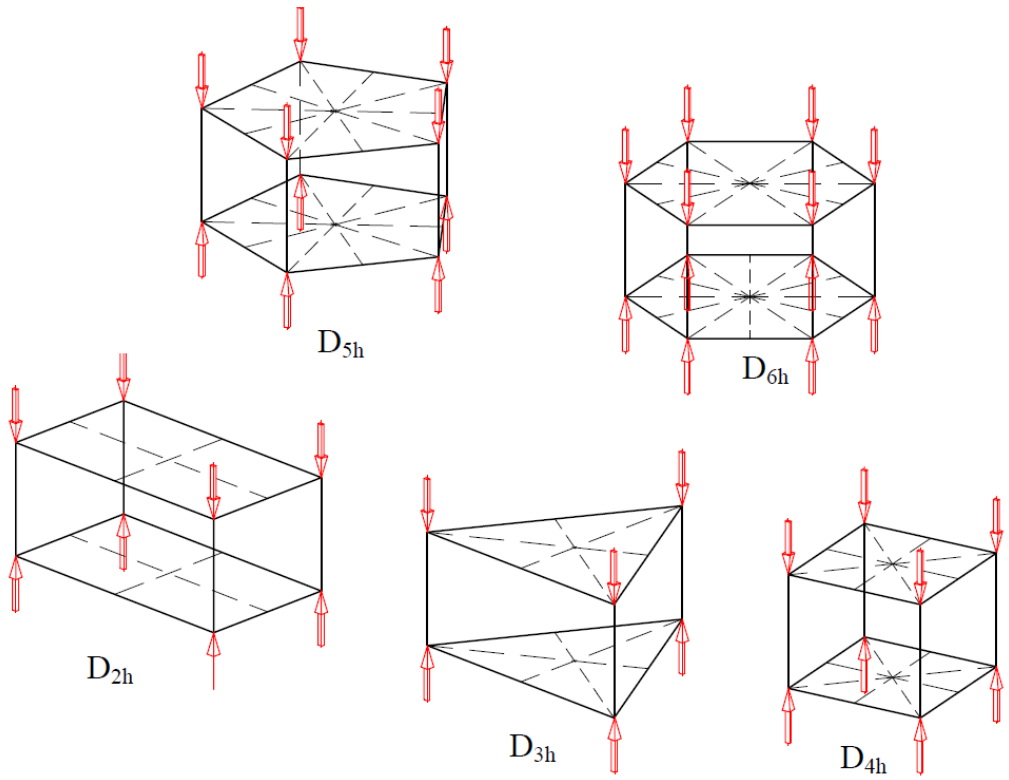

Figure 1.3:D_{nh} Space Frames

1.4 Limitations of study

This study was limited to:

I. Analytical investigations of elastic buckling loads using linear eigenvalue analysis;
II. numerical analyses with ABAQUS finite element software packages provided by the Structural Engineering and Mechanics Research Group, University of Cape Town; and
III. no experimental tests of the space frames were conducted.

.....

1.5 Outline of Thesis

This thesis is presented in seven chapters, with the current chapter containing a brief background to the study and scope of the research. An overview of each of the remaining chapters is as follows:

Chapter 2 reviews the literature of previous research on elastic stability, global stability behaviour of symmetric structures and the application of group theory to the analysis of symmetric structures. The development of theories on elastic stability is reviewed, starting with the work of Euler in 1774 to the time of writing this study. Studies on the stability behaviour of lattice domes, and rigidly jointed plane and space frames are then reviewed. The methods of buckling analysis and post-buckling analysis of plane and space frames are discussed. Symmetry groups and group theory applications in the analysis of symmetric structures are discussed. Previous studies on the influence of symmetry on the stability behaviour of symmetric structures are also discussed. Lastly, the rationale and objectives of the study are presented.

Chapter 3 presents the numerical and analytical methods used to conduct this study. The developed group theoretic methods for buckling analysis of symmetric plane frames are presented. The group theoretic methods presented are based on the matrix stiffness method and slope deflection methods. Examples on how to apply the group theoretic matrix stiffness method are provided and, the results are validated using the results obtained from the conventional approach. Further, the methods used to trace the post buckling paths of space frames and lattice domes are presented. The method is validated using results available in literature.

Chapter 4 discusses and presents the results of the investigation of the stability behaviour of C_{nv} plane frames. The group theoretic slope deflection method is used to obtain analytical results. The

analytical results are then used to validate the finite element models created in Abaqus. The finite element models created in Abaqus are then used to carry out more detailed studies on the influence of symmetry on the stability behaviour of plane frames. Different combinations of the symmetry of applied loads and stiffness are investigated and their effect on buckling behaviour is determined. The symmetry of the eigenmodes for every eigenvalue produced using a linear eigenvalue analysis is categorised and observations and conclusions are made on the order of emergence of symmetries.

Chapter 5 discusses and presents the results on the investigation of the stability behaviour of C_{nv} symmetric space frames which are laterally unrestrained. Again, analytical results obtained from the group theoretic slope deflection method are used to obtain analytical results on simplified models of C_{nv} space frames that are laterally unrestrained. The finite element models in Abaqus are then used to carry out more detailed studies on the buckling behaviour using linear eigenvalue analysis. The symmetry of buckling modes is categorised and the order of emergence of these symmetries is discussed.

Chapter 6 discusses and presents the results on the stability behaviour of D_{nh} symmetric space frames. First, a linear eigenvalue analysis is carried out in Abaqus on each finite element model of a space frame. The analytical results obtained in Chapter 4 are used to validate the results obtained from finite element model for eigenvalues whose eigenmode symmetries are compatible with those obtained for plane frames in Chapter 4. Further detailed studies on the buckling and post buckling behaviour of D_{nh} space frames are made.

Chapter 7 presents the benefits of the current study and opportunities for future research. The possible applications of the methods and results presented in this study are discussed. The limitations of this study that provide scope for further studies are also presented.

Chapter 2

2. Literature review

2.1 Concepts of Stability

The concept of stability is used in many different scientific fields, such as structural mechanics, fluid mechanics, control theory and astronomy. In structural mechanics, stability refers to the response of the state of a system to small changes in its equilibrium position. The state of a system is the collection of values of the system parameters at any instant of time. A stable system is one in which relatively small changes in the system parameters produce relatively small changes in the existing state of the system (Farshad, 1994). In fact, while Euler (1744) is widely recognised as being the first to systematically handle the problem of elastic stability, he did not formally define stability. Bryan (1888) as will later be discussed, was the first to present a formal definition of stability. However, we shall begin our discussion with a more descriptive definition of stability which is quite useful in structural engineering, before proceeding to discuss the contributions of Bryan (1888) and others.

It is generally accepted that the critical equilibrium state can be identified in the equilibrium path of a structure as either an extremum or a branching point (Britvec, 1960; Thompson, 1963). An example of an extremum and branching point on a load displacement curve is given by points *A* and *B* respectively, as shown in Figure *2.1* below. A structure can be said to be stable if an increase in the deformation of the structure requires an increase in the applied loading. In the case of the load-displacement diagram, the curve or equilibrium path is ascending. On the other hand, a structure will be said to be unstable if increasing the deformation of a structure requires a decrease in the applied loading.

In the case where the tangent of the equilibrium path is horizontal, the state of the system can be stable, neutral or unstable. It is the loading at this point of the equilibrium path that is defined as the buckling load or critical load. Here the system is in a transition state from stable to unstable (Thompson, 1963).

At a critical point, a new branch or several other branches will emanate from the equilibrium path. Thus, such a point is sometimes referred to as a bifurcation point and the process by which new equilibrium paths emanate from an equilibrium path is referred to as bifurcation (Thompson & Hunt, 1973). The initial equilibrium path is referred to as the fundamental or primary equilibrium path and the post-critical path is referred to as the post-bifurcation or secondary equilibrium path. In the figure shown below, the structure would lose stability by bifurcation at the point *B*. If the bifurcation point *B* were absent, the structure will lose stability at the local maximum labelled *A*. The loss of stability at point *A* is referred to as snapping, snap buckling or more commonly as limit-point instability. The bifurcation point is very important in the analysis of imperfect structures as it's the asymptote of the load deformation curve of imperfect structures. An imperfect structure is a structure with geometric inaccuracies leading to, for example, eccentric loadings or initial deformations in the direction of the buckling deformation.

A critical distinction between loss of stability by limit point and bifurcation is that, in the former case, there is no new path emanating from the fundamental equilibrium path *OB*. In fact, in an imperfect structure, loss of stability will be caused by limit point instability when post-buckling curve of the perfect structure is descending (Budiansky, 1974).

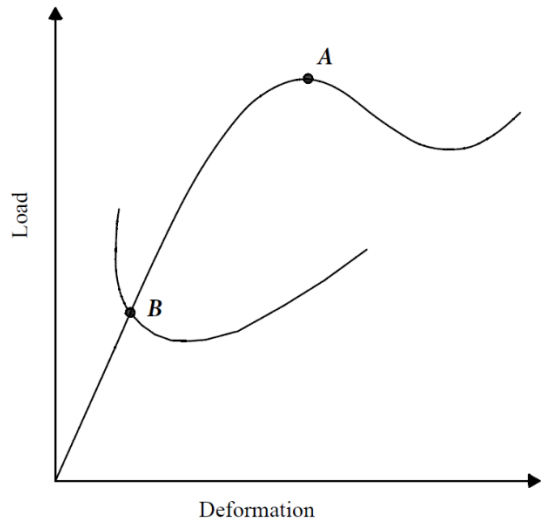

Figure 2.1: Bifurcation and Snapping

There is another context within which the term snapping is used, and this is usually referred to as snap-through buckling. This type of buckling is characterised by a sudden visible jump from the primary equilibrium path. It is accompanied by motion of the structure as it seeks to find another

stable equilibrium state (See Figure 2.2 *b* below) (Kounadis et al., 1977). As shown in figure *b* below, in snap-through buckling after reaching the limit point rather than the structure following the load-displacement curve on the descending section, the load displacement curve 'jumps' over to the stable section of the load-displacement curve. This type of buckling phenomenon is often observed in transversely loaded shallow arches and axially compressed thin shells.

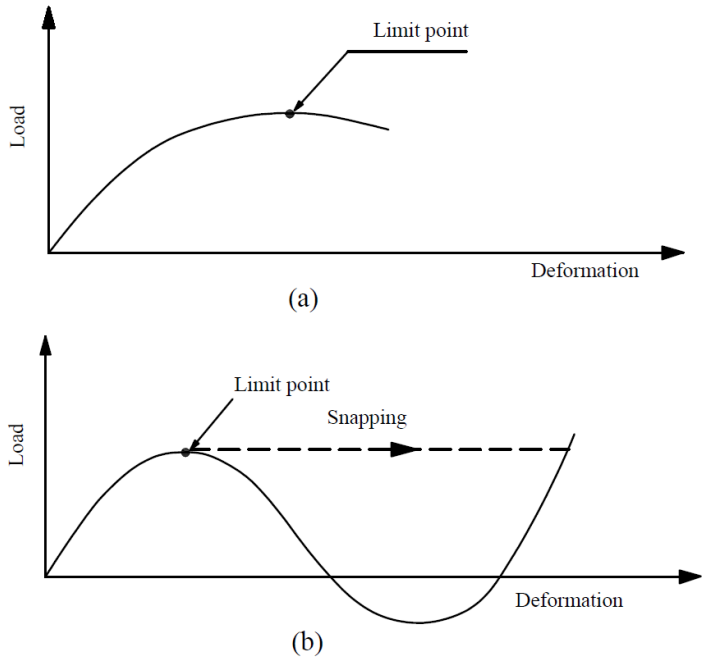

Figure 2.2:(a) Limit point instability (b) snap-through buckling

The descriptive definition of stability given earlier requires mention of some of its inadequacies. The load versus deflection curve can be increasing, but the equilibrium path can still be unstable if there is an undetected bifurcation point on a rising load displacement curve. This kind of phenomenon is usually a problem in highly symmetric structures (Budiansky, 1974).

2.2 Historical Developments on Theory of Elastic Stability

The theory of elastic stability in statics began with the work of Euler in 1744 on the critical buckling load of columns (Euler, 1744). Euler demonstrated that a straight, slender column under a load along its longitudinal axis may buckle. This was achieved by applying calculus of variations to the minimisation of elastic strain energy, to derive the equation of the elastic curve, and to deduce the Euler buckling formula, or Euler critical load (W. A. Oldfather et al., 1933). Euler (1744) considered the specific case of a column with one fixed end and the other end free. The buckling formula he derived is the basis for the famous buckling equation used to determine the

elastic buckling strength of slender columns under concentric axial loading and is usually expressed as:

$$P_{cr} = \frac{\pi^2 EI}{(kL)^2} \qquad (2.1)$$

Where:

- P_{cr}-buckling load or maximum axial load on the column just before it begins to buckle;
- E-the modulus of elasticity for the material;
- I -least second area moment of the cross-section of the column;
- L-length of the column; and
- k-effective length factor.

The result of Euler (1744) shows one very important fact about elastic stability, i.e., the stability of elastic structures is dependent on the geometric properties of the structure. Further, one other very important basic feature of instability phenomena used by Euler (1744), was the influence of deformations on internal forces. This is the reason why equilibrium equations are written for the deformed or buckled shape of the structure in stability problems.

Despite Euler's (1744) contribution, experiments to determine the critical loads of columns showed some discrepancies with theoretical results, which were resolved by Young (1807). Young explained that imperfections such as initial curvature, initial bending moments, and load eccentricity were the cause of the discrepancy. He further went on to derive modification factors for deflections and bending moments influenced by the effect of axial compressive forces in members (Young, 1807).

The work of Euler was restricted to small deflections, the theory was later extended to geometrically non-linear large deflections for the elastic curve by employing elliptic integrals in the solution.

Euler's theory only considered the effect of bending deformations, and shear deformations were ignored. The effect of shear stresses on the buckling load, which is significant in columns with low shear stiffness, was initially studied by Engesser, (1889).

As we stated earlier, Euler (1744) did not formally define a general theory of stability. One of the early formal definitions of stability for elastic structures was proposed by Bryan (1888). This general theory of stability was based on the energy criterion for a system under conservative forces. A system is stable when the second variation of its potential energy is positive about a static equilibrium state and unstable when the second variation of energy is negative (Bryan, 1888). Mathematically, the total potential energy of the system for an isotropic body as given by Bryan 1888 was:

$$W = \iiint \Phi dxdydz + \iiint \rho V dxdydz + \int \Psi dS \qquad (2.2)$$

Where W is the total potential energy, ρ is the density, V is the potential of the body forces, and Ψ for the surface tractions acting on the boundary S. The condition for equilibrium was defined as the first variation of the total potential energy.

$$\delta W = 0 \qquad (2.3)$$

for some variations in displacement.

As has been earlier stated, an unstable equilibrium is only possible when the second variation of the total potential is negative, and this was expressed as:

$$\delta^2 W = \iiint \delta^2 \Phi dxdydz + \iiint \rho \delta^2 V dxdydz + \int \delta^2 \Psi dS < 0 \qquad (2.4)$$

for some variations in displacement.

Bryan (1888) when calculating Φ, only took quadratic terms into account, and consequently $\delta^2\Phi$ would always be positive. Therefore, the only possibility of having a negative $\delta^2 W$ was if the load terms were negative and larger than the strain terms. The implication of this argument was that the equilibrium of solid bodies under small strains should always be stable, provided that rigid body movements are restrained. Koiter notes in his 1945 PhD thesis that this conclusion does not hold for an axially compressed prismatic member subject to a prescribed end shortening (Koiter, 1970).

In addition to the energy criterion of stability as proposed by Bryan (1888), there is also the method of small vibrations. This method consists of the derivation of equations of motion for small displacements from the equilibrium position of a system. The resulting equations are homogeneous

and linear because of the small displacements. The equilibrium state is considered stable for the conditions for which the solution of the resulting characteristic equation has a real part that is nonpositive (Kerr, 1977). This approach was utilised by Southwell (1914), when he derived the equations that govern the neutral equilibrium state of uniform stress and deformation (R. V. Southwell, 1914). Extensions to work by Southwell (1914) were made by (Biezeno & Hencky, 1928), and (Biot, 1938), however, this work was restricted to the analysis of neutral equilibrium. The primary concern was the determination of the stability limit and thus the stability behaviour in the neighbourhood of the stability limit was not explored. This limitation would later be systematically addressed by Koiter (1945).

In modern times, the general theory of elastic buckling, post-buckling behaviour and imperfection sensitivity analysis was developed by Koiter (1945) and is based on the principle of stationery potential energy. Koiter was trying to resolve the problem of the discrepancy between the theoretical buckling and experimental buckling strengths of shells and plates. He employed perturbation theory to develop an asymptotic analysis that enabled him to follow the post-buckling path in its early stages. This was achieved by enforcing equilibrium on a conservative elastic system by employing a variational approach on the energy potential of the system. This then results in homogeneous equilibrium equations, which are solved by perturbation procedures. The advantage of this method is that the effects of introducing small geometric imperfections (deviations from the exact shape) can be examined. Through this approach, Koiter (1945) was able to show that shells were very sensitive to imperfections of about *1/8* to *1/3* of the critical load, when the critical point belonged to the unstable part of the loading curve. Thus, an explanation for the difference between the theoretical and experimental buckling strengths of shells was provided. Koiter (1945) also showed how different types of bifurcation points possessed different types of imperfection sensitivities, i.e., changes in the lowest critical load for the structure when imperfections are introduced either in the geometry or loading of the structure. Koiter (1945) found that structures with symmetric stable bifurcation points were not sensitive to initial imperfections (see Figure 2.3 below). In Figure 2.3 below, curve A is the curve of the perfect system once it bifurcates at point B. The curves C D and E are the curves of the imperfect system due to a geometric imperfection w_0 introduced to the system. The curves monotonically increase with the increasing load P and displacement w, and thus they are not sensitive to geometric imperfections.

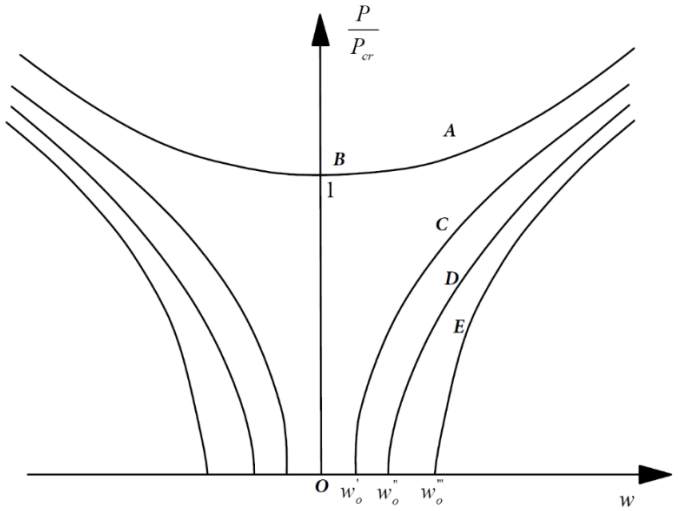

Figure 2.3: Behaviour of a system with symmetric stable bifurcation

Koiter (1945) also found that structures with symmetric unstable points were imperfection sensitive and those with asymmetric bifurcation being most sensitive to initial imperfections (see Figure 2.*4* below). From Figure 2.*4* below, we can see that the maximum stability of the imperfect system is lower than that of the perfect system. In effect, the introduction of imperfections has turned the bifurcation point at *B* into a limit point. Further, the limit load progressively reduces as the imperfection w_0 is increased. In general, Koiter (1945) showed that for all elastic structures, the imperfections cause a reduction according to either the *2/3* or the *1/2* power of the imperfection magnitude for symmetric unstable and asymmetric unstable bifurcations, respectively.

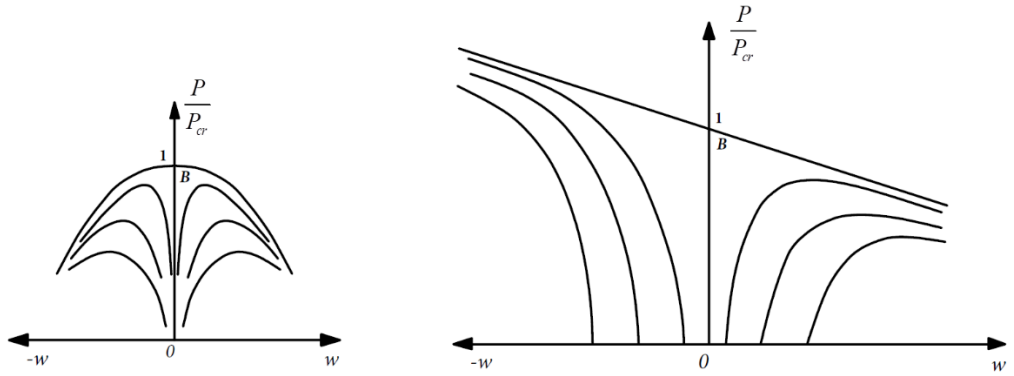

Figure 2.4:(a) Symmetric unstable bifurcation (b) Asymmetric unstable bifurcation

Koiter (1945) is a seminal work on the subject of elastic stability theory, and this work has been translated into English (Koiter, 1970). The essential features of this work (Koiter, 1945) have also been presented using much fewer mathematical arguments than in the original publication

(Wempner, 1972). Equivalent forms of this general theory of elastic stability were also independently proposed by other researchers (Britvec, 1960; Thompson, 1963).

The work of Koiter (1945), Britvec (1960), and Thompson (1963) was mainly motivated by the problem of the stability behaviour of shells. Initially, researchers of stability of structures observed that linear stability analysis was accurate at predicting the strength of compressed columns and plates, and thus linear analysis was considered sufficient for predicting the load carrying capacity of structures (Kounadis et al., 1977). However, this did not prove to be the case for structures such as thin shells, where the discrepancy between theoretical and experimental results was quite large (Hoff, 1966). We shall conclude this subsection by stating some general features of elastic stability theory that have generally remained the same.

The theory of elastic systems subject to conservative loads is founded on the energy criterion: A positive definite second variation of the potential energy of a system about a static equilibrium position is a sufficient condition for stability of that system (Hutchinson & Koiter, 1970). This energy criterion presupposes elastic material behaviour, and it can be broadly classified as either linear or nonlinear. Linear studies are primarily concerned with the determination of critical points, and the nature of the equilibrium paths beyond the critical points is not investigated. Linear elastic stability analysis usually results in eigenvalue problems, with the lowest eigenvalue being of prime importance in structural engineering applications (Kerr, 1977). This type of analysis is concerned with the stability analysis of perfect structures, and the lowest eigenvalue sort is that for which the second variation of potential elastic energy of a structure is semidefinite (Hutchinson & Koiter, 1970). The stability load obtained in this manner is referred to as the classical elastic buckling load. For a structure that exhibits initial stable post-bucking behaviour, the classical buckling load is usually a good measure of the load level at which an imperfect structure begins to undergo significant deformations (Thompson, 1963; Hutchinson & Koiter, 1970).

Nonlinear elastic stability analysis on the other hand, is concerned with the nature of the equilibrium path in the neighbourhood of the critical point, and a major contributor to this field is Koiter (1945). Perturbation theory is normally employed in nonlinear stability problems, as we have previously discussed.

2.3 Stability Behaviour of Trusses and Frames

As was earlier stated in the section on elastic stability theory, loss of elastic stability can either be by: bifurcation, limit point instability, or snap-through. Bifurcation analysis is also referred to as buckling analysis or the mechanical model of stability analysis. On the load displacement curve, buckling is characterised by a splitting/bifurcation of the fundamental equilibrium path (Le-Wu, 1963). This model applies to perfect frames, i.e., frames where there are no geometric imperfections in the members and no eccentrically applied loads (pre-buckling moments). In the bifurcation model, all loads are concentrically applied at the column joints of a frame (Douglas, 1964). Thus, this model of analysis is ideal because it rarely reflects the actual situation of frame loads. It is analogous to the buckling of an initially straight, perfect Euler column. The stability load obtained from this type of analysis is usually an upper limit of the stability load for an imperfect frame (Chilver, 1956). Loss of stability by bifurcation usually occurs in symmetric structures. As we shall later discuss, this is related to a process known as symmetry breaking in the elastic buckling of structures.

In Figure *2.5*, shown below, we have an example of buckling for a perfect frame (case I) and an imperfect frame (case II). The frame in case II is classified as an imperfect frame because the frame has a lateral loading. We must also take note that the lateral load here is applied in a direction orthogonal to the vertical loading, causing the buckling instability, and the effect of this lateral load is to turn a bifurcation point into a limit point.

In limit point instability, the lateral deflection of the frame begins upon the initial application of loads. As the applied loading is increased, the internal stiffness of the structure is progressively reduced until it reaches zero at the limit point. Most frames lose stability through limit point instability (Le-Wu, 1963; Lu, 1963; Douglas, 1964). The exceptions for loss of stability by limit point are for perfect frames where the vertical loads have been applied at the column joints (Le-Wu, 1963; Lu, 1963; Douglas, 1964). This type of instability is shown in cases (Ia) and (Ib) of Figure *2.5* below. The stability behaviour briefly discussed here has also been observed in space frames.

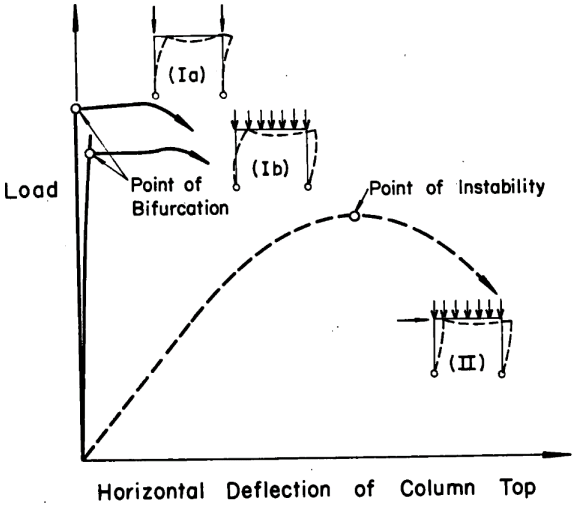

Figure 2.5: Types of overall frame

Source:(Douglas, 1964)

Harrison (1965) studied the stability behaviour of a space frame with an equilateral triangular plan, subject to a lateral and vertical loading, as shown in Figure *2.6* (a) below. The load displacement curve of this space frame from experimental and numerical results is shown in Figure *2.6* (b) below. As would be expected, the frame does not display bifurcation instability as a lateral load is applied to the frame and the vertical load is not applied at the column joints. However, if only vertical loads were applied at column joints, we expect the column to lose stability by bifurcation with a sideway buckling mode, and this kind of behaviour was both analytically and experimentally observed for a similar space frame with an equilateral triangular plan (LeRoy, 1961; Shosuke, 1970).

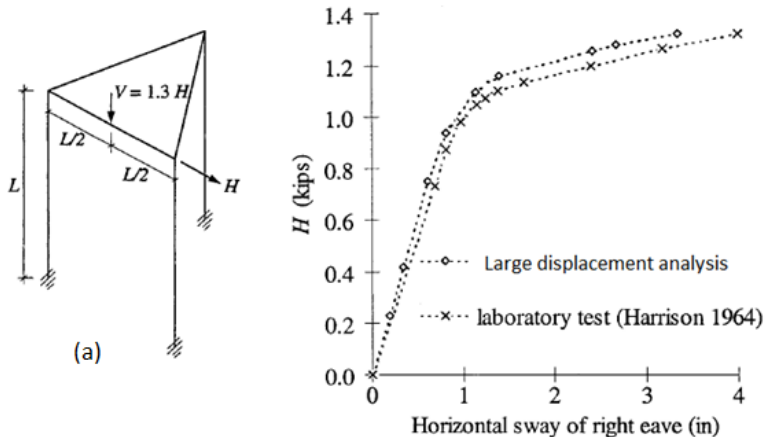

Figure 2.6: (a) Triangular space frame (b) Load displacement curve of triangular space frame

Source:(Harrison, 1965)

Citipitioglu (1965) numerically studied the bifurcation behaviour of a space frame with a rectangular plan, with vertical loads applied at all four column joints (see Figure *2.7* below). The loss of stability of this frame was observed to be due to buckling. An experimental study of the space frame was not carried out in this study, and there was no report on the buckling mode. We should take note that the vertical loading of this frame was not symmetrical; however, the frame displayed a loss of stability through bifurcation.

We have discussed the loss of elastic stability of space frames by bifurcation and limit point instability. Another possible mode of loss of instability is by snap-through. Structures with positive curvature, such as shallow reticulated domes, have been known to lose stability by snap-through (Gioncu, 1995). In addition, a common feature of structures that lose stability by snap-through is that the dominant mode of force transfer, is axial loading. The simplest structure commonly used to illustrate snap-through behaviour is the simple planar two-member truss. An extensive numerical study of such a frame was carried out and the stability behaviour of the truss was noted under various loading conditions (Healey, 1985; Pecknold et al., 1985).

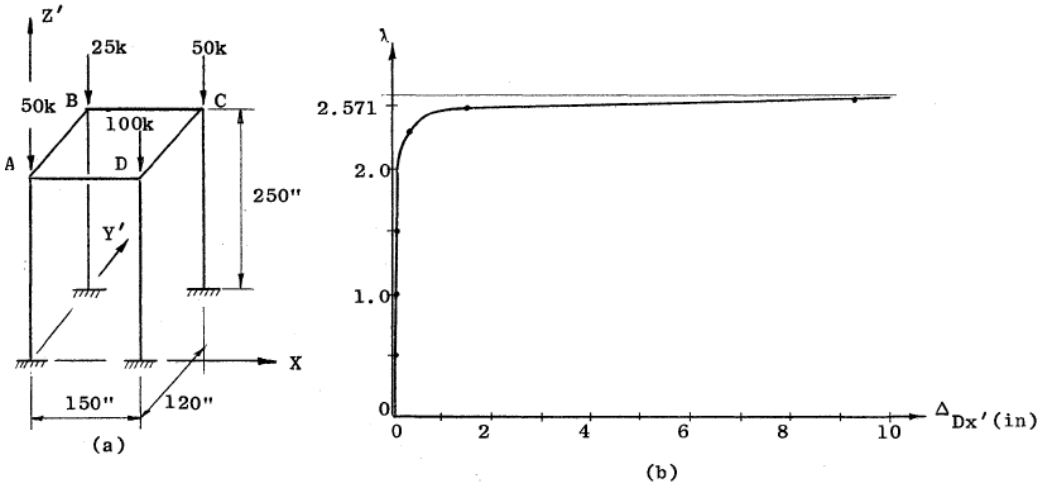

Figure 2.7:(a) Rectangular space frame (b) Load displacement curve space frame

Source:(Citipitioglu, 1965)

In the study by Pecknold et al. (1985), for the case where the truss was subject to a vertical symmetric loading and the truss was shallow with an angle ($\alpha<54.7^o$, refer to Figure 2.*8 a,* for details), only snap-through behaviour was observed. Further, the shape of the primary path was independent of the angle α (see Figure 2.*8 b* below). However, in the case where the truss was steep with $\alpha>54.7^o$, bifurcation of the primary path was observed, which appears as a straight line

on the load displacement curve (see Figure 2.*9* below). It was reported that bifurcation could be made to occur anywhere on the primary path with the adjustment of α. However, the study did not report on how the location of the bifurcation point changed with variations of α. The study did report that a snap-through point and a bifurcation occurred simultaneously in the case where the vertical spring constant was unity and $\alpha=54.7^{o}$. Here, the bifurcation path was observed to have shrunk to a point.

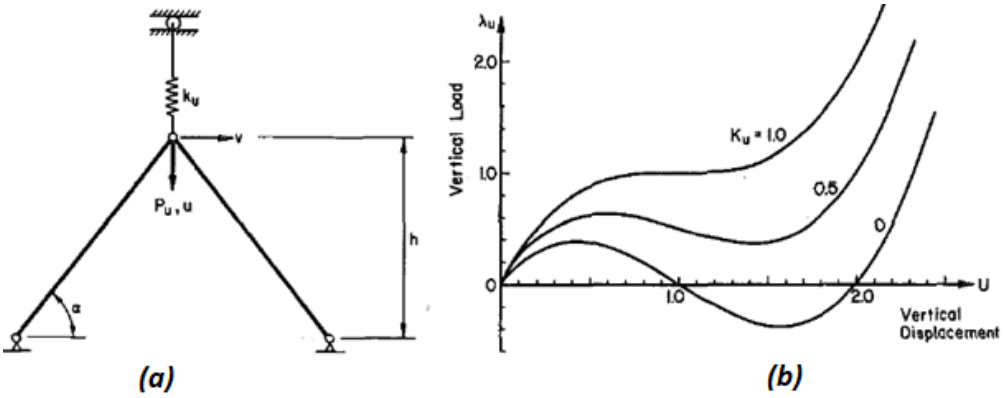

Figure 2.8:Effect of Linear Spring Stiffness K_u on Primary Response for Vertical Loading

Source: Pecknold et al. (1985)

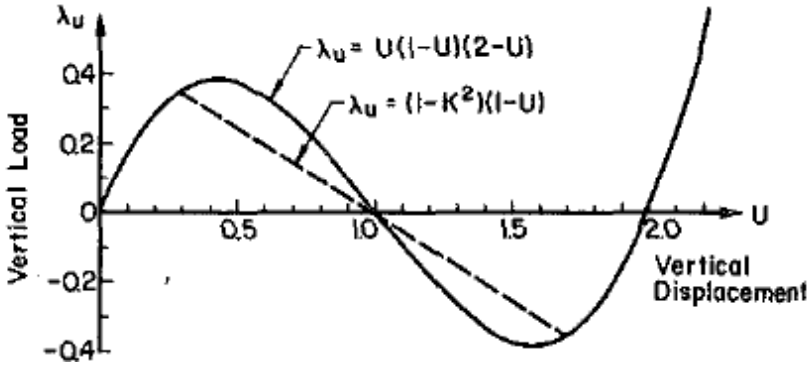

Figure 2.9: Vertical Loading Response ($P_{,,}$ = 0), Ku = 0, K^2 = 0.5 (a = 63.4 deg)

Source: Pecknold et al. (1985)

For cases where the truss was loaded with a combined asymmetric load (i.e. $P_v=\epsilon P_u$), the primary path asymptotically approached the bifurcation path (see Figure 2.*10* below). From Figure *2.10*, we can observe that the introduction of a load imperfection $P_v=\epsilon P_u$ to the existing vertical load P_u such that the load pattern P_v is not orthogonal to the bifurcation mode, effectively transforms a bifurcation point into a limit point. This forms the basis of the analytical distinction between a

limit point and a bifurcation point, that is, given a load vector $\boldsymbol{P}$ and eigenvector $\boldsymbol{\Phi}$ we have: at a bifurcation point $(\boldsymbol{\Phi}^T\boldsymbol{P}=0)$ and at a limit point ($\boldsymbol{\Phi}^T\boldsymbol{P}\neq 0$) with operations in the brackets indicating the dot product of the two vectors (Lee & Han, 2012; Nishino et al., 1984; Pecknold et al., 1985).

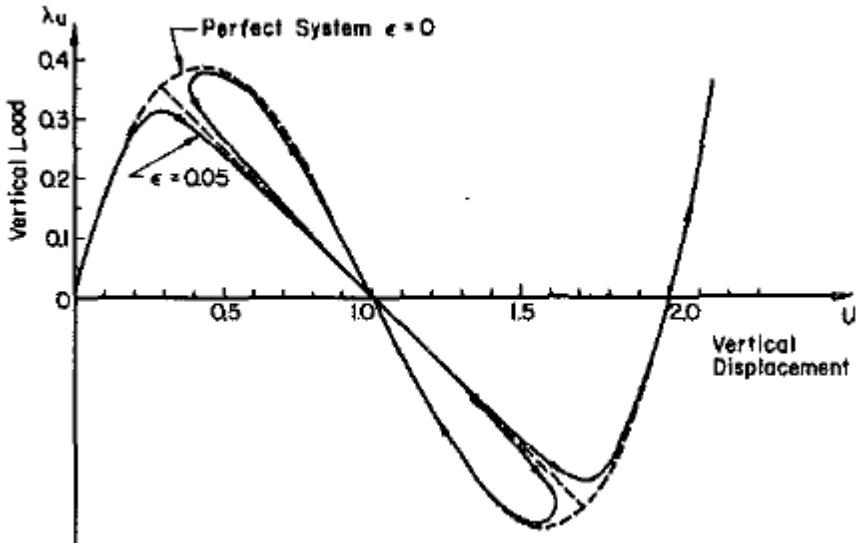

Figure 2.10: Asymmetrically loaded truss with α=63.4 and k_u=0

The snap-through stability behaviour discussed above has also been observed even in the case where the two-member truss is rigid-jointed. However, the snap-through load of the rigidly jointed two-member truss is higher (Williams, 1964). Snap-through behaviour is not limited only to truss structures, it has also been observed in polygonal portal frames (Horne, 1961) of the type shown in Figure *2.11* below. It is easy to see, however, that the dominant mode of load transfer in the inclined members shown in Figure *2.11*, will be by axial load transfer.

Snap-through behaviour has also been observed in the following structures: shallow-arches loaded at the apex with a concentrated load (Haisler et al., 1977); pin jointed shallow reticulated domes (Rothert et al., 1981); and rigid-jointed reticulated domes (Meek & Hoon Swee Tan, 1984) with a single concentrated load at the apex. However, for the equivalent rigidly jointed shallow domes the limit load is higher than that of the pin jointed shallow dome. For cases where all the nodes of the dome are symmetrically loaded by vertical concentrated loads, the snap-through behaviour has been observed to be the same as that of the dome with a single concentrated load at its apex. The unsymmetrical loading condition also exhibits snap-through behaviour, though at a load level lower than that for symmetrical loading (Riks, 1979; Meek & Hoon Swee Tan, 1984). Lastly, we

shall state that loss of stability by bifurcation is also possible in structures that display snap-through behaviour particularly in cases where such a structure has a high order of symmetry.

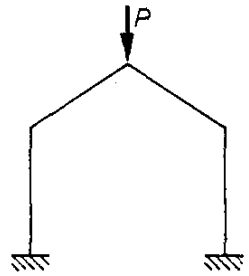

Figure 2.11: Polygonal portal frame exhibiting snap-through

As we have seen from the two-member pinned truss, when a bifurcation occurs before the limit point, the peak load is drastically reduced, and this behaviour is often observed in shallow domes (see Figure *2.12* below). A truss dome such as the one shown in Figure *2.12* will exhibit snapping behaviour on the primary equilibrium path, as shown in Figure *2.13*. However, before the limit point is reached, the truss dome can fail at loads much lower than the limit point (LP_1) as shown in Figure *2.13*. For this truss dome, there are three bifurcation points before the limit point is reached (Fujii & Choong, 1992; Crisfield, 1997; Lee & Han, 2012). We shall return to this truss problem in the section on symmetry breaking and tracing of bifurcation paths of this study.

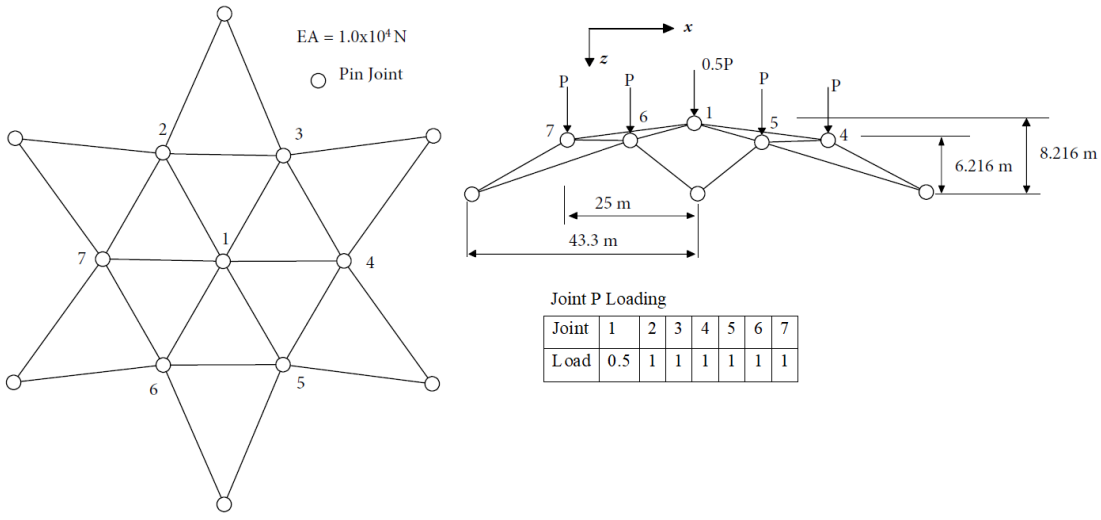

Joint P Loading

Joint	1	2	3	4	5	6	7
Load	0.5	1	1	1	1	1	1

Figure 2.12: Star Dome Truss

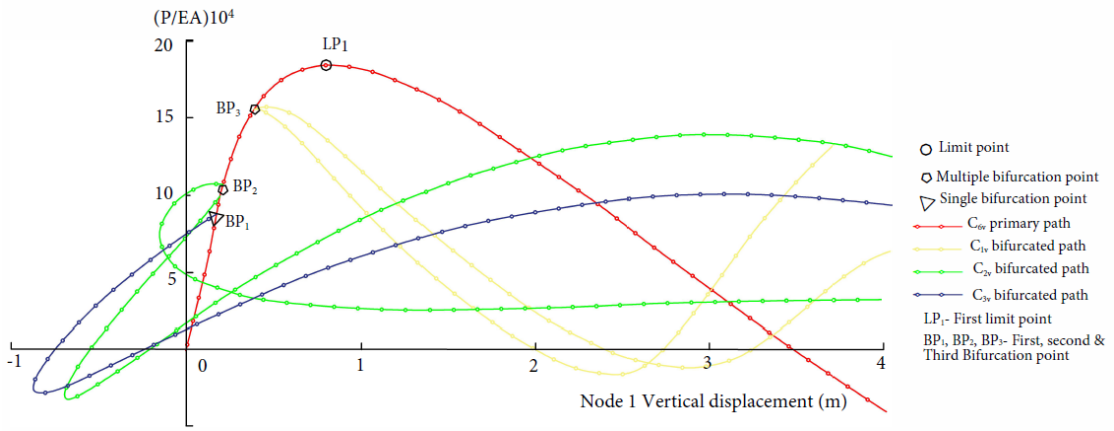

Figure 2.13: Star Dome Primary and Bifurcation paths

2.4 Methods of Stability Analysis for Plane Frames

The conventional methods for structural analysis of frames have been adapted for stability analysis. The slope deflection method was one of the earliest conventional methods of structural analysis of plane frames adapted for stability analysis. The slope deflection equations were modified through the use of what are termed as stability functions, which are functions that take account of the influence of axial loads in columns on the stiffness of the columns (Berry, 1919; James, 1935; Chwalla & Jokisch, 1941; Livesley, R. K., Chandler,D.B., 1968). The application of displacement methods such as the slope deflection method usually results in a system of homogenous linear equations with displacement quantities of the buckling shape as unknowns. Buckling occurs when the determinant of such systems of equations equals zero. Simplification of the determinant results in a characteristic equation of trigonometric functions, which are a function of the influence of axial forces on deformations and moments. The roots of such characteristic equations yield the buckling load of the structure.

The moment distribution method is another displacement method of structural analysis that was adapted for the elastic stability analysis of plane frames (Lundquist, 1937). Lundquist (1937) modified the stiffness of members to take account of the influence of axial loads. Proof of the uniqueness and convergence of Lundquist's method was also provided for the case of stable equilibrium by applying energy considerations (Hoff, 1941). The moment distribution approach for stability analysis developed by Lundiquist was later adapted for the analysis of out-of-plane buckling (Masur & Cukurs, 1957).

A much simpler displacement method approach to stability analysis of plane frames is the stiffness matrix method of structural analysis, which was adapted to the stability analysis of plane frames by taking account of the effect of axial loads on the stiffness of members (James, 1935; Masur, 1955; Carter, 1963; Livesley, R. K., Chandler,D.B., 1968). This method is particularly well suited for computer applications. The stiffness matrix of the frame is assembled, and at buckling the determinant of the stiffness matrix is equal to zero.

The flexibility matrix method of structural analysis of frames was also adapted for stability analysis of frames by modifying the flexibility matrix to take account of the effect of the axial forces on the stiffness of the columns (Mises & Ratzersdorfer, 1926; Chwalla, 1928; Zweig, 1984). The matrix stiffness method has, however, proven to be more suitable than the flexibility method because it is more amenable to computer programming (Zweig, 1984). Further, the flexibility method can give erroneous results in highly indeterminate structures, as the flexibility matrix of the primary structure can lose positive definitiveness prior to the first critical load (Bažant, 2000). The primary structure is the determinate structure obtained from the original indeterminate structure in the conventional application of the flexibility method (Zweig, 1984). The other reason why the displacement approach has been preferred over the flexibility approach is that the determinant of the displacement method varies more smoothly than that of the flexibility approach, making it easier to determine the smallest buckling load (Bažant, 2000).

Energy methods are based on the principle that the work done by external loads through a change in deformation configuration due to a disturbance is smaller than the change in strain energy. The frame returns to its initial deformed state after any small disturbance in its pre-buckled state (Masur, 1954). Masur (1954) developed lower and upper bound theorems for determining the buckling load of plane frames and trusses. These methods were later extended to multi-story, multi-bay frames (Johnson, 1961). Energy methods also lead to a system of linear equations analogous to those resulting from equilibrium methods. The buckling load is determined by an eigenvalue problem for the vanishing of the determinant of the coefficients of the equilibrium equations (Johnson, 1961). Approximate methods based on the energy method have also been proposed for the computation of the buckling load. All these methods require knowledge of the deflected shape of buckling, and their accuracy depends on how close the assumed buckled shape is to the true buckled shape (Stevens, 1967). The instability condition of these methods is to equate

the change in strain energy due to lateral displacements caused by lateral loads to that done by vertical loads moving through an equivalent lateral displacement (Horne, 1963).

2.5 Methods of Stability Analysis for Space Frames

As was stated in the discussion on concepts of stability in the introduction to chapter two of this study, the stability behaviour of space frames can be categorised into two categories: Bifurcation instability; and Limit-load instability.

2.5.1 Bifurcation Analysis

The methods of buckling analysis that were discussed for plane frames also apply for space frames. However, the buckling analysis of space frames is not just a simple generalisation of the methods developed for planar frames. This is because of the effects of the torsional stiffness of members and the possibility of torsional buckling of columns. Further, there are more degrees of freedom in space frames than in plane frames. Thus, many of the methods introduced for the stability analysis of space frames require the use of computers. One such method, implemented by LeRoy (1961) and Renton (1962) was based on the vanishing determinant of the stiffness matrix (the determinantal criterion). The application of this method required the use of computers. The effects of warping stiffness, pre-buckling moments, axial forces on torsional stiffness were ignored. Shosuke (1970) accounted for the effects of warping stiffness in the stability analysis of space frames. Further research studies on how to account for warping deformation behaviour in the stability analysis of space frames have been carried out (Barsoum & Gallagher, 1970; Ettouney & Kirby, 1981; Yang & McGuire, 1984) details of which will not be discussed here because this is particularly important for space frames composed of thin-walled members. The effects of axial loads on torsional stiffness in space frames were first accounted for by Vaart (1965).

For the case of rectangular space frames with pre-buckling moments, Citipitioglu (1965) and Vaart (1965) were one of the first researchers to use a second-order analysis to determine the buckling load of such frames. The buckling load was defined as the load level at which deflections become infinite on the load displacement curve without any load increment. This type of buckling criterion was referred to as the convergence criterion (Vaart, 1965). The instability load determined by the convergence criterion is what we have previously referred to as the limit point load. Citipiloglu (1965) found that the buckling load of a rectangular space frame with pre-buckling moments was about 10% lower than that of space frames without pre-buckling moments. This observation was

also previously made for the case of rectangular plane frames with pre-buckling moments (Le-Wu, 1963). Citipitioglu (1965) notes that the convergence criterion for elastic buckling of space frames with symmetric pre-buckling moments fails, and the determinantal criterion should be used as the approximate solution for the elastic buckling load. No explanation was given by Citipiloglu (1965) as to the cause of the failure of the convergence criterion for such frames. However, if one notes that symmetric structures have multiple repeating eigenvalues (buckling modes), then it becomes clear the source of the failure of the convergence criterion (Healey, 1985; Ikeda et al., 1986b; Healey, 1988; Ikeda et al., 1991) .

The second-order analysis of space frames considering the effects of large displacements has received the attention of many researchers and is discussed in the next section below.

2.5.2 Large displacement analysis

In cases where the loss of stability is caused by limit point and snap-through, a large displacement approach is required for the stability analysis. The work by Euler (1744) on the elastic buckling load of a column and general buckling analysis was based on small deflection theory. Later, Euler and Lagrange (1770) presented the first works on nonlinear large displacement theory of the post-buckling behaviour of elastic columns (Timoshenko, 1983). The major difference between buckling analysis and large displacement analysis is the inclusion of the effect of large displacements on the stiffness matrix. In the large displacement approach, the equilibrium path of the space frame is traced in an iterative numerical procedure, and deflections and stresses are continuously monitored and updated (Zienkiewicz, 1971). During this process, the limit and bifurcation points are identified; however, bifurcation points require special path switching methods from the primary equilibrium path in order to trace the secondary paths.

To carry out a large displacement analysis, the description of all stresses, deflections, and forces must be based on some coordinate system. The Eulerian or Lagrangian reference systems are used, with the latter being more commonly used in the analysis of space frames as it is particularly suitable for the step-by-step nonlinear analysis of solid bodies (Izzuddin & Lloyd, 1996).

There are basically two types of Lagrangian formulations: the total Lagrangian formulation and the updated Lagrangian formulation. In the total Lagrangian formulations, all deformations in subsequent iterations are based on the initial undeformed configuration (Mallett & Marcal, 1968; El-Zanaty & Murray, 1983; Nishino et al., 1984). In the updated Lagrangian formulation, on the

other hand, all configurations are referenced incrementally to the last known equilibrium configuration. The updated Lagrangian approach results in much simpler strain-displacement relationships than the total Lagrangian approach (Wen & Jalil, 1983).

The total Lagrangian formulation has been used in the nonlinear analysis of space frames with thin-walled members to derive the linear and geometric components of the stiffness matrix for frames in which the effects of warping have been ignored (Attard, 1986; Trahair & Teh, 2001). The updated Lagrangian formulation, on the other hand, has been used to derive the linear and geometric components of the stiffness matrix for frame structures with thin-walled members, taking into account the effects of warping (Yang & McGuire, 1986; Yang & Kuo, 1991a; Yang & Kuo, 1991b).

A critical assessment of the total and updated Lagrangian formulation has been performed, and it was concluded that the two formulations yield identical element stiffness matrices and nodal point vectors. Further, it was also found that the updated Lagrangian formulation was computationally more efficient (Bathe & Bolourchi, 1979).

In addition to the total and updated Lagrangian formulations normally used in the large displacement analysis of space frames, the co-rotational approach is also used. Here, the frame of reference for the deformation of an element continuously rotates with the element but does not deform with it. It has been shown that the co-rotational approach more conveniently considers the coupling of the bow and bending effects of a beam element (Teh & Clarke, 1998). Further, the corotational formulation has an advantage over the updated and total Lagrangian formulations in that, the number of degrees of freedom involved in the formulation at the element level is reduced by the number of rigid body movements. On the other hand, the updated formulation has been found to be more accurate at predicting flexural torsional buckling (Teh & Clarke, 1998). The co-rotational approach and the tangent stiffness matrix for the tracing of the nonlinear equilibrium paths of space frames have been formulated by several researchers (Oran, 1973; Belytschko et al., 1977; Belytschko & Glaum, 1979; Meek & Hoon Swee Tan, 1984; Crisfield, 1990; Meek & Xue, 1998).

The co-rotational approach has also been combined with either the total or the updated Lagrangian approach. A co-rotational Lagrangian formulation for three-dimensional beam elements has been proposed for the nonlinear analysis of space frames, capturing the coupling among the bending,

twisting, and stretching deformations among the beam elements (Hsiao, 1992; Hsiao et al., 1998a; Hsiao et al., 1998b; Hsiao & Lin, 2000).

2.5.3 Second-order nonlinear analysis

To trace the nonlinear equilibrium path of a space frame, the equilibrium and kinematic relationships must be written with respect to the deformed configuration of the structure. This analysis is referred to as a second-order elastic analysis when the material nonlinearities are not accounted for in the analysis. One approach to this analysis is the use of stability functions to take account of the influence of axial loads on the stiffness of the structure. Stability functions have been used to derive the tangent stiffness matrix of space frames for geometrically nonlinear elastic analysis based on the assumption of small relative deformations but large rotations (Oran, 1973). Stability functions have also been expressed in the form of a power series for digital computer implementation for the analysis of space frames (Goto & Chen, 1987). Other forms of stability functions for space frames have also been proposed (Ekhande et al., 1989).

The other approach for the second-order analysis of space frames is the finite element method. The simplest nonlinear element that has been used for space structures is the cubic Hermite element. This has been implemented by including the geometric terms into the linear stiffness matrix to form the tangent stiffness matrix (Connor et al., 1968; Bathe & Bolourchi, 1979; Meek & Hoon Swee Tan, 1984). For the analysis of highly nonlinear space frames, a higher order element has been proposed by employing a fourth-order polynomial displacement function in the element derivation (Chan & Zhou, 1994; Izzuddin & Lloyd, 1996).

The finite element method of the two approaches discussed is the most widely used because of its simplicity. The stability approach has the inconvenience of requiring the separation of the solution for tensile, compressive, and zero load cases. However, it is more accurate as it satisfies equilibrium along the whole length of the element, unlike the finite element method.

2.5.4 Numerical Methods for Plotting Equilibrium Paths

In the large displacement analysis of space frames, the stiffness matrix changes corresponding to the load level and changes in geometry. We have already discussed the formulations that are used to track changes in the configuration of the space frame. We now divert our attention to the numerical methods to trace the nonlinear equilibrium paths of space frames.

The numerical methods are iterative in nature since the geometry of the structure changes at each load step. The five commonly used numerical methods for nonlinear problems are (Clarke & Hancock, 1990): the Newton-Raphson method; the displacement control method; the arc-length control method; the minimum residual displacement method; and the work control method.

A simple, straight forward load incremental method can be used to trace the nonlinear equilibrium path of a space frame. However, the disadvantage of such an approach is that the iterative numerical solution drifts away from the true equilibrium solution. To overcome this drawback, the Newton-Raphson method is often employed. However, this method also has a drawback in that it fails to trace the equilibrium path beyond the limit points and bifurcation points, where the tangent stiffness matrix is singular (Ramm, 1981). To overcome this drawback, the displacement control method was proposed.

In the displacement control method, some particular displacement is chosen as the independent variable, while the remaining components of displacement and the load are taken as the dependent variables. The resulting system of equations is then solved by an iterative procedure such as the Newton-Raphson method (Wempner, 1971). The displacement control method can trace the equilibrium path in the neighbourhood and beyond the limit points of the equilibrium path. However, it fails to trace the equilibrium path at a snap-back point where the equilibrium path does not increase with the load. Thus, other methods, such as the arc length method, were proposed (Riks, 1979; Wempner, 1971). The arc length method does not iterate at a constant load or displacement. To the standard equilibrium equation of a nonlinear problem, a constraint equation is added to fix the length of the incremental load step (Riks, 1979). The arc length method can be used for problems that exhibit either limit point instability, snap-through or snap-back instability. The arc length method that was initially proposed by Riks (1979) was modified by several researchers to make it more suitable for use with the finite element method and to improve its convergence characteristics (Crisfield, 1981; Ramm, 1981; Crisfield, 1983; Schweizerhof & Wriggers, 1986).

Another method that was developed to overcome the shortcomings of the displacement or load control methods in tracing the equilibrium path is the work control method (Bathe & Dvorkin, 1983; Yang & McGuire, 1986). In this approach, the value of the work done in each iteration is

fixed. While this method is able to handle nonlinear problems, it has been shown to have a slower convergence rate than the arc length method (Yang & McGuire, 1986).

The arc length method and the work control method employ some constraints for each iteration to enable the analysis to traverse critical points. Another approach, referred to as the minimum residual displacement method, controls the load steps of each iteration by using a load factor, which follows the shortest path to obtain the solution point (Chan, 1988). This method has been found to have good convergence (Clarke & Hancock, 1990).

We have discussed the methods used to trace the equilibrium path in nonlinear problems beyond limit points. However, when a bifurcation point is present along the equilibrium path, the post-buckling equilibrium path must be switched to by using a path switching algorithm. One approach to locating a bifurcation point is to simply infer bifurcation points by introducing some kind of imperfection into the system and thus perturbing the bifurcation points into limit points (Hangai & Kawamata, 1972; Holzer et al., 1981; Vannucci et al., 1998). The major drawback of this method is that the selection of a sufficient imperfection to excite a particular secondary path is difficult for complex three-dimensional structures such as space frames.

Another method to locate the buckling points is to successively solve a linearized eigenvalue problem for the incremental loading (Maewal & Nachbar, 1977; Riks, 1979; Kim et al., 2002). A similar method is the determinant check, which investigates the vanishing of the determinant of the stiffness matrix. The determinant method is computationally more efficient; however, it has problems detecting double critical points. The eigenvalue method is more reliable as it utilises more information, such as the eigenvalues and eigenvectors of the stiffness matrix (Ikeda & Murota, 1991).

2.6 Symmetry

Many structures are constructed with symmetry for functionality reasons and also for aesthetics. The symmetry of a physical system is a geometric transformation of the system that leaves the system physically indistinguishable from its initial configuration (Zingoni, 2014). These transformations can either be continuous, such as in the rotations of a circle, or discrete such as the rotation or reflection of a regular polygon. In this study, the transformations that will be considered will be discrete rotations, and reflections, and combinations of these transformations.

The concepts of symmetry and anti-symmetry have been used to simplify the analysis of structures that exhibit planes or axes of symmetry. This involves the familiar methods of dividing structures into substructures based on planes of symmetry, applying appropriate boundary conditions at the plane of symmetry, and analysing the substructure. This is, however, a very simple approach to the utility of the application of principles of symmetry.

The main developments in the structural analysis of symmetric structures have come mainly through two approaches: the Fourier approach, which exploits only rotational symmetry, and the Group-theoretic approach which can exploit both rotational and reflection symmetries (Kangwai et al., 1999).

The Fourier approach is based on the discrete Fourier transformation. When the transformation matrix known as the Fourier transformation matrix is applied to the basis vectors of a symmetric system, the governing matrix equations of the system reduce to block-diagonalized form (Kangwai et al., 1999). One of the earliest applications of this method was for the buckling analysis of symmetric structures (Hussey, 1967; Renton, 1964). The vibrations of rotary symmetric structures have also been studied using the Fourier approach, and it has been shown that any forced vibrations can be decomposed into independent rotating components (Thomas, 1979). One major drawback of the Fourier approach is that it is unable to take full advantage of all the possible symmetries of a physical configuration. This is where group theory has proved to be very useful, as it can take account of all possible symmetries of a physical configuration.

Group theory and group representation theory are widely used in chemistry and physics to simplify calculations of molecules and crystals (Hamermesh, 1962). In the field of structural engineering, one of the first applications of group representation theory to structural analysis was by (Zloković, (1989), who formulated the so-called G-vector analysis based on group representation theory and applied it to problems in static, vibration, and stability. Zingoni made further developments showing how group theory can be exploited not only to simplify computations, but also to gain insights into the structural behaviour of symmetric structures (Zingoni et al., 1993; Zingoni et al., 1994; Zingoni & Pavlovic, 1994; Zingoni, 1996; Zingoni, 2001a; Zingoni, 2001b; Zingoni, 2005a; Zingoni, 2005b; Zingoni, 2008; Zingoni, 2009; Zingoni, 2012a; Zingoni, 2012b; Zingoni, 2014; Zingoni, 2015; Zingoni, 2018).

2.6.1 Basic Concepts of Symmetry Groups

Group theory is a formal mathematical approach used to analyse the symmetry characteristics of a system. It can be used to simplify the structural computations of symmetric structures, and it can also be used to explain the structural behaviour of symmetric structures. It has been applied in the stability analysis of symmetric structures by several researchers (Renton, 1964; Healey, 1985; Ikeda et al., 1986b; Ikeda et al., 1986a; Ikeda & Torii, 1987a; Ikeda & Torii, 1987b; Healey, 1988; Zloković, 1989; Ikeda & Murota, 1991; Ikeda et al., 1991; Kaveh & Nikbakht, 2010; Chen & Feng, 2018). Group theory has also been applied to the vibration analysis of symmetric structures (Zingoni, 1996; Zingoni, 2005b; Zingoni, 2008; Zingoni, 2014; Zingoni, 2015; Zingoni, 2018). An extensive discussion of the applications of group theory in structural mechanics can be found in Zingoni (2009).

Before discussing exactly how group theory is applied in the stability analysis of symmetric structures, the basic concepts of group theory shall first be discussed.

A symmetry group G describes all the symmetries inherent in a structure by use of a set of symmetry elements $\{a,b, c, \ldots, g, \ldots\}$. In order for these symmetry elements to comprise a group they must satisfy four axioms with respect to a binary operation (for example, multiplication) if the following axioms are satisfied (Zingoni, 1996; Zingoni, 2009; Zingoni, 2014):

i. Closure - The product c of any two elements a and b of the group must be a unique element which must also belong to the group;
ii. Identity - For each element a in the group, the identity element e must exist such that: $ea=ae=a$;
iii. Inverses - For each element a in the group, an inverse d must exist in the group such that $ad=da=e$, where e is the identity $e;$ and
iv. Associativity - for any elements a, b, and c in the group it must be true that: $a(bc)=(ab)c$.

Groups for which commutativity holds, i.e., $ab=ba$ (for any elements a and b of the group) are called *Abelian* groups.

Symmetry elements of a group are operations or transformations that bring an object into coincidence with itself, while leaving it indistinguishable from its original configuration. For finite

objects (whose symmetry groups are referred to as point groups), symmetry operations are of the following types (Zingoni, 1996; Zingoni, 2009; Zingoni, 2014):

i. reflections in planes of symmetry, which we will denote by σ_l, where l is the plane of symmetry;
ii. rotations about an axis of symmetry, which we will denote by C_n, if the angle of rotation is $2\pi/n$;
iii. rotation–reflections, which we will denote by S_n; these represent a rotation through an angle $2\pi/n$, combined with a reflection in the plane perpendicular to the axis of rotation.

Symmetry groups are classified according to the types of symmetry elements that they have. Groups for which one point remains stationary upon the application of symmetry operations are called point group symmetries and are the only type of symmetry group considered in this study. We shall now discuss the groups considered in this study.

Groups denoted by C_n and C_{nv} all possess a single principle n-fold axis of rotational symmetry (giving n rotation elements, one of which is equivalent to the identity element e), with the C_{nv} groups possessing additional n reflection elements (Kangwai et al., 1999; Zingoni, 1996; Zingoni, 2015). For our discussion, we shall take our principal *n-fold* axis C_n be about the *z-axis* of the cartesian coordinate system. Examples of geometric configurations belonging to the C_8 and C_{8v} symmetry groups are shown in Figure *2.14* below.

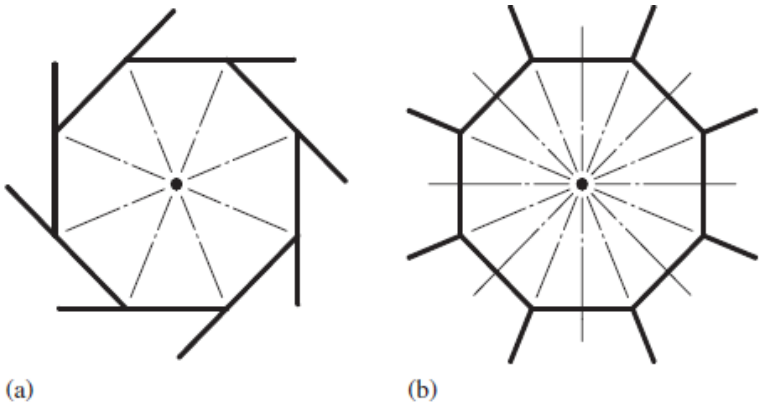

Figure 2.14:C_8 configuration and (b) C_{8v} configuration

Source: Zingoni (2009)

The C_n and C_{nv} symmetry groups have orders n and $2n$ respectively. The order is the number of elements in a group.

In three-dimensional configurations, if, in addition to the principal n-fold axis C_n, there is a system of nC_2 fold secondary axes at right angles to the principle axis C_n, then we have the dihedral groups D_n of order $2n$. Addition of a horizontal plane to these symmetry operations of D_n we obtain the groups D_{nh} of order $4n$ (Zingoni, 2012b).

Table *2.1* below presents a summary of the elements of some of the point groups that will be considered in this study. Reference axes and reflection planes are labelled as *x, y, z* (or *xy,xz,yz*) where these can be related to the cartesian coordinate directions, or otherwise as *1, 2, 3*,…or *A,B,C*,…., depending on whether they pass through corners, mid-sides, or mid-faces of configurations. The element σ_h refers to the reflection in the horizontal plane perpendicular to the *principal n-fold* axis.

Examples of C_{nv} and D_{nh} symmetric space frames that will be considered in this study are shown in Figure *1.1, 1.2* and *1.3*. It is important to take note that the D_n and C_{nv} groups are isomorphic as abstract groups when applied to regular n-sided polygons (Ikeda & Murota, 2010). A group isomorphism is a function between two groups that sets up a one-to-one correspondence between the elements of the groups in a way that respects the given group operations.

Each symmetry group has itself as a subgroup and proper subgroups. A subgroup is basically a subset of a symmetry group, which also satisfies the four axioms of symmetry groups outlined above. Taking the example of the D_3 symmetry group, it has the following elements:

$$D_3 = \left\{e, \mathrm{C}_3, \mathrm{C}_3^{-1}, C_2^1, C_2^2, C_2^3\right\}$$

The subsets of D_3 are the following:

$$D_3,\ C_3 = \left\{e, \mathrm{C}_3, \mathrm{C}_3^{-1}\right\}, D_1^1 = \left\{e, C_2^1\right\}, D_1^2 = \left\{e, C_2^2\right\}, D_1^3 = \left\{e, C_2^3\right\}, C_1 = \left\{e\right\}$$

The D_3 group is of order six. The ratio of elements in a group to those of its subgroup is called the index. It is an indicator of the level of difference in symmetry between a group and its subgroup. The index for a group D_n and its subgroup D_m is given by (Ikeda et al., 1991):

$$\left|\frac{D_n}{D_m}\right| = \frac{2n}{2m} = \frac{n}{m} \qquad (2.5)$$

Table 2.1: Examples of point group symmetries

Group	order	elements
C_1	1	e
C_{1v}	2	e, σ_v
C_{2v}	4	$e, \mathrm{C}_2, \sigma_x, \sigma_y$
C_{3v}	6	$e, \mathrm{C}_3, C_3^{-1}, \sigma_1, \sigma_2, \sigma_3$
C_{4v}	8	$e, \mathrm{C}_4, C_4^{-1}, \mathrm{C}_2, \sigma_x, \sigma_y, \sigma_1, \sigma_2$
C_{6v}	12	$e, \mathrm{C}_6, C_6^{-1}, \mathrm{C}_3, \mathrm{C}_3^{-1}, C_2, \sigma_A, \sigma_B, \sigma_C, \sigma_1, \sigma_2, \sigma_3$
C_{8v}	16	$e, \mathrm{C}_8, C_8^{-1}, \mathrm{C}_8^3, \mathrm{C}_8^5, C_4, \mathrm{C}_4^{-1}, C_2, \sigma_A, \sigma_B, \sigma_C, \sigma_D, \sigma_1, \sigma_2, \sigma_3, \sigma_4$
D_2	4	$e, \mathrm{C}_2^x, C_2^y, C_2^z$
D_3	6	$e, \mathrm{C}_3, \mathrm{C}_3^{-1}, C_2^1, C_2^2, C_2^3$
D_4	8	$e, \mathrm{C}_4, \mathrm{C}_4^{-1}, \mathrm{C}_2, C_2^x, C_2^y, C_2^1, C_2^2$
D_6	12	$e, \mathrm{C}_6, \mathrm{C}_6^{-1}, \mathrm{C}_2, \mathrm{C}_3, \mathrm{C}_3^{-1}, C_2^A, C_2^B, C_2^C, C_2^1, C_2^2, C_2^3$
D_8	16	$e, \mathrm{C}_8, C_8^{-1}, \mathrm{C}_8^3, \mathrm{C}_8^5, C_4, \mathrm{C}_4^{-1}, C_2, \mathrm{C}_2^A, \mathrm{C}_2^B, \mathrm{C}_2^C, \mathrm{C}_2^D, \mathrm{C}_2^1, \mathrm{C}_2^2, \mathrm{C}_2^3, \mathrm{C}_2^4$
D_{2h}	8	$e, \mathrm{C}_2^x, C_2^y, C_2^z, S_2, \sigma_{xy}, \sigma_{xz}, \sigma_{yz}$
D_{3h}	12	$e, \mathrm{C}_3, \mathrm{C}_3^{-1}, \mathrm{S}_3, \mathrm{S}_3^{-1} C_2^1, C_2^2, C_2^3, \sigma_h, \sigma_1, \sigma_2, \sigma_3$
D_{4h}	16	$e, \mathrm{C}_4, \mathrm{C}_4^{-1}, \mathrm{S}_4, \mathrm{S}_4^{-1}, \mathrm{S}_2, C_2^x, C_2^y, \mathrm{C}_2^z, C_2^1, C_2^2, \sigma_h, \sigma_x, \sigma_y, \sigma_1, \sigma_2$
D_{5h}	20	$e, \mathrm{C}_5, \mathrm{C}_5^{-1}, \mathrm{C}_5^2, \mathrm{C}_5^{-2}, \mathrm{S}_5, \mathrm{S}_5^{-1}, \mathrm{S}_5^3, \mathrm{S}_5^{-3}, C_2^1, C_2^2, \mathrm{C}_2^3, C_2^4, C_2^5, \sigma_h, \sigma_1, \sigma_2, \sigma_3, \sigma_4, \sigma_5$
D_{6h}	24	$e, \mathrm{C}_6, \mathrm{C}_6^{-1}, \mathrm{S}_6, \mathrm{S}_6^{-1}, \mathrm{C}_2, \mathrm{S}_2, \mathrm{C}_3, \mathrm{C}_3^{-1}, \mathrm{S}_3, \mathrm{S}_3^{-1}, C_2^A, C_2^B, C_2^C, C_2^1, C_2^2, C_2^3, \sigma_h, \sigma_A, \sigma_B, \sigma_C, \sigma_1, \sigma_2, \sigma_3$
D_{8h}	32	$e, \mathrm{C}_8, C_8^{-1}, \mathrm{S}_8, \mathrm{S}_8^{-1}, \mathrm{C}_8^3, \mathrm{C}_8^5, \mathrm{S}_8^3, \mathrm{S}_8^5 C_4, \mathrm{C}_4^{-1}, \mathrm{S}_4, \mathrm{S}_4^{-1}, C_2, \mathrm{S}_2, \mathrm{C}_2^A, \mathrm{C}_2^B, \mathrm{C}_2^C, \mathrm{C}_2^D, \mathrm{C}_2^1, \mathrm{C}_2^2, \mathrm{C}_2^3, \mathrm{C}_2^4, \sigma_h, \sigma_A, \sigma_B, \sigma_C, \sigma_D, \sigma_1, \sigma_2, \sigma_3, \sigma_4$

For each symmetry group, it is possible to write down a multiplication table of the symmetry operations. These multiplication tables are used to facilitate the multiplication of three or more

elements and are widely available (Hamermesh, 1962; Altmann & Herzig, 1994). An example of the C_{2v} multiplication table of symmetry operations is given in Table *2.2* below.

Table 2.2: Group table for C_{2v}

$\boldsymbol{C_{2v}}$	$\boldsymbol{e}$	$\boldsymbol{C_2}$	$\boldsymbol{\sigma_x}$	$\boldsymbol{\sigma_y}$
$\boldsymbol{e}$	e	C_2	σ_x	σ_y
$\boldsymbol{C_{2v}}$	C_2	e	σ_y	σ_x
$\boldsymbol{\sigma_x}$	σ_x	σ_y	e	C_2
$\boldsymbol{\sigma_y}$	σ_y	σ_x	C_2	e

Lastly, it should be noted that even though all cyclic and dihedral symmetries are assumed to be known in advance in this study, automated symmetry detection algorithms have been developed to identify the symmetry of a system (Zhang et al., 2022; Chen et al., 2018; Zingoni, 2012b). These algorithms are computational methods designed to identify and analyse symmetrical patterns within data or systems. They utilise mathematical and computational techniques to assess the spatial relationships and arrangements of elements within the system (Chen et al., 2018). By automating the process of symmetry detection, these algorithms enhance efficiency and accuracy, particularly in scenarios where human observation and analysis may be impractical due to the complexity or size of the system.

2.6.2 Matrix representations of groups

When we attach a coordinate system to a structure with a configuration belonging to a symmetry group G, it becomes possible to represent the symmetry operations of a group G in terms of a set of matrices $R(G)$ for an n-dimensional vector space V. This set of matrices $R(G)$ depends on the set of basis vectors chosen for the vector space V and is thus termed as reducible. If a different set of basis vectors is chosen, a different set of matrices $R'(G)$ results. According to Group representation theory, a set of basis vectors can be found such that our set of matrices $R(G)$ will be in a block-diagonal form, with the blocks being as small as possible. These blocks are called the irreducible matrix representations of the group and will have the following general form (Kangwai et al., 1999; Zingoni, 2009; Zingoni, 2015):

$$R(G)=\begin{bmatrix} R^{(1)}G & 0 & . & 0 \\ 0 & R^{(2)}G & . & 0 \\ . & . & . & . \\ 0 & 0 & . & R^{(k)}G \end{bmatrix} \qquad (2.6)$$

The set of submatrices in Equation (2.6) is the set of all the symmetry operations for the group *G*. While the blocks of matrices in Equation (2.6) are irreducible, the representation *R(G)* is reducible, and Equation (2.6) may be rewritten as (Zingoni, 2009):

$$R(G)=R^{(1)}(G)+R^{(2)}(G)+\cdots+R^{(k)}(G) \quad (2.7)$$

The matrix *R(G)* is of size *nxn*, whereas the submatrices $R^{(1)}(G)$, $R^{(2)}(G)$,…, $R^{(k)}(G)$ are sizes n_1xn_1, n_2xn_2, …, n_kxn_k respectively, where $n_1+n_2+...n_k=n$.

The diagonal representation of *R(G)* effectively splits the vector space *V* into a number of independent group invariant subspaces $U^{(i)}$ of smaller dimensions, such that none of these subspaces can be divided into invariant subspaces of smaller dimensions (Ikeda & Murota, 1991; Zingoni, 2009).

At this point, we have not discussed exactly how the irreducible submatrices $R^{(1)}(G)$, $R^{(2)}(G)$,…, $R^{(k)}(G)$ are obtained. To do this, we must discuss some additional concepts used in group representation theory.

An element α of a group *G* is said to be conjugate to an element β in the same group if there exists an element ρ in *G* such that $\alpha=\rho^{-1}\beta\rho$. The class of β is the collection of all elements formed by evaluating $\rho^{-1}\beta\rho$ for all ρ in the group *G* (Zingoni, 2009).

Earlier, we stated that the set of matrices *R(G)* depends on the set of basis vectors chosen for the vector space. However, one quantity remains constant irrespective of the basis vectors chosen. This is the sum of diagonal elements for a submatrix representing a symmetry operation *a* (Kangwai et al., 1999; Zingoni, 2009; Zingoni, 2015). We shall denote the trace for a symmetry operation *a* as $\chi(a)$.

The traces of conjugate elements in a group are equal, and thus, in any irreducible representation, all elements belonging to the same class have the same character. Further, according to group representation theory, the number of different irreducible representations for a group *G* is finite

and equal to k for a group G of order h and k different classes (Zingoni, 2009; Zingoni, 2015). A character table is then a table whose rows $R^{(i)}$ correspond to irreducible group representations and columns to conjugacy classes $K^{(i)}$ of group elements. The entries of the table consist of traces $\chi_j^{(i)}$ of the matrices representing group elements of the column's class in the given row's group representation (see Table 2.3 below).

In essence, the character table provides a useful way of encoding the important information of a symmetry group. Character tables for common symmetry groups can be found in literature (Hamermesh, 1962; Altmann & Herzig, 1994).

If we add addition to the four axioms previously presented that define a symmetry group G, we obtain a vector space termed *group algebra* (Zingoni, 2009; Zingoni, 2015). Thus, the elements of the group algebra Z are all the linear combinations of the group elements. Since a set of linearly independent vectors constitutes a basis for a vector space (Axler, 1997) and the elements of G are linearly independent, they, therefore, constitute a basis for Z.

Table 2.3: General format of character table

G	K_1	K_2	.	K_J	.	K_K
$R^{(1)}$	$\chi_1^{(1)}$	$\chi_2^{(1)}$	.	$\chi_j^{(1)}$	.	$\chi_k^{(1)}$
$R^{(2)}$	$\chi_1^{(2)}$	$\chi_2^{(2)}$	.	$\chi_j^{(2)}$	.	$\chi_k^{(2)}$
.	.	.	.	.	.	.
$R^{(I)}$	$\chi_1^{(i)}$	$\chi_2^{(i)}$	.	$\chi_j^{(i)}$	.	$\chi_k^{(i)}$
.	.	.	.	.	.	.
$R^{(K)}$	$\chi_1^{(k)}$	$\chi_2^{(k)}$	.	$\chi_j^{(k)}$	.	$\chi_k^{(k)}$

Idempotents of the group algebra are its non-zero elements, which satisfy the relation $P^{(i)}\,P^{(i)} = P^{(i)}$. Further, orthogonal idempotents satisfy the relation $P^{(i)}P^{i)}=0$, *if* $\neq j$. Idempotents are linearly independent, and the sum of orthogonal idempotents is also an idempotent. The orthogonal idempotents $P^{(i)}$ of the group algebra for the subspace $U^{(i)}$ *(for i=1,2,…,k)* can be written down directly from the character table using the relation (Zingoni, 2009; Zingoni, 2015).

$$P^{(i)} = \frac{\delta^{(i)}}{h} \sum_{g} \chi^{(i)}\left(g^{-1}\right) g \tag{2.8}$$

Where h is the order of G, $\delta^{(i)}$ is the dimension of the ith irreducible representation, given by $\delta^{(i)}=\chi^{(i)}(e)$, the first character of the ith row of the character table, $\chi(i)$ is a character of the ith irreducible representation, g is an element of G, and g^{-1} its inverse.

When an idempotent $P^{(i)}$ corresponding to the reducible $R^{(i)}$ is applied to vectors of a vector space V, it nullifies every vector that does not belong to the subspace $U^{(i)}$ of $R^{(i)}$. The idempotent $P^{(i)}$ acts as an operator, selecting all vectors that belong to $U^{(i)}$ which all have the symmetry characteristics of the subspace $U^{(i)}$ (Zingoni, 2009; Zingoni, 2015).

The standard basis *((1,0,0), (0,1,0), (0,0,1))* of three-dimensional space is not a unique basis. Any set of linearly independent vectors that span a vector space can be used to describe any vector in that vector space (Axler, 1997). If a physical system possesses symmetry properties that can be described by a symmetry group, application of the procedure described above effectively changes the basis vectors to symmetry adapted basis vectors. This decomposes the vector space to which the physical system belongs into independent subspaces. This makes it possible to separate the matrix equations that describe the behaviour of the physical system into a block-diagonal form (Zingoni, 1996; Zingoni, 2009; Zingoni, 2015).

2.6.3 Group theory and analysis of symmetric structures

As was earlier stated, a common feature of the bifurcation behaviour of symmetric structures are double critical points, which appear several times on the equilibrium paths of such structures (Healey, 1985; Ikeda et al., 1986b; Healey, 1988; Ikeda et al., 1991; Ikeda & Murota, 1991; Wohlever & Healey, 1995).

The tracing of all branching paths at double critical points of the equilibrium path has been challenging in structural engineering. In the global bifurcation analysis of symmetric structures, the group-theoretic approach has proved to be effective (Ikeda & Murota, 1991). Healey (1985, 1988) employed the group-theoretic approach to the problem of tracing the equilibrium path, identifying bifurcation points and directions of new branches of a lattice dome with regular-hexagonal symmetry. The bifurcation points were detected by testing the tangent-stiffness matrix of the system at particular points of the equilibrium path. Other researchers who have used the

group-theoretic approach for the tracing of the equilibrium path of symmetric structures include: (Ikeda & Murota, 1991; Wohlever, 1996; Wohlever & Healey, 1995; Chen & Feng, 2018).

In order to understand how group theory is applied in the analysis of symmetric structures, we must first note that the standard basis vectors ((1,0,0), (0,1,0),(0,0,1) are not unique, and any other convenient set of basis vectors can be used (Axler, 1997). Thus, in what is referred to as the group-theoretic approach to the analysis of symmetric structures, the basis vectors used are based on the symmetry group to which the physical configuration of a system belongs (Zingoni, 1996; Zingoni, 2009; Zingoni, 2015). Each symmetry operation of a symmetry group is a linear transformation in space, which can be represented by a transformation matrix. By using these linear transformations, symmetry-adapted coordinate systems are obtained that decompose the vector space of a structural problem into several independent subspaces. The matrix of equations describing the behaviour of the system will be in block-diagonal form. Thus, these equations are placed into independent sets of equations belonging to separate subspaces of the vector space of the system (Healey, 1988; Ikeda & Murota, 1991; Zingoni, 2009).

The linear transformation referred to above is facilitated by a suitable orthogonal matrix $\boldsymbol{H}$, such that the transformed stiffness matrix $\boldsymbol{H^T K H}$ takes the block diagonal form (Ikeda & Murota, 1991). In this way, the test for the singularity of $\boldsymbol{K}$ is decomposed into mutually independent tests for the singularity of the diagonal blocks. We shall use the example of the Newton-Raphson procedure to illustrate how the group-theoretic method is used in stability analysis (Wohlever & Healey, 1995; Zingoni, 2009): Consider the vector equilibrium equation in vector space V:

$$\boldsymbol{f(u,\lambda)=0} \tag{2.9}$$

where $\boldsymbol{f}$ is a column-vector function, $\boldsymbol{u}$ is a displacement vector, λ is a loading parameter, and the tangent-stiffness matrix $\boldsymbol{K}=d\boldsymbol{f}/d\boldsymbol{u}$. The matrix $\boldsymbol{K}$ is now block diagonalized $\boldsymbol{H^T K H}$. Taking the Newton-Raphson procedure as an example, this results in the following incremental equations of the Newton-Raphson procedure:

$$\begin{bmatrix} \mathbf{K}^{(1)} & 0 & . & 0 \\ 0 & \mathbf{K}^{(2)} & . & 0 \\ . & . & . & . \\ 0 & 0 & 0 & \mathbf{K}^{(k)} \end{bmatrix} \begin{Bmatrix} \Delta\mathbf{u}^{(1)} \\ \Delta\mathbf{u}^{(2)} \\ . \\ \Delta\mathbf{u}^{(k)} \end{Bmatrix} = \begin{Bmatrix} -\mathbf{f}_{\lambda} \\ 0 \\ . \\ 0 \end{Bmatrix} \tag{2.10}$$

Where $\boldsymbol{u}^{(i)}$ belongs to subspace $U^{(i)}$. Thus, the vector space V of the full problem has now been reduced into independent subspaces $U^{(k)}$ which reflect the different symmetries to which the system belongs (Ikeda & Murota, 1991; Zingoni, 2009). This makes the singularity test of the stiffness matrix much more efficient, as the singularity test is based on smaller matrices than the full stiffness matrix. A further advantage of this approach is that critical points are systematically categorised, and the directions of the bifurcation paths are determined automatically (Ikeda & Torii, 1987b; Ikeda et al., 1991).

There are two major methods of detecting critical points: the determinant-check method, which investigates the vanishing of the determinant *det(K)* of K; and the eigenvalue method which observes the vanishing of eigenvalues of K. Ikeda and Murota (1991) compared the efficiency of the determinant method in the conventional and group-theoretic approaches to detecting double points for a hexagonal lattice dome. The determinant method failed to properly detect double points in the conventional approach. However, the determinant check was able to efficiently detect double points when the group theoretic method was used. LeyRoy (1961) also found that the determinant method failed to detect critical points with the conventional approach to bifurcation analysis of a symmetric space frame, and no mention was made in this study as to the influence of double points on this kind of behaviour. The determinant method is able to work in the group theoretic approach because the problem of numerical ill-conditioning at double critical points is circumvented since the double points belong to different diagonal blocks (Ikeda & Murota, 1991).

In tracing the equilibrium path of symmetric structure by using equation (2.10), the subspace that reflects the symmetry of the full problem will be the fundamental equilibrium path, and the paths traced from the other subspaces will be bifurcated paths (Ikeda & Murota, 1991; Ikeda et al., 1991).

The group-theoretic method highlighted above, while effective at avoiding the numerical ill-conditioning of closely spaced bifurcation points has one major drawback in the sense that, in order to assemble the diagonalized stiffness matrix, the full non-diagonalized stiffness matrix has to be assembled first (Zingoni, 2009). This can be computationally expensive for very large problems. Instead of following this approach, the governing equilibrium equation (2.10) may be restricted to a specific subspace $U^{(i)}$ (Zingoni, 2009). Recall that this subspace is obtained from the vector space of a system with a configuration belonging to the symmetry group G. Following this approach, equation (2.10) can be written as:

$$\mathbf{f}^{(i)}(\mathbf{v},\lambda)=0 \qquad (2.11)$$

where $\boldsymbol{f}^{(i)}$ is a load vector belonging to subspace $U^{(i)}$, and $\boldsymbol{v}$ is the displacement vector belonging to subspace $U^{(i)}$. The reduced problem of equation (2.11) only captures the solutions of equation (2.10) belonging to the space $U^{(i)}$ (Healey, 1988; Zingoni, 2009). Further detailed discussions on the group-theoretic approach to bifurcation analysis can be found in Sattinger (1979) and Golubitsky and Schaeffer (1985). These works are, however, related to local bifurcation behaviour.

2.7 Influence of Symmetry on Stability

The principles of symmetry have been used to explain a wide variety of phenomena in the fields of physics and chemistry. Before discussing the influence of symmetry on stability, we shall first discuss the concept of symmetry breaking.

2.7.1 Symmetry Breaking

Symmetry breaking is the process by which the symmetry of a system is reduced when the system becomes unstable (Stewart & Golubitsky, 1992). Generally, the breaking of the symmetry of a system does not imply that symmetry no longer exists. Often, a lower order of symmetry will result, that is, the subgroup of the symmetry group of the system before symmetry breaks (Stewart, 1999). As it relates to bifurcation, we may state that symmetry breaking is a phenomenon where slight disturbances acting on a system at the critical point of the fundamental equilibrium path determine which branch (bifurcation path) of the fundamental path is taken (Stewart & Golubitsky, 1992). In this case, the fundamental equilibrium path has a higher order of symmetry than the bifurcated path (Chiba & Nagahama, 2001). The concept of symmetry breaking was first introduced in physics in the study of physical objects and phenomena by Pierre Curie in 1894 (Castellani, 2003). The kind of symmetry breaking being discussed here is referred to as spontaneous symmetry breaking (Castellani, 2003), and the simple example of the buckling of a perfect column is used here to explain this concept. The configuration and energy of a Euler column subjected to an axial load are invariant for all rotations about the longitudinal axis of the column. That is, rotations of the column about any angle about the longitudinal axis do not change the nature of the fundamental equilibrium path. For example, the column does not bend. However, this invariance only holds if the applied load is below the buckling load. At the buckling load, the symmetric equilibrium configuration becomes unstable, and an infinite number of stable bent configurations that are no longer rotationally symmetric appear. Symmetry breaking can now

occur due to the effect of an asymmetric cause, for example, a slight lateral disturbance of the column at the buckling load. Thus, in the buckled configuration, the equilibrium configuration is no longer invariant under rotations about the longitudinal axis, and thus rotational symmetry has been broken. The buckling of a compressed cylinder under an axial load may also be similarly used to explain the concept of spontaneous symmetry breaking (Stewart & Golubitsky, 1992).

The concept of symmetry breaking has been used to explain various phenomena, such as the pattern of dimples on a buckled cylinder, spirals in galaxies, and the patterns on the barks of trees just to mention a few (Weinberg, 2009). The theory of symmetry breaking, like other theories such as the theory of chaos and thermodynamics, is applicable to a wide variety of phenomena, but its applicability is not unlimited (Weinberg, 2009). For our purposes, however, we shall focus on the global bifurcation behaviour of systems that are equivariant to a symmetry group. The principle of equivariance is explained below.

If we have a symmetry group G describing the overall symmetry of the system and g any element belonging to G. Further, if $T(g)$ for $g \in G$ is an NxN orthogonal matrix of a linear representation of G on R^N, then the equation:

$$\boldsymbol{f}(\boldsymbol{u},\lambda)=\boldsymbol{0} \qquad (2.9)$$

is said to be equivariant under the action of T if:

$$\boldsymbol{f}(T(g)\boldsymbol{u},\lambda)=T(g)\boldsymbol{f}(\boldsymbol{u},\lambda) \text{ for all } g \in G \qquad (2.11)$$

The equivariance of equation 2.*9* to a symmetry group must hold in order to apply the group theoretic approach to the analysis of symmetric structures (Ikeda et al., 1991). It is important to note that our system must be invariant to the symmetry group G not only in the geometrical configuration, but in the stiffness distribution, loading pattern, and support conditions as well. We must also add that in the discretization of a system, the elements chosen must not violate the symmetry group of the system. For example, Wohlever and Healey (1995), in their study of the post-buckling behaviour of an axially compressed cylindrical shell, adopted ring elements to preserve the axis-symmetry of the full cylinder. The displacement fields of the shell (within each ring) were represented by a finite number of Fourier terms along the circumference of the cylinder.

Some bifurcation properties of systems equivariant to a symmetry group G that have been established (Fuji's theorems) can be stated as follows (Ikeda et al., 1986a):

I. The deformation patterns of a structure on the bifurcated paths of a G equivariant system will have G_i symmetry, which is a proper subgroup of G;
II. the deformation patterns of the structure on the fundamental equilibrium path will have G group symmetry;
III. the deformation pattern of the structure on a path will preserve its symmetry group until it reaches a bifurcation point;
IV. when bifurcation paths branch from an equilibrium path at a bifurcation point with a single root, the symmetry groups of the structure deformation pattern on the bifurcated paths are subgroups of the symmetry group of the equilibrium path from which the bifurcated path branched off from; and
V. all the single critical points on the path with trivial symmetry group E (the group with only the identity element), in general are stationery points of the loading parameter f.

In the study by Ikeda et al., (1986a) of a hexagonal-sided lattice dome, it was numerically observed that Fujii's theorem (IV) holds for the cases of double roots as well; that is, the symmetry groups of the structure deformation pattern on bifurcation paths are the subgroups of the symmetry group of the main path for both single and double roots.

As we can see from the statements listed above, an important question to answer in the theory of symmetry breaking is the kind of subgroups that can occur when the symmetry of a system is broken. Thus, by using the concept of symmetry breaking and the group-theoretic approach to the analysis of symmetric structures, it is possible to gain insight into the kind of subgroups that will occur when a symmetric structure loses stability by bifurcation (Ikeda et al., 1991). We can now return to the example of the shallow truss dome in Figure *2.12* and provide more explanation on its primary and bifurcated paths shown in Figure *2.13*. On the primary equilibrium path, the deformation pattern of the free nodes of the truss dome shown in Figure *2.12* is C_{6v} symmetric. However, on the bifurcated paths emerging at critical points BP_1, BP_2, and BP_3, the deformation patterns of the truss dome are a subgroup of C_{6v} (Ikeda & Murota, 2010). Thus, at bifurcation, the symmetry of the dome is reduced, or, in other words, the symmetry is broken. Further, observe that at each double critical point, two bifurcation paths emerge. Therefore, by applying the concept

of symmetry breaking, it is possible to have a priori knowledge of the symmetry pattern of a symmetric structure that loses stability by bifurcation. Further, it is also possible to know the symmetry patterns of the dome on the double critical points using the group-theoretic approach, even before detailed numerical computations are carried out. Recall that the group theoretic approach reduces the vector space V of a system into independent subspaces $U^{(i)}$ by using the irreducible matrix representations of a symmetry group for the linear transformations of basis vectors of a vector space V.

Similar applications of the group-theoretic approach have been used in the vibration analysis of symmetric systems to gain insights on the vibration characteristics, such as the number of repeating and distinct frequencies of vibration, and the subspaces (thus eigenmodes) to which these frequencies belong (Zingoni, 1996; Zingoni, 2005b; Zingoni, 2008; Zingoni, 2014; Zingoni, 2018). All this insight is gained even before a full numerical analysis is even carried out.

2.7.2 Bifurcation points

The concept of symmetry breaking is a qualitative approach to the bifurcation of symmetric structures, i.e., at bifurcation, the symmetry of the deformation pattern of the structure on the equilibrium path is broken. Numerically, bifurcation can also be interpreted as an instability induced by a singular tangent-stiffness matrix in the linearized eigenvalue problem of structural systems (Ikeda et al., 1991). The points at which one or more eigenvalues of the stiffness matrix vanish are referred to as singular points or critical points (Ikeda et al., 1991).

Symmetric structures are known to produce several multiple critical points (Thompson & Hunt, 1973; Ikeda & Murota, 1991; Ikeda et al., 1991; Orlando et al., 2013). Multiple critical points can also occur in non-symmetric structures; however, these occur as a coincidence of a pair of simple critical points due to a change of various physical parameters in the system. In symmetric structures, on the other hand, multiple critical points appear generically with the change of one physical parameter (e.g., the loading parameter) (Healey, 1985; Healey, 1988; Ikeda & Murota, 1991; Ikeda et al., 1991). Multiple points that appear in non-symmetric structures are classified as parametric, and those in symmetric structures as group theoretic multiple points (Ikeda et al., 1991).

The explanation for the occurrence of multiple critical points (repeating eigenvalues) in symmetric structures is based on the dimensions of the irreducible representations (Ikeda & Murota, 1991;

Zingoni, 1996; Zingoni, 2005b; Zingoni, 2014; Zingoni, 2018). The group theoretic double points emerge in the subspaces with irreducible representations of two dimensions. This is because the subspaces $U^{(i)}$ with irreducible representations of two dimensions can be split into two independent subspaces $U_1^{(i)}$ and $U_2^{(i)}$ such that these two independent subspaces are spanned by new basis vectors obtained by linearly combining the basis vectors of $U^{(i)}$ in such a way as to form two orthogonal sets. The set of basis vectors for $U_1^{(i)}$ and $U_2^{(i)}$ are identical except for their orientations. The orientation of a set of basis vectors does not affect the physical properties of the subspace, and thus the symmetry of such subspaces is physically indistinguishable. Only one of the two subspaces needs to be considered for computations as they yield identical eigenvalues. Thus, the subspace $U^{(i)}$, has a set of repeating eigenvalues. It is also important to note, however, that simple critical points are also present in symmetric structures, and these are associated with subspaces with irreducible representations of one dimension.

From the foregoing discussion, we can state the following about critical points along an equilibrium path for a system that is equivariant to a symmetry group G (Ikeda et al., 1986b; Ikeda et al., 1991):

- A critical point in a distinct subspace is a simple point;
- a critical point in a repeated subspace is a group-theoretic double point; and
- a critical point in a subspace that reflects the deformation pattern of symmetry group G of the system, is a limit point.

The categorization of a critical point in a subspace as a limit point requires further discussion. First, recall that a point in a system is a critical point if the stiffness matrix of that system for that point is singular. Thus, we can test for the singularity of a point in any subspace by testing the singularity of the diagonalized stiffness matrix for that subspace. Using the example of the symmetrically loaded two-member truss in section *2.3*, we first note that this truss system belongs to the C_{1v} symmetry group. This symmetry group has two irreducible subspaces both of one dimension, that is: a symmetric and antisymmetric subspace. A singularity in the symmetric subspace is a limit point, while a singularity in the antisymmetric subspace is a simple point, which happens to be a bifurcation point in this case. It should also be clear that such a system cannot have a group-theoretic double point.

2.7.3 Studies on influence of symmetry on Stability

Studies on the influence of symmetry on the stability of space frames usually involve some application of group theory. One of the first studies to take advantage of the invariance transformations (reflection and rotation) of an overall coordinate system was by Renton (1964). This study did not address the question of the influence of symmetry on the bifurcation behaviour of symmetric structures; it merely took advantage of the rotational symmetry of the structure in the bifurcation analysis for computational efficiency. Much of the literature on the influence of symmetry on the stability of structures has been carried out on lattice domes.

2.7.3.1 Lattice Domes

As we have already stated, symmetric structures are known to inherently possess double critical points. The tracing of equilibrium paths at double critical points is challenging because of numerical ill-conditioning. Healey (1985, 1988) applied the group-theoretic approach to study the bifurcation behaviour of a hexagonal lattice dome. The geometry of this structure belongs to the C_{6v} symmetry group. In this study, the equilibrium paths were traced from the subspaces obtained by applying the irreducible matrix representations of C_{6v} to the geometry and loading of the lattice dome. The resulting subspaces had smaller dimensions than the full vector space of the problem. For each separate subspace, the equilibrium path was traced, and the critical points in each were separately determined. The principle of stationery potential energy was used to derive the equilibrium equations for this problem and the equilibrium paths traced via the reduced Euler-Newton algorithm. By using the group-theoretic approach, the ill-conditioning due to symmetry breaking bifurcation points was avoided, as they were in separate subspaces. Further, accidental branch switching was avoided as the bifurcated paths were in independent subspaces.

Other researchers used the conventional *FEM* displacement analysis technique to trace equilibrium paths, which are shown in Figure *2.13* (Hangai & Kawamata, 1972; Lee & Han, 2012). Others applied the conventional equilibrium tracing approach and then qualitatively explained the bifurcation behaviour using a hierarchy of bifurcations. Through the results of group-theoretic bifurcation theory and heuristic case studies, a framework was designed to describe the bifurcation hierarchy of symmetric structural systems equivariant to the C_{nv} and Cyclic C_n groups (Ikeda et al., 1986b; Ikeda et al., 1986a; Ikeda & Torii, 1987a; Ikeda & Torii, 1987b; Ikeda et al., 1991).

In order to use the hierarchical approach to explain bifurcation behaviour, the hierarchy of successive bifurcations must be described in terms of the symmetry group and its subgroups (Ikeda et al., 1986a; Ikeda & Murota, 1991). We shall use the example of a triangular truss dome (see Figure below *2.15*) that is equivariant to the C_{3v} symmetric group.

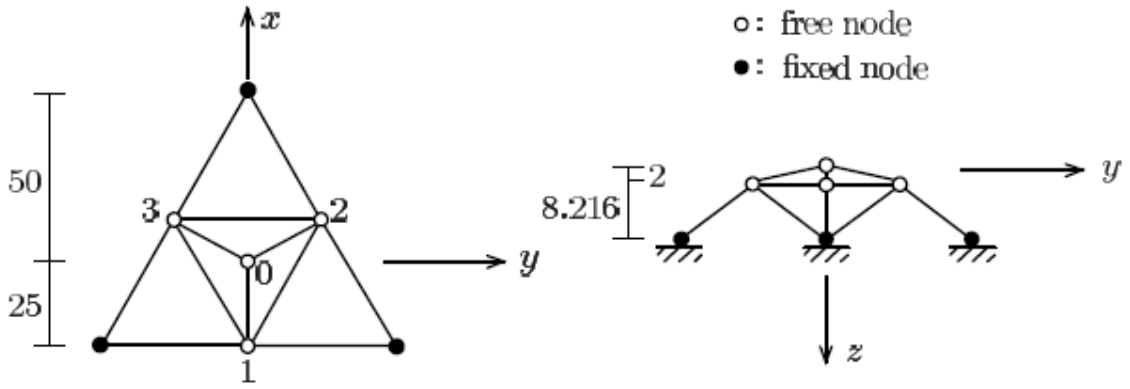

Figure 2.15: Regular-triangular truss dome (C_{3v}-symmteric)

Source: (Ikeda et al., 1991)

The deformation patterns of this triangular truss dome as it successively bifurcates will be invariant to the C_{3v} symmetry group and its subgroups, and these are:

$$C_3 = \{e, C_3, C_3^{-1}\}, C_{1v}^1 = \{e, \sigma_1\}, C_{1v}^2 = \{e, \sigma_2\}, C_{1v}^3 = \{e, \sigma_3\}, C_1 = \{e\}$$

The symmetry operations are as previously defined for the C_{nv} symmetry group.

The deformation patterns of this dome are labelled by C_{3v} on the fundamental equilibrium path and by its subgroups after bifurcation, and these are shown in Figure *2.16* below. The plane views of the deformation patterns presented in Figure *2.15* are for free nodes *1*, *2,* and *3* of the truss dome expressed as subgroups of C_{3v}: C_{3v} for a uniform expansion or shrinking of the regular triangle, accompanied by a uniform float or drop; C_3 for a rotated regular-triangular pattern indicating a rotation about the *z*-axis, along with a uniform expansion or shrinking and a uniform float or drop; C_{1v}^k *(k=1,2,3)* for isosceles-triangular patterns with a reflection symmetry; and C_1 for an asymmetric scalene-triangular pattern.

We can now present the hierarchy of bifurcation of the triangular truss dome, as shown below in Figure *2.17,* with *n=3*. This truss deforms with a deformation pattern symmetric to C_{3v} on the fundamental equilibrium path, and upon bifurcation, the deformation patterns will be symmetric

to subgroups of C_{3v} as they have a lower order of symmetry. This process of successive bifurcations continues until the truss becomes completely asymmetric, that is:

$$C_{3v} \rightarrow C_{1v}^{k} \dashrightarrow C_1 \text{ or } C_{3v} \dashrightarrow C_3 \rightarrow C_1 .$$

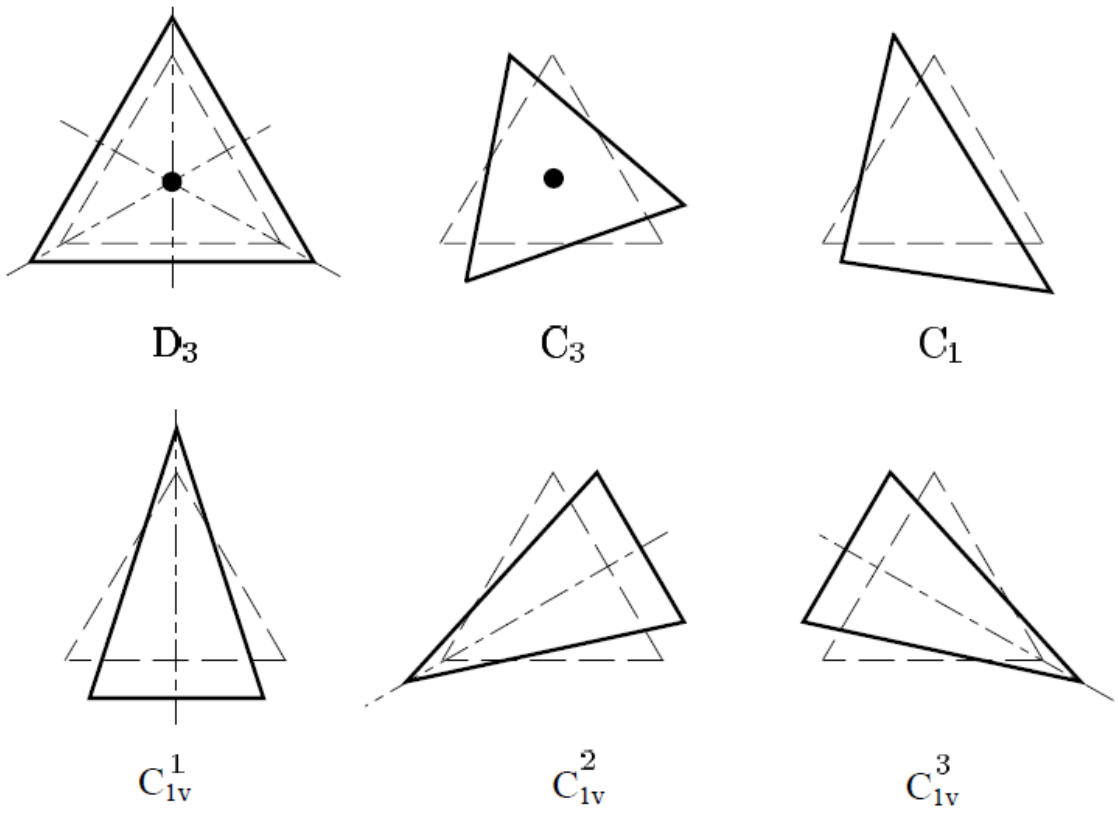

Figure 2.16: Plane views of the deformation patterns of the regular-triangular free nodes of the regular-triangular truss dome

Source: (Ikeda et al., 1991)

The solid arrows in Figure *2.17* indicate that during the bifurcation process, the solid arrows can be bypassed but not the dotted arrows. Thus, the dashed arrow in Figure 2.16 below, indicates that a C_1 cannot directly emanate from a C_{3v} path, but the C_{1v}^{k} symmetric path can. This point becomes much clearer when we consider the bifurcation pattern of a truss dome equivariant to the C_{4v} symmetry group, as shown in Figure *2.17* below. The bifurcation process, $C_{4v} \rightarrow C_{2v} \rightarrow C_{1v}^{1}$, made of only solid arrows, indicates that a C_{1v}^{1} symmetric path can directly branch from a C_{4v} symmetric path. On the other hand, $C_{4v} \dashrightarrow C_4 \rightarrow C_2$, indicates that a C_4 symmetric path can directly branch

from a C_{4v} symmetric path, while a C_2 symmetric path cannot. The C_{4v} symmetric group is the symmetry group for a regular four-sided polygon with four reflection symmetries and four rotational symmetries. The subgroups of C_{4v} are:

- C_4, with four rotational symmetries of a four-sided polygon;
- C^k_{2v} (k=1, 2), with one rotational symmetry and two reflection symmetries for a four-sided polygon; and
- C^k_{1v} (k=1, 2, 3, 4), with one reflection symmetry for a four-sided polygon.

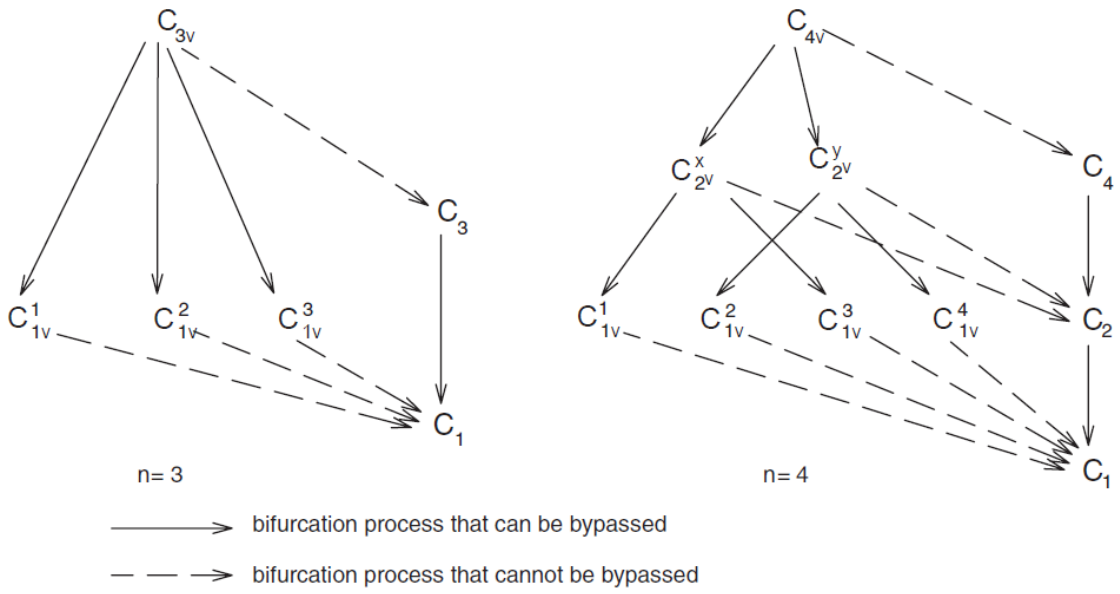

Figure 2.17: Bifurcation hierarchy of truss Dome equivariant to C_{nv}

Source: (Ikeda et al., 1991)

We have described how symmetry breaking bifurcation behaviour can be explained in terms of a hierarchy of possible subgroups of an equivariant system to a symmetry group. It should be noted that any bifurcation path with a deformation pattern symmetric to a particular subgroup is potentially reachable, and its existence in a particular bifurcation problem depends on the numerical properties of the problem in question. A review of literature shows no studies on how numerical properties of a problem can be used to predict the symmetry subgroup that exists in a particular bifurcation behaviour.

The group-theoretic approach to symmetry breaking bifurcation has also been used to predict the number of bifurcation paths that emanate at a critical point and the symmetry of such paths. For structures equivariant to the C_{nv} symmetry group, the number of paths emanating at a critical point is twice the group index (n/m), where n and m represent the number of symmetry elements in a group and its subgroup, respectively (Ikeda & Torii, 1987b; Ikeda et al., 1991). It has also been observed that the symmetry of the bifurcated path depends on whether the index is odd or even. When the index is equal to two, the critical point is a simple point, and the bifurcated path is symmetric. When the index is greater than two and even, then the critical point is a double critical point, and the bifurcation path is symmetric. In instances where the index is greater than two and odd, the critical point is a double point, and the bifurcated path is asymmetric (Ikeda et al., 1991). We shall again use the triangular truss dome example to explain how these concepts can be used to predict the bifurcation behaviour of a system equivariant to the dihedral group. Ikeda and Murota (1991) used the conventional finite element displacement analysis technique to trace the equilibrium paths of this truss, and the equilibrium paths are shown in Figure *2.18* below. Figure *2.18 (a)* shows the space views of the relationship between the loading parameter *f* and the *X*-and *Y*-directional displacements of the centre node *0*. Figure *2.18 (b)* displays the relationship *f* and the vertical displacement of node *0*. From Figures *2.18* (b) and *2.13*, notice that the bifurcation paths are unstable, while the primary equilibrium path displays a loss of stability by snapping. Such stability behaviour is characteristic of shallow truss domes.

Returning to Figure *2.18 (a)*, at point *a* of the equilibrium path, there is an asymmetric double point with six paths since the index is three and odd. As shown in Chapter 4 of this study, the C_{1v} symmetry group emerges from a subspace with two repeating critical points. It is also shown in Chapter 4 of this study, how this subspace can be split into two identical subspaces. Thus, for each of the two identical subspaces, three bifurcation paths can emerge. Also, by analysis of the symmetry of the eigenvectors of the subspace symmetric to C^k_{1v} (k=1, 2, 3), it can be shown that the deformation modes of paths P_1, P_3, and P_5; and P_2, P_4, P_6 are respectively rotationally symmetric (Ikeda et al., 1991). Thus, only paths P_1 and P_4 are required to be traced, as shown in Figure *2.18 (b)*. On the bifurcated path P_1, the critical point will be simple, as the index is equal to 2. Recall that the C^k_{1v} subgroup has two symmetry elements and the C_1 subgroup has one symmetry element. Lastly, we can observe that the complex bifurcation path shown in Figure *2.18 (b)* can be qualitatively explained by the symmetry breaking bifurcation shown in Figure *2.17.*

Similar observations can be made for the bifurcation paths shown in Figure *2.13* for the truss dome in Figure *2.12*. For the C_{3v} path, the group index is *2*, and the bifurcation point is simple. For the C_{1v} and C_{2v} paths, the group index is *2* and *4,* respectively. The bifurcation points from which each path emanates are both double critical points.

From the foregoing discussion, the bifurcation phenomena of structures belonging to the C_{nv} point group can be systematically analysed even before they are analysed using computer software packages for structural analysis. This could then be used as an aid in the verification and validation of the results obtained from software packages.

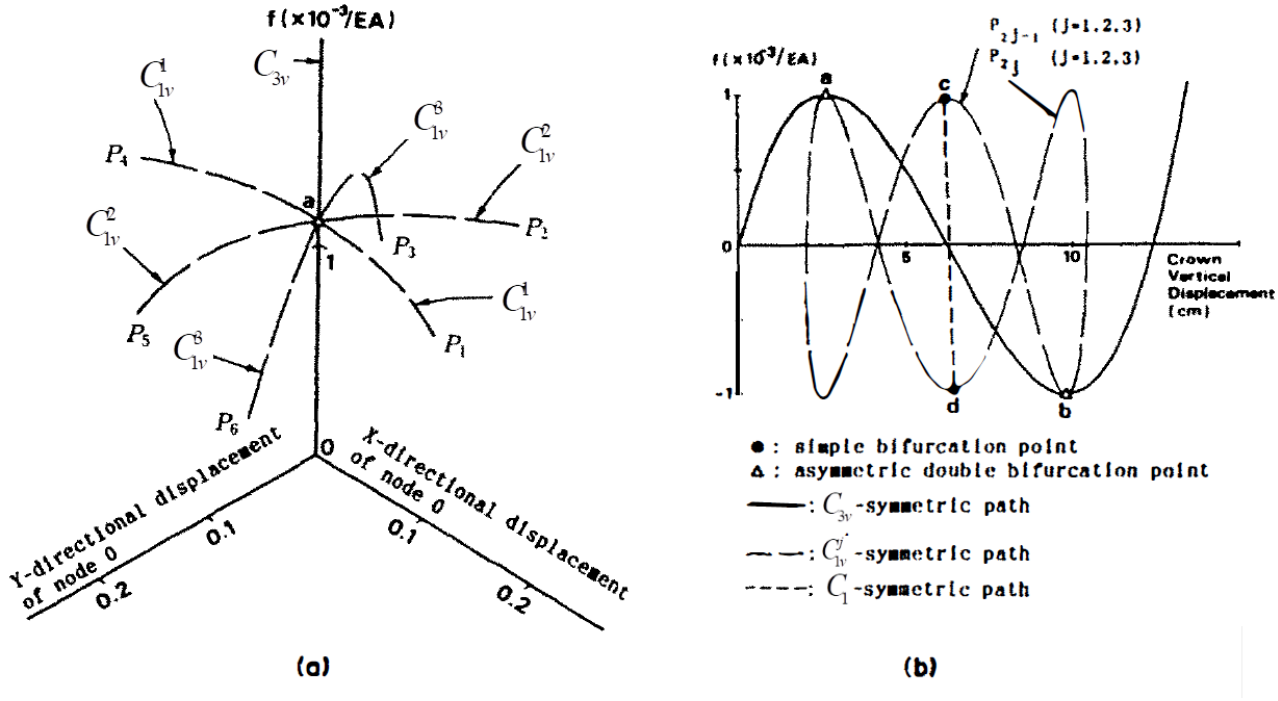

Figure 2.18: Equilibrium paths of a D_3 equivariant truss dome, (a) space views (b) plane views

Source: (Ikeda et al., 1991)

The group-theoretic approach just described has also been used to study the bifurcation behaviour of prestressed truss structures (Chen & Feng, 2015). Chen and Feng (2015) studied the buckling behaviour of the following prestressed trusses: plane trusses equivariant to C_{1v} symmetry; a Geiger dome equivariant to the C_{12v} symmetry group; and a suspension dome equivariant to the C_{24v} symmetry group. In this study, the buckling analysis was carried out using the group-theoretic approach, which was implemented using the software package *Matlab,* and the conventional buckling analysis was carried out using *Matlab* and the software package *Abaqus*. It was found

that the group-theoretic approach was computationally less costly than the conventional approach, either using *Matlab* or *Abaqus*. Further, Chen & Feng (2015) were able to accurately predict the number of distinct and repeating eigenvalues using the group theoretic approach even before using either *Matlab* or *Abaqus* for the buckling analysis. The study also investigated the effect of the ratio of height to span (*h/L*) of the domes on the stability behaviour of the C_{24v} symmetric suspension-dome. It was observed that the lower the *h/L* ratio, the lower the buckling capacity of the dome. In particular, it was observed that with small values *(0.06)* of the *h/L* ratio, the first buckling modes were low and close to each other (see Figure *2.19* below). Pecknold et al. (1985) also varied the *h/L* ratio to change the location of the bifurcation point on the load displacement curve of a two-member truss. The study by Chen and Feng (2015) did not report on which subspaces these buckling modes belonged to; this would be useful information for developing a framework to use to predict which subgroups exist in a particular stability problem.

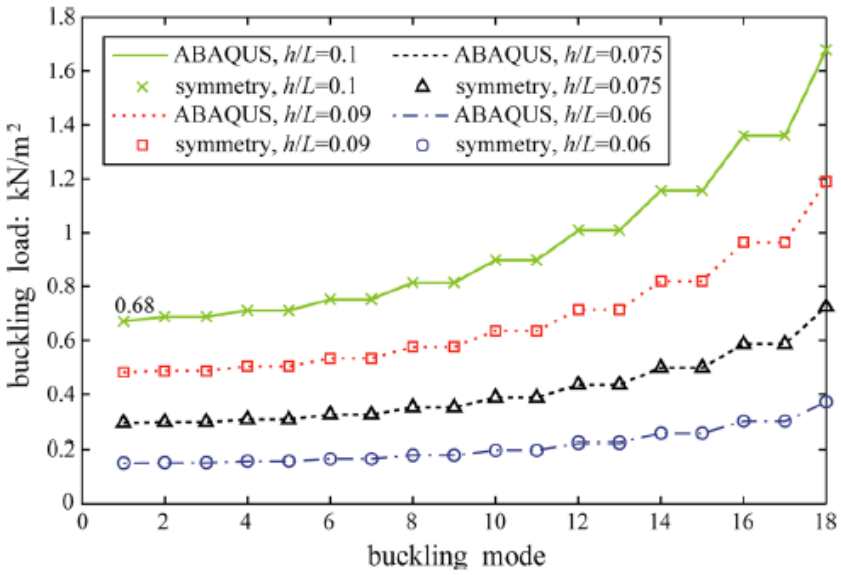

Figure 2.19:The first 18 buckling loads of the symmetric suspension-domes with different rise-span ratios
Source: (Chen & Feng, 2015)

2.7.3.2 Two-Dimensional Moment Frames

Research on the influence of symmetry on plane frames appears to be very limited. Perhaps this is because the order of symmetry that a practical plane frame can have is usually only one plane of reflection symmetry. Furthermore, space frames have traditionally been designed as plane frames, and engineers have designed such structures as separate plane frames in orthogonal directions,

ignoring the three-dimensional nature of the structure (Zalka, 2002). And when approached from this perspective, the only level of symmetry that can be addressed belongs to the C_{1v} point group symmetry, which is the symmetry group that describes the symmetry of any physical configuration with one plane of reflection symmetry. For such frames that are unbraced, the first property of instability behaviour at bifurcation that can be noted is that the bifurcation mode is either symmetric or antisymmetric (Bleich, 1952; Douglas, 1964). And indeed, this fact also follows from group representation theory: the C_{1v} symmetry group has only two subspaces, that is, a symmetric and an antisymmetric subspace (Zingoni, 2015). Since bifurcation of symmetric structures is achieved by symmetry breaking, the bifurcation mode has to be the sway antisymmetric mode. On the other hand, the symmetric buckling mode is due to limit point instability and not bifurcation instability.

The loss of stability in plane frames by bifurcation is associated with a plane frame where the vertical loads have been applied at the column joints. However, Chwalla (1938), analytically demonstrated that a plane frame with symmetric transverse beam loading will experience a loss of elastic stability through bifurcation. This was demonstrated by employing the classical approach of integrating the differential equations, which define the equilibrium of the buckled state of all the members in the frame. The resulting solution showed the existence of a bifurcation point on the load displacement curve. Further, Chwalla (1938), found that the buckling load of such frames is lower than that of equivalent frames with a statically equivalent vertical loading applied at the joints (see Figure 2.20 below).

The results of a numerical study by Lu (1963) found that the critical load for the symmetric buckling mode with initial bending moments was as much as 17% lower than that for a symmetrical frame with no initial moments but with an equivalent vertical loading, as shown in Figure 2.20 (a) and (b) below.

On the other hand, for the antisymmetric sway bucking mode, the results of a numerical study by Lu (1963) found that for frames with beam to column length ratios of less than three, the buckling mode for a frame with pre-buckling moments did not exceed about 10% of that of a frame with no initial moments.

Douglas (1964) also found that for the sway buckling mode, the buckling mode of a frame with pre-buckling moments was not significantly lower than that without pre-buckling moments.

In conclusion, for an unrestrained symmetric plane frame, the antisymmetric sway buckling mode will always be lower than the symmetric buckling mode.

However, this reduction in the buckling load was found not to be significant (Chwalla, 1938; Masur et al., 1962; Le-Wu, 1963; Douglas, 1964). The only exception to this result is the case of frames with very long beams in comparison to the columns. In such cases, the presence of initial moments significantly reduces the elastic buckling load for the symmetric buckling mode (Masur et al., 1962).

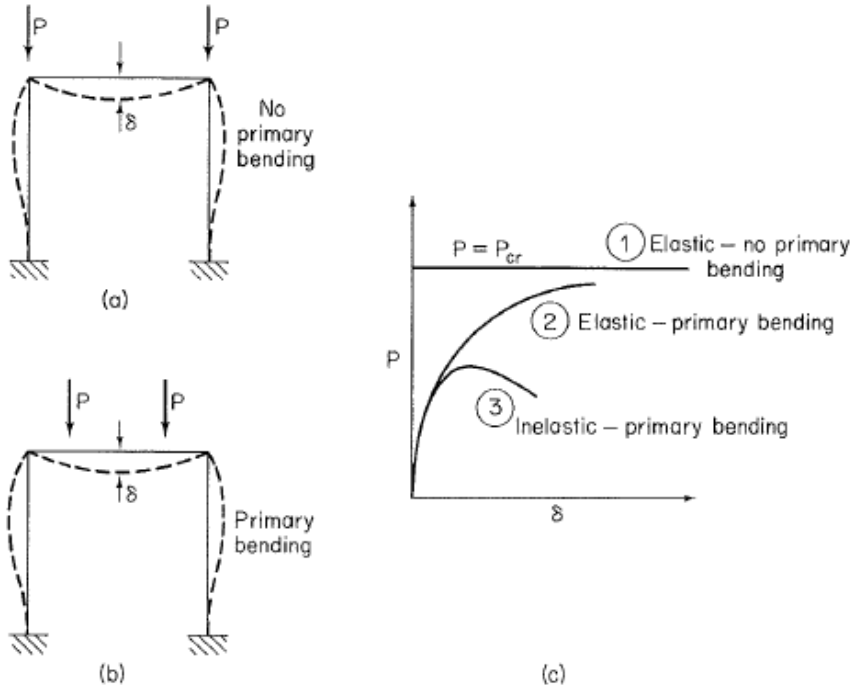

Figure 2.20:Stability Behaviour symmetric plane frame

Source:(Douglas, 1964)

The provision of support conditions limits the types of symmetrical configurations that can be studied in plane frames. If, however, support conditions are ignored then frames of several regular polygon shapes can be studied. For example, Timošenko and Gere, (1963) presented the case of a rectangular frame symmetrical about the vertical and horizontal reflection planes (see Figure 2.21 below). It is easy to see that the symmetrical mode will have the lowest buckling mode in this case, since every member in the symmetrical mode (Figure *2.21 a*) is in the condition of a column with pinned ends.

Mises and Ratzersdorfer (1926) studied the buckling behaviour of regular *n*-sided polygons (see Figure *2.22* below) with symmetric loading. They found that the critical force in the members is given by (Timošenko & Gere, 1963):

$$\text{For } n>3 \qquad P_{cr}=\left(\frac{4\pi}{n}\right)^2\frac{EI}{l^2} \qquad 2.12\text{ a}$$

$$\text{For } n=3 \qquad P_{cr}=(1.23\pi)^2\frac{EI}{l^2} \qquad 2.12\text{ b}$$

The study did not report on the symmetry of eigenmode for the eigenvalues predicted by equation 2.12.

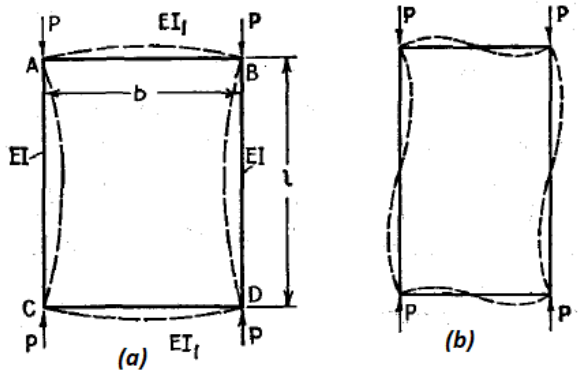

Figure 2.21: Rectangular plane frame

Source: (Timošenko & Gere, 1963)

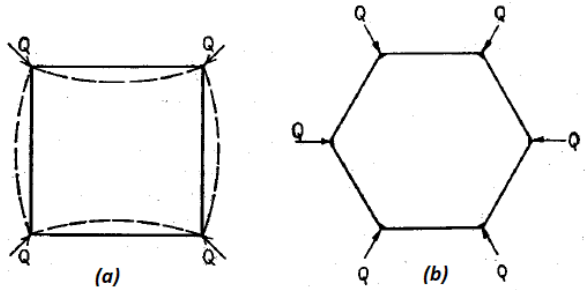

Figure 2.22: Plane frames examples for regular sided polygons

Source:(Timošenko & Gere, 1963)

2.7.3.3 Space Frames

From the few studies that have addressed the bifurcation behaviour of space frames, the bifurcation behaviour of space frames is characterised by three types of buckling modes: Sway buckling;

torsional buckling; and combined sway-torsional buckling (LeRoy, 1961; Shosuke, 1970). LeRoy (1961) studied the buckling of a frame with an equilateral triangular plan (see Figure *2.23* below) numerically and experimentally, and the numerical results matched the experimental results. For the case in which the loading was asymmetric ($\alpha_1=\alpha_2=1/3\alpha_3$) the buckling mode was found to be the torsional mode (see Figure below *2.24 a*), in which the frame rotates about the centre of gravity of the triangle. The triangular frame studied by LeRoy (1961) and Shosuke (1970) was symmetric in stiffness and for case where the loading was symmetric ($\alpha_1=\alpha_2=\alpha_3$) three buckling modes were considered: two equal sway modes about either axis of symmetry of the triangular plan and a twisting mode about the centroid of the plan (see Figure *2.24 a, b, c*). In this study, the sway buckling mode was found to have the lowest buckling load, and this result was also experimentally verified by LeRoy (1961). Shosuke (1970), however, reports that the graph for the determinantal criterion shows that the determinant does not become negative past the sway mode. Another method for determining the buckling load was employed by Shosuke (1970). In this method, referred to as the method of excitation, a vertical load *P* below the buckling load was first applied, and the reduced member stiffness was computed. Small disturbances that excite a particular buckling mode were then introduced, and the corresponding displacements were computed using the computed reduced stiffness. Following this approach, the value obtained for the twisting buckling load was found to be the same as that using the determinantal criterion. Shosuke (1970) did not report on whether the method of excitation was able to confirm the result of the determinantal method for the sway mode buckling load.

Citipitioglu (1965), on the other hand, found that the determinantal criterion for buckling converged for symmetric space frames with symmetrical vertical loading with no pre-buckling moments. However, in the case where the pre-buckling moments were present, the iterative method used to determine the buckling load failed to converge in the case of symmetrical loading. It should be noted that this study was not clear on whether the symmetrical space frame with pre-buckling moments studied was either rectangular or square in plan.

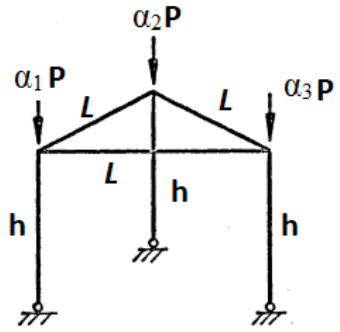

Figure 2.23: Space frame C_{3v} symmetry group

Source:(Shosuke, 1970)

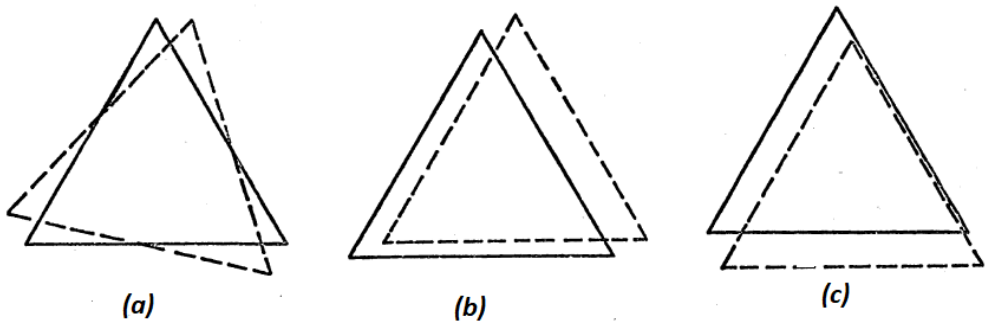

Figure 2.24: Buckling modes of Space frame C_{3v} symmetry group (a) Twisting mode, (b) and (c) sway mode

Source:(Shosuke, 1970)

Aristizábal-Ochoa (1997), (2002), and (2003) studied the influence of symmetry on the stability of three-dimensional frames that are rectangular and triangular in plan (Figure 2.26 and Figure 2.27). This means that the symmetry groups that were being investigated were the C_{2v} group and C_{3v} symmetry groups.

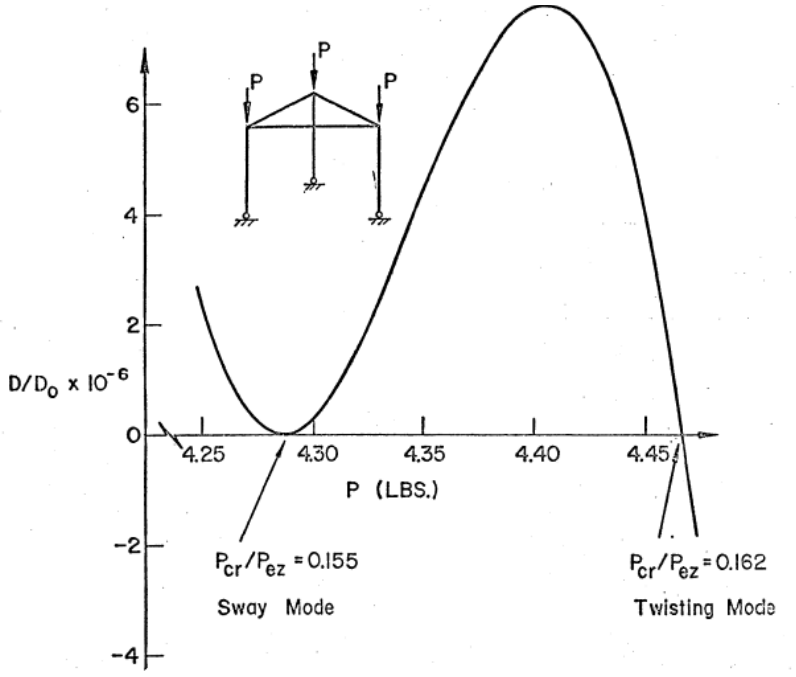

Figure 2.25: Buckling for a space frame with C_{3v} symmetry

Source:(Shosuke, 1970)

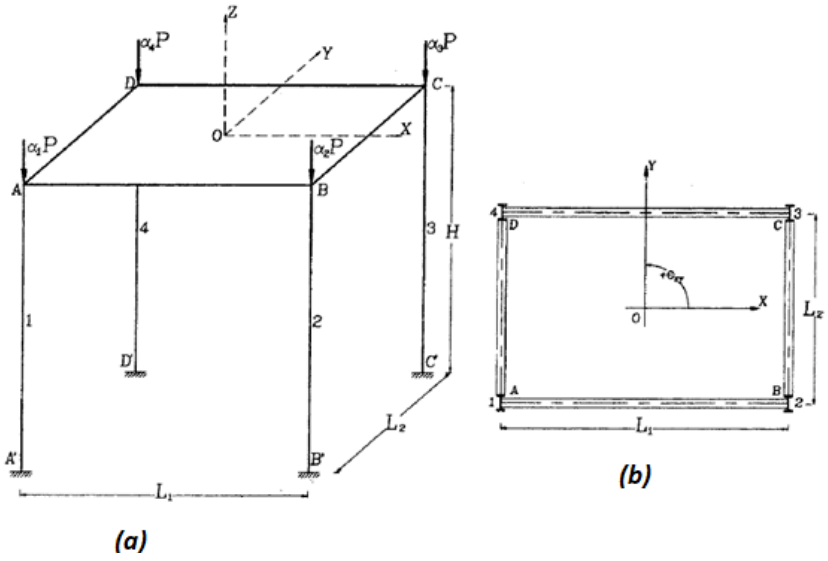

Figure 2.26:Simple space frame and column layout

Source: Aristizábal-Ochoa 2003

In the studies by Aristizábal-Ochoa (1997), (2002), and (2003), the following types of buckling modes were considered for sidesway and twist uninhibited or partially inhibited three dimensional frames in which column sections lie in the *XY* plane (Figure 2.27):

1. Overall sidesway buckling that occurs when the whole story moves along a line on the *XY* plane;
2. overall sidesway-twist buckling that occurs with sway along the *XY* plane and twist about the *Z*-axis; and
3. pure overall twist buckling about the *Z*-axis.

Individual flexural buckling of columns was also considered; however, individual torsional buckling of columns was not considered.

Aristizábal-Ochoa (2003) found that the maximum buckling load for an unrestrained three-dimensional frame was obtained for a system that was symmetric both in geometry and loading, with the columns oriented in such a manner that their minor axis was tangent to a circumscribed circle of a triangle or rectangle (Figure *2.27 a*). This happens to be the system that offers the minimum sidesway-twist coupling and maximum sidesway stiffness (Aristizábal-Ochoa, 2003). Incidentally, these are the configurations for which all the elements of the C_{3v} and C_{2v} symmetry groups apply to the triangular and rectangular column arrangements, respectively. If the column and load arrangement were symmetrical and the columns were oriented in such a manner that the major axis of the sections was tangent to the circumscribed circle, the maximum bucking load was significantly reduced when compared to the preceding case.

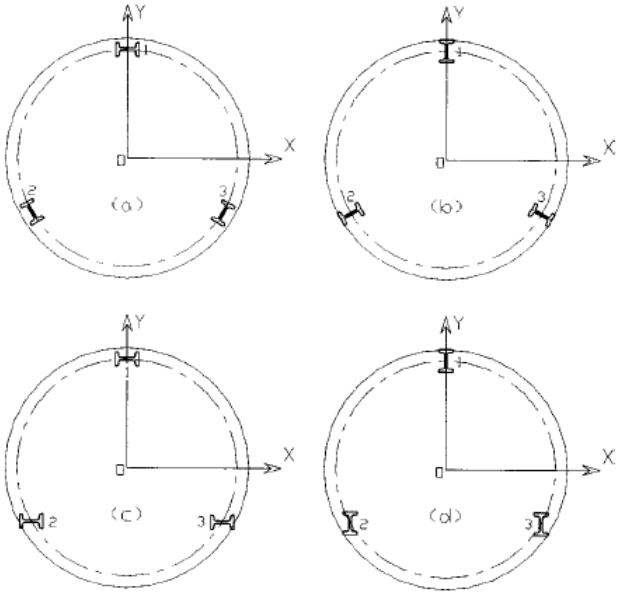

Figure 2.27:Column orientations of triangular column layout

Source: Aristizábal-Ochoa 2003

With this type of arrangement (Figure 2.27 *b*), in which the columns are oriented in a cruciform arrangement, the column system failed due to overall twist instability (Aristizábal-Ochoa, 2003). This column arrangement also corresponds to the configurations for which all the symmetry operations of the C_{2v} and C_{3v} symmetry groups apply.

Further, it was found that the total critical load of a symmetrical frame with optimum column orientation was reduced significantly by either asymmetry in the load distribution among the columns or asymmetry in the column layout. This is because the asymmetry of the frame induces the sidesway-twist buckling mode, whose critical load is always below the pure sidesway buckling load (Aristizabal, 1997). Unsymmetrical space frames always buckle in a sidesway-twist mode, since the stability behaviour of an asymmetrical space frame is similar to that of a three-dimensional single column in which its shear centre and centroid do not coincide (Aristizabal, 1997). It should be noted here that overall twist instability or global torsional failure of structures has received little attention in university textbooks and in national and international codes of practice, despite the emergence of computer-aided structural analysis (Zalka, 2012).

In summary, from the foregoing discussion, the buckling of a totally symmetrical three-dimensional framed structure with sidesway has three buckling modes with sidesway that are uncoupled. These buckling modes include: buckling along the *X* and *Y* axes and overall twist around the *Z* axis. The governing buckling mode with the lowest critical load will depend on the sizes, heights, end restraints, plan layout, and load distribution of the columns (Aristizábal-Ochoa, 2002). This is the same behaviour exhibited in the buckling of columns with doubly symmetric cross-sections (Chajes, 1974).

When the column and load distribution are only symmetric about one axis, say the *X*-axis, then the flexural buckling mode with sidesway along the *Y* axis and the torsional one about the vertical *Z* axis become coupled. This leads to combined torsional-flexural buckling in a single symmetrical space frame under symmetrical loads about the same axes. Thus, a space frame that is symmetric in column layout and loads about one axis, may buckle with sidesway by bending along the axis of symmetry or by a combination of twisting around the *Z* axis and bending along the axis perpendicular to the axis of symmetry (Aristizábal-Ochoa, 2002). This is also the buckling behaviour exhibited by columns with singly symmetric cross-sections (Chajes, 1974).

Finally, if the three-dimensional frame structure does not possess any symmetry in loading and column layout, then the system will always buckle in sidesway-twist mode. A column with an asymmetric cross-section also behaves the same way (Chajes, 1974).

We must note that the studies by Aristizábal-Ochoa (1997), (2002), (2003) did not systematically address the influence of symmetry from a group-theoretic approach, in conjunction with the fact that loss of stability by bifurcation is essentially caused by symmetry breaking in symmetric structures. This meant that there was some limitation in terms of the conclusion that the researcher was able to draw from the sizeable numerical results generated in the study. The group theory approach has been very useful in explaining the bifurcation behaviour of lattice structures. Third, the model for frames did not include the effect of the stiffness of the beams, and it was assumed that the frame consisted of rigid flat floors with no beams, providing pin supports at top of the columns and fixed supports at the base. Lastly, only doubly symmetric sections were studied, and the effect of the warping stiffness of the columns was ignored. However, some studies have shown that the effects of the warping stiffness of the beams and columns have little effect on the stability analysis of three-dimensional frames (Aristizábal-Ochoa, 2002).

Space frames constructed as shallow domes are known to display snapping behaviour bifurcation similar to that of shallow space trusses. One such space frame (Figure 2.28) has been studied by several researchers (Papadrakakis & Ghionis, 1986; Shi & Atluri, 1988; Aslam & Reza, 1991; Lee & Han, 2012). The equilibrium path has been investigated by all researchers cited, however, only Lee and Han (2012) have investigated the first two bifurcation paths. These paths were traced using a method for large deformation analysis of the space frame based on a Eulerian formulation, taking into account the effects of large joint rotations with finite rotations. A path switching algorithm based on the non-negative eigenvalue and its corresponding eigenvector was used to trace the bifurcated paths (Lee & Han, 2012). As can be seen from Figure *2.29,* the space frame dome displays snapping behaviour just as in the case of shallow space truss domes. However, the bifurcated paths are not initially unstable, as in the case of shallow space truss domes (Figure 2.13). It was difficult to determine the symmetry of eigenmodes for the bifurcated paths from the sketches presented by Lee and Han (2012). However, the deformation pattern of the space dome on the primary path was C_{6v}.

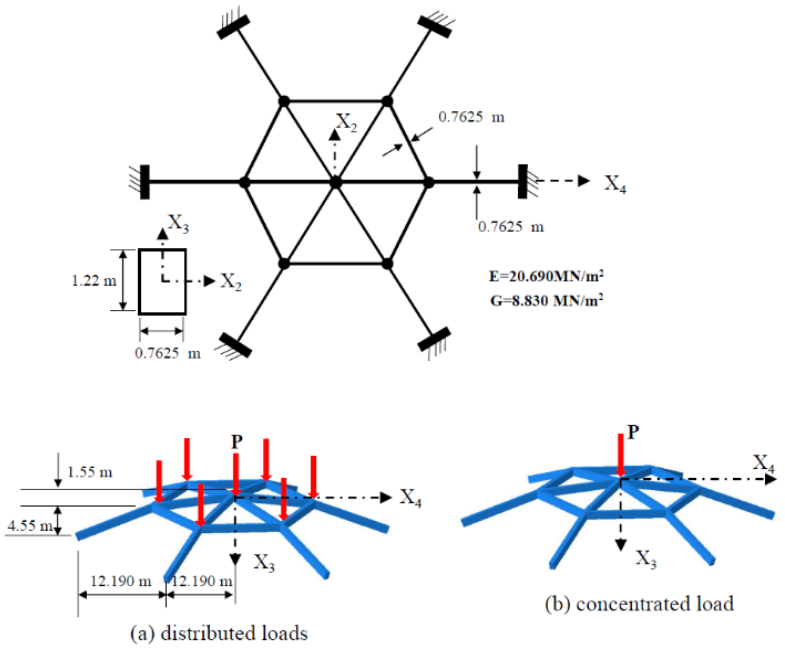

Figure 2.28: Space frame dome

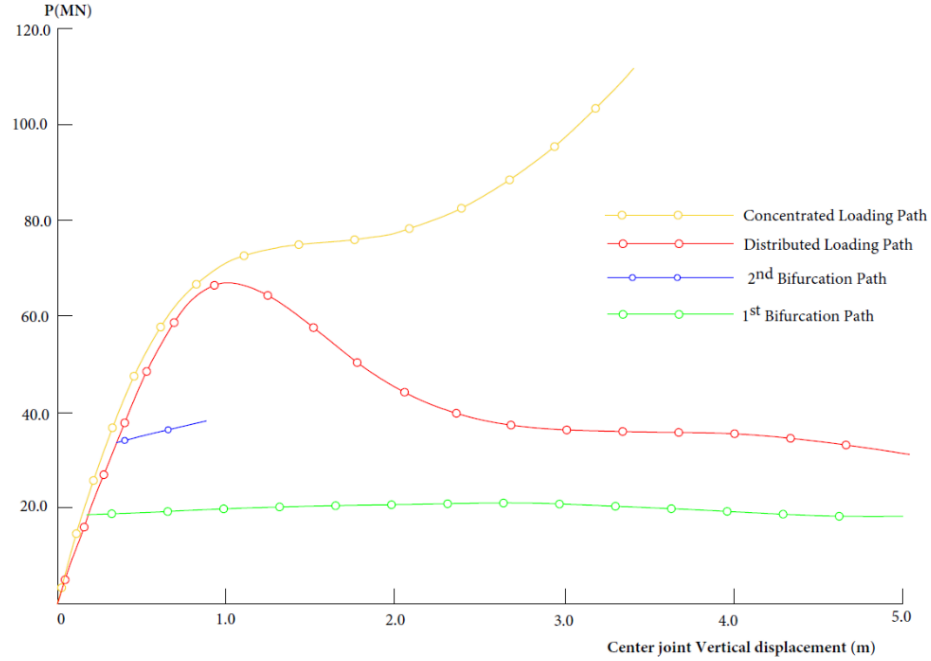

Figure 2.29: Space frame dome equilibrium and bifurcation paths

It should be noted that the studies discussed above did not investigate exactly how the buckling load would change with the variation of other factors, such as the ratio of stiffnesses of columns and beams. Further, these studies did not investigate the types of symmetries in the deformation

patterns of the structure on the bifurcated paths. In addition, all but one of the studies did not investigate the nature of the post-buckling paths. As has been earlier stated, a review of the literature seems to indicate that no other studies have been carried out on the stability behaviour of frames of other symmetry groups in the dihedral symmetry group. This is quite different for lattice domes, where the study of the bifurcation behaviour of domes belonging to several groups of the C_{nv} symmetry group has been quite extensive.

2.8. Rationale

Symmetry is known to generate complex bifurcation behaviour in symmetric structures, as we have previously discussed. The complex bifurcation behaviour of lattice domes symmetric to the C_{nv} symmetry group, has been explained using the group-theoretic approach. The basic idea is that at the onset of bifurcation on an equilibrium path, the symmetry of the deformation pattern is reduced. On each successive bifurcated path, the symmetry of the deformation pattern is further reduced until a path with an asymmetric deformation pattern is reached. This recursive bifurcation is associated with a hierarchy of subgroups. This framework provides a tool for engineers to have a priori knowledge of the bifurcation behaviour of a lattice dome equivariant to a particular symmetry group of C_{nv}. We would expect that space frames that are C_{nv} equivariant to have bifurcation behaviour similar to that of lattice domes that are C_{nv} equivariant. However, we should note that the hierarchy of bifurcations that has been developed for lattice domes is based on all the subgroups of C_{nv}. This is possible since the deformations considered were elongations, contractions, and member rotations. There is no curvature considered in the members since the members of the lattice domes were modelled as truss members. In the case of C_{nv} symmetric space frames the members are beams and thus have curvature, and because of this it is not clear that all subgroups of the C_{nv} symmetry group are applicable, as is the case with lattice domes. Thus, the aim of this study was to determine the possible symmetries in the bifurcation of C_{nv} symmetric plane and space frames of the type shown in Figures *1.1* and *1.2*.

A survey of the literature also found no studies where the hierarchy of bifurcation approach has been used to explain the bifurcation behaviour of structures with D_{nh} symmetric configurations, either in the case of space frames or lattice domes. Thus, another aim of this study was to determine the possible symmetry produced in the bifurcation behaviour of D_{nh} symmetric space frames of the type shown in Figure *1.3*.

The group theoretic approach has been successively used in the bifurcation analysis of lattice domes and shells. With this approach, the numerical problems of ill conditioning associated with bifurcation problems in highly symmetric structures can be avoided. This has been successively implemented in the case of lattice domes. A survey of literature found no existing studies on the use of the group theoretic approach based on the slope deflection method to the buckling analysis of space frames symmetric either to the C_{nv} or D_{nh} symmetry groups as shown in Figure *1.1, 1.2* and *1.3*. Application of the group theoretic approach to the buckling analysis of frames would be computationally cost effective especially for large problems. Thus, this study sought to develop a group theoretic approach for the buckling analysis of plane frames by using a symmetry adapted slope deflection method.

Studies have been carried out on the bifurcation behaviour of lattice domes that are symmetric with respect to the geometry, loading, stiffness, and support conditions. A review of literature shows no systematic studies on either lattice or space frames where the geometry of a structure is symmetric to a particular symmetry group but either the stiffness or loading have a lower order of symmetry. This study sought to determine the bifurcation behaviour of space frames which are symmetric to the C_{nv} and D_{nh} groups in terms of geometry, loading, and support conditions but with a lower order of symmetry in terms of stiffness or loading.

2.9 Research Questions

In order to provide usable information for the analysis of the stability behaviour of space frames, the following are the research questions that this study sought to answer:

I. How can the group theoretic approach be utilised to determine the buckling load of symmetric frames?
II. How can group theory be applied to gain a priori knowledge on the bifurcation behaviour of symmetric frames?
III. What is the nature of the primary and bifurcated equilibrium paths of D_{nh} Space frames?

2.10 Objectives

The main objective of this study was to investigate the influence of symmetry on the global stability behaviour of space frames under static loading.

Chapter 3

3. Methodology

3.1 Introduction

In order to study the bifurcation behaviour of C_{nv} and D_{nh} symmetric space frames, group theory was used to identify the possible subgroups that appear in symmetries of the eigenmodes from a buckling analysis. The deformation patterns of beam members were used to identify the potential subgroups for C_{nv} symmetric plane frames.

Group-theoretic formulations of the matrix stiffness approach, and the slope deflection method (*SDM*) was developed and used to determine the buckling loads of C_{nv} plane frames. The group theoretic *SDM* was used to obtain analytical results that were used to validate the *FEM* created using Abaqus. The developed group theoretic *SDM* was also used to gain insights on the number of distinct and repeating eigenvalues in each subspace for each geometric configuration of the plane frames considered in this study.

FEM's created using Abaqus were used to determine the eigen loads and eigenmodes using a linear eigenvalue analysis. The nature of the primary equilibrium path and bifurcated paths for D_{nh} space frames was investigated using the Riks method in Abaqus. The primary equilibrium path can be traced using the Riks method, even in cases that involve snapping. However, in order to trace the bifurcated paths, imperfections consisting of superimposed buckling modes produced from a linear eigenvalue analysis must be introduced in the geometry of the *FEM* model. This is because the Riks method by itself cannot trace paths that bifurcate off the primary path. The load excitation method explained in *2.7.3.3* can also be used to trace the bifurcated paths using the Riks method. This is especially useful in symmetric structures where the bifurcation is a symmetry breaking bifurcation.

3.2 Group-theoretic buckling analysis of plane frames

In this section, a method for the group-theoretic eigenvalue buckling analysis of plane frames of C_{nv} symmetry was proposed. This group-theoretic approach is based on the matrix stiffness method. The frames are subjected to point loads at the joints of the frame, and compression forces are induced in some members.

As was discussed in Chapter two of this research, many researchers have applied the group theoretic approach to bifurcation and vibration problems in lattice domes and shells. At the time of writing this proposed group-theoretic buckling analysis of plane frames, a survey of the literature only managed to find works by Kaveh and Nikbakht (2006, 2008, 2010) on this subject. In these studies, the researchers used transformation matrices to convert the conventional stiffness matrix into symmetry-adapted stiffness matrices. This results in a non-overlapping block-diagonal matrix, with each independent block being associated with a subspace of the problem (Kaveh & Nikbakht, 2006; Kaveh & Nikbakht, 2008; Kaveh et al., 2010). This approach is amenable to computer programming. However, it can also be computationally demanding, since the conventional structural matrix has to be first assembled, then converted into a block-diagonal matrix using suitable matrix transformations.

The approach used in the current proposed method, obtains the symmetry-adapted stiffness matrices directly by simple superimposition of the appropriate values of the conventional stiffness coefficients in accordance with the coordinates of the symmetry adapted basis vectors of the problem. This approach has been applied in the vibration analysis of symmetric frames (Zingoni & Pavlovic, 1994; Zingoni, 1996; Zingoni, 2015; Zingoni, 2019).

Some of the results reported in this section have been published by the American Society of Civil Engineers (Kaluba & Zingoni, 2021).

3.2.1 Matrix stiffness method

The matrix stiffness method can be used to study the flexural behaviour of a member subject to axial loading as well as bending. Provided displacements and elastic stresses are within small limits, the force-deflection relationship of a flexural member subject to axial and bending loading is given by:

$$[Q] = \{[K_1] + P[K_2]\}[\Delta] \qquad (3.1)$$

where

$[Q]$ -contains the transverse loads that cause bending

$[\Delta]$ -contains the corresponding bending deformations

P - the axial load

$[K_1]$ -the stiffness matrix of a member subject only to flexure

$[K_2]$ -the stiffness matrix that accounts for effect that the axial load *P* has on the stiffness of the flexural member.

The force-deflection equation *3.1* given above can be rewritten as:

$$[\Delta] = \{[K_1] + P[K_2]\}^{-1}[Q] \qquad (3.2)$$

From the above equation the flexural member buckles when [Δ] increases without bound for finite values of $[Q]$. This happens when the inverse of the stiffness matrix becomes infinitely large.

Since the inverse of a matrix is obtained by dividing the adjoint matrix by the determinant, the inverse will blow up when the determinant vanishes. Therefore, the buckling load can be found by setting the determinant of the stiffness matrix equal to zero (Carter, 1963; Citipitioglu, 1965; Douglas, 1964). The characteristic equation then becomes:

$$|K| = 0 \qquad (3.3)$$

where

$$K = [K_1] + P[K_2]$$

To implement the matrix stiffness method in our current study, we shall use a beam-column element subject to an axial load *P* and a set of loads *[q],* as shown in Figure *3.1 a* and with corresponding displacements *[δ]* as shown in Figure *3.1 b*.

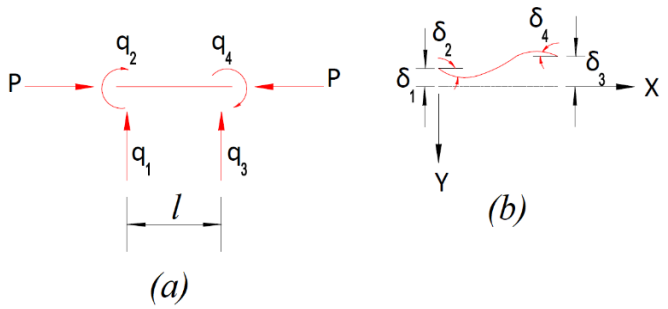

Figure 3.1: Beam column element (a) forces and (b) displacements

The stiffness matrix for such a beam-column element is well known (Farshad, 1994; Hartz, 1965) and may be expressed as:

$$[k]=\frac{EI}{l^3}\left(\begin{bmatrix}12 & -6 & -12 & -6\\ -6 & 4 & 6 & 2\\ -12 & 6 & 12 & 6\\ -6 & 2 & 6 & 4\end{bmatrix}-\lambda\begin{bmatrix}36 & -3 & -36 & -3\\ -3 & 4 & 3 & -1\\ -36 & 3 & 36 & 3\\ -3 & -1 & 3 & 4\end{bmatrix}\right) \qquad (3.4)$$

In equation 3.4 the eigenvalue (λ) is given by:

$$\lambda=\frac{Pl^2}{30EI} \qquad (3.5)$$

where:

- P as the axial load in the beam element;
- l the length of the beam element; and
- EI the flexural rigidity of the beam element.

In the derivation of Equation *3.4* following assumptions are made:

- The material is assumed to be elastic;
- the member is perfectly straight, and the load is applied along its centroidal axis;
- deformations are so small that the slope of the elastic curve is negligible when compared with unity; and
- the elastic curve is a cubic function.

Further, it also should be noted that the terms given in Equation *3.4* have been adjusted so that every term in the matrix has the same dimensions. This simplification is achieved by adjusting the force and displacement matrices so that all terms in the former have dimensions of force, and those

in the latter have dimensions of distance, and this is expressed in the stiffness equation given below.

$$\begin{bmatrix} q_1 \\ \frac{q_2}{l} \\ q_3 \\ \frac{q_4}{l} \end{bmatrix} = \left(\frac{EI}{l^3} \begin{bmatrix} 12 & -6 & -12 & -6 \\ -6 & 4 & 6 & 2 \\ -12 & 6 & 12 & 6 \\ -6 & 2 & 6 & 4 \end{bmatrix} - \frac{P}{30l} \begin{bmatrix} 36 & -3 & -36 & -3 \\ -3 & 4 & 3 & -1 \\ -36 & 3 & 36 & 3 \\ -3 & -1 & 3 & 4 \end{bmatrix} \right) \begin{bmatrix} \delta_1 \\ \delta_2 l \\ \delta_3 \\ \delta_4 l \end{bmatrix}$$

In the matrix stiffness method, the element stiffness matrices $[k_n]$ must be transformed from element coordinates (δ) to structure coordinates (ϕ) in order to assemble the stiffness matrix of the structure. The element stiffness matrix in structure coordinates $[K_n]$ is given as:

$$\left[K_n\right] = \left[D_n\right]^T \left[k_n\right]\left[D_n\right] \qquad (3.6)$$

in which $\left[D_n\right]$, the transformation matrix for the *nth* element, and is defined by

$$\left[\delta_n\right] = \left[D_n\right]\left[\phi_n\right] \qquad (3.7)$$

To obtain the eigenvalues of a frame using the stiffness element presented here the characteristic equation applied can be expressed as:

$$\left|\left[K_1\right] - \lambda\left[K_2\right]\right| = 0 \qquad (3.8)$$

It is important to note that in most engineering literature, the parameter in equations *3.5, 3.8* and *4.4* is referred to as an eigenvalue, even though the problem itself is in the form $[\boldsymbol{K_1-\lambda K_2]x=0}$ and not $\boldsymbol{[K-\lambda I]x=0}$, where *I* is the identity matrix, *K* is the coefficient matrix of the linear system, and *x* is the undetermined displacement column matrix. For the problems in this thesis, the parameter λ does not only appear in the *diagonal terms* of the coefficient matrix. Thus, it is not an eigenvalue in the mathematical linear algebra form of $\boldsymbol{[K-\lambda I]x=0}$.

3.2.2 Group-theoretic formulation of the buckling problem

In our Group-theoretic formulation of the buckling problem, we first obtain the symmetry adapted basis vectors (Φ) from the conventional basis vectors (ϕ) of the given problem. This is achieved by applying idempotents of the symmetry group applicable to the vector space of the problem.

Idempotents $P^{(i)}$ of a symmetry group G are linear combinations of its symmetry elements satisfying the relation $P^{(i)}P^{(i)} = P^{(i)}$, and $P^{(i)}\,P^{(j)} = 0$ if $i \neq j$. Each subspace of a vector space has its own idempotent. Application of an idempotent $P^{(i)}$ to the basis vectors of a vector space V of dimension n, results in the selection of only those basis vectors that belong to the subspace $S^{(i)}$. These basis vectors all have a definite symmetry type characteristic of the subspace. In particular, when idempotents are applied to the basis vectors $\phi_1, \phi_2, \ldots, \phi_n$ of an n-dimensional physical problem, *symmetry-adapted basis vectors* are generated for each respective subspace. These symmetry-adapted basis vectors of the various subspaces are of smaller dimension r than n of the full vector space. Further details can be obtained from Zingoni (1996, 2005b, 2008, 2014, 2015, 2018), which will also be illustrated in our subsequent numerical examples.

After the symmetry adapted basis vectors have been selected from the basis vectors of the full vector space V. The next step is to generate the symmetry-adapted stiffness matrices $\boldsymbol{B}$ for each subspace $S^{(i)}$ from the conventional stiffness matrix $\boldsymbol{A}$ of the problem in the full vector space $\boldsymbol{V}$. The matrix B for each subspace $S^{(i)}$, will be of a smaller dimension than the matrix $\boldsymbol{A}$ of the conventional approach. Zingoni (1996, 200b, 2008, 2014, 2015, 2018) has outlined how this step is implemented, and this will also be illustrated in our subsequent three numerical examples. Once the symmetry adapted stiffness matrices are obtained, the eigenvalues of the problem for each subspace can then be separately computed.

Upon obtaining the symmetry adapted stiffness matrices for each subspace, the eigenvalues of the respective subspaces can then be computed conventionally. The eigenvalues computed for each subspace are also the eigenvalues for the full vector space of the problem (Zingoni, 1996; Zingoni, 2005b; Zingoni, 2008; Zingoni, 2012b; Zingoni, 2014; Zingoni, 2018; Zingoni, 2019). This is because the eigenvalues of a problem are independent of the basis vectors chosen for the problem, and therein lies one of the computational advantages of the group theoretic approach. To obtain the eigenvalues for each subspace, a characteristic equation is applied to each subspace. The stiffness matrix B, of our characteristic equation has two components: one component (C_1) that takes account of flexure only and the other (C_2) that takes account of effects of the axial load P on stiffness. Therefore, the characteristic equation to compute the r eigenvalues for each subspace is expressed as:

$$\left|[C_1]-\lambda[C_2]\right|=0 \qquad (3.9)$$

The eigenvectors for each subspace are obtained by substituting the *r* eigenvalues for each subspace into the eigenvalue equation for each subspace (Zingoni, 2019). The eigenvector equation can be expressed as:

$$\left[[C_1]-\lambda[C_2]\right]\{\Psi\}=0 \qquad (3.10)$$

Where Ψ is the eigenvector of the subspace.

The symmetry pattern of these eigenvectors is always in accordance with the symmetry pattern of the subspace. Further, while the eigenvalues of *r*-dimensional subspaces are the eigenvalues of the full *n*-dimensional space of the original problem. The eigenvectors of a *r*-dimensional subspace are not the eigenvectors of the full *n*-dimensional space of the original problem. To obtain the eigenvectors of the full *n*-dimensional space, we must first note that the *r* components of $\Psi_1, \Psi_2, \ldots\ldots, \Psi_r$ of a subspace eigenvector correspond to the basis vectors Φ of the same subspace. To obtain the eigenvector {**U**} in the original *n*-dimensional vector space of the problem, for each eigenvalue $\lambda_1, \lambda_2, \ldots. \lambda_r$ of a *r*-dimensional subspace we must allocate the calculated value of a subspace-eigenvector component Ψ to all beam element nodes associated with the basis vectors of the subspace. These allocations must be in accordance with the positive or negative signs of the basis vector terms (Zingoni, 2019).

3.2.2.1 Plane Frames with C_{1v} symmetry

In our first numerical example, we show how the group-theoretic approach can be applied to the buckling analysis of a symmetric portal frame such as the one shown in Figure *3.2* (a) below. This frame has one vertical plane of symmetry, and therefore the symmetry of the problem belongs to the C_{1v} symmetry group.

Let's assume that the portal frame is pinned at the base and laterally restrained as shown above. To implement the matrix stiffness method to determine the buckling load of this frame, we shall divide it into six elements with seven nodes ten degrees of freedom $\Delta_1, \Delta_2, \ldots, \Delta_{10}$, as shown in Figure *3.2 (b)*.

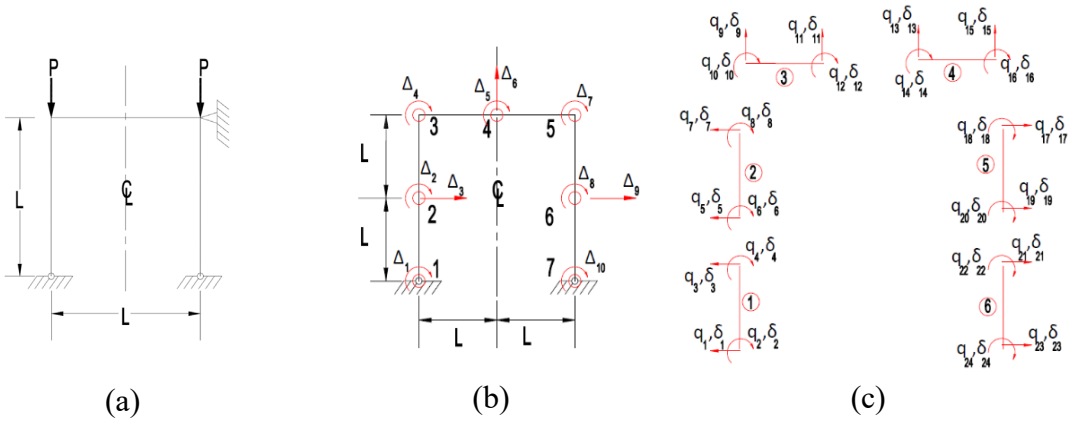

Figure 3.2: C_{1v} symmetric portal frame

The sign convention used for the displacements shown in Figure *3.2* is as follows: clockwise rotations are positive; anticlockwise rotations are negative; vertical upward deflections are positive; vertical downward deflections are negative; and horizontal deflections to the right are positive and to the left are negative.

This problem, while having ten degrees of freedom, will only have eight eigenvalues. This is because there is no axial load in the beam. Thus, rather than having ten eigenvalues for ten degrees of freedom, we only have eight eigenvalues for the eight degrees of freedom in the two columns of the frame. To compute the eigenvalues using the conventional matrix stiffness method, a *10x10* stiffness matrix would be required to determine the eight eigenvalues for the eight distinct buckling loads. However, if we implement the group-theoretic approach to the problem, the number of degrees of freedom can be reduced. This is achieved by applying the idempotents of the C_{1v} symmetry group to each of the basis vectors of our problem.

The idempotents for a system with one plane of reflection symmetry, as in our given portal frame are (Zingoni, 1996; Zingoni, 2005b; Zingoni, 2014; Zingoni, 2015):

$$P^1 = \frac{1}{2}(e + \sigma_v), \qquad P^2 = \frac{1}{2}(e - \sigma_v), \qquad (3.11 - 3.12)$$

Where e is the identity element and σ_v is a reflection about a vertical plane of symmetry.

Since the C_{1v} symmetry group has two idempotents, the symmetry-adapted functions of the two subspaces S^1 and S^2 are obtained by applying the respective idempotents (P^1 in the case of subspace S^1, and P^2 in the case of subspace S_2) to the system functions $\phi_1 (= \Delta_1)$, $\phi_2 (= \Delta_2)$, $\phi_3 (= \Delta_3)$, $\phi_4 (=$

Δ_4), $\phi_5(=\Delta_5)$, $\phi_6(=\Delta_6)$, $\phi_7(=\Delta_7)$, $\phi_8(=\Delta_8)$, $\phi_9(=\Delta_9)$, and $\phi_{10}(=\Delta_{10})$. This process is carried out as follows:

Subspace S^1

$$P^1\phi_1 = \frac{1}{2}\phi_1(e+\sigma_v) = \frac{1}{2}(\phi_1 - \phi_{10}) = -P^1\phi_{10}$$

$$P^1\phi_2 = \frac{1}{2}\phi_2(e+\sigma_v) = \frac{1}{2}(\phi_2 - \phi_8) = -P^1\phi_8$$

$$P^1\phi_3 = \frac{1}{2}\phi_3(e+\sigma_v) = \frac{1}{2}(\phi_3 - \phi_9) = -P^1\phi_9$$

$$P^1\phi_4 = \frac{1}{2}\phi_4(e+\sigma_v) = \frac{1}{2}(\phi_4 - \phi_7) = -P^1\phi_7$$

$$P^1\phi_5 = \frac{1}{2}\phi_5(e+\sigma_v) = \frac{1}{2}(\phi_5 - \phi_5) = 0$$

$$P^1\phi_6 = \frac{1}{2}\phi_6(e+\sigma_v) = \frac{1}{2}(\phi_6 + \phi_6) = \phi_6$$

Therefore, subspace S^1 is five-dimensional, and the basis vectors are:

$$\Phi_1^1 = \phi_1 - \phi_{10}, \quad \Phi_2^1 = \phi_2 - \phi_8, \quad \Phi_3^1 = \phi_3 - \phi_9, \quad \Phi_4^1 = \phi_4 - \phi_7, \quad \Phi_5^1 = \phi_6, \quad (3.13-3.17)$$

Subspace S^2

The basis vectors for subspace S^2 are obtained in a similar manner, by applying the idempotent P^2. Subspace S^2 was also found to be five dimensional and the basis vectors are:

$$\Phi_1^2 = \phi_1 + \phi_{10}, \quad \Phi_2^2 = \phi_2 + \phi_8, \quad \Phi_3^2 = \phi_3 + \phi_9, \quad \Phi_4^2 = \phi_4 + \phi_7, \quad \Phi_5^2 = \phi_5, \quad (3.18-3.22)$$

The basis vectors of subspaces S^1 and S^2 are shown in Figures *3.3* and *3.4* respectively below.

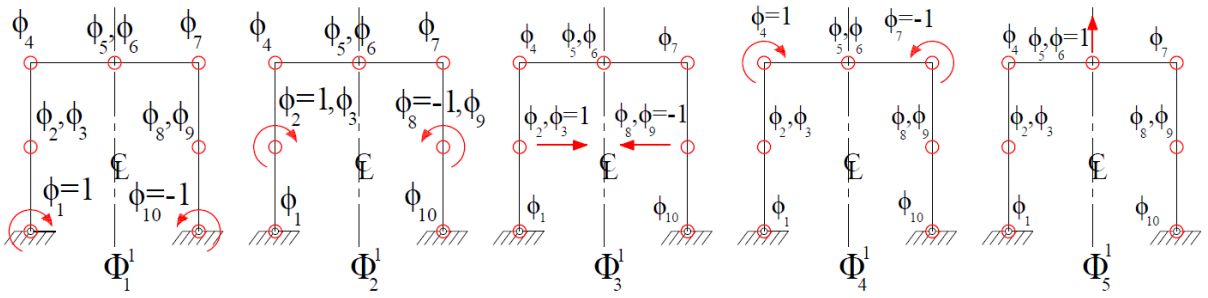

Figure 3.3:C_{1v} Frame unit moments applied in accordance with the coordinates of the basis vectors of subspace S^1

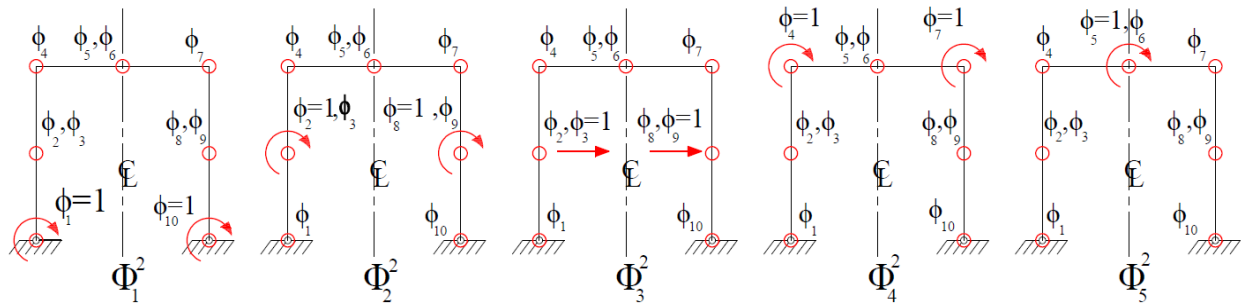

Figure 3.4:C_{1v} Frame unit moments applied in accordance with the coordinates of the basis vectors of subspace S^2

The conventional stiffness matrix for the portal frame shown in Figure *3.2* may be written down as $A_{i,j}$ (i = 1,2,...,10; j = 1,2,...,10), where, $A_{i,j}$ is the force at node i due to a unit displacement applied at node j. Therefore, the conventional stiffness matrix will be of the form given in equation *3.23* below.

It should be noted that, as a consequence of the reciprocal theorem of elasticity, the stiffness matrix $\boldsymbol{A}$ is symmetrical, i.e. $\boldsymbol{A_{i,j}=A_{j,i}}$.

$$A=\begin{bmatrix} a_{1,1} & a_{1,2} & a_{1,3} & . & . & . & a_{1,10} \\ a_{2,1} & a_{2,2} & a_{2,3} & . & . & . & a_{2,10} \\ . & . & . & & & & . \\ . & . & . & & & & . \\ . & . & . & & & & . \\ . & . & . & & & & . \\ a_{10,1} & a_{10,2} & a_{10,3} & . & . & . & a_{10,10} \end{bmatrix} \qquad (3.23)$$

In the group-theoretic formulation of the problem, let us consider any subspace of dimension r. We will define the *symmetry-adapted stiffness coefficient* $B_{i,j}$ (i = 1,2,...,r; j = 1,2,...,r) as the force at any of the nodes of the basis vector Φ_i, due to unit displacements at all the nodes of the basis vector Φ_j. In our current example, r = *5* for subspaces S^1 and S^2. The symmetry-adapted stiffness matrix B for S^1 and S^2 will be of the form shown in equation *3.24*:

$$B = \begin{bmatrix} b_{1,1} & b_{1,2} & b_{1,3} & b_{1,4} & b_{1,5} \\ b_{2,1} & b_{2,2} & b_{2,3} & b_{2,4} & b_{2,5} \\ b_{3,1} & b_{3,2} & b_{3,3} & b_{3,4} & b_{3,5} \\ b_{4,1} & b_{4,2} & b_{4,3} & b_{4,4} & b_{4,5} \\ b_{5,1} & b_{5,2} & b_{5,3} & b_{5,4} & b_{5,5} \end{bmatrix} \qquad (3.24)$$

At this stage, the coefficients of ***B*** for each subspace are obtained by superimposing the appropriate values of the conventional stiffness coefficients appearing in matrix *A* of equation *3.23* in accordance with the combinations of unit displacements of Φ_j appearing in Figure *3.3* for subspace S^1 and Figure *3.4* for subspace S^2, and these coefficients are as follows:

Subspace S^1

$$b_{1,1} = a_{1,1} - a_{1,10}, \quad b_{1,2} = a_{1,2} - a_{1,8}, \quad b_{1,3} = a_{1,3} - a_{1,9}, \quad b_{1,4} = a_{1,4} - a_{1,7}, \quad (3.25-3.28)$$

$$b_{1,5} = a_{1,6}, \quad (3.29)$$

$$b_{2,1} = a_{2,1} - a_{2,10}, \quad b_{2,2} = a_{2,2} - a_{2,8}, \quad b_{2,3} = a_{2,3} - a_{2,9} \quad b_{2,4} = a_{2,4} - a_{2,7}, \quad (3.30-3.33)$$

$$b_{2,5} = a_{2,6}, \quad (3.34)$$

$$b_{3,1} = a_{3,1} - a_{3,10}, \quad b_{3,2} = a_{3,2} - a_{3,8}, \quad b_{3,3} = a_{3,3} - a_{3,9}, \quad b_{3,4} = a_{3,4} - a_{3,7} \quad (3.35-3.38)$$

$$b_{3,5} = a_{3,6} \quad (3.39)$$

$$b_{4,1} = a_{4,1} - a_{1,10}, \quad b_{4,2} = a_{4,2} - a_{4,8}, \quad b_{4,3} = a_{4,3} - a_{4,9} \quad b_{4,4} = a_{4,4} - a_{4,7} \quad (3.40-3.43)$$

$$b_{4,5} = a_{4,6} \quad (3.44)$$

$$b_{5,1} = a_{6,1} - a_{6,10}, \quad b_{5,2} = a_{6,2} - a_{6,8}, \quad b_{5,3} = a_{6,3} - a_{6,9}, \quad b_{5,4} = a_{6,4} - a_{6,7} \quad (3.45-3.48)$$

$$b_{5,5} = a_{6,6} \quad (3.49)$$

Subspace S^2

$$b_{1,1} = a_{1,1} + a_{1,10}, \quad b_{1,2} = a_{1,2} + a_{1,8}, \quad b_{1,3} = a_{1,3} + a_{1,9} \quad b_{1,4} = a_{1,4} + a_{1,7} \quad (3.50-3.53)$$

$$b_{1,5} = a_{1,5} \quad (3.54)$$

$$b_{2,1} = a_{2,1} + a_{2,10}, \quad b_{2,2} = a_{2,2} + a_{2,8}, \quad b_{2,3} = a_{2,3} + a_{2,9}, \quad b_{2,4} = a_{2,4} + a_{2,7} \quad (3.55-3.58)$$

$$b_{2,5} = a_{2,5} \quad (3.59)$$

$$b_{3,1} = a_{3,1} + a_{3,10}, \quad b_{3,2} = a_{3,2} + a_{3,8} \quad b_{3,3} = a_{3,3} + a_{3,9} \quad b_{3,4} = a_{3,4} + a_{3,7} \quad (3.60-3.63)$$

$$b_{3,5} = a_{3,5} \quad (3.64)$$

$$b_{4,1} = a_{4,1} + a_{1,10} \qquad b_{4,2} = a_{4,2} + a_{4,8}, \qquad b_{4,3} = a_{4,3} + a_{4,9} \qquad b_{4,4} = a_{4,4} + a_{4,7} \qquad (3.65 - 3.68)$$

$$b_{4,5} = a_{4,5} \qquad (3.69)$$

$$b_{5,1} = a_{5,1} + a_{5,10}, \qquad b_{5,2} = a_{5,2} + a_{5,8}, \qquad b_{5,3} = a_{5,3} + a_{5,9} \qquad b_{5,4} = a_{5,4} + a_{5,7} \qquad (3.70 - 3.73)$$

$$b_{5,5} = a_{5,5} \qquad (3.74)$$

Before applying equations *3.25* to *3.74*, we must first conventionally obtain the matrix ***A***. Assuming that the portal frame shown in Figure 3.*2* has member lengths *l* and constant flexural rigidity *EI*. The stiffness matrix for elements *1*, *2*, *5* and *6* of Figure *3.2b* is denoted as: k_1, k_2, k_5; *and* k_6 respectively. From Equation *3.4,* these element stiffness matrices are given as:

$$[k_1] = [k_2] = [k_5] = [k_6] = \frac{EI}{l^3}\left(\begin{bmatrix} 12 & -6 & -12 & -6 \\ -6 & 4 & 6 & 2 \\ -12 & 6 & 12 & 6 \\ -6 & 2 & 6 & 4 \end{bmatrix} - \lambda \begin{bmatrix} 36 & -3 & -36 & -3 \\ -3 & 4 & 3 & -1 \\ -36 & 3 & 36 & 3 \\ -3 & -1 & 3 & 4 \end{bmatrix}\right)$$

$$[k_3] = [k_4] = \frac{EI}{l^3}\begin{bmatrix} 12 & -6 & -12 & -6 \\ -6 & 4 & 6 & 2 \\ -12 & 6 & 12 & 6 \\ -6 & 2 & 6 & 4 \end{bmatrix}$$

To transform the element stiffness matrices in structure coordinates, we must first obtain the transformation matrices. The transformation matrices for elements of Figure *3.2c* are:

$$[D_1] = \begin{matrix} \phi_1 & \phi_2 & \phi_3 l \end{matrix}\begin{bmatrix} 0 & 0 & 0 \\ 1 & 0 & 0 \\ 0 & 0 & -1 \\ 0 & 1 & 0 \end{bmatrix}\begin{matrix} \delta_1 \\ \delta_2 l \\ \delta_3 \\ \delta_4 l \end{matrix} \qquad [D_2] = \begin{matrix} \phi_2 & \phi_3 l & \phi_4 \end{matrix}\begin{bmatrix} 0 & -1 & 0 \\ 1 & 0 & 0 \\ 0 & 0 & 0 \\ 0 & 0 & 1 \end{bmatrix}\begin{matrix} \delta_5 \\ \delta_6 l \\ \delta_7 \\ \delta_8 l \end{matrix} \qquad [D_3] = \begin{matrix} \phi_4 & \phi_5 & \phi_6 l \end{matrix}\begin{bmatrix} 0 & 0 & 0 \\ 1 & 0 & 0 \\ 0 & 0 & 1 \\ 0 & 1 & 0 \end{bmatrix}\begin{matrix} \delta_9 \\ \delta_{10} l \\ \delta_{11} \\ \delta_{12} l \end{matrix}$$

$$[D_4] = \begin{matrix} \phi_5 & \phi_6 l & \phi_7 \end{matrix}\begin{bmatrix} 0 & 1 & 0 \\ 1 & 0 & 0 \\ 0 & 0 & 0 \\ 0 & 0 & 1 \end{bmatrix}\begin{matrix} \delta_{13} \\ \delta_{14} l \\ \delta_{15} \\ \delta_{16} l \end{matrix} \qquad [D_5] = \begin{matrix} \phi_7 & \phi_8 & \phi_9 l \end{matrix}\begin{bmatrix} 0 & 0 & 0 \\ 1 & 0 & 0 \\ 0 & 0 & 1 \\ 0 & 1 & 0 \end{bmatrix}\begin{matrix} \delta_{17} \\ \delta_{18} l \\ \delta_{19} \\ \delta_{20} l \end{matrix} \qquad [D_6] = \begin{matrix} \phi_8 & \phi_9 l & \phi_{10} \end{matrix}\begin{bmatrix} 0 & 1 & 0 \\ 1 & 0 & 0 \\ 0 & 0 & 0 \\ 0 & 0 & 1 \end{bmatrix}\begin{matrix} \delta_{21} \\ \delta_{22} l \\ \delta_{23} \\ \delta_{24} l \end{matrix}$$

Using these transformation matrices and carrying out the operations indicated in equation 3.6, the element stiffness matrix in structure coordinates now become:

$$[K_1]=\begin{matrix}\begin{matrix}\phi_1 & \phi_2 & \phi_3 l\end{matrix}\\ \begin{bmatrix}4-4\lambda & 2+\lambda & -6+3\lambda\\ 2+\lambda & 4-4\lambda & -6+3\lambda\\ -6+3\lambda & -6+3\lambda & 12-36\lambda\end{bmatrix}\end{matrix}\begin{matrix}\phi_1\\ \phi_2\\ \phi_3 l\end{matrix} \qquad [K_2]=\begin{matrix}\begin{matrix}\phi_2 & \phi_3 l & \phi_4\end{matrix}\\ \begin{bmatrix}4-4\lambda & 6-3\lambda & 2+\lambda\\ 6-3\lambda & 12-36\lambda & 6-3\lambda\\ 2+\lambda & 6-3\lambda & 4-4\lambda\end{bmatrix}\end{matrix}\begin{matrix}\phi_2\\ \phi_3 l\\ \phi_4\end{matrix}$$

$$[K_3]=\begin{matrix}\begin{matrix}\phi_4 & \phi_5 & \phi_6 l\end{matrix}\\ \begin{bmatrix}4 & 2 & 6\\ 2 & 4 & 6\\ 6 & 6 & 12\end{bmatrix}\end{matrix}\begin{matrix}\phi_4\\ \phi_5\\ \phi_6 l\end{matrix} \qquad [K_4]=\begin{matrix}\begin{matrix}\phi_5 & \phi_6 l & \phi_7\end{matrix}\\ \begin{bmatrix}4 & -6 & 2\\ -6 & 12 & -6\\ 2 & -6 & 4\end{bmatrix}\end{matrix}\begin{matrix}\phi_5\\ \phi_6 l\\ \phi_7\end{matrix}$$

$$[K_5]=\begin{matrix}\begin{matrix}\phi_7 & \phi_8 & \phi_9 l\end{matrix}\\ \begin{bmatrix}4-4\lambda & 2+\lambda & 6-3\lambda\\ 2+\lambda & 4-4\lambda & 6-3\lambda\\ 6-3\lambda & 6-3\lambda & 12-36\lambda\end{bmatrix}\end{matrix}\begin{matrix}\phi_7\\ \phi_8\\ \phi_9 l\end{matrix} \qquad [K_6]=\begin{matrix}\begin{matrix}\phi_8 & \phi_9 l & \phi_{10}\end{matrix}\\ \begin{bmatrix}4-4\lambda & -6+3\lambda & 2+\lambda\\ -6+3\lambda & 12-36\lambda & -6+3\lambda\\ 2+\lambda & -6+3\lambda & 4-4\lambda\end{bmatrix}\end{matrix}\begin{matrix}\phi_8\\ \phi_9 l\\ \phi_{10}\end{matrix}$$

Notice that the element stiffness matrices in structure coordinates have been obtained by only using the transformation matrices obtained with reference to a single coordinate system, in this case Figure 3.*2b*. Recall that the stiffness matrix defined by equation 3.23 was based on Figure 3.*2b*. This approach also applies to any problem with more than two subspaces, as will be shown in subsequent examples.

To obtain the structure stiffness matrix, we only need to combine the coefficients of each element stiffness matrix K_1, K_2, K_3, K_4, K_5 and K_6 in accordance with equations *3.25-3.49* and *3.50-3.74* for subspaces S^1 and S^2 respectively. The stiffness matrices for each subspace are as follows:

Subspace S^1

$$B^1=\begin{bmatrix}4-4\lambda & \lambda+2 & 3\lambda-6 & 0 & 0\\ \lambda+2 & 8-8\lambda & 0 & \lambda+2 & 0\\ 3\lambda-6 & 0 & 24-72\lambda & 6-3\lambda & 0\\ 0 & \lambda+2 & 6-3\lambda & 8-4\lambda & 6\\ 0 & 0 & 0 & 12 & 24\end{bmatrix}$$

Subspace S^2

$$B^2 = \begin{bmatrix} 4-4\lambda & 2+\lambda & -6+3\lambda & 0 & 0 \\ 2+\lambda & 8-8\lambda & 0 & 2+\lambda & 0 \\ -6+3\lambda & 0 & 24-72\lambda & 6-3\lambda & 0 \\ 0 & 2+\lambda & 6-3\lambda & 8-4\lambda & 2 \\ 0 & 0 & 0 & 4 & 8 \end{bmatrix}$$

We can now proceed to obtaining the eigenvalues and eigenvectors for each subspace by simply applying equations *3.9* and *3.10*, respectively, to the stiffness matrix for each subspace. To obtain the eigenvectors for the full space, we allocate the calculated value of a subspace-eigenvector component Ψ to all beam element nodes associated with the basis vectors of the subspace. This has been worked out in Tables *3.1* and *3.2* below.

Subspace S^1

$\lambda_1 = 0.1084$

$$\Psi_1 = \begin{bmatrix} 1.0000 \\ -0.0889 \\ 0.5954 \\ -0.6988 \\ 0.3494 \end{bmatrix}$$

$\lambda_2 = 0.4447$

$$\Psi_2 = \begin{bmatrix} -0.9643 \\ 1.0000 \\ 0.0649 \\ -0.8528 \\ 0.4264 \end{bmatrix}$$

$\lambda_3 = 1.1718$

$$\Psi_3 = \begin{bmatrix} 1.0000 \\ 0.1543 \\ -0.0796 \\ -0.9331 \\ 0.4666 \end{bmatrix}$$

$\lambda_4 = 2.0973$

$$\Psi_4 = \begin{bmatrix} 0.7721 \\ 0.8271 \\ -0.0005 \\ 1.0000 \\ -0.5000 \end{bmatrix}$$

Table 3.1:C_{1v} frame deflection ordinates of mode shapes of subspace S^1

ϕ_i	1	2	3	4	5	6	7	8	9	10
$\mathbf{U^1_1}$	1.0000	-0.0889	0.5954	-0.6988	0.0000	0.3494	0.6988	0.0889	-0.5954	-1.0000
$\mathbf{U^1_2}$	-0.9643	1.0000	0.0649	-0.8528	0.0000	0.4264	0.8528	-1.0000	-0.0649	0.9643
$\mathbf{U^1_3}$	1.0000	0.1543	-0.0796	-0.9331	0.0000	0.4666	0.9331	-0.1543	0.0796	-1.0000
$\mathbf{U^1_4}$	0.7721	0.8271	-0.0005	1.0000	0.0000	-0.5000	-1.0000	-0.8271	0.0005	-0.7721

Subspace S^2

$\lambda_1 = 0.1331$

$$\Psi_1 = \begin{bmatrix} -1.0000 \\ 0.1789 \\ -0.5510 \\ 0.4181 \\ -0.2090 \end{bmatrix}$$

$\lambda_2 = 0.5034$

$$\Psi_2 = \begin{bmatrix} 0.9691 \\ -1.0000 \\ -0.1288 \\ 0.6180 \\ -0.3090 \end{bmatrix}$$

$\lambda_3 = 1.3359$

$$\Psi_3 = \begin{bmatrix} -1.0000 \\ -0.3747 \\ 0.0469 \\ 0.6982 \\ -0.3491 \end{bmatrix}$$

$\lambda_4 = 2.3832$

$$\Psi_4 = \begin{bmatrix} 0.4560 \\ 0.5767 \\ -0.0042 \\ 1.0000 \\ -0.5000 \end{bmatrix}$$

Table 3.2: C_{1v} frame deflection ordinates of mode shapes of subspace S^2

ϕ_i	1	2	3	4	5	6	7	8	9	10
U^2_1	-1.0000	0.1789	-0.5510	0.4181	-0.2090	0	0.4181	0.1789	-0.5510	-1.0000
U^2_2	0.9691	-1.0000	-0.1288	0.6180	-0.3090	0	0.6180	-1.0000	-0.1288	0.9691
U^2_3	-1.0000	-0.3747	0.0469	0.6982	-0.3491	0	0.6982	-0.3747	0.0469	-1.0000
U^2_4	0.4560	0.5767	-0.0042	1.0000	-0.5000	0	1.0000	0.5767	-0.0042	0.4560

The sketches of the buckling modes for subspaces S^1 and S^2 are shown in Figure *3.5* and *3.6* below. It is easy to see that see buckling modes are all in accordance with the basis vectors illustrated in Figures *3.5* and *3.6*.

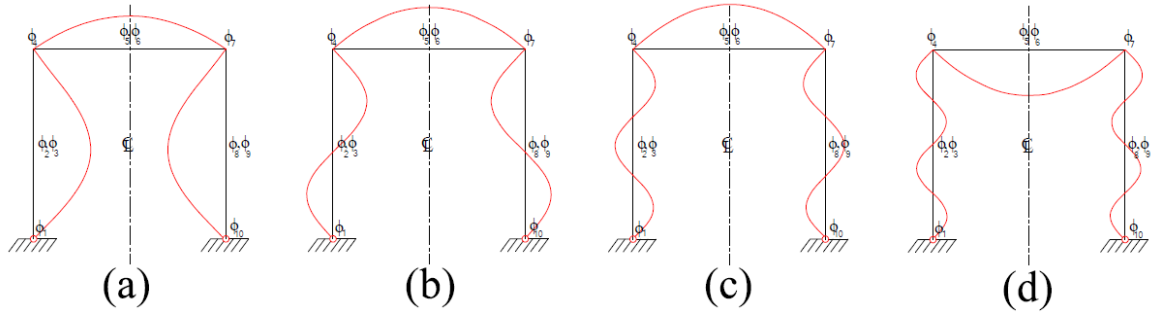

Figure 3.5: Buckling modes of C_{1v} example for subspace S^1:(a) U^1_1; (b) U^1_2; (c) U^1_3; (d) U^1_4

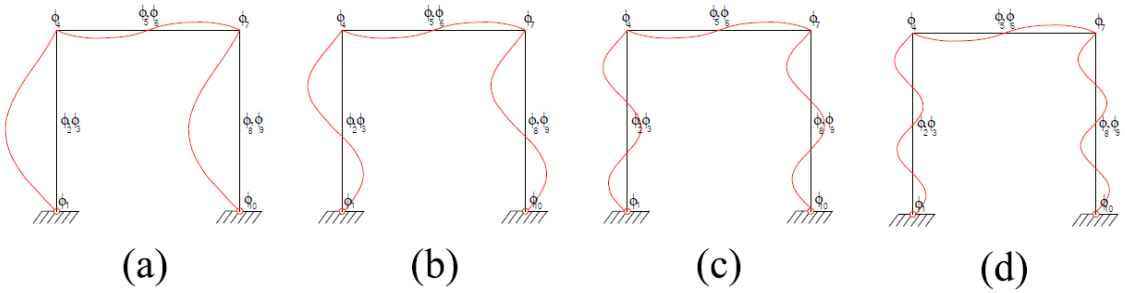

Figure 3.6: Buckling modes of C_{1v} example for subspace S^2:(a) U^2_1; (b) U^2_2; (c) U^2_3; (d) U^2_4

From this example, we note that the highest eigenvalue is obtained in the antisymmetric subspace S^2, while on the other hand the lowest eigenvalue is obtained in the symmetric subspace S^1.

It should be noted that the model used here is merely meant to illustrate the group theoretic approach to buckling analysis. To obtain results that approach the analytical results for the eigenvalues, we would have to use more elements in the model.

3.2.2.2 Plane Frames with C_{2v} symmetry

Let us now consider the case of a laterally restrained rectangular plane frame symmetrical about the vertical and horizontal reflection planes (see Figure *3.7* below). Such a frame belongs to the

C_{2v} symmetry, which has the following idempotents (Zingoni, 1996; Zingoni, 2005b; Zingoni, 2014; Zingoni, 2015):

$$P^1 = \frac{1}{4}\left(e + C_2 + \sigma_x + \sigma_y\right), \qquad P^2 = \frac{1}{4}\left(e + C_2 - \sigma_x - \sigma_y\right), \qquad (3.75-3.76)$$

$$P^3 = \frac{1}{4}\left(e - C_2 + \sigma_x - \sigma_y\right), \qquad P^4 = \frac{1}{4}\left(e - C_2 - \sigma_x + \sigma_y\right), \qquad (3.77-3.78)$$

First, we note that the model for this problem has twelve degrees of freedom, as shown in Figure *3.7* (b). However, there are only eight eigenvalues for eight buckling loads since degrees of freedom ϕ_5, ϕ_6, ϕ_{11} and ϕ_{12} are in members where there is no axial load. To obtain these eight eigenvalues using the conventional method of buckling analysis, we are required to evaluate the determinant of a *12x12* stiffness matrix, resulting in an eight-degree polynomial.

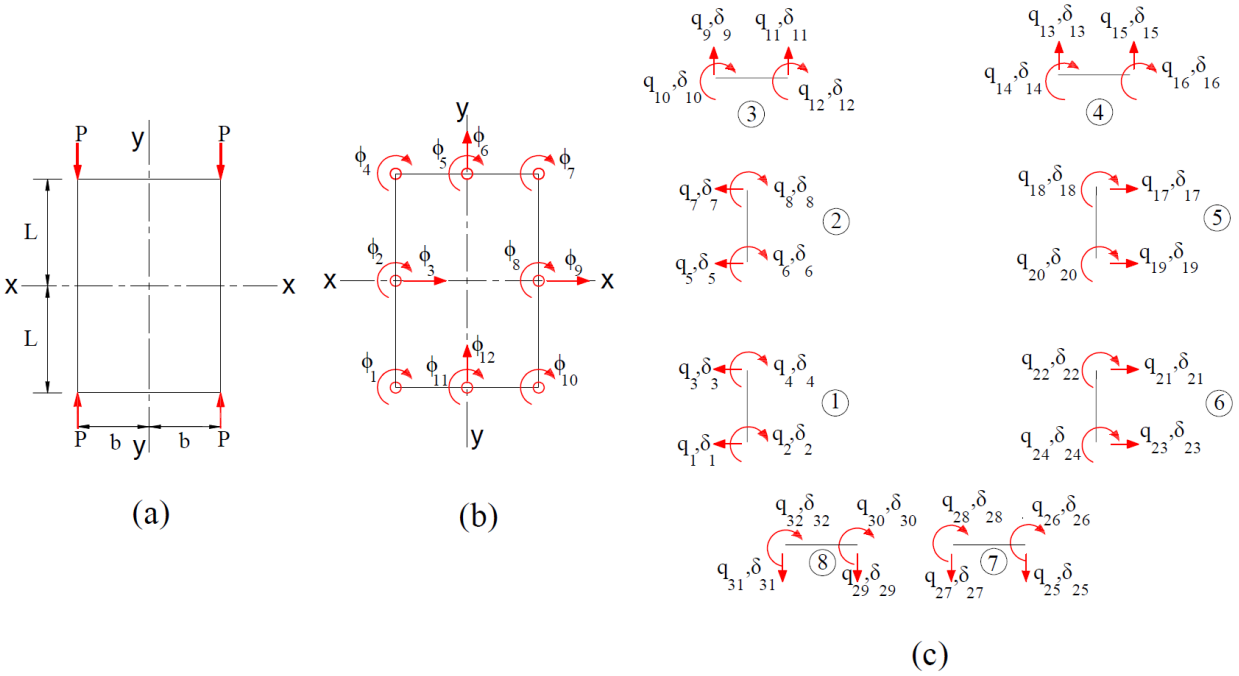

Figure 3.7: C_{2v} plane frame model

To obtain symmetry adapted basis vectors for this frame we apply each idempotent $P^k(k=1,2,3,4)$ of each equations *3.75-3.78* to all the twelve positional functions $\phi_1, \phi_2, \phi_3, \ldots\ldots, \phi_{12}$ shown in Figure *3.7 b.*

Subspace S^1

$$P^1\phi_1 = \frac{1}{4}\left(e + C_2 + \sigma_x + \sigma_y\right)\phi_1 = \frac{1}{4}\left(\phi_1 + \phi_7 - \phi_4 - \phi_{10}\right) = P^1\phi_7 = -P^1\phi_4 = -P^1\phi_{10}$$

$$P^1\phi_2 = \frac{1}{4}\left(e + C_2 + \sigma_x + \sigma_y\right)\phi_2$$
$$= \frac{1}{4}\left(\phi_2 + \phi_8 - \phi_2 - \phi_8\right) = -P^1\phi_8$$
$$= 0$$

$$P^1\phi_3 = \frac{1}{4}\left(e + C_2 + \sigma_x + \sigma_y\right)\phi_3$$
$$= \frac{1}{4}\left(\phi_3 - \phi_9 + \phi_3 - \phi_9\right) = -P^1\phi_9$$
$$= \frac{1}{2}\left(\phi_3 - \phi_9\right)$$

$$P^1\phi_5 = \frac{1}{4}\left(e + C_2 + \sigma_x + \sigma_y\right)\phi_5$$
$$= \frac{1}{4}\left(\phi_5 + \phi_{11} - \phi_{11} - \phi_5\right) = P^1\phi_{11}$$
$$= 0$$

$$P^1\phi_6 = \frac{1}{4}\left(e + C_2 + \sigma_x + \sigma_y\right)\phi_6$$
$$= \frac{1}{4}\left(\phi_6 - \phi_{12} - \phi_{12} + \phi_6\right) = -P^1\phi_{12}$$
$$= \frac{1}{2}\left(\phi_6 - \phi_{12}\right)$$

The basis vector of Subspace S^1

$$\Phi_1^1 = \phi_1 + \phi_7 - \phi_4 - \phi_{10}, \quad \Phi_2^1 = \phi_3 - \phi_9, \quad \Phi_3^1 = \phi_6 - \phi_{12}, \quad (3.79 - 3.81)$$

The basis vectors for the remaining three subspaces are similarly obtained. Application of idempotents P^2, P^3, P^4 to the twelve positional functions shown in Figure *3.7 b* results in subspaces; S^2, S^3, and S^4 respectively. The basis vectors for these three subspaces are as follows:

Subspace S^2

$$\Phi_1^2 = \phi_1 + \phi_7 + \phi_4 + \phi_{10}, \quad \Phi_2^2 = \phi_2 + \phi_8, \quad \Phi_3^2 = \phi_5 + \phi_{11}, \quad (3.82 - 3.84)$$

Subspace S^3

$$\Phi_1^3 = \phi_1 - \phi_7 - \phi_4 + \phi_{10}, \quad \Phi_2^3 = \phi_3 + \phi_9, \quad \Phi_3^3 = \phi_5 - \phi_{11} \quad (3.85 - 3.87)$$

Subspace S^4

$$\Phi_1^4 = \phi_1 - \phi_7 + \phi_4 - \phi_{10}, \quad \Phi_2^4 = \phi_2 - \phi_8, \quad \Phi_3^4 = \phi_6 + \phi_{12}, \quad (3.88 - 3.90)$$

From this example, we notice that rather than having to evaluate the determinant of a *12x12* stiffness matrix to determine the eight eigenvalues for the plane frame, we only need to work with *3x3* stiffness matrices to determine the eight eigenvalues. Further, it is important to note that while each subspace in this problem is three-dimensional, the basis vectors in equations *3.81*, *3.84*, *3.87*, and *3.90* relate to degrees of freedom in members of the frames where there is no axial load. Therefore, for each of the four subspaces, we shall obtain two eigenvalues. The basis vectors for our C_{2v} problem are illustrated in Figure 3.8 below.

At this point we proceed the conventional way and derive the transformation matrices for of the four elements shown in Figure *3.7*.

$$[D_1] = \begin{matrix} \phi_1 & \phi_2 & \phi_3 l \end{matrix} \begin{bmatrix} 0 & 0 & 0 \\ 1 & 0 & 0 \\ 0 & 0 & -1 \\ 0 & 1 & 0 \end{bmatrix} \begin{matrix} \delta_1 \\ \delta_2 l \\ \delta_3 \\ \delta_4 l \end{matrix} \quad [D_2] = \begin{matrix} \phi_2 & \phi_3 & \phi_4 \end{matrix} \begin{bmatrix} 0 & -1 & 0 \\ 1 & 0 & 0 \\ 0 & 0 & 0 \\ 0 & 0 & 1 \end{bmatrix} \begin{matrix} \delta_5 \\ \delta_6 l \\ \delta_7 \\ \delta_8 l \end{matrix} \quad [D_3] = \begin{matrix} \phi_4 & \phi_5 & \phi_6 l \end{matrix} \begin{bmatrix} 0 & 0 & 0 \\ 1 & 0 & 0 \\ 0 & 0 & 1 \\ 0 & 1 & 0 \end{bmatrix} \begin{matrix} \delta_9 \\ \delta_{10} l \\ \delta_{11} \\ \delta_{12} l \end{matrix}$$

$$[D_4] = \begin{matrix} \phi_5 & \phi_6 l & \phi_7 \end{matrix} \begin{bmatrix} 0 & 1 & 0 \\ 1 & 0 & 0 \\ 0 & 0 & 0 \\ 0 & 0 & 1 \end{bmatrix} \begin{matrix} \delta_{13} \\ \delta_{14} l \\ \delta_{15} \\ \delta_{16} l \end{matrix} \quad [D_5] = \begin{matrix} \phi_7 & \phi_8 & \phi_9 l \end{matrix} \begin{bmatrix} 0 & 0 & 0 \\ 1 & 0 & 0 \\ 0 & 0 & 1 \\ 0 & 1 & 0 \end{bmatrix} \begin{matrix} \delta_{17} \\ \delta_{18} l \\ \delta_{19} \\ \delta_{20} l \end{matrix} \quad [D_6] = \begin{matrix} \phi_8 & \phi_9 l & \phi_{10} \end{matrix} \begin{bmatrix} 0 & 1 & 0 \\ 1 & 0 & 0 \\ 0 & 0 & 0 \\ 0 & 0 & 1 \end{bmatrix} \begin{matrix} \delta_{21} \\ \delta_{22} l \\ \delta_{23} \\ \delta_{24} l \end{matrix}$$

$$[D_7] = \begin{matrix} \phi_{10} & \phi_{11} & \phi_{12} l \end{matrix} \begin{bmatrix} 0 & 0 & 0 \\ 1 & 0 & 0 \\ 0 & 0 & -1 \\ 0 & 1 & 0 \end{bmatrix} \begin{matrix} \delta_{25} \\ \delta_{26} l \\ \delta_{27} \\ \delta_{28} l \end{matrix} \quad [D_8] = \begin{matrix} \phi_1 & \phi_{11} & \phi_{12} l \end{matrix} \begin{bmatrix} 0 & 0 & -1 \\ 0 & 1 & 0 \\ 0 & 0 & 0 \\ 1 & 0 & 0 \end{bmatrix} \begin{matrix} \delta_{29} \\ \delta_{30} l \\ \delta_{31} \\ \delta_{32} l \end{matrix}$$

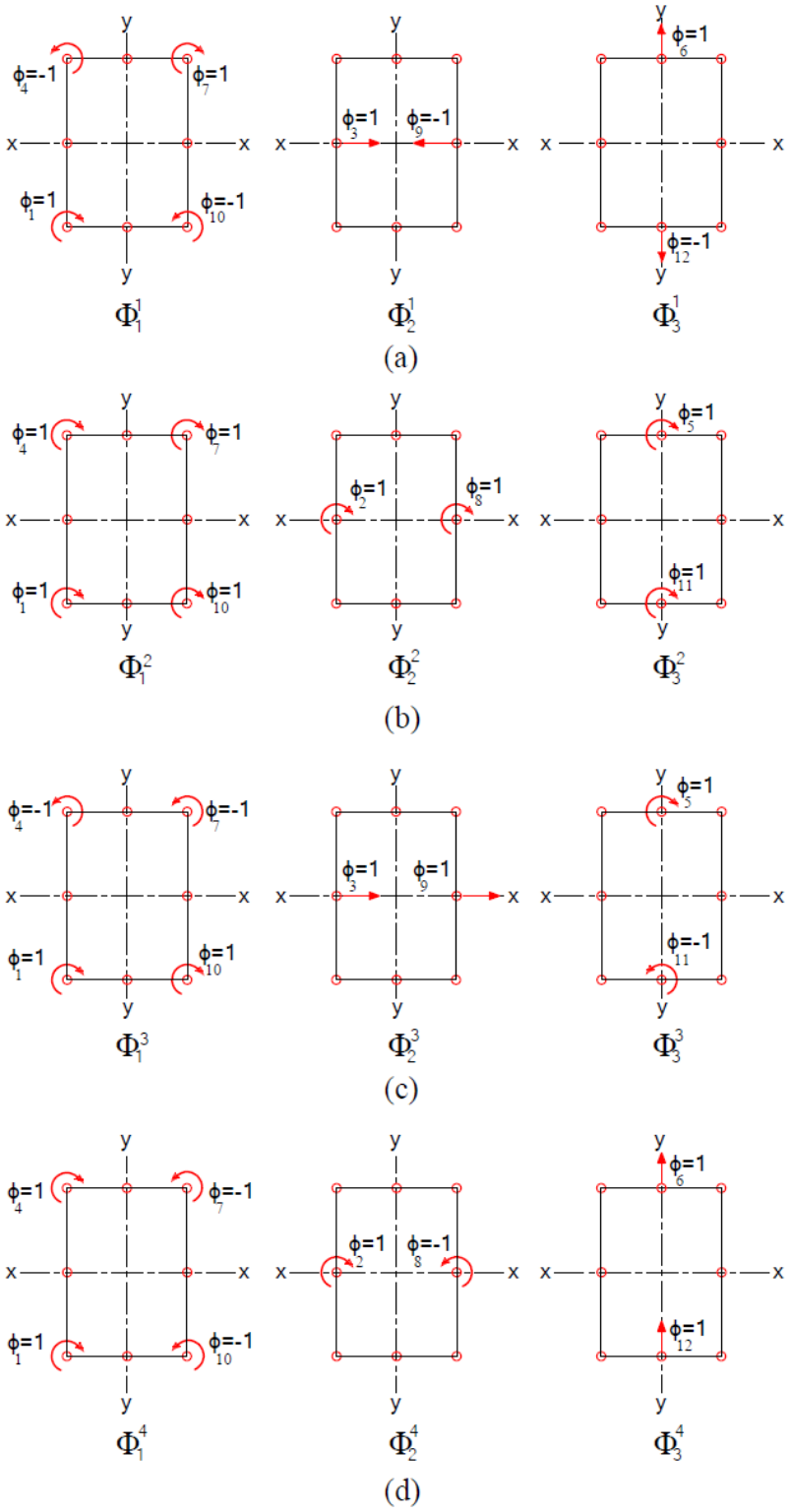

Figure 3.8:C_{2v} plane frame: Unit moments and unit forces applied in accordance with the coordinates of the basis vectors: (a) subspace S^1; (b) subspace S^2; (c) subspace S^3; and (d) subspace S^4.

Notice that the transformation matrices derived here are all based on the structure coordinate system of Figure *3.7 (b)*. Now applying equation *3.6,* we obtain the element stiffness matrices in structure coordinates for the case where *b=l/2* and these are:

$$[K_1]=\begin{matrix}\phi_1 & \phi_2 & \phi_3 l\end{matrix}\begin{bmatrix}4-4\lambda & 2+\lambda & -6+3\lambda\\ 2+\lambda & 4-4\lambda & -6+3\lambda\\ -6+3\lambda & -6+3\lambda & 12-36\lambda\end{bmatrix}\begin{matrix}\phi_1\\ \phi_2\\ \phi_3 l\end{matrix}$$

$$[K_2]=\begin{matrix}\phi_2 & \phi_3 l & \phi_4\end{matrix}\begin{bmatrix}4-4\lambda & 6-3\lambda & 2+\lambda\\ 6-3\lambda & 12-36\lambda & 6-3\lambda\\ 2+\lambda & 6-3\lambda & 4-4\lambda\end{bmatrix}\begin{matrix}\phi_2\\ \phi_3 l\\ \phi_4\end{matrix}$$

$$[K_3]=\begin{matrix}\phi_4 & \phi_5 & \phi_6 l\end{matrix}\begin{bmatrix}8 & 4 & 12\\ 4 & 8 & 12\\ 12 & 12 & 24\end{bmatrix}\begin{matrix}\phi_4\\ \phi_5\\ \phi_6 l\end{matrix}$$

$$[K_4]=\begin{matrix}\phi_5 & \phi_6 l & \phi_7\end{matrix}\begin{bmatrix}8 & -12 & 4\\ -12 & 24 & -12\\ 4 & -12 & 8\end{bmatrix}\begin{matrix}\phi_5\\ \phi_6 l\\ \phi_7\end{matrix}$$

$$[K_5]=\begin{matrix}\phi_7 & \phi_8 & \phi_9 l\end{matrix}\begin{bmatrix}4-4\lambda & 2+\lambda & 6-3\lambda\\ 2+\lambda & 4-4\lambda & 6-3\lambda\\ 6-3\lambda & 6-3\lambda & 12-36\lambda\end{bmatrix}\begin{matrix}\phi_7\\ \phi_8\\ \phi_9 l\end{matrix}$$

$$[K_6]=\begin{matrix}\phi_8 & \phi_9 l & \phi_{10}\end{matrix}\begin{bmatrix}4-4\lambda & -6+3\lambda & 2+\lambda\\ -6+3\lambda & 12-36\lambda & -6+3\lambda\\ 2+\lambda & -6+3\lambda & 4-4\lambda\end{bmatrix}\begin{matrix}\phi_8\\ \phi_9 l\\ \phi_{10}\end{matrix}$$

$$[K_7]=\begin{matrix}\phi_{10} & \phi_{11} & \phi_{12} l\end{matrix}\begin{bmatrix}8 & 4 & -12\\ 4 & 8 & -12\\ -12 & -12 & 24\end{bmatrix}\begin{matrix}\phi_{10}\\ \phi_{11}\\ \phi_{12} l\end{matrix}$$

$$[K_8]=\begin{matrix}\phi_1 & \phi_{11} & \phi_{12} l\end{matrix}\begin{bmatrix}8 & 4 & 12\\ 4 & 8 & 12\\ 12 & 12 & 24\end{bmatrix}\begin{matrix}\phi_1\\ \phi_{11}\\ \phi_{12} l\end{matrix}$$

The conventional stiffness matrix for the frame shown in Figure *3.7 b* may be written down as $A_{i,j}$ (i = 1,2,3,….,12; j = 1,2,3,….,12), where, A_{ij} is the force at node i due to a unit displacement applied at node j. Therefore, the conventional stiffness matrix will be of the form:

$$A=\begin{bmatrix}a_{1,1} & a_{1,2} & a_{1,3} & . & . & . & a_{1,12}\\ a_{2,1} & a_{2,2} & a_{2,3} & . & . & . & a_{2,12}\\ . & . & & & & & .\\ . & . & & & & & .\\ . & . & & & & & .\\ . & . & & & & & .\\ a_{12,1} & a_{12,2} & a_{12,3} & . & . & . & a_{12,12}\end{bmatrix} \qquad (3.91)$$

For this problem each of the four subspaces is three dimensional and therefore, the stiffness matrix ***B***, of each subspace will be of the form:

$$B = \begin{bmatrix} b_{1,1} & b_{1,2} & b_{1,3} \\ b_{2,1} & b_{2,2} & b_{2,3} \\ b_{3,1} & b_{3,2} & b_{3,3} \end{bmatrix} \qquad (3.92)$$

It is important to note that while matrix ***A***, in equation *3.91* is always symmetric, matrix ***B*** in equation *3.92* is not always symmetric.

The coefficients of ***B*** for each subspace, can be obtained by superimposing the appropriate values of the conventional stiffness coefficients appearing in matrix ***A*** of equation *3.91* in accordance with the combinations of unit displacements of Φ_j appearing in Figures *3.8-3.9* for each subspace. The stiffness coefficients and stiffness matrices for each subspace are then:

Subspace S^1

$$b_{1,1} = a_{1,1} + a_{1,7} - a_{1,4} - a_{1,10}, \quad b_{1,2} = a_{1,3} - a_{1,9}, \quad b_{1,3} = a_{1,6} - a_{1,12}, \quad (3.93-3.95)$$

$$b_{2,1} = a_{3,1} + a_{3,7} - a_{3,4} - a_{3,10}, \quad b_{2,2} = a_{3,3} - a_{3,9}, \quad b_{2,3} = a_{3,6} - a_{3,12}, \quad (3.96-3.98)$$

$$b_{3,1} = a_{6,1} + a_{6,7} - a_{6,4} - a_{6,10}, \quad b_{32} = a_{6,3} - a_{6,9} \quad b_{3,3} = a_{6,6} - a_{6,12}, \quad (3.99-3.101)$$

$$B^1 = \begin{bmatrix} 12-4\lambda & -6+3\lambda & -12 \\ -12+6\lambda & 24-72\lambda & 0 \\ -24 & 0 & 48 \end{bmatrix}$$

Subspace S^2

$$b_{11} = a_{1,1} + a_{1,7} + a_{1,4} + a_{1,10}, \quad b_{1,2} = a_{1,2} + a_{1,8}, \quad b_{1,3} = a_{1,5} + a_{1,11} \quad (3.102-3.104)$$

$$b_{2,1} = a_{2,1} + a_{2,7} + a_{2,4} + a_{2,10}, \quad b_{2,2} = a_{2,2} + a_{2,8}, \quad b_{2,3} = a_{2,5} + a_{2,11}, \quad (3.105-3.107)$$

$$b_{3,1} = a_{5,1} + a_{5,7} + a_{5,4} + a_{5,10}, \quad b_{3,2} = a_{5,2} + a_{5,8}, \quad b_{3,3} = a_{5,5} + a_{5,11}, \quad (3.108-3.110)$$

$$B^2 = \begin{bmatrix} 12 - 4\lambda & 2+\lambda & 4 \\ 4+2\lambda & 8 - 8\lambda & 0 \\ 8 & 0 & 16 \end{bmatrix}$$

Subspace S^3

$$b_{1,1} = a_{1,1} - a_{1,7} - a_{1,4} + a_{1,10}, \quad b_{1,2} = a_{1,3} + a_{1,9}, \quad b_{1,3} = a_{1,5} - a_{1,11}, \quad (3.111-3.113)$$

$$b_{2,1} = a_{3,1} - a_{3,7} - a_{3,4} + a_{3,10}, \quad b_{2,2} = a_{3,3} + a_{3,9}, \quad b_{2,3} = a_{3,5} - a_{3,11}, \quad (3.114-3.116)$$

$$b_{3,1} = a_{5,1} - a_{5,7} - a_{5,4} + a_{5,10}, \quad b_{3,2} = a_{5,3} + a_{5,9}, \quad b_{3,3} = a_{5,5} - a_{5,11}, \qquad (3.117 - 3.119)$$

$$B^3 = \begin{bmatrix} 12-4\lambda & -6+3\lambda & -4 \\ -12+6\lambda & 24-72\lambda & 0 \\ -8 & 0 & 16 \end{bmatrix}$$

Subspace S^4

$$b_{1,1} = a_{1,1} - a_{1,7} + a_{1,4} - a_{1,10} \quad b_{1,2} = a_{1,2} - a_{1,8}, \quad b_{1,3} = a_{1,6} + a_{1,12}, \qquad (3.120 - 3.122)$$

$$b_{2,1} = a_{2,1} - a_{2,7} + a_{2,4} - a_{2,10}, \quad b_{2,2} = a_{2,2} - a_{2,8}, \quad b_{2,3} = a_{2,6} + a_{2,12}, \qquad (3.123 - 3.125)$$

$$b_{3,1} = a_{6,1} - a_{6,7} + a_{6,4} - a_{6,10} \quad b_{3,2} = a_{6,2} - a_{6,8}, \quad b_{3,3} = a_{6,6} + a_{6,12} \qquad (3.126 - 3.128)$$

$$B^4 = \begin{bmatrix} 12-4\lambda & 2+\lambda & 12 \\ 4+2\lambda & 8-8\lambda & 0 \\ 24 & 0 & 48 \end{bmatrix}$$

To obtain the eigenvalues λ and eigenvectors Ψ, we simply apply equations *3.9* and *3.10,* respectively to the stiffness matrix for each subspace and obtain the eigenvalues and vectors for each subspace as follows:

Subspace S^1

$$\lambda_1 = 0.1763 \qquad \lambda_2 = 1.5126$$

$$\Psi_1 = \begin{bmatrix} 1.0000 \\ 0.9678 \\ 0.5000 \end{bmatrix} \qquad \Psi_2 = \begin{bmatrix} 1.0000 \\ -0.0344 \\ 0.5000 \end{bmatrix}$$

Table 3.3: C_{2v} deflection ordinates of mode shapes of subspace S^1

ϕ_i	1	2	3	4	5	6	7	8	9	10	11	12
$\mathbf{U^1_1}$	1.0000	0	0.9678	-1.0000	0	0.5000	1.0000	0	-0.9678	-1.0000	0	-0.5000
$\mathbf{U^1_2}$	1.0000	0	-0.0344	-1.0000	0	0.5000	1.0000	0	0.0344	-1.0000	0	-0.5000

Subspace S_2

$$\lambda_1 = 0.7351 \qquad \lambda_2 = 3.2649$$

$$\Psi_1 = \begin{bmatrix} 0.3874 \\ -1.0000 \\ -0.1937 \end{bmatrix} \qquad \Psi_2 = \begin{bmatrix} 1.0000 \\ 0.5811 \\ -0.5000 \end{bmatrix}$$

Table 3.4: C_{2v} deflection ordinates of mode shapes of subspace S^2

ϕ_i	1	2	3	4	5	6	7	8	9	10	11	12
$\mathbf{U^1_1}$	0.3874	-1.0000	0	0.3874	-0.1937	0	0.3874	-1.0000	0	0.3874	-0.1937	0
$\mathbf{U^1_2}$	1.0000	0.5811	0	1.0000	-0.5000	0	1.0000	0.5811	0	1.0000	-0.5000	0

Subspace S^3

$$\lambda_1 = 0.2482 \qquad \lambda_2 = 2.5074$$

$$\Psi_1 = \begin{bmatrix} 0.5835 \\ 1.0000 \\ 0.2917 \end{bmatrix} \qquad \Psi_2 = \begin{bmatrix} 1.0000 \\ 0.0194 \\ 0.5000 \end{bmatrix}$$

Table 3.5: C_{2v} deflection ordinates of mode shapes of subspace S^3

ϕ_i	1	2	3	4	5	6	7	8	9	10	11	12
$\mathbf{U^1_1}$	0.5835	0	1.0000	-0.5835	0.2917	0	-0.5835	0	1.0000	0.5835	-0.2917	0
$\mathbf{U^1_2}$	1.0000	0	0.0194	-1.0000	0.5000	0	-1.0000	0	0.0194	1.0000	-0.5000	0

Subspace S^4

$$\lambda_1 = 0.5624 \qquad \lambda_2 = 2.3710$$

$$\Psi_1 = \begin{bmatrix} -0.6832 \\ 1.0000 \\ 0.3416 \end{bmatrix} \quad \Psi_2 = \begin{bmatrix} -1.0000 \\ -0.7971 \\ 0.5000 \end{bmatrix}$$

Table 3.6: C_{2v} deflection ordinates of mode shapes of subspace S^4

ϕ_i	1	2	3	4	5	6	7	8	9	10	11	12
$\mathbf{U^1_1}$	-0.6832	1.0000	0	-0.6832	0	0.3416	0.6832	-1.0000	0	0.6832	0	0.3416
$\mathbf{U^1_2}$	-1.0000	-0.7971	0	-1.0000	0	0.5000	1.0000	0.7971	0	1.0000	0	0.5000

The eigenmodes for the plane frame for each subspace can now be sketched and are presented in Figure 3.9. From Figure *3.9 a-b* we observe that the eigenmodes for each subspace are in accordance with the basis vectors derived for each subspace. Further, we also notice that the eigenmode in each subspace has a particular type of symmetry. The eigenmodes of Subspace S^1 have two vertical planes of symmetry (x and y), that is, they have the full symmetry of the C_{2v} symmetry group. On the other hand, the eigenmodes for S^2 are C_2 symmetric. The eigenmodes for subspaces S^3 and S^4 have one vertical plane of symmetry, x and y, respectively. Therefore, these eigenmodes belong to the C_{1v} symmetry group.

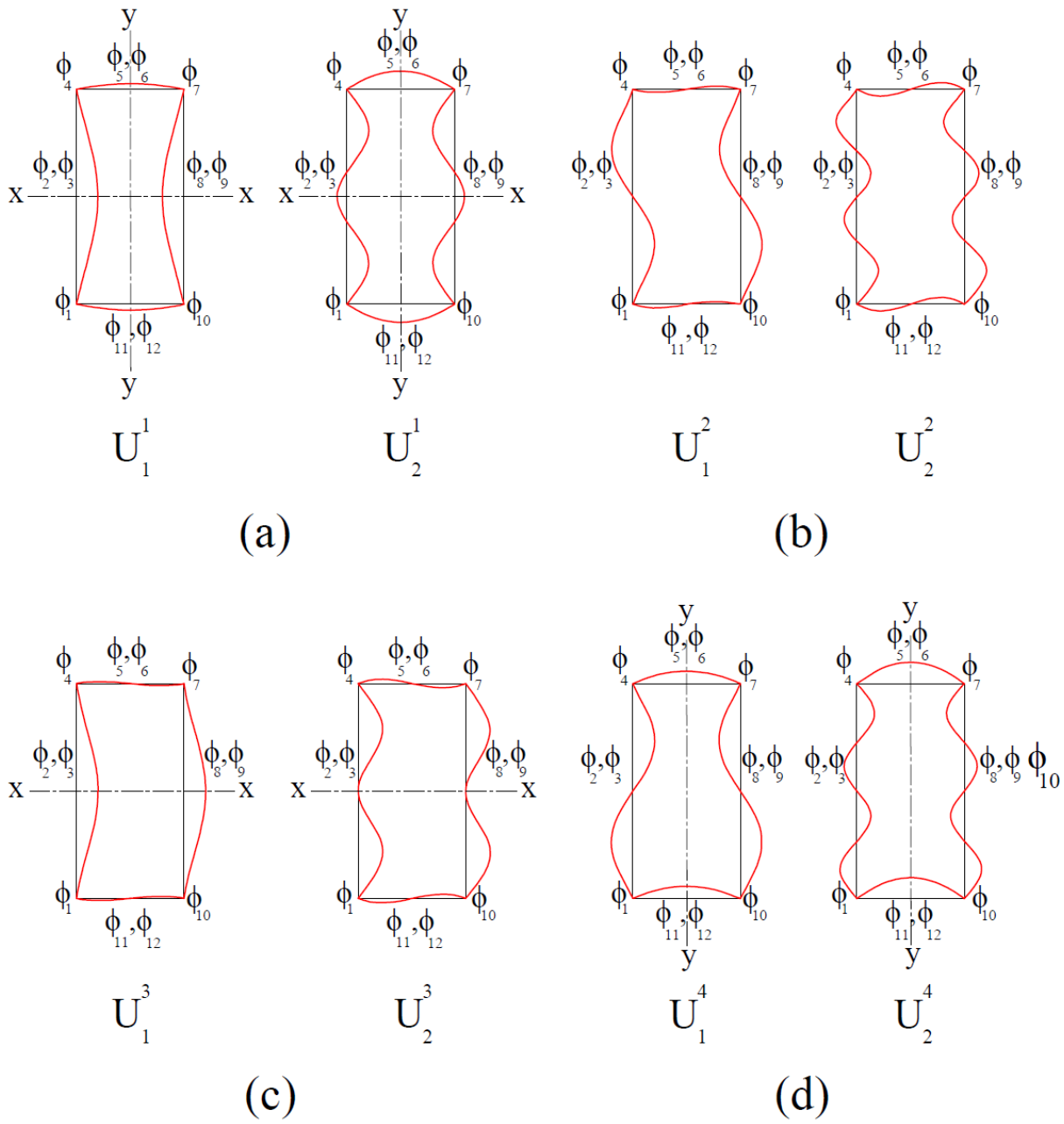

Figure 3.9: Buckling modes of C_{2v} numerical example: (a) subspace S^1; (b) subspace S^2; (c) subspace S^3; and (d) subspace S^4.

The computed eigenvalues and corresponding subspace and symmetry groups are summarized in Table 3.7. From Table *3.7*, we observe that the lowest eigenvalue is obtained from the subspace S^1, with eigenmodes that have the highest order of symmetry, that is, the C_{2v} symmetry group. On the other hand, the highest eigenvalue is obtained from subspace S^2, with eigenmodes with the lowest order of symmetry (subspace), that is, the C_2 symmetry group.

Table 3.7: C_{2v} Eigenvalues and corresponding symmetry groups

No	λ	Subspace	Symmetry Group
1	0.1763	S^1	C_{2v}
2	0.2482	S^3	C_{1v}
3	0.5624	S^4	C_{1v}
4	0.7351	S^2	C_2
5	1.5126	S^1	C_{2v}
6	2.3710	S^4	C_{1v}
7	2.5074	S^3	C_{1v}
8	3.2649	S^2	C_2

It is important to note that the eight-element model employed for the C_{2v} frame is only intended to serve as an example of the group theoretic method of buckling analysis. We would need to add more elements to create a model that would yield eigenvalues that were close to the true or analytical result. Alternatively, if we used the stability stiffness matrix given by Equation *4.1* of this study, only four elements would be necessary to yield accurate results. Such a model is presented in chapter four of this study.

3.2.2.3 Plane Frames with C_{4v} symmetry

We shall now use the group theoretic approach to analyse the buckling of plane frame which belongs to the C_{4v} symmetry group as shown in Figure *3.10*.

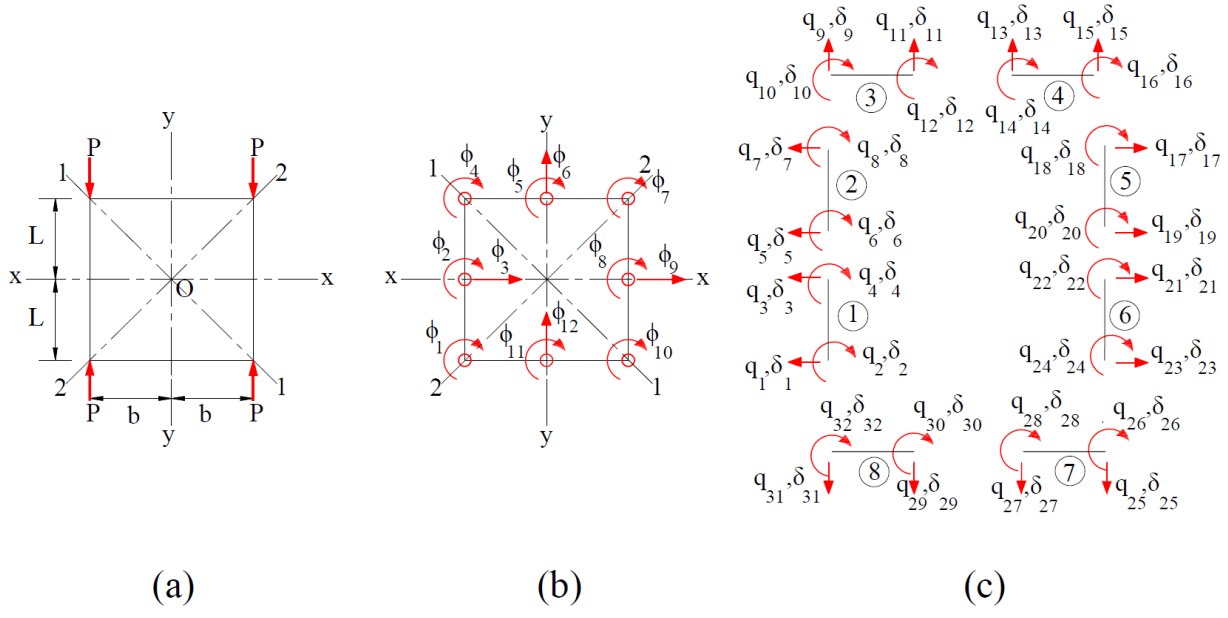

Figure 3.10: C_{4v} symmetric frame

This is the symmetry group of a square and the idempotents are (Zingoni, 1996; Zingoni, 2005b; Zingoni, 2014; Zingoni, 2015):

$$P^1 = \frac{1}{8}\left(e + C_4 + C_4^{-1} + C_2 + \sigma_x + \sigma_y + \sigma_1 + \sigma_2\right) \qquad (3.129)$$

$$P^2 = \frac{1}{8}\left(e + C_4 + C_4^{-1} + C_2 - \sigma_x - \sigma_y - \sigma_1 - \sigma_2\right) \qquad (3.130)$$

$$P^3 = \frac{1}{8}\left(e - C_4 - C_4^{-1} + C_2 + \sigma_x + \sigma_y - \sigma_1 - \sigma_2\right) \qquad (3.131)$$

$$P^4 = \frac{1}{8}\left(e - C_4 - C_4^{-1} + C_2 - \sigma_x - \sigma_y + \sigma_1 + \sigma_2\right) \qquad (3.132)$$

$$P^5 = \frac{1}{2}\left(e - C_2\right) = P^{5,1} + P^{5,1} \qquad (3.133)$$

$$P^{5,1} = \frac{1}{4}\left(e - C_2 + \sigma_1 - \sigma_2\right), \quad P^{5,2} = \frac{1}{4}\left(e - C_2 - \sigma_1 + \sigma_2\right) \qquad (3.134 - 3.135)$$

Alternatively

$$P^{5,1} = \frac{1}{4}\left(e - C_2 + \sigma_x - \sigma_y\right), \quad P^{5,2} = \frac{1}{4}\left(e - C_2 - \sigma_x + \sigma_y\right) \qquad (3.136 - 3.137)$$

For the symmetry group C_{4v}, Zingoni (2014) has presented the conceptual splitting of the idempotent P^5 of subspace S^5 into independent operators $P^{5,1}$ and $P^{5,2}$, as a means of decomposing the subspace S^5, into two identical subspaces, $S^{5,1}$ and $S^{5,2}$. To generate the symmetry adapted basis vectors for S^5 we only need to apply one of the idempotents given by $P^{5,1}$ or $P^{5,2}$, and we obtain one set of the double eigenvalues of S^5 from either $S^{5,1}$ or $S^{5,2}$. The eigenvalues in $S^{5,1}$ and $S^{5,2}$ are identical, however, their eigenvectors are orthogonal to each other.

To obtain symmetry adapted basis vectors for this frame, we apply each idempotent $P^k(k=1,2,3,4,5)$ of equations *3.129-3.132* and *3.134* to all the twelve positional functions $\phi_1, \phi_2, \phi_3, .., \phi_{12}$ shown in Figure *3.10 b*.

Subspace S^1

$$P^1\phi_1 = \frac{1}{8}\left(e + C_4 + C_4^{-1} + C_2 + \sigma_x + \sigma_y + \sigma_1 + \sigma_2\right)\phi_1$$

$$= \frac{1}{8}\left(\phi_1 + \phi_{10} + \phi_4 + \phi_7 - \phi_4 - \phi_{10} - \phi_7 - \phi_1\right) = P^1\phi_{10} = P^1\phi_4 = P^1\phi_7$$

$$= \frac{1}{8}\left(\phi_1 - \phi_1 + \phi_{10} - \phi_{10} + \phi_4 - \phi_4 + \phi_7 - \phi_7\right) = 0$$

$$P^1\phi_2 = \frac{1}{8}\left(e + C_4 + C_4^{-1} + C_2 + \sigma_x + \sigma_y + \sigma_1 + \sigma_2\right)\phi_2$$
$$= \frac{1}{8}\left(\phi_2 + \phi_{11} + \phi_5 + \phi_8 - \phi_2 - \phi_8 - \phi_5 - \phi_{11}\right) = P^1\phi_{11} = P^1\phi_5 = P^1\phi_8$$
$$= \frac{1}{8}\left(\phi_2 - \phi_2 + \phi_{11} - \phi_{11} + \phi_5 - \phi_5 + \phi_8 - \phi_8\right) = 0$$

$$P^1\phi_3 = \frac{1}{8}\left(e + C_4 + C_4^{-1} + C_2 + \sigma_x + \sigma_y + \sigma_1 + \sigma_2\right)\phi_3$$
$$= \frac{1}{8}\left(\phi_3 + \phi_{12} - \phi_6 - \phi_9 + \phi_3 - \phi_9 - \phi_6 + \phi_{12}\right) = P^1\phi_{12} = -P^1\phi_6 = -P^1\phi_9$$
$$= \frac{1}{8}\left(\phi_3 + \phi_3 + \phi_{12} + \phi_{12} - \phi_6 - \phi_6 - \phi_9 - \phi_9\right)$$
$$= \frac{1}{4}\left(\phi_3 + \phi_{12} - \phi_6 - \phi_9\right)$$

The basis vector of Subspace S^1

$$\Phi^1 = \phi_3 + \phi_{12} - \phi_6 - \phi_9 \qquad (3.138)$$

The basis vectors for the remaining four subspaces are similarly obtained, and they are as follows:

Subspace S^2

$$\Phi_1^2 = \phi_1 + \phi_{10} + \phi_4 + \phi_7, \quad \Phi_2^2 = \phi_2 + \phi_{11} + \phi_5 + \phi_8, \quad (3.139 - 3.140)$$

Subspace S^3

$$\Phi_1^3 = \phi_1 - \phi_{10} - \phi_4 + \phi_7, \quad \Phi_2^3 = \phi_3 - \phi_{12} + \phi_6 - \phi_9, \quad (3.141 - 3.142)$$

Subspace S^4

$$\Phi^4 = \phi_2 - \phi_{11} - \phi_5 + \phi_8 \qquad (3.143)$$

Subspace $S^{5,1}$

$$\Phi_1^{5,1} = \phi_1 - \phi_7 - \phi_4 + \phi_{10}, \quad \Phi_2^{5,1} = \phi_3 + \phi_9, \quad \Phi_3^{5,1} = \phi_5 - \phi_{11} \quad (3.144 - 3.145)$$

The derived basis vectors for each subspace are illustrated below in Figures *3.11 a-e*.

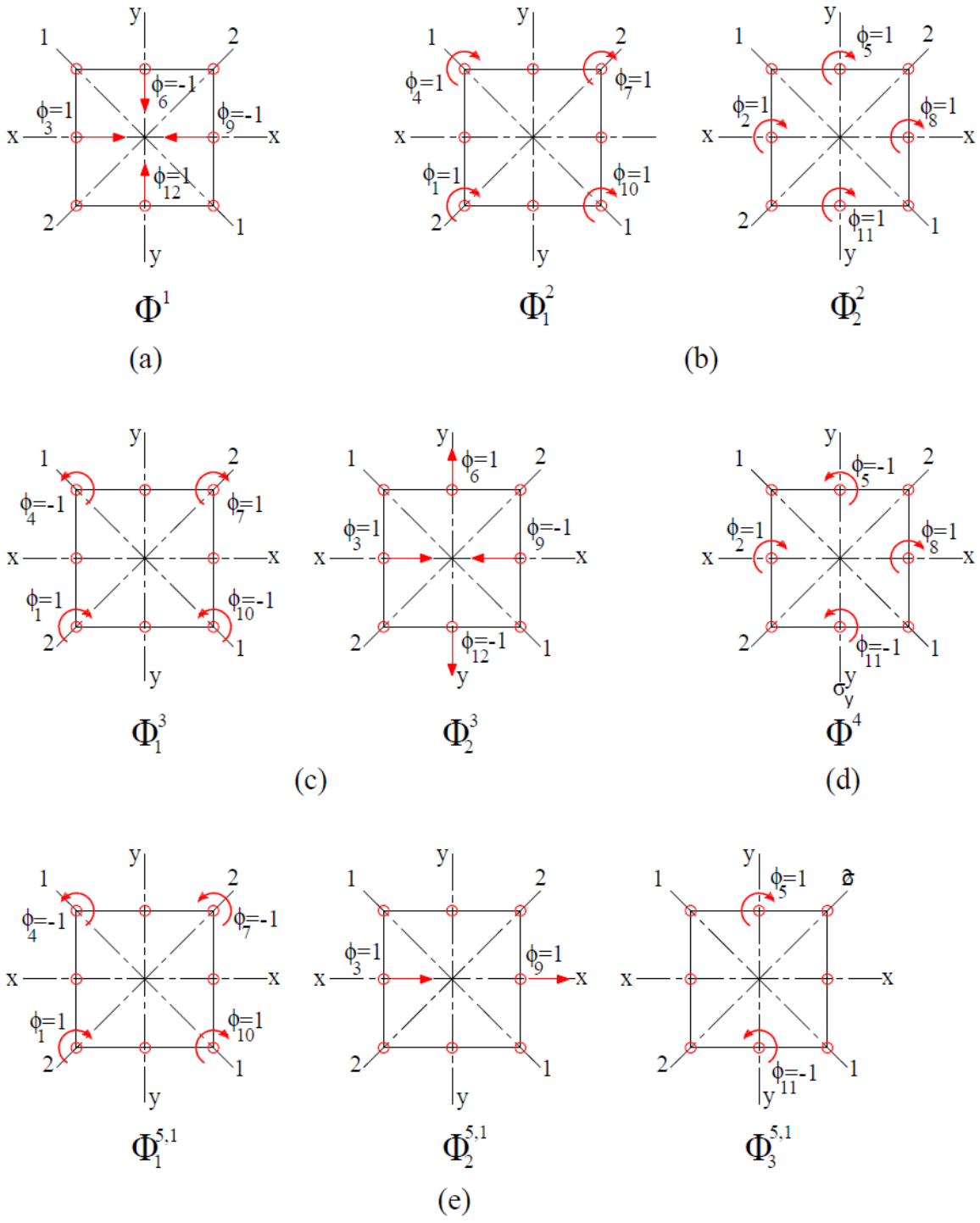

Figure 3.11: C_{4v} plane frame: unit moments and unit forces applied in accordance with the coordinates of the basis vectors: (a) subspace S^1; (b) subspace S^2; (c) subspace S^3; (d) subspace S^4; and (e) subspace $S^{5,1}$.

At this point, we proceed the conventional way and derive the transformation matrices for each of the eight elements shown in Figure 3.10 *b*. For this example, the transformation matrices are

identical to the transformation matrices for the C_{2v} example previously presented. Applying equation *3.6,* we obtain the element stiffness matrices in structure coordinates as:

$$[K_1]=\begin{matrix}\phi_1 & \phi_2 & \phi_3 l\end{matrix}\begin{bmatrix}4-4\lambda & 2+\lambda & -6+3\lambda\\ 2+\lambda & 4-4\lambda & -6+3\lambda\\ -6+3\lambda & -6+3\lambda & 12-36\lambda\end{bmatrix}\begin{matrix}\phi_1\\ \phi_2\\ \phi_3 l\end{matrix}$$

$$[K_2]=\begin{matrix}\phi_2 & \phi_3 l & \phi_4\end{matrix}\begin{bmatrix}4-4\lambda & 6-3\lambda & 2+\lambda\\ 6-3\lambda & 12-36\lambda & 6-3\lambda\\ 2+\lambda & 6-3\lambda & 4-4\lambda\end{bmatrix}\begin{matrix}\phi_2\\ \phi_3 l\\ \phi_4\end{matrix}$$

$$[K_3]=\begin{matrix}\phi_4 & \phi_5 & \phi_6 l\end{matrix}\begin{bmatrix}4-4\lambda & 2+\lambda & 6-3\lambda\\ 2+\lambda & 4-4\lambda & 6-3\lambda\\ 6-3\lambda & 6-3\lambda & 12-36\lambda\end{bmatrix}\begin{matrix}\phi_4\\ \phi_5\\ \phi_6 l\end{matrix}$$

$$[K_4]=\begin{matrix}\phi_5 & \phi_6 l & \phi_7\end{matrix}\begin{bmatrix}4-4\lambda & -6+3\lambda & 2+\lambda\\ -6+3\lambda & 12-36\lambda & -6+3\lambda\\ 2+\lambda & -6+3\lambda & 4-4\lambda\end{bmatrix}\begin{matrix}\phi_5\\ \phi_6 l\\ \phi_7\end{matrix}$$

$$[K_5]=\begin{matrix}\phi_7 & \phi_8 & \phi_9 l\end{matrix}\begin{bmatrix}4-4\lambda & 2+\lambda & 6-3\lambda\\ 2+\lambda & 4-4\lambda & 6-3\lambda\\ 6-3\lambda & 6-3\lambda & 12-36\lambda\end{bmatrix}\begin{matrix}\phi_7\\ \phi_8\\ \phi_9 l\end{matrix}$$

$$[K_6]=\begin{matrix}\phi_8 & \phi_9 l & \phi_{10}\end{matrix}\begin{bmatrix}4-4\lambda & -6+3\lambda & 2+\lambda\\ -6+3\lambda & 12-36\lambda & -6+3\lambda\\ 2+\lambda & -6+3\lambda & 4-4\lambda\end{bmatrix}\begin{matrix}\phi_8\\ \phi_9 l\\ \phi_{10}\end{matrix}$$

$$[K_7]=\begin{matrix}\phi_{10} & \phi_{11} & \phi_{12} l\end{matrix}\begin{bmatrix}4-4\lambda & 2+\lambda & -6+3\lambda\\ 2+\lambda & 4-4\lambda & -6+3\lambda\\ -6+3\lambda & -6+3\lambda & 12-36\lambda\end{bmatrix}\begin{matrix}\phi_{10}\\ \phi_{11}\\ \phi_{12} l\end{matrix}$$

$$[K_8]=\begin{matrix}\phi_1 & \phi_{11} & \phi_{12} l\end{matrix}\begin{bmatrix}4-4\lambda & 2+\lambda & 6-3\lambda\\ 2+\lambda & 4-4\lambda & 6-3\lambda\\ 6-3\lambda & 6-3\lambda & 12-36\lambda\end{bmatrix}\begin{matrix}\phi_1\\ \phi_{11}\\ \phi_{12} l\end{matrix}$$

To assemble the stiffness matrices for each subspace, we must first note that the conventional stiffness matrix for the frame shown in Figure *3.10 b* may be written down as $A_{i,j}$ (i = 1,2,3,….,12; j = 1,2,3,….,12), where, $A_{i,j}$ is the force at node i due to a unit displacement applied at node j. Therefore, the conventional stiffness matrix will be of the form:

$$A = A = \begin{bmatrix} a_{1,1} & a_{1,2} & a_{1,3} & . & . & . & a_{1,12} \\ a_{2,1} & a_{2,2} & a_{2,3} & . & . & . & a_{2,12} \\ . & . & & & & & . \\ . & . & & & & & . \\ . & . & & & & & . \\ . & . & & & & & . \\ a_{12,1} & a_{12,2} & a_{12,3} & . & . & . & a_{12,12} \end{bmatrix} \qquad (3.146)$$

For this problem subspaces S^1 and S^4 are one dimensional and therefore, the stiffness matrix $\boldsymbol{B}$, for each subspace will be of the form:

$$B = \left[b \right] \qquad (3.147)$$

Subspaces S^2 and S^3 are two dimensional and therefore the stiffness matrix $\boldsymbol{B}$ for each subspace will be of the form:

$$B = \begin{bmatrix} b_{1,1} & b_{1,2} \\ b_{2,1} & b_{2,2} \end{bmatrix} \qquad (3.148)$$

Subspace $S^{5,1}$ was obtained by decomposing the six-dimensional subspace S^5 into two identical three-dimensional subspaces. Subspace $S^{5,1}$ is therefore, of the form:

$$B = \begin{bmatrix} b_{1,1} & b_{1,2} & b_{1,3} \\ b_{2,1} & b_{2,2} & b_{2,3} \\ b_{3,1} & b_{3,2} & b_{3,3} \end{bmatrix} \qquad (3.149)$$

The coefficients of $\boldsymbol{B}$ for each subspace, can be obtained by superimposing the appropriate values of the conventional stiffness coefficients appearing in matrix A of equation *3.146* in accordance with the combinations of unit displacements of Φ_j appearing in Figure *3.11* for each subspace. The stiffness coefficients and stiffness matrices for each subspace are then:

Subspace S^1

$$b = a_{3,3} + a_{3,12} - a_{3,6} - a_{3,9} \qquad (3.150)$$
$$B^1 = \left[24 - 72\lambda \right]$$

Subspace S^2

$$b_{1,1} = a_{1,1} + a_{1,10} + a_{1,4} + a_{1,7}, \quad b_{1,2} = a_{1,2} + a_{1,11} + a_{1,5} + a_{1,8}, \qquad (3.151 - 3.152)$$
$$b_{2,1} = a_{2,1} + a_{2,10} + a_{2,4} + a_{2,7}, \quad b_{2,2} = a_{2,2} + a_{2,11} + a_{2,5} + a_{2,8}, \qquad (3.153 - 3.154)$$
$$B^2 = \begin{bmatrix} 8 - 8\lambda & 4 + 2\lambda \\ 4 + 2\lambda & 8 - 8\lambda \end{bmatrix}$$

Subspace S^3

$$b_{1,1} = a_{1,1} - a_{1,10} - a_{1,4} + a_{1,7}, \quad b_{1,2} = a_{1,3} - a_{1,12} + a_{1,6} - a_{1,9}, \qquad (3.155 - 3.156)$$
$$b_{2,1} = a_{3,1} - a_{3,10} - a_{3,4} + a_{3,7}, \quad b_{2,2} = a_{3,3} - a_{3,12} + a_{3,6} - a_{3,9}, \qquad (3.157 - 3.158)$$

$$B^3 = \begin{bmatrix} 8-8\lambda & -12+6\lambda \\ -12+6\lambda & 24-72\lambda \end{bmatrix}$$

Subspace S^4

$$b = a_{2,2} - a_{2,11} - a_{2,5} + a_{2,8}, \qquad (3.159)$$

$$B^4 = [8-8\lambda]$$

Subspace $S^{5,1}$

$$b_{1,1} = a_{1,1} - a_{1,7} - a_{1,4} + a_{1,10}, \quad b_{1,2} = a_{1,3} + a_{1,9}, \quad b_{1,3} = a_{1,5} - a_{1,11} \qquad (3.160-3.162)$$

$$b_{2,1} = a_{3,1} - a_{3,7} - a_{3,4} + a_{3,10}, \quad b_{2,2} = a_{3,3} + a_{3,9}, \quad b_{2,3} = a_{3,5} - a_{3,11}, \qquad (3.163-3.165)$$

$$b_{3,1} = a_{5,1} - a_{5,7} - a_{5,4} + a_{5,10}, \quad b_{3,2} = a_{5,3} + a_{5,9}, \quad b_{3,3} = a_{5,5} - a_{5,11} \qquad (3.166-3.168)$$

$$B^5 = \begin{bmatrix} 8-8\lambda & -6+3\lambda & -2-\lambda \\ -12+6\lambda & 24-72\lambda & 0 \\ -4-2\lambda & 0 & 8-8\lambda \end{bmatrix}$$

The conventional procedure for buckling analysis would require the evaluation of the determinant of a *12x12* stiffness matrix resulting in a twelfth-degree polynomial to obtain all the twelve eigenvalues of this problem. However, with the group theoretical approach, we only need to evaluate, at most, the determinant of a *3x3* stiffness matrix. Thus, by implementing the group theoretic approach, the computational effort required to evaluate all the eigenvalues of this problem is reduced. This is especially the case for repeating eigenvalues such as those for S^5, since with the group theoretic approach, the numerical ill conditioning due to repeating eigenvalues is avoided.

To obtain the eigenvalues λ and eigenvectors, Ψ we simply apply equation *3.9* and *3.10* respectively to the stiffness matrix for each subspace and obtain the eigenvalues and vectors as follows:

Subspace S^1

$$\lambda = \frac{1}{3} = 0.3333$$

$$\Psi = [1]$$

Table 3.8: C_{4v} deflection ordinates of mode shapes of subspace S^1

ϕ_i	1	2	3	4	5	6	7	8	9	10	11	12
$\mathbf{U^1}$	0	0	1.0000	0	0	-1.0000	0	0	-1.0000	0	0	1.0000

Subspace S^2

$\lambda_1 = 0.4 \qquad \lambda_2 = 2$

$\Psi_1 = \begin{bmatrix} -1 \\ 1 \end{bmatrix} \qquad \Psi_2 = \begin{bmatrix} 1 \\ 1 \end{bmatrix}$

Table 3.9: C_{4v} deflection ordinates of mode shapes of subspace S^2

ϕ_i	1	2	3	4	5	6	7	8	9	10	11	12
$\mathbf{U^2_1}$	-1.0000	1.0000	0	-1.0000	1.0000	0	-1.0000	1.0000	0	-1.0000	1.0000	0
$\mathbf{U^2_2}$	1.0000	1.0000	0	1.0000	1.0000	0	1.0000	1.0000	0	1.0000	1.0000	0

Subspace S^3

$\lambda_1 = 0.0829 \qquad \lambda_2 = 1.0727$

$\Psi_1 = \begin{bmatrix} -1.0000 \\ -0.6379 \end{bmatrix} \qquad \Psi_1 = \begin{bmatrix} -1.0000 \\ 0.1045 \end{bmatrix}$

Table 3.10: C_{4v} deflection ordinates of mode shapes of subspace S^3

ϕ_i	1	2	3	4	5	6	7	8	9	10	11	12
$\mathbf{U^3_1}$	-1.0000	0	-0.6379	1.0000	0	-0.6379	-1.0000	0	0.6379	1.0000	0	0.6379
$\mathbf{U^3_2}$	-1.0000	0	0.1045	1.0000	0	0.1045	-1.0000	0	-0.1045	1.0000	0	-0.1045

Subspace S^4

$\lambda_1 = 1.0000$

$\Psi = 1.0000$

Table 3.11: C_{4v} deflection ordinates of mode shapes of subspace S^4

ϕ_i	1	2	3	4	5	6	7	8	9	10	11	12
$\mathbf{U^4_1}$	0	1.0000	0	0	-1.0000	0	0	1.0000	0	0	-1.0000	0

Subspace S^5

$\lambda_1 = 0.1726 \qquad \lambda_2 = 0.6258 \qquad \lambda_3 = 1.6460$

$\Psi_1 = \begin{bmatrix} 1.0000 \\ 0.9473 \\ 0.6564 \end{bmatrix} \qquad \Psi_2 = \begin{bmatrix} -0.5700 \\ 0.2231 \\ -1.0000 \end{bmatrix} \qquad \Psi_3 = \begin{bmatrix} 0.7087 \\ -0.0159 \\ -1.0000 \end{bmatrix}$

Table 3.12: C_{4v} deflection ordinates of mode shapes of subspace $S^{5,1}$

ϕ_i	1	2	3	4	5	6	7	8	9	10	11	12
$\mathbf{U^{5,1}_1}$	1.0000	0	0.9473	-1.0000	0.6564	0	-1.0000	0	0.9473	1.0000	-0.6564	0
$\mathbf{U^{5,1}_2}$	-0.5700	0	0.2231	0.5700	-1.0000	0	0.5700	0	0.2231	-0.5700	1.0000	0
$\mathbf{U^{5,1}_3}$	0.7087	0	-0.0159	-0.7087	-1.0000	0	-0.7087	0	-0.0159	0.7087	1.0000	0

The eigenmodes for the plane frame for each subspace can now be sketched and are presented in Figure *3.12*.

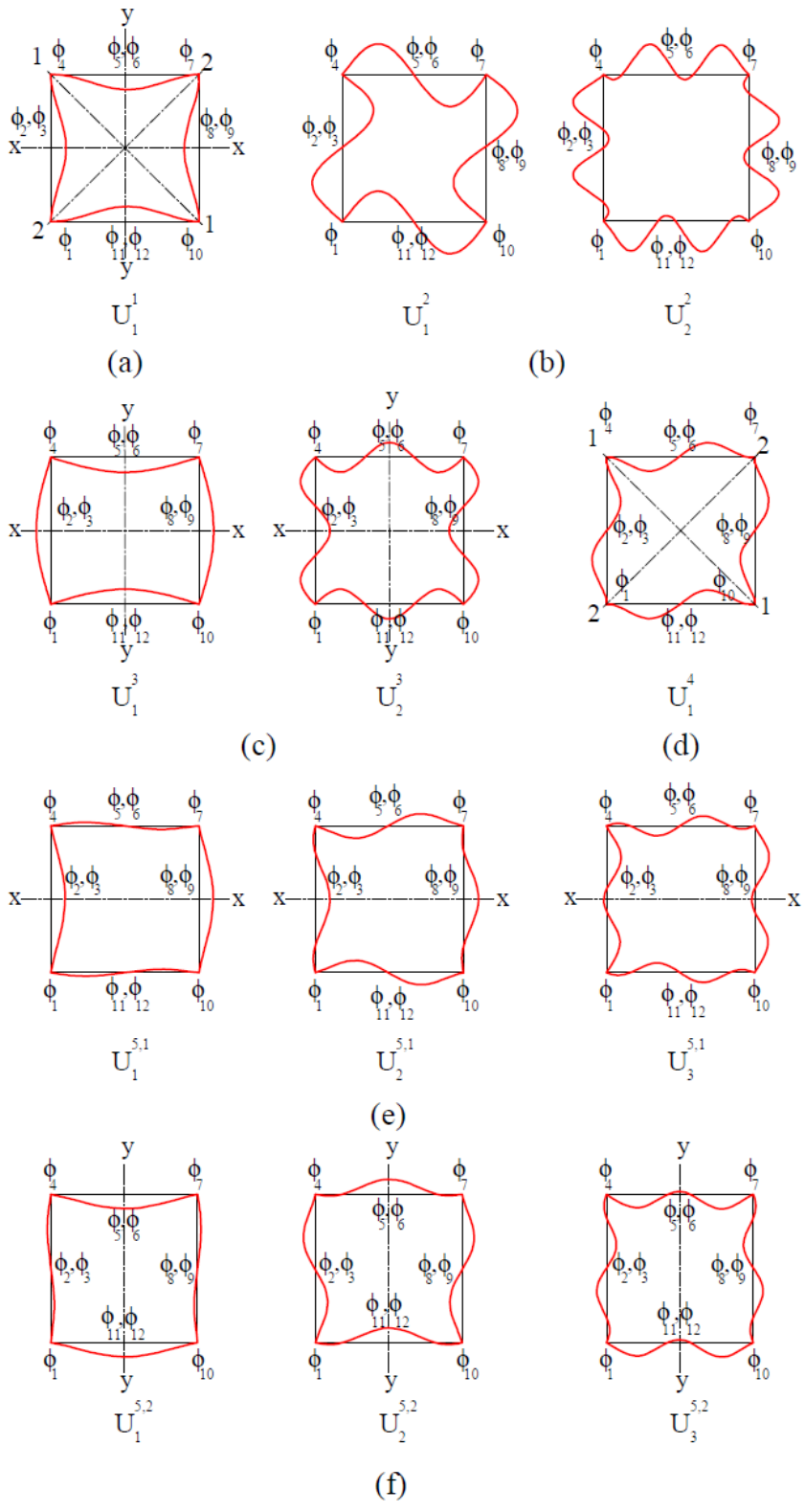

Figure 3.12: Buckling modes of C_{4v} numerical example: (a) subspace S^1; (b) subspace S^2; (c) subspace S^3; (d) subspace S^4; (e) subspace $S^{5;1}$; and (f) subspace $S^{5;2}$.

As in the previous numerical examples, the eigenmodes for each subspace are all in accordance with the basis vectors for each subspace. The eigenmode of $S,^{1}$ as shown in Figure *3.12 (a)* above, has the full symmetry of the C_{4v} Symmetry group. The eigenmodes of S^{2}, Figure 3.12 (b), are C_2 symmetric. Eigenmodes of Subspaces S^{3} and S^{4} in Figures *3.12 (c) and (d)*, have the same order of symmetry. They all have two vertical planes of symmetry and thus belong to the C_{2v} symmetry group. The subspace with repeating eigenvalues, subspace $S^{5,1}$ has eigenmodes with one plane of vertical symmetry and therefore belongs to the C_{1v} symmetry group.

The computed eigenvalues and corresponding subspace and symmetry groups are summarised in Table *3.13*, shown below.

Table 3.13: C_{4v} Eigenvalues and corresponding symmetry groups

No	λ	Subspace	Symmetry Group
1	0.0829	S^3	C_{2v}
2	0.1726, 0.1726	S^5	C_{1v}
3	0.3333	S^1	C_{4v}
4	0.4000	S^2	C_2
5	0.6258, 0.6258	S^5	C_{1v}
6	1.0000	S^4	C_{2v}
7	1.0727	S^3	C_{2v}
8	1.6460, 1.6460	S^5	C_{1v}
9	2.000	S^2	C_2

From Table *3.13*, we observe that the lowest eigenvalue is obtained from the subspace with eigenmodes that belong to the C_{2v} symmetry group. The eigenmode with the highest order of symmetry (C_{4v}), is not the eigenmode with the lowest eigenvalue, as was the case for the C_{2v} plane frame problem. However, as in the previous two examples, the eigenmode with the highest eigenvalue is from subspace whose eigenmodes are C_2 symmetric, which in this case is subspace S^{2}.

Finally, it is important to note that the eight-element model used for the C_{4v} frame is merely meant to function as an illustration of the buckling analysis using the group theoretic approach. To build a model that produced eigenvalues that were almost identical to the real or analytical result, we would need to add more elements. Alternatively, we might utilise the stability stiffness matrix provided by this study's Equation *4.1*, which would require only four elements to produce reliable findings. Such a model is presented in chapter four of this study.

3.2.2.4 Verification of Group Theoretic Results for C_{1v}

The group theoretic results were verified by using the conventional approach to compute the eigenvalues and eigenmodes for the C_{1v} numerical example presented earlier. We first assemble the global stiffness matrix A of equation *3.23* by summing together the element stiffness matrices as follows:

$$A = K_1 + K_2 + K_3 + K_4 + K_5 + K_6$$

$$A = \begin{bmatrix}
4-4\lambda & 2+\lambda & -6+3\lambda & 0 & 0 & 0 & 0 & 0 & 0 & 0 \\
2+\lambda & 8-8\lambda & 0 & 2+\lambda & 0 & 0 & 0 & 0 & 0 & 0 \\
-6+3\lambda & 0 & 24-72\lambda & 6-3\lambda & 0 & 0 & 0 & 0 & 0 & 0 \\
0 & 2+\lambda & 6-3\lambda & 8-4\lambda & 2 & 6 & 0 & 0 & 0 & 0 \\
0 & 0 & 0 & 2 & 8 & 0 & 2 & 0 & 0 & 0 \\
0 & 0 & 0 & 6 & 0 & 24 & -6 & 0 & 0 & 0 \\
0 & 0 & 0 & 0 & 2 & -6 & 8-4\lambda & 2+\lambda & 6-3\lambda & 0 \\
0 & 0 & 0 & 0 & 0 & 0 & 2+\lambda & 8-8\lambda & 0 & \lambda+2 \\
0 & 0 & 0 & 0 & 0 & 0 & 6-3\lambda & 0 & 24-72\lambda & -6+3\lambda \\
0 & 0 & 0 & 0 & 0 & 0 & 0 & \lambda+2 & -6+3\lambda & 4-4\lambda
\end{bmatrix}$$

The eigenvalues for the full space of the problem can then be obtained by applying equation *3.8* to matrix A and the resulting characteristic equation is:

$$0.125971\lambda^8 - 1.030164\lambda^7 + 3.348283\lambda^6 - 5.549683\lambda^5 + 5.022797\lambda^4 - 2.477969\lambda^3 + 0.634674\lambda^2 - 0.074742\lambda + 0.003185 = 0$$

From which we obtain using MATLAB the eigenvalues as:

$$\lambda = \begin{Bmatrix} 2.3832 \\ 2.0973 \\ 1.3359 \\ 1.1718 \\ 0.5034 \\ 0.4447 \\ 0.1331 \\ 0.1084 \end{Bmatrix}$$

These are the same eigenvalues obtained using the group theoretic approach presented earlier. Applying equation *3.10* to the full space yields the same eigenvectors for each eigenvalue as those obtained from the group theoretic approach.

3.2.2.5 Verification of Group Theoretic Results for C_{2v}

To verify the group theoretic results obtained for the C_{2v}, we simply use the conventional approach to compute the eigenvalues and eigenmodes. We first assemble the global stiffness matrix A of equation *3.91* by summing together the element stiffness matrices as follows:

$$A = K_1 + K_2 + K_3 + K_4 + K_5 + K_6 + K_7 + K_8$$

$$A = \begin{bmatrix}
12 - 4\lambda & \lambda + 2 & 3\lambda - 6 & 0 & 0 & 0 & 0 & 0 & 0 & 0 & 4 & 12 \\
\lambda + 2 & 8 - 8\lambda & 0 & \lambda + 2 & 0 & 0 & 0 & 0 & 0 & 0 & 0 & 0 \\
3\lambda - 6 & 0 & 24 - 72\lambda & 6 - 3\lambda & 0 & 0 & 0 & 0 & 0 & 0 & 0 & 0 \\
0 & \lambda + 2 & 6 - 3\lambda & 12 - 4\lambda & 4 & 12 & 0 & 0 & 0 & 0 & 0 & 0 \\
0 & 0 & 0 & 4 & 16 & 0 & 4 & 0 & 0 & 0 & 0 & 0 \\
0 & 0 & 0 & 12 & 0 & 48 & -12 & 0 & 0 & 0 & 0 & 0 \\
0 & 0 & 0 & 0 & 4 & -12 & 12 - 4\lambda & \lambda + 2 & 6 - 3\lambda & 0 & 0 & 0 \\
0 & 0 & 0 & 0 & 0 & 0 & \lambda + 2 & 8 - 8\lambda & 0 & \lambda + 2 & 0 & 0 \\
0 & 0 & 0 & 0 & 0 & 0 & 6 - 3\lambda & 0 & 24 - 72\lambda & 3\lambda - 6 & 0 & 0 \\
0 & 0 & 0 & 0 & 0 & 0 & 0 & \lambda + 2 & 3\lambda - 6 & 12 - 4\lambda & 4 & -12 \\
4 & 0 & 0 & 0 & 0 & 0 & 0 & 0 & 0 & 4 & 16 & 0 \\
12 & 0 & 0 & 0 & 0 & 0 & 0 & 0 & 0 & -12 & 0 & 48
\end{bmatrix}$$

The eigenvalues for the full space of the problem can be obtained by applying equation *3.8* to matrix A and the resulting characteristic equation is:

$$0.038698\lambda^8 - 0.440301\lambda^7 + 2.005511\lambda^6 - 4.695242\lambda^5 + 6.054998\lambda^4 - 4.317692\lambda^3 + 1.640726\lambda^2 - 0.300579\lambda + 0.020547 = 0$$

From which we obtain using MATLAB, the eigenvalues as:

$$\lambda = \begin{Bmatrix} 3.2649 \\ 2.5074 \\ 2.3710 \\ 1.5126 \\ 0.7351 \\ 0.5624 \\ 0.2482 \\ 0.1763 \end{Bmatrix}$$

These are the same eigenvalues obtained using the group theoretic approach earlier presented. Applying equation *3.10* to the full space yields the same eigenvectors for each eigenvalue as those obtained from the group theoretic approach.

3.2.2.6 Verification of Group Theoretic Results for C_{4v}

To verify the group theoretic results obtained for the C_{4v}, we simply use the conventional approach to compute the eigenvalues and eigenmodes. We first assemble the global stiffness matrix A of equation *3.146* by summing together the element stiffness matrices as follows:

$$A = K_1 + K_2 + K_3 + K_4 + K_5 + K_6 + K_7 + K_8$$

$$A = \begin{bmatrix}
8-8\lambda & \lambda+2 & 3\lambda-6 & 0 & 0 & 0 & 0 & 0 & 0 & 0 & 2+\lambda & 6-3\lambda \\
\lambda+2 & 8-8\lambda & 0 & \lambda+2 & 0 & 0 & 0 & 0 & 0 & 0 & 0 & 0 \\
3\lambda-6 & 0 & 24-72\lambda & 6-3\lambda & 0 & 0 & 0 & 0 & 0 & 0 & 0 & 0 \\
0 & \lambda+2 & 6-3\lambda & 8-8\lambda & 2+\lambda & 6-3\lambda & 0 & 0 & 0 & 0 & 0 & 0 \\
0 & 0 & 0 & 2+\lambda & 8-8\lambda & 0 & 2+\lambda & 0 & 0 & 0 & 0 & 0 \\
0 & 0 & 0 & 6-3\lambda & 0 & 24-72\lambda & -6+3\lambda & 0 & 0 & 0 & 0 & 0 \\
0 & 0 & 0 & 0 & 2+\lambda & 3\lambda-6 & 8-8\lambda & \lambda+2 & 6-3\lambda & 0 & 0 & 0 \\
0 & 0 & 0 & 0 & 0 & 0 & \lambda+2 & 8-8\lambda & 0 & \lambda+2 & 0 & 0 \\
0 & 0 & 0 & 0 & 0 & 0 & 6-3\lambda & 0 & 24-72\lambda & 3\lambda-6 & 0 & 0 \\
0 & 0 & 0 & 0 & 0 & 0 & 0 & \lambda+2 & 3\lambda-6 & 8-8\lambda & 2+\lambda & -6+3\lambda \\
2+\lambda & 0 & 0 & 0 & 0 & 0 & 0 & 0 & 0 & 2+\lambda & 8-8\lambda & 0 \\
6-3\lambda & 0 & 0 & 0 & 0 & 0 & 0 & 0 & 0 & -6+3\lambda & 0 & 24-72\lambda
\end{bmatrix}$$

The eigenvalues for the full space of the problem can be obtained by applying equation 3.*9* to matrix A and the resulting characteristic equation is:

$$\begin{Bmatrix} 0.034828517376 \\ -0.340545503232 \\ 1.44389573443584 \\ -3.494837716254720 \\ 5.353589855748096 \\ -5.442129648156672 \\ 3.745755719899546 \\ -1.749680549108122 \\ 0.547392306806784 \\ -0.111184221044736 \\ 0.013828720951296 \\ -0.000939309347635 \\ 0.000026091926323 \end{Bmatrix} \begin{bmatrix} \lambda^{12} & \lambda^{11} & \lambda^{10} & \lambda^{9} & \lambda^{8} & \lambda^{7} & \lambda^{6} & \lambda^{5} & \lambda^{4} & \lambda^{3} & \lambda^{2} & \lambda & 1 \end{bmatrix} = 0$$

From which we obtain using MATLAB the eigenvalues as:

$$\lambda = \begin{Bmatrix} 2.0000 \\ 1.6460 \\ 1.6460 \\ 1.0727 \\ 1.0000 \\ 0.6258 \\ 0.6258 \\ 0.4000 \\ 0.3333 \\ 0.1726 \\ 0.1726 \\ 0.0829 \end{Bmatrix}$$

These are the same eigenvalues obtained using the group theoretic approach presented earlier. Applying equation 3.*10* to the full space yields the same eigenvectors for each eigenvalue as those obtained from the group theoretic approach.

3.2.3 Imperfect structures

The method proposed above can also be used for the analysis of plane frames with symmetric imperfections. These imperfections can then be transformed into initial equivalent bending

moments, and a second order elastic analysis would have to be carried out. Now that the problem is no longer an eigenvalue problem, the results obtained, for example for deflections, in each subspace would have to be summed up to obtain the deflection for the full space of the problem (Zingoni et al., 1994). The buckling load would then be defined as the load level at which deflections become infinite on the load displacement curve without any load increment (Vaart, 1965).

For cases where the imperfections are not symmetric The Load Excitation Method proposed in Section 3.3.1 of this study can be used.

3.3 Plotting Equilibrium Paths

Linear eigenvalue buckling analysis does not provide information about the post buckling behaviour of a structure, especially truss structures and lattice domes. A post buckling analysis can be carried out by tracing the bifurcated paths, using path switching algorithms. However, it is still possible to trace bifurcated paths without using path switching algorithms. This can be done by using either superimposed buckling modes or load excitation to trace bifurcated equilibrium paths using the Riks method in *FEM* software such as Abaqus. The Nlgeom tab has to be selected in Abaqus in order for the nonlinear effects of large deformations and displacements to be accounted for.

3.3.1 The Load Excitation Method

In the load excitation method, we introduce a small load imperfection that excites a particular bifurcation path, which we seek to trace. To show how this method can be employed, we shall return to the problem of tracing the equilibrium paths of the star dome shown in Figure *2.12* of this study. The star dome shown in Figure *2.12* was modelled in Abaqus using *24* truss linear line elements of type *T3D2*. Lee and Han (2012) also used truss elements in their study.

To excite a particular bifurcation path, to the star dome with C_{6v} loading, we introduce an additional load. This additional load is a load imperfection with a symmetry characteristic that is the same as the deformation pattern of the dome on the bifurcated path. The imperfection load patterns are shown in Table *3.14* with reference to Figures *2.12* and *3.13*.

Table 3.14: Star Dome Load Imperfection

Joint	C_{6v} Load	C_{3v} Load	C_{2v} Load	C_{1v} Load
1	0.5			
2	1	γ_1		γ_3
3	1		γ_2	
4	1	γ_1	γ_2	
5	1			
6	1	γ_1	γ_2	γ_3
7	1		γ_2	γ_3

To trace the C_{6v} primary equilibrium, the imperfection load parameters γ_1, γ_2 and γ_3 are set as zero, and an elastic nonlinear analysis is carried out in Abaqus. To trace the C_{3v}, γ_2 and γ_3 are set to zero. Similarly, for C_{2v} and C_{1v} paths, we set $\gamma_1 = \gamma_3 = 0$ and $\gamma_1 = \gamma_2 = 0$ respectively. The sketches of the load patterns are shown in the figure below.

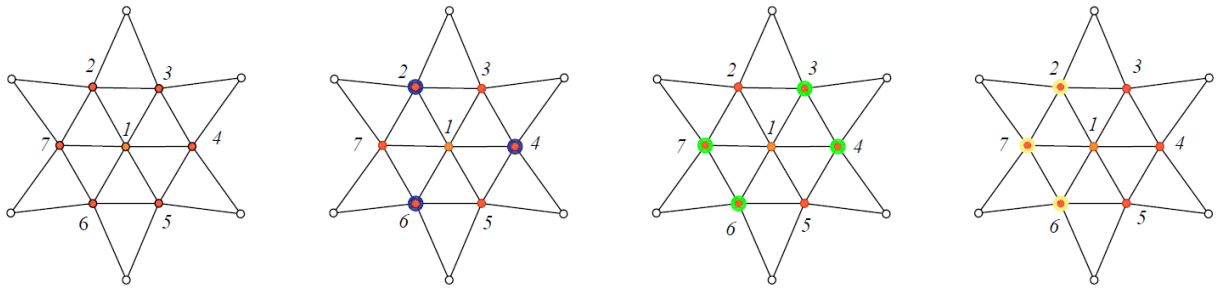

(a) C_{6v} (b) C_{3v} (c) C_{2v} (d) C_{1v}

Figure 3.13: Star Load Imperfection patterns

An important question that arises, is how to select the correct magnitude of γ to excite a specific bifurcation path. First, it is important to note that each type of imperfection load pattern, for sufficiently small values of γ, produces a specific type of bifurcation path and symmetry deformation pattern of the structure. A sensitivity analysis has to be carried out for different values of γ, the value of γ that results in the maximum bifurcation load is the value of γ that produces the bifurcation path that approaches the 'true' bifurcation path. This is evaluated by two factors: the type of bifurcation path and the symmetry of the deformation. This is a consequence of the *Resonance of symmetry*. The worst imperfection pattern for a symmetric structure displays symmetric characteristics by inheriting the symmetry of the critical eigenvectors at a critical point.

It is this inheritance, that is referred to as Resonance of symmetry (Ikeda & Murota, 2010). The figures below show the results of the sensitivity analysis for each load imperfection case.

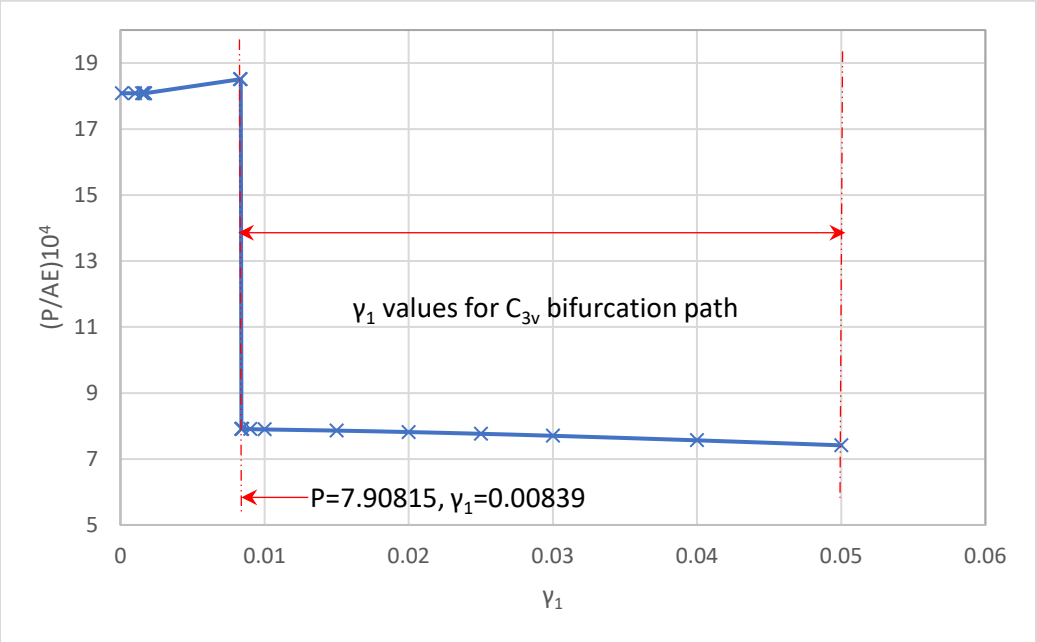

Figure 3.14: C_{3v} Sensitivity analysis

For the values of γ highlighted in Figures *3.14*, *3.15*, and *3.16*, the deformation pattern of the dome was C_{3v}, C_{2v} and C_{1v} respectively. Thus, it is within this range of γ that the bifurcation load is to be determined.

A comparison of the equilibrium paths obtained by Lee and Han (2012) with those obtained in the current study is shown in Figure *3.17*.

As can be seen from Figure *3.17* above, there is good agreement between the results obtained by Lee and Han (2012) using a path switching algorithm and the current study using the Load excitation method. Table *3.15* presents the results obtained for the Limit point (LP_1) load, and for the three Bifurcation point loads (BP_1, BP_2 and BP_3) in the current and previous studies.

From Table *3.15*, the results obtained from the load excitation method are in good agreement with the results obtained by using path switching algorithms. From the results presented in Figure *3.17* and Table *3.15*, the load excitation method can be used to trace bifurcated paths.

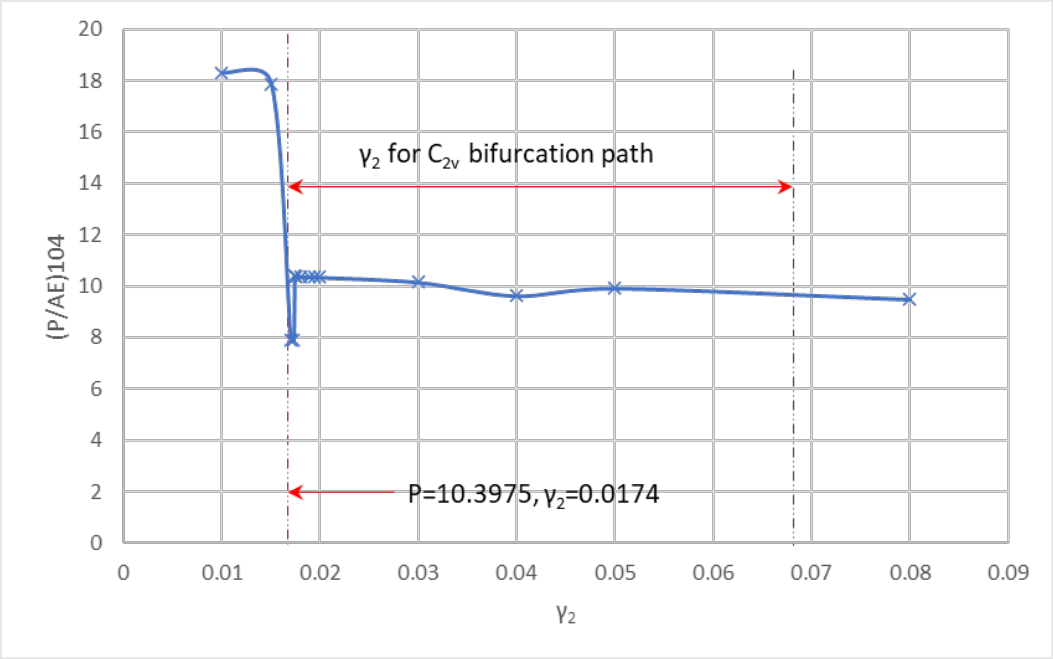

Figure 3.15: C_{2v} Sensitivity Analysis

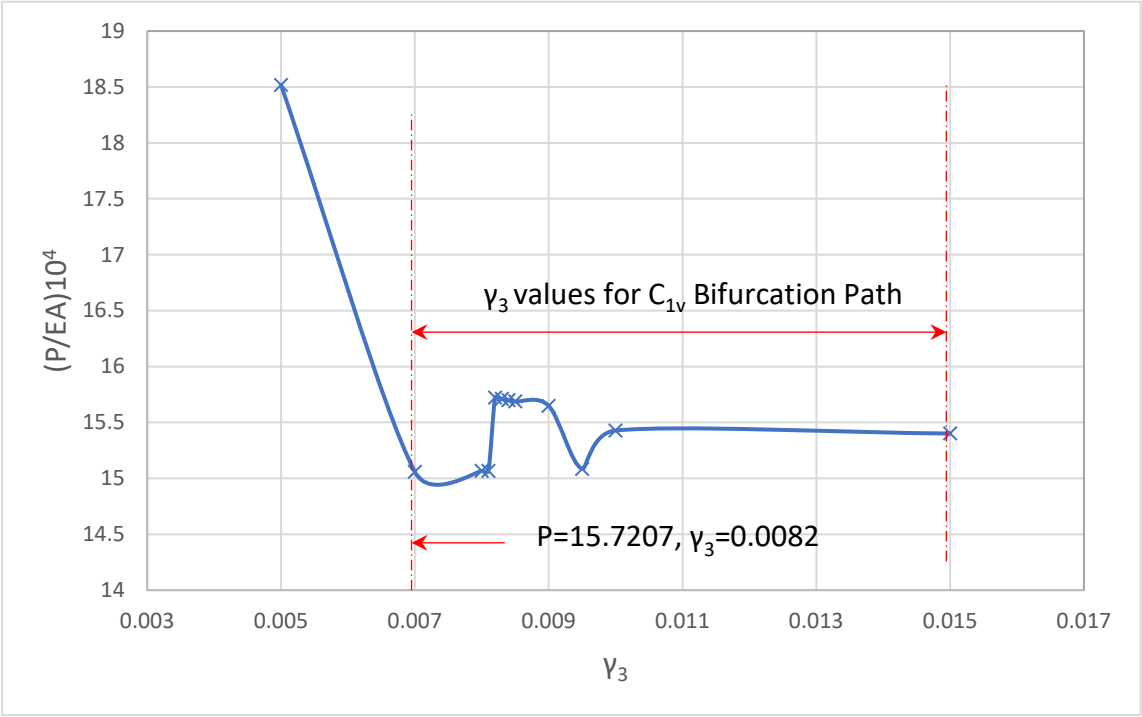

Figure 3.16:C_{1v} Sensitivity Analysis

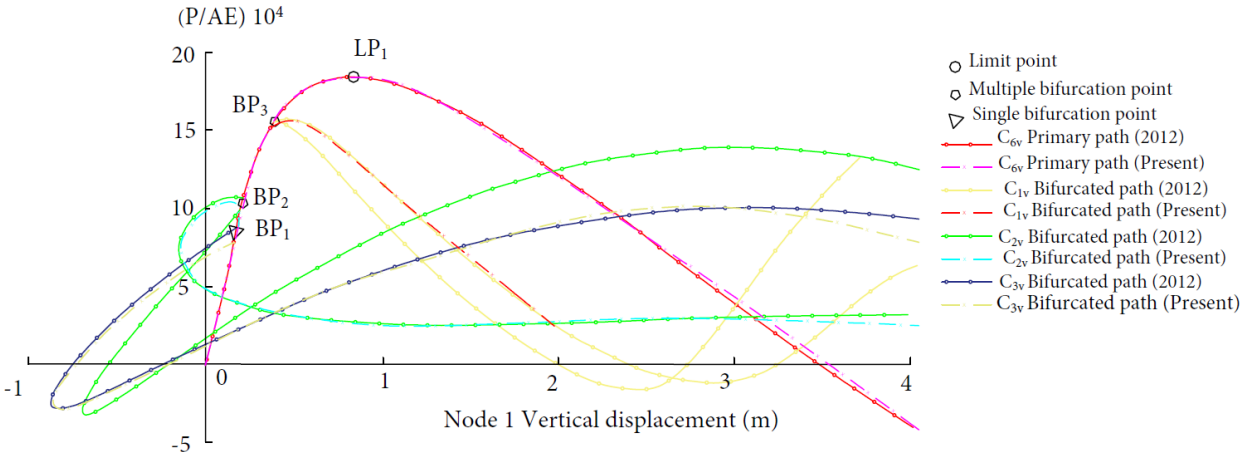

Figure 3.17: Star Dome Bifurcation Paths by Load Excitation Method

Table 3.15: Star Dome Load Parameters at Critical Points

	BP_1	BP_2	BP_3	LP_1
Current	7.908	10.398	15.721	18.683
Lee and Han (2012)	8.700	10.282	15.662	18.420
Crisfield (1997)	8.680	10.260	15.670	18.40
Fujii and Choong (1992)	8.689	10.267	15.606	-

3.3.2 The method of superimposed eigenmodes

In cases where the structure is modelled with beam elements, linear eigenvalue analysis can be carried out to obtain eigenmodes for each bifurcation load. The eigenmode for a particular bifurcation load is then superimposed on the geometry of the structure. The Riks method is then used to trace the bifurcated path in Abaqus, as described for the load excitation method.

As in the previous method, each type of imperfection geometry pattern produces a specific type of bifurcation path and deformation pattern of the structure, for sufficiently small values of the imperfection. Thus, the appropriate magnitude of the imperfection parameter is selected based on how close the load at which the bifurcation path emerges from the primary path is to that predicted from the linear eigenvalue analysis, the type of bifurcation path, and the symmetry pattern of the deformation of the structure. The type of bifurcation path refers to whether, a path is stable or unstable. The method of superimposed eigenmodes was used to trace the bifurcation paths for the space frame dome shown in Figure *2.28*, and they are in good agreement with those obtained by Lee and Han (2012) as shown in Figure *3.18*.

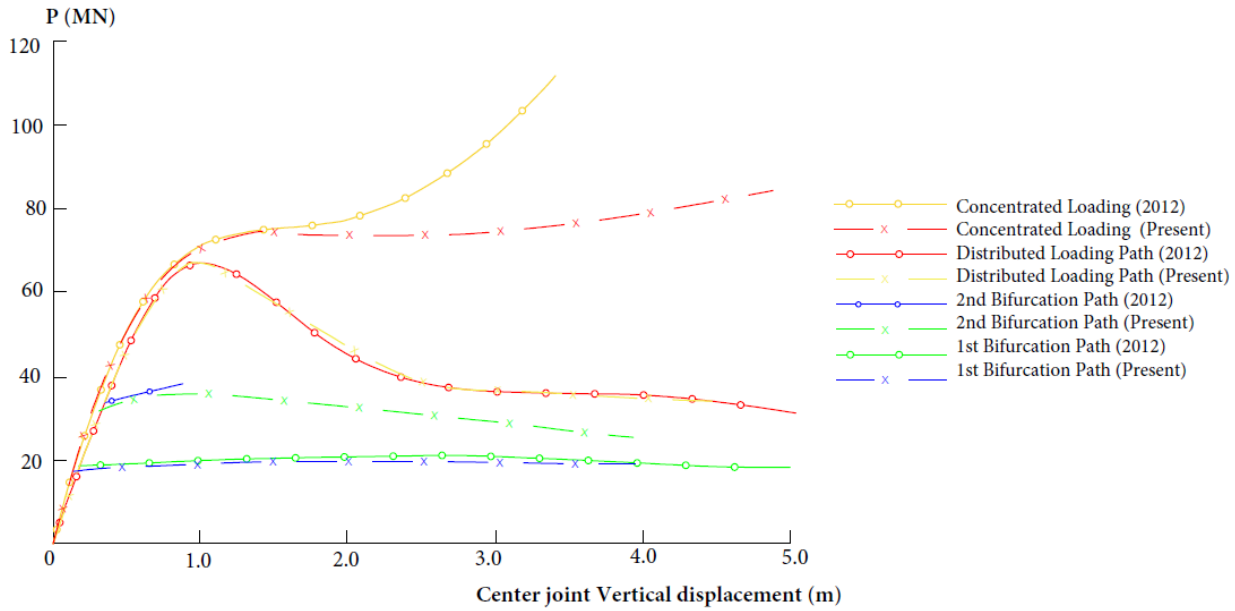

Figure 3.18: Space frame dome equilibrium and bifurcation paths by method of superimposed eigenmodes

The results of the sensitivity analysis carried out for the first bifurcation path are shown in Figure *3.19*. From the linear eigenvalue analysis carried out in this study, the eigenmodes at the first and second buckling loads were C_6 and C_{1v} symmetric, respectively. The dome was created in Abaqus using linear beam line elements of type *B31* elements. The geometric nonlinear analysis using the Riks method showed that the deformation pattern of the dome was C_{6v} symmetric on the primary path (Distributed load) in Figure *3.19*. When the sensitivity analysis was carried out it was observed that at γ=*0.0001*, the deformation pattern of the Dome was C_{6v} symmetric, thus we notice that the bifurcation path (BP1,γ=*0.0001*) is similar to that of the primary path. When the value of γ is increased to *0.001*, *0.01* and *0.1* the deformation pattern of the Dome was C_6 symmetric. Notice that at γ=0.001, the highest bifurcation load is produced with the C_6 deformation pattern of the dome.

Lastly, the method of superimposed eigenmodes was also used to trace the bifurcation of a plane frame. The plane frame shown in Figure *3.20 (a)* has been previously studied to validate proposed bifurcation path tracing methods (Fujii & Ramm, 1997; Lee & Han, 2012). In both cited studies, a path switching algorithm was used to trace the bifurcated paths. In this study, the method of superimposed eigenmodes was used. The model in Abaqus used *B21* type elements.

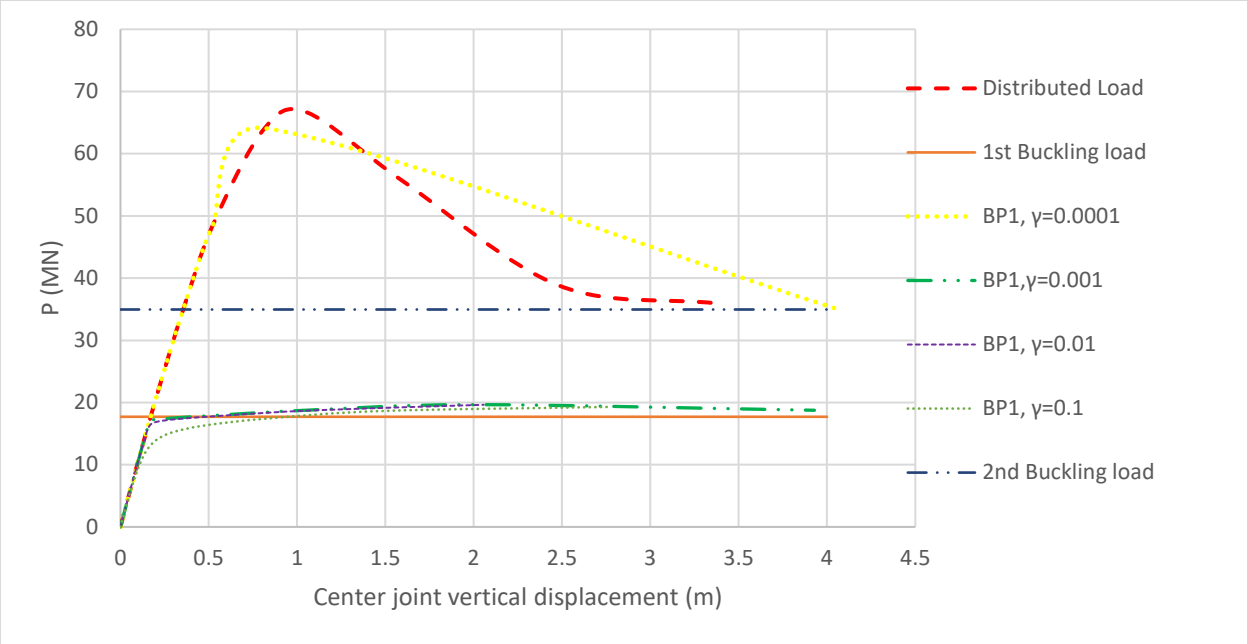

Figure 3.19: Space frame dome 1st bifurcation path sensitivity analysis

The eigenmodes produced from a linear eigenvalue analysis in Abaqus are shown in Figure *3.20 (b)*, *(c)*, *(d),* and *(e)*. The traced primary and bifurcated paths produced in this study and the two other cited studies are shown in Figure *3.21* below. Again, the results produced from the method of superimposed eigenmodes compare very well with results produced using path switching algorithms. It should be noted, however, that the results produced by Fujii and Ramm (1997) are more conservative than the results produced by Lee and Han (2012), and in this study. Notwithstanding, the method of superimposed eigenmodes was able to accurately trace the bifurcated paths, provided an appropriate magnitude of the imperfection parameter was used. Again, in this case, a sensitivity analysis was carried out and the results are summarised in Figure *3.22* for the third bifurcation point for bifurcation path *BP3,* shown in Figure *3.21*. From Figure 3.22, it can be seen that as the imperfection parameter reduces in magnitude from *0.8*, to a value below 0.09, the shape of the bifurcation path is no longer smooth as the other curves. To clearly observe that at $\gamma=0.09$, we obtain the correct third bifurcation path, we need to plot a curve of the imperfection parameter against the bifurcation load as shown in Figure *3.23*. Then we must note the values of γ that produce similar bifurcation paths and, in addition, a deformation pattern of the frame as shown in Figure *3.20 (d).* Again, it becomes clear that at $\gamma=0.09$, we obtain the correct third bifurcation path.

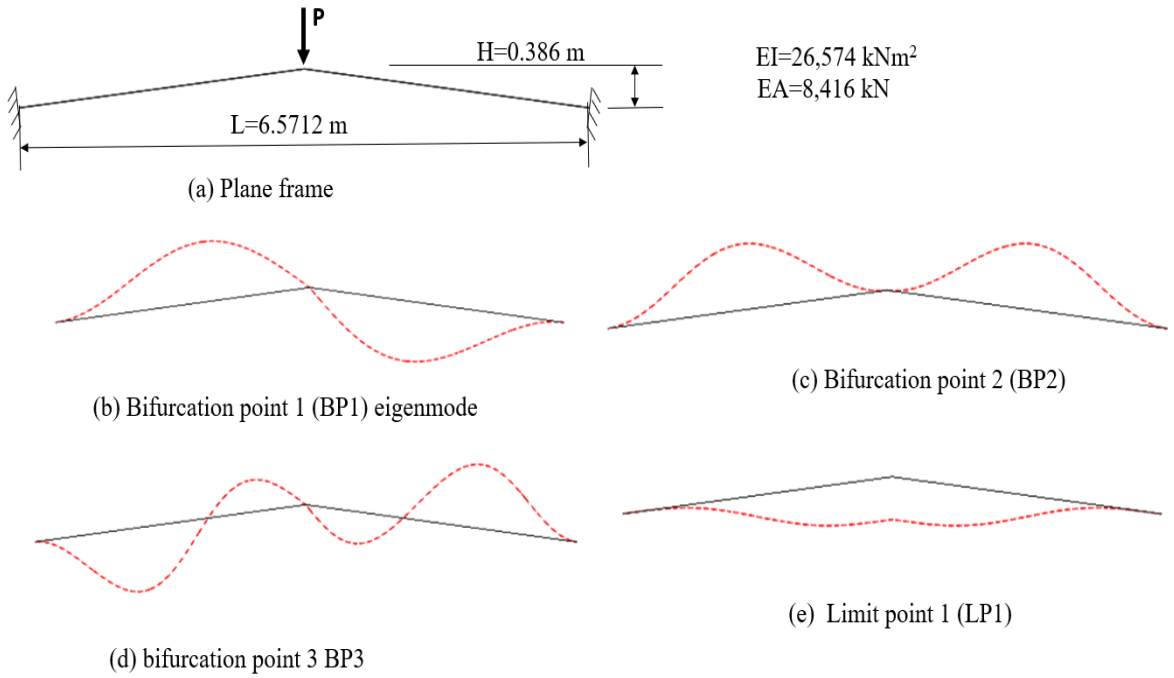

Figure 3.20: Plane frame and Eigenmodes

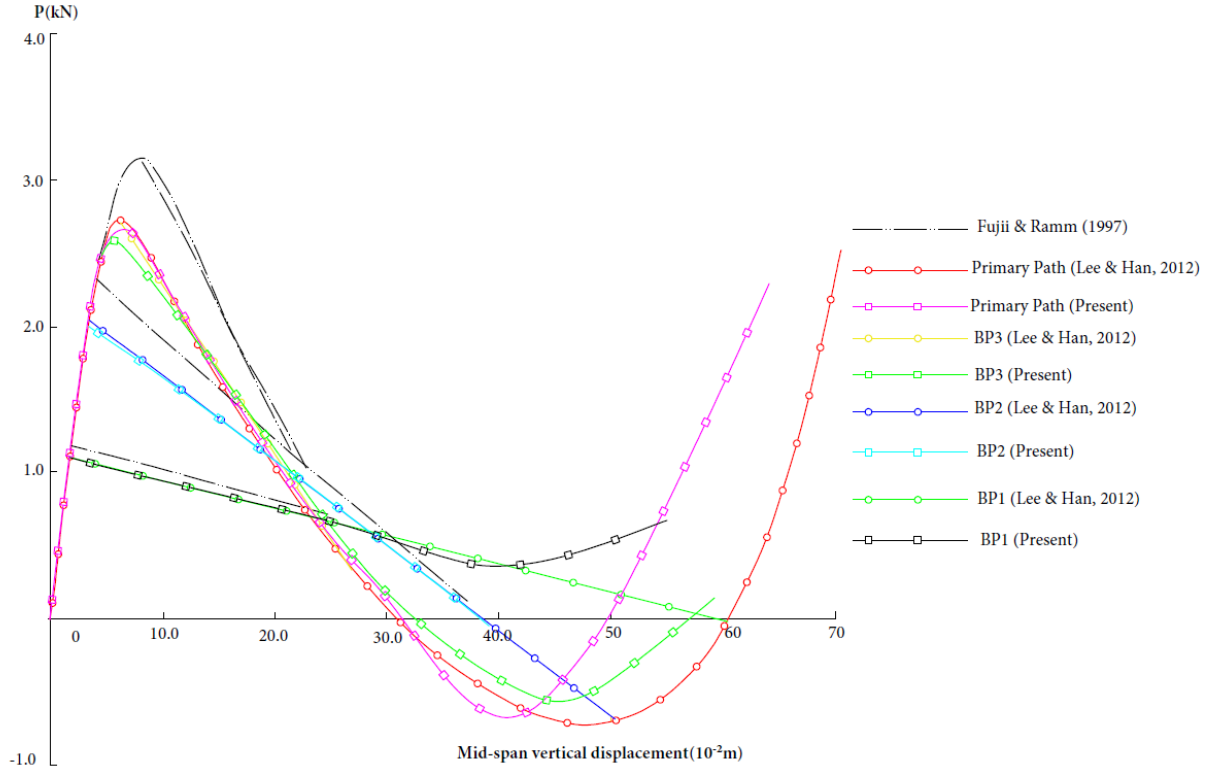

Figure 3.21: Plane Frame, equilibrium paths

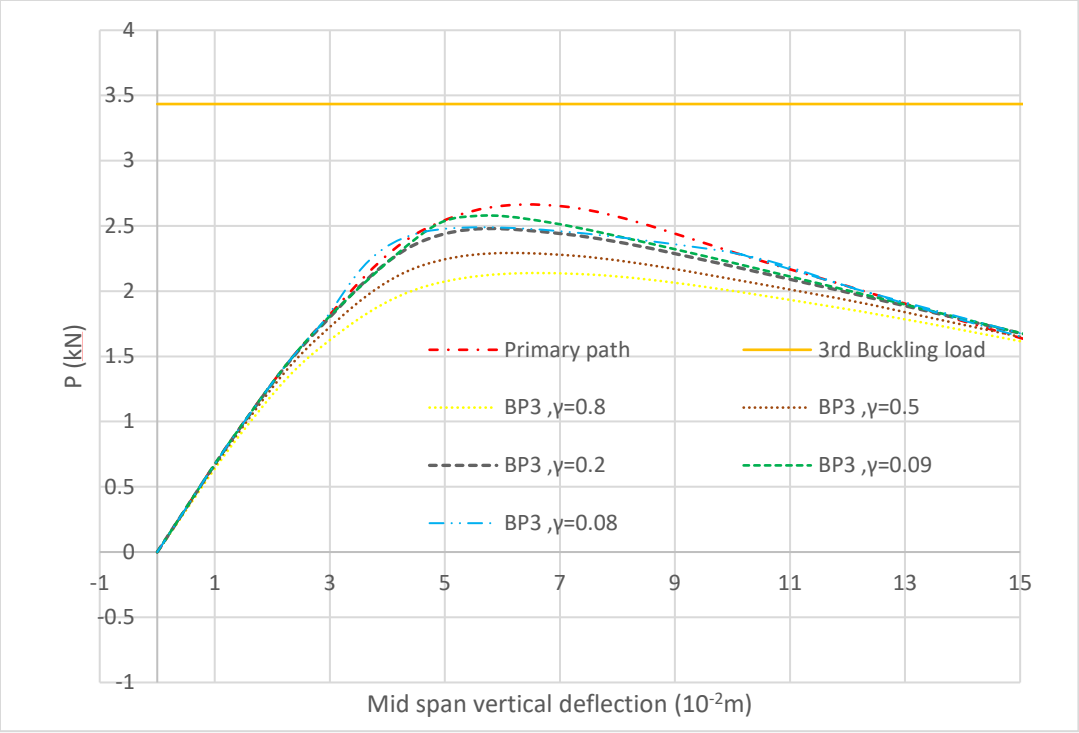

Figure 3.22: BP3 Sensitivity Analysis

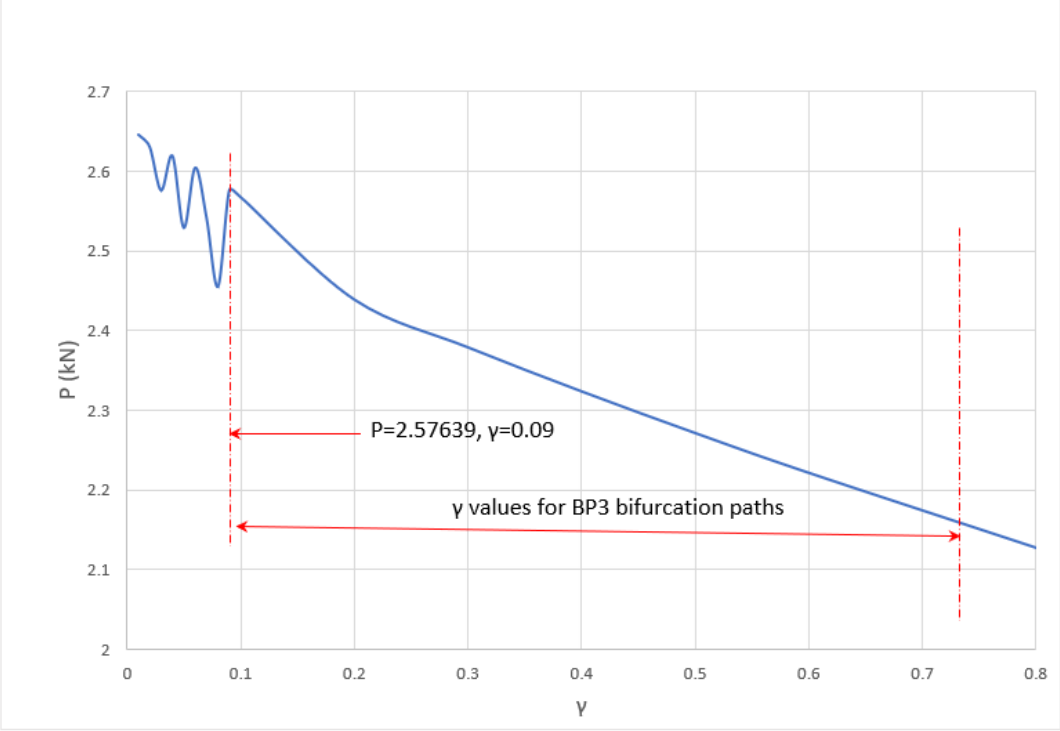

Figure 3.23: BP3 Sensitivity analysis, γ values

3.4 Summary and concluding remarks

In this chapter, the methods that were used for the analysis of the symmetric frames studied in this research are presented. The group theoretic approach to buckling using the matrix stiffness method was proposed, and examples were provided. In addition, the method was validated using the conventional matrix stiffness method. It was demonstrated that by using this approach, the computational effort required to compute the eigenvalues and eigenvectors is reduced. For example, for the C_{4v} problem presented in this chapter, a *12x12* stiffness matrix was required to compute the *12* eigenvalues using the conventional approach, while for the group theoretic approach, only five independent symmetry adapted stiffness matrices of at most a size of 3x3 were required to compute the *12* eigenvalues.

For the analysis of flexible structures such as lattice domes and space trusses, a load excitation method was proposed for the determination of buckling loads and the tracing of post buckling paths. In this analysis, a conventional second order analysis of a structure is carried out; however, a load imperfection with a symmetry characteristic that is the same as the deformation pattern of the dome on the bifurcated path was introduced. By adjusting the magnitude of the imperfection, the buckling load is determined, and the post buckling path is traced using the Riks method.

Finally, the method used to trace the post buckling paths of space frames studied in this research was presented. In this method, a linear eigenvalue analysis is carried out to obtain eigenmodes for each bifurcation load. The eigenmode for a particular bifurcation load is then superimposed on the geometry of the structure. The Riks method is then used to trace the bifurcated path in Abaqus, as described for the load excitation method.

Chapter 4

4. Influence of symmetry on the stability behaviour of C_{nv} plane symmetric frames

4.1 Introduction

In this part of this study, we attempt to establish the influence of symmetry on the stability behaviour of C_{nv} symmetric frames of the type shown in Figure *1.1*. Plane frames symmetric to seven point-group symmetries were investigated, and these are: C_{2v}, C_{3v}, C_{4v}, C_{5v}, C_{6v} and C_{8v}. Some of the results reported in this chapter were presented at the Eighth International Conference on Structural Engineering, Mechanics and Computation (Kaluba & Zingoni, 2022).

In this part of the study, each frame except for the C_{8v} frame was first studied using the slope deflection method to obtain analytical results. These analytical results were subsequently used to validate *FEMs* created in the software Abaqus.

As stated in Chapter two of this study, symmetric structures display repeating eigenvalues, which result in numerical ill conditioning when computing eigenvalues. Therefore, the group-theoretic approach was applied to the conventional slope deflection method when computing eigenvalues. This was the same approach that was used for the group-theoretical matrix stiffness method outlined in Chapter *3* of this study. However, here the element stiffness matrix was not defined by equation 3.4.

To implement the slope deflection method in the stability analysis of plane frames, we shall use a beam-column element subject to an axial load P and a set of loads $[q]$, as shown in Figure *4.1 (a)* and with corresponding displacements $[\delta]$ as shown in Figure *4.1(b)*.

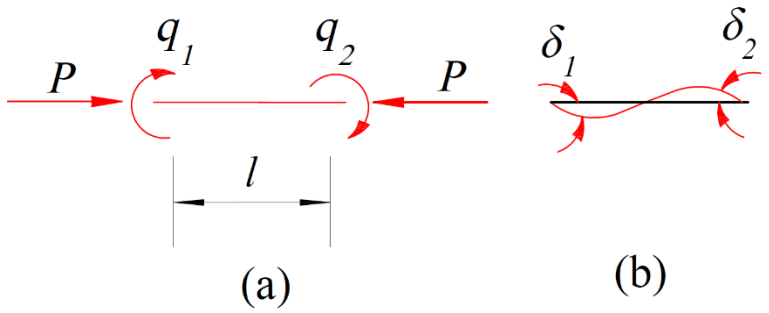

Figure 4.1: Beam column element

The element stiffness matrix for the element shown in Figure *4.1* member was defined as (Bažant & Luigi 2010):

$$[k] = \frac{EI}{l}\begin{bmatrix} s & sc \\ sc & s \end{bmatrix} \qquad (4.1)$$

where,

$$s = \frac{\lambda(\sin\lambda - \lambda\cos\lambda)}{2 - 2\cos\lambda - \lambda\sin\lambda} \qquad (4.2)$$

$$c = \frac{\lambda - \sin\lambda}{\sin\lambda - \lambda\cos\lambda} \qquad (4.3)$$

$$\lambda = l\sqrt{\frac{P}{EI}} \qquad (4.4)$$

with: P as the axial load in the beam element; l the length of the beam element; EI the flexural rigidity of the beam element; and λ the critical load parameter.

The assumptions used to derive the stiffness matrix given by Equation *4.1* are the same as those used to derive the stiffness matrix defined by Equation *3.4*. However, for Equation *4.1*, the elastic curve is assumed to be a trigonometric curve rather than a cubic curve. In addition, only rotational displacements are considered for Equation *4.1*. It can easily be observed that if we only consider rotational displacements, the stiffness matrices given by Equations *3.1* and *4.1* are the same if we neglect the second order terms of the Taylor series expansion s and sc of Equation *4.1*:

$$s = 4 - \frac{2\pi^2}{15}\left(\frac{P}{P_E}\right) - \frac{11\pi^4}{6300}\left(\frac{P}{P^E}\right)^2 - .....$$

$$sc = 2 + \frac{\pi^2}{30}\left(\frac{P}{P_E}\right) + \frac{13\pi^4}{12600}\left(\frac{P}{P^E}\right)^2 + ...$$

where P and P_E are the applied load and Euler buckling loads respectively. It is also easy to see that if there is no axial force (i.e. P=0), the values of the parameters s and c reduce to: $s=4$ and $c=1/2$.

The buckling load was found by setting the determinant of the frame stiffness matrix equal to zero.

$$|K| = 0 \qquad (4.5)$$

$$|B| = 0 \qquad (4.6)$$

where: K is the stiffness matrix of the frame and B is the symmetry adapted stiffness matrix.

The resulting simplified trigonometric equation from Equation *4.6* was then solved in the software Matlab to obtain the first fifty eigenvalues. The eigenvectors for the first fifty eigenvalues were then computed by substituting the computed eigenvalues into the stiffness matrix for the full space Equation *4.7*.

$$[K]\{\phi\} = 0 \qquad (4.7)$$

where ϕ is the eigenvector.

Once the analytical results were obtained, they were then used to validate the FEMs in Abaqus. These FEMs were then used to study the effects of different symmetric configurations on buckling behaviour. The models were created from a circular hollow section with an inner diameter of *40 mm*, a thickness of *6 mm*, a length of *2 m*, a modulus of elasticity of *200 GPa,* and a Poisson's ratio of *0.3*. Two-node linear *B21* elements were used in the model, and mesh refinement was validated using results obtained from the analytical analysis.

4.2 C_{2v} Plane Frame

We begin by considering the influence of symmetry on the buckling behaviour of a C_{2v} symmetric frame as shown in Figure *4.2 (a)* below.

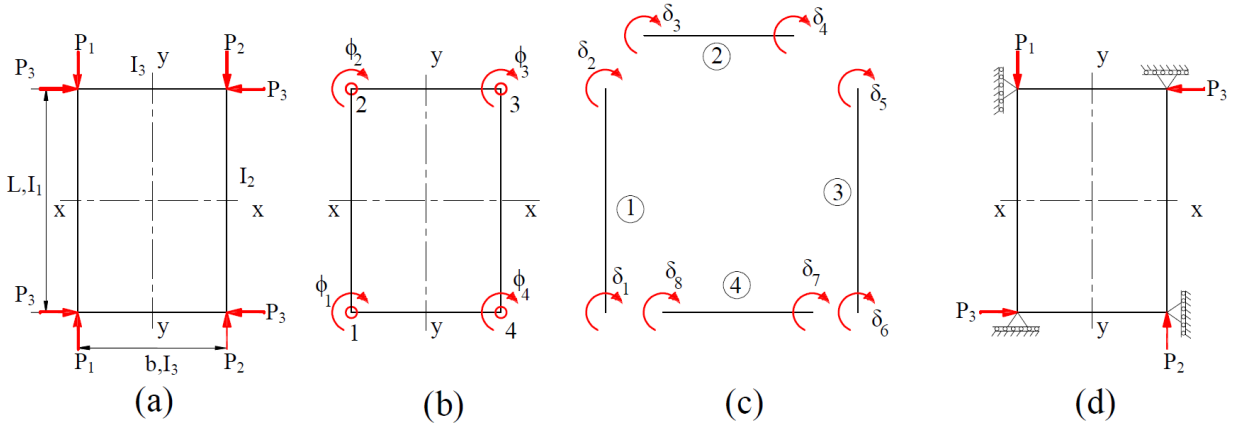

Figure 4.2: C_{2v} Frame Model

We can obtain the symmetry adapted basis vectors for the frame shown in Figure *4.2 (b)* by applying idempotent equations *3.75-3.78* to the positional vectors in Figure *4.2 (b)* as outlined in Section *3.2.2.2* of this study. The symmetry adapted basis vectors for the four subspaces of the problem are:

$$\Phi_1^1 = \phi_1 - \phi_2 + \phi_3 - \phi_4 \qquad (4.8)$$

$$\Phi_1^2 = \phi_1 + \phi_2 + \phi_3 + \phi_4 \qquad (4.9)$$

$$\Phi_1^3 = \phi_1 - \phi_2 - \phi_3 + \phi_4 \qquad (4.10)$$

$$\Phi_1^4 = \phi_1 + \phi_2 - \phi_3 - \phi_4 \qquad (4.11)$$

The sketches of these basis vectors are shown in Figure *4.3,* and the symmetries for the basis vectors are summarised in Table *4.1*. To identify the symmetry pattern of each subspace, unit moments must be applied in accordance with the coordinates of the basis vectors, as shown in Table *4.1*.

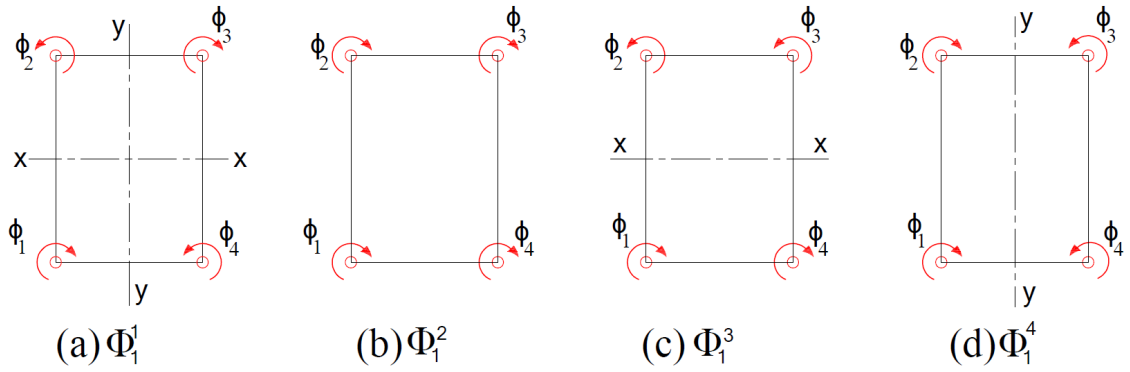

Figure 4.3: C_{2v} symmetry adapted basis vectors

Table 4.1: C_{2v} Basis vector symmetries

Figure 4.2	Subspace	Symmetry Group	order (*n*)	Group index (*m/n*)	Applied unit moments
(a)	S^1	C_{2v}	4	1	$\phi_1 = \phi_3 = 1, \quad \phi_2 = \phi_4 = -1$
(b)	S^2	C_2	2	2	$\phi_1 = \phi_2 = \phi_3 = \phi_4 = 1,$
(c)	S^3	C^x_{1v}	2	2	$\phi_1 = \phi_4 = 1, \quad \phi_2 = \phi_3 = -1$
(d)	S^4	C^y_{1v}	2	2	$\phi_1 = \phi_2 = 1, \quad \phi_3 = \phi_4 = -1$

4.2.1 Buckling behaviour of C_{2v} symmetric frame (Loading)

In this section, we seek to study the buckling behaviour of a plane frame with C_{2v} stiffness and C_{2v} loading or C_{1v} loading. That is, for all load arrangements, the stiffness was as follows: $I_1=I_2=I_3$. The load arrangements were summarised in Table *4.2*.

Table 4.2: C_{2v} Frame load arrangements

C_{2v} ($\gamma_1=P_3/P_1$) values, with $P_2=P_1$	0	1	1/2	1/3	1/4	1/5	1/6	1/7	1/8	1/9	1/10
C_{1v} γ_2 (P_2/P_1) values, with $P_3=0$	-	1	2	3	4	5	6	7	8	-	-

First, let us obtain analytical solutions for this buckling problem using a symmetry adapted slope deflection method. The approach outlined in Section *3.2* of this study is used. First, the frame is divided into four elements, as shown in Figure *4.2 (c),* and the transformation matrices for each element are:

$$[D_1]=\begin{matrix}\phi_1 & \phi_2\end{matrix}\begin{bmatrix}1 & 0\\ 0 & 1\end{bmatrix}\begin{matrix}\delta_1\\ \delta_2\end{matrix} \qquad [D_2]=\begin{matrix}\phi_2 & \phi_3\end{matrix}\begin{bmatrix}1 & 0\\ 0 & 1\end{bmatrix}\begin{matrix}\delta_3\\ \delta_4\end{matrix} \qquad [D_3]=\begin{matrix}\phi_3 & \phi_4\end{matrix}\begin{bmatrix}1 & 0\\ 0 & 1\end{bmatrix}\begin{matrix}\delta_5\\ \delta_6\end{matrix} \qquad [D_4]=\begin{matrix}\phi_4 & \phi_1\end{matrix}\begin{bmatrix}1 & 0\\ 0 & 1\end{bmatrix}\begin{matrix}\delta_7\\ \delta_8\end{matrix}$$

For the case of C_{2v} (γ_1=0) loading and C_{2v} stiffness, the element stiffness matrices of the C_{2v} frame ($b=l/2$) shown in Figure *4.2* (b) are obtained by applying Equation *3.6,* and these are:

$$[K_1]=\begin{matrix}\phi_1 & \phi_2\end{matrix}\begin{bmatrix}s & sc\\ sc & s\end{bmatrix}\begin{matrix}\phi_1\\ \phi_2\end{matrix} \qquad [K_2]=\begin{matrix}\phi_2 & \phi_3\end{matrix}\begin{bmatrix}8 & 4\\ 4 & 8\end{bmatrix}\begin{matrix}\phi_2\\ \phi_3\end{matrix} \qquad [K_3]=\begin{matrix}\phi_3 & \phi_4\end{matrix}\begin{bmatrix}s & sc\\ sc & s\end{bmatrix}\begin{matrix}\phi_3\\ \phi_4\end{matrix} \qquad [K_4]=\begin{matrix}\phi_4 & \phi_1\end{matrix}\begin{bmatrix}8 & 4\\ 4 & 8\end{bmatrix}\begin{matrix}\phi_4\\ \phi_1\end{matrix}$$

The global stiffness matrix is then given as:

$$A=K_1+K_2+K_3+K_4=\frac{EI}{L}\begin{bmatrix}s+8 & sc & 0 & 4\\ sc & s+8 & 4 & 0\\ 0 & 4 & s+8 & sc\\ 4 & 0 & sc & s+8\end{bmatrix} \qquad (4.12)$$

The stability functions s and c are as previously defined in Equations *4.2* and *4.3*.

The coefficients of $\boldsymbol{B}$ for each subspace can be obtained by superimposing the appropriate values of the conventional stiffness coefficients appearing in matrix $\boldsymbol{A}$ of equation *4.12* in accordance with the combinations of basis vectors of Φ_j appearing in Figure *4.2* for each subspace. The stiffness matrices for each subspace are then:

Subspace S^1

$$\begin{aligned}B^1 &= a_{11}-a_{12}+a_{13}-a_{14}\\ &=(s+8)-sc+0-4\\ &=s-sc+4\\ &=s(1-c)+4\\ |B^1| &= s(1-c)+4=0\end{aligned}$$

Solving this trigonometric equation in Matlab, we find the first five eigenvalues, as shown in Table *4.3*.

Solving the eigenvectors for each eigenvalue using the full space solution equation *4.7*, shows that for each eigenvalue, the eigenvector is C_{2v} symmetric. For example, for $\lambda_1=4.5779$, the stability

functions are now: *s=-0.2537* and *c=-14.7658*. Substituting equation *4.12* into equation *4.7,* we obtain:

$$\begin{bmatrix} 7.7463 & 3.7461 & 0 & 4.0000 \\ 3.7461 & 7.7463 & 4.0000 & 0 \\ 0 & 4.0000 & 7.7463 & 3.7461 \\ 4.0000 & 0 & 3.7461 & 7.7463 \end{bmatrix} \begin{Bmatrix} \phi_1 \\ \phi_2 \\ \phi_3 \\ \phi_4 \end{Bmatrix} = \begin{Bmatrix} 0 \\ 0 \\ 0 \\ 0 \end{Bmatrix}$$

Solving the above equation using Matlab we obtain:

$$\begin{Bmatrix} \phi_1 \\ \phi_2 \\ \phi_3 \\ \phi_4 \end{Bmatrix} = \begin{Bmatrix} -0.5000 \\ 0.5000 \\ -0.5000 \\ 0.5000 \end{Bmatrix}$$

The eigenvalues and eigenvectors obtained from the analytical analysis for S^I are summarised in Table *4.3* below.

Table 4.3: C_{2v} plane frame: subspace S^I eigenvalues and eigenvectors

λ_n	ϕ_1	ϕ_2	ϕ_3	ϕ_4
4.5779	-0.5	0.5	-0.5	0.5
10.1740	-0.5	0.5	-0.5	0.5
16.1923	-0.5	0.5	-0.5	0.5
22.3454	-0.5	0.5	-0.5	0.5

The eigenvectors shown in Table *4.3* are all consistent with C_{2v} symmetric eigenmodes. The classification of the symmetry of the eigenmodes is based on the positional displacements at the set of *n-vertices* of the frame, and in the above problem, it is based on the set of four positional displacements for each eigenvalue as shown in Table *4.3*. This suffices to classify the symmetry of the eigenmode. This is because for a plane figure, it is not possible for the positional displacements at any other set of *n* positions to contradict those obtained from the classification based on the *n-vertices* positional displacements. For example, if the set of positional displacements at the vertices of a rectangle is C_{2v}, any other four sets of positional displacements at a set of locations forming a rectangle cannot be of C_{1v} or any other C_{nv} or C_n symmetry. The only exception is for a totally asymmetric mode belonging to the C_1 symmetry group. Furthermore,

the stability functions of Equations *4.2* and *4.3* assume a trigonometric elastic curve, and thus only four elements for the above problem are sufficient to obtain accurate results.

Subspace S^2

$$B^2 = a_{11} + a_{12} + a_{13} + a_{14}$$
$$B^2 = (s+8) + sc + 0 + 4$$
$$= s + sc + 12$$
$$\left|B^2\right| = s + sc + 12 = 0$$

Solving for eigenvalues and eigenvectors for each eigenvalue using the full space solution equation *4.7* shows that for each eigenvalue, the eigenmode is C_2 symmetric. The eigenvalues and eigenvectors obtained from the analytical analysis for S^2 are summarised in Table *4.4* below.

Table 4.4: C_{2v} plane frame: subspace S^2 eigenvalues and eigenvectors

λ_n	ϕ_1	ϕ_2	ϕ_3	ϕ_4
7.9440	0.5	0.5	0.5	0.5
13.8773	0.5	0.5	0.5	0.5
19.8841	0.5	0.5	0.5	0.5
25.9721	0.5	0.5	0.5	0.5

Subspace S^3

$$B^3 = a_{11} - a_{12} - a_{13} + a_{14}$$
$$B^3 = (s+8) - sc + 0 + 4$$
$$= s - sc + 12$$
$$\left|B^3\right| = s - sc + 12 = 0$$

Solving the for eigenvalue and eigenvector for each eigenvalue using the full space solution *4.7* shows that for each eigenvalue, the eigenmode is $C^x{}_{1v}$ symmetric. The results for the first five eigenvalue and respective eigenvectors are shown in Table *4.5*.

Table 4.5: C_{2v} plane frame: subspace S^3 eigenvalues and eigenvectors

λ	ϕ_1	ϕ_2	ϕ_3	ϕ_4
5.4329	0.5	-0.5	-0.5	0.5
11.0756	0.5	-0.5	-0.5	0.5
16.9406	0.5	-0.5	-0.5	0.5
22.9545	0.5	-0.5	-0.5	0.5

Subspace S^4

$$B^4 = a_{11} + a_{12} - a_{13} - a_{14}$$

$$B^4 = (s+8) + sc - 0 - 4$$

$$= s + sc + 4$$

$$|B_4| = s + sc + 4 = 0$$

Solving for eigenvalues and eigenvectors for each eigenvalue using the full space solution *4.7* shows that for each eigenvalue, the eigenmode is $C^y{}_{1v}$ symmetric. The results for the first five eigenvalues and respective eigenvectors are shown in Table *4.6*.

Table 4.6: C_{2v} subspace S^4 eigenvalues and eigenvectors

λ	ϕ_1	ϕ_2	ϕ_3	ϕ_4
7.1818	-0.5	-0.5	0.5	0.5
13.1329	-0.5	-0.5	0.5	0.5
19.2509	-0.5	-0.5	0.5	0.5
25.4409	-0.5	-0.5	0.5	0.5

Table 4.7 below presents a summary of the results obtained from the analytical analysis for all subspaces.

Table 4.7: C_{2v} Eigenvalues obtained by analytical method

No	Eigenvalue	Eigenmode symmetry
1	4.578	C_{2v}
2	5.433	$C^x{}_{1v}$
3	7.182	$C^y{}_{1v}$
4	7.944	C_2
5	10.174	C_{2v}
6	11.076	$C^x{}_{1v}$
7	13.133	$C^y{}_{1v}$
8	13.877	C_2
9	16.192	C_{2v}
10	16.941	$C^x{}_{1v}$
11	19.251	$C^y{}_{1v}$
12	19.884	C_2
13	22.345	C_{2v}
14	22.955	$C^x{}_{1v}$

The analytical solution shows that the lowest eigenvalue is 1.4572π and its eigenmode is C_{2v} symmetric. Timoshenko and Jere (1963) report the lowest eigenvalue as 1.2915π. However, they also report that the eigenmode of the lowest eigenvalue is C_{2v} symmetric (Timošenko & Gere, 1963).

A *FEM* of a C_{2v} frame with C_{2v} ($\gamma_1=0$) loading and C_{2v} stiffness was created using Abaqus, and the first fifty eigenmodes and eigenvalues were analysed. The loading and applied boundary conditions employed for this *FEM* are shown in Figure *4.2 (d)*. The validation of the *FEM* was made by comparison with the buckling loads obtained analytically in this study. Figure *4.4* below shows the convergence analyses for *FEM* for which $I_1=I_2=I_3$ and $P_3=0$ (see Figure *4.2*). The convergence analysis was based on the eigenvalues obtained from the analytical results using the symmetry adapted slope deflection method.

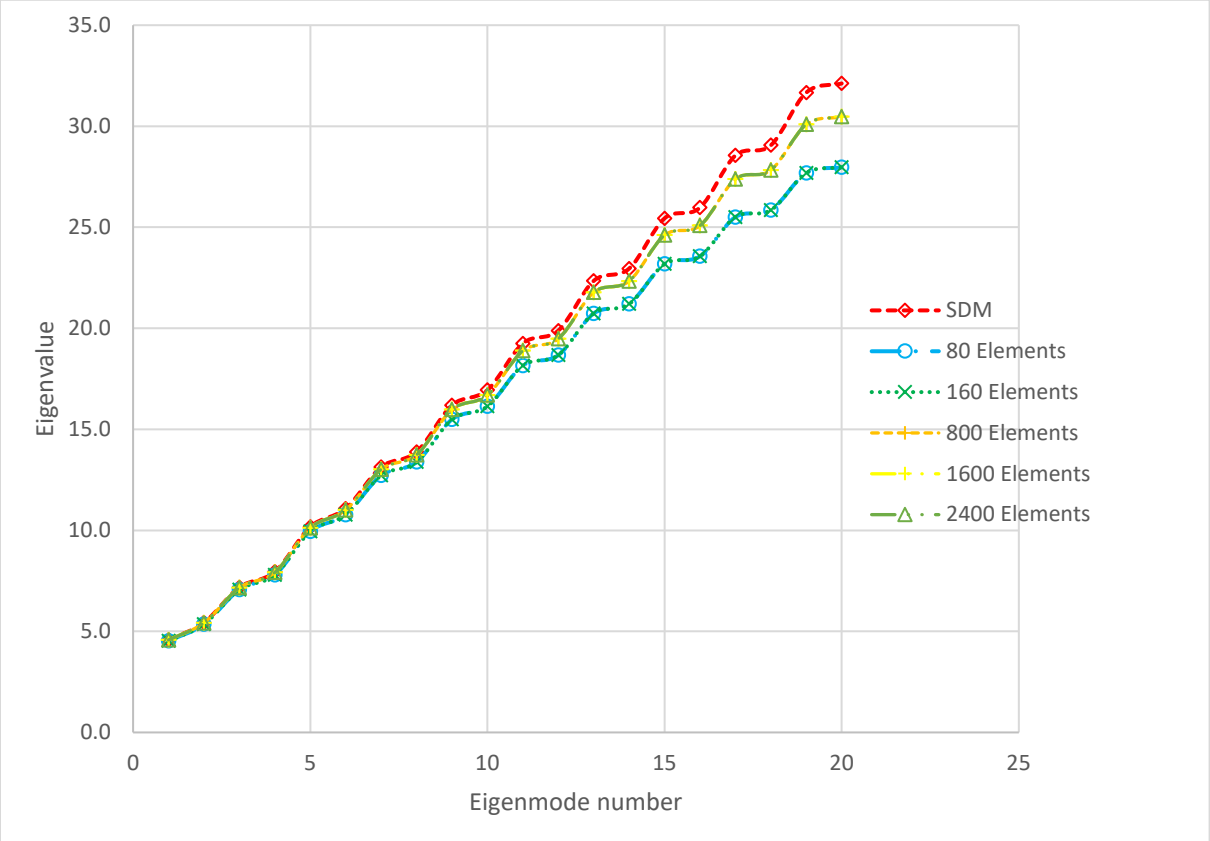

Figure 4.4: Convergence analysis of C_{2v} plane frame

The symmetry of eigenmodes for each eigenvalue was also categorised, and these are shown for the first fourteen eigenvalues in Table *4.8* below. It is clear that the results obtained from the finite

element analysis agree with the results obtained from the analytical solution in terms of eigenvalues and symmetry of eigenmode. Samples of the eigenmodes produced from Abaqus are shown in Figure *4.5*.

It should be noted that the terms eigenvalue and eigenmode are used for the *FEM* results, even though these results were not obtained analytically. A more appropriate term to use would be normalised critical load factors and buckling modes. The terms eigenvalues and eigenmodes are used in this study for the purposes of comparing the analytical and *FEM* results. Furthermore, it is common practice in engineering literature to refer to the normalised critical load factors as eigenvalues. This practice is maintained for the other *FEM* results of this study.

Table 4.8: C_{2v} Eigenvalues obtained from FEM

Number	Eigenvalue	Eigenmode symmetry
1	4.575	C_{2v}
2	5.424	C^{x}_{1v}
3	7.167	C^{y}_{1v}
4	7.916	C_2
5	10.125	C_{2v}
6	11.005	C^{x}_{1v}
7	13.021	C^{y}_{1v}
8	13.737	C_2
9	15.978	C_{2v}
10	16.689	C^{x}_{1v}
11	18.888	C^{y}_{1v}
12	19.477	C_2
13	21.778	C_{2v}
14	22.334	C^{x}_{1v}

From Tables *4.7* and *4.8*, we observe that the lowest eigenvalue has an eigenmode that belongs to a symmetry group with the lowest group index from Table *4.1*. It is also observed that although the C_{1v} and C_2 symmetry groups have an equal group index, the C_{1v} eigenmode is produced first from the sequence of eigenmode symmetries shown in Tables *4.7* and *4.8*. Further, the pattern of

the emergence of symmetries of eigenmodes shown in Table *4.8* was repeating for all the eigenmodes of the fifty eigenvalues produced from the finite element analysis. As can be seen from Table *4.8*, the pattern repeats every four eigenvalues, and four happens to be the order of the C_{2v} group. The reason for this repeating pattern in Table *4.8* can be seen from Figures *4.6* and *4.7* shown below. These figures are plots of eigenvalues produced from each subspace from the analytical analysis and finite element analysis results, respectively. It is observed that the curves have the same general trend and thus the symmetries of the eigenmodes emerge in a very clear and repeating pattern. Further, it was also observed that the eigenvalues whose eigenmodes have the C_2 symmetries (*S2*) formed the higher bound eigenvalues, and the eigenvalues with C_{2v} symmetric eigenmodes (*S1*) formed the lower bound eigenvalues.

The buckling behaviour of the C_{2v} symmetric frame with different C_{2v} load arrangements was also studied in Abaqus. This was achieved by varying the parameter $\gamma_1=P_3/P_1$, with $P_1=P_2$ for the ranges from 0 to *10* as shown in Table *4.2*. It was observed that the symmetry of the buckling modes was the same regardless of the value of γ_1. That is, all the buckling modes had the following symmetries: C_{2v}, C_{1v}, and C_2. Further, for the first five buckling values as defined by Equation *4.4*, the buckling modes for all values γ_1 were exactly in the order shown in Table *4.8*. For the sixth and higher buckling values, no common pattern in the emergence of the symmetries of buckling modes was apparent. The reason is apparent from Figures *4.8*, *4.9*, and *4.10* of buckling values plotted by symmetry of buckling modes for each value of γ_1. The curves for each value of γ_1 intersect at different points, and therefore, no common pattern in the emergence of symmetries of buckling modes for all values of γ_1 was possible. It was also observed that the case of $\gamma_1=1$ was the only load arrangement that produced a repeating buckling. The symmetry of buckling modes of the repeating buckling value was always C_2 and C_{2v} symmetric. It was also observed that for $\gamma_1=1$, the pattern of emerging symmetries was every twelve buckling values. A pattern of repeating symmetries for other values of γ_1 was not observed for the first fitty buckling values produced.

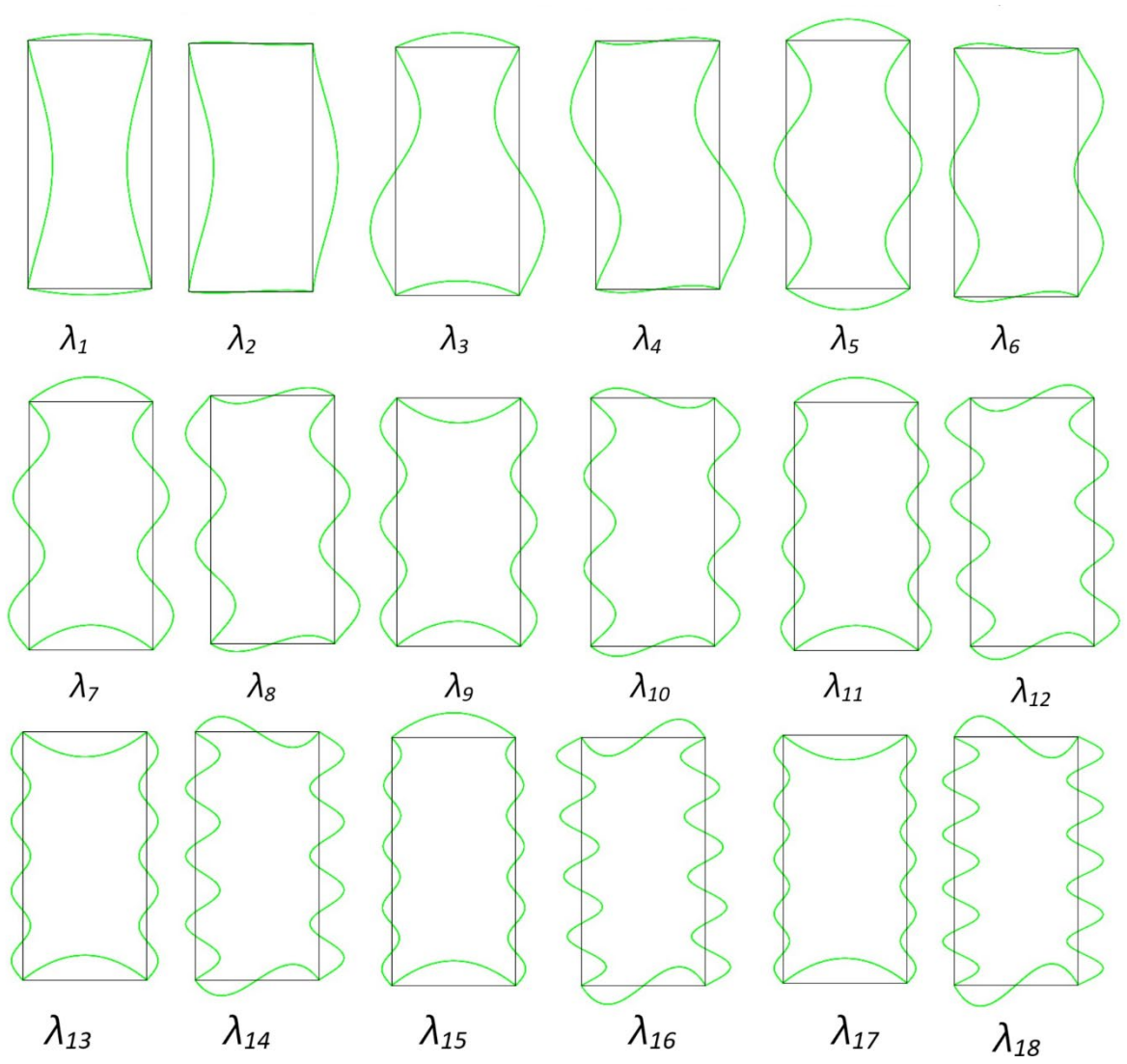

Figure 4.5: C_{2v} plane eigenmodes

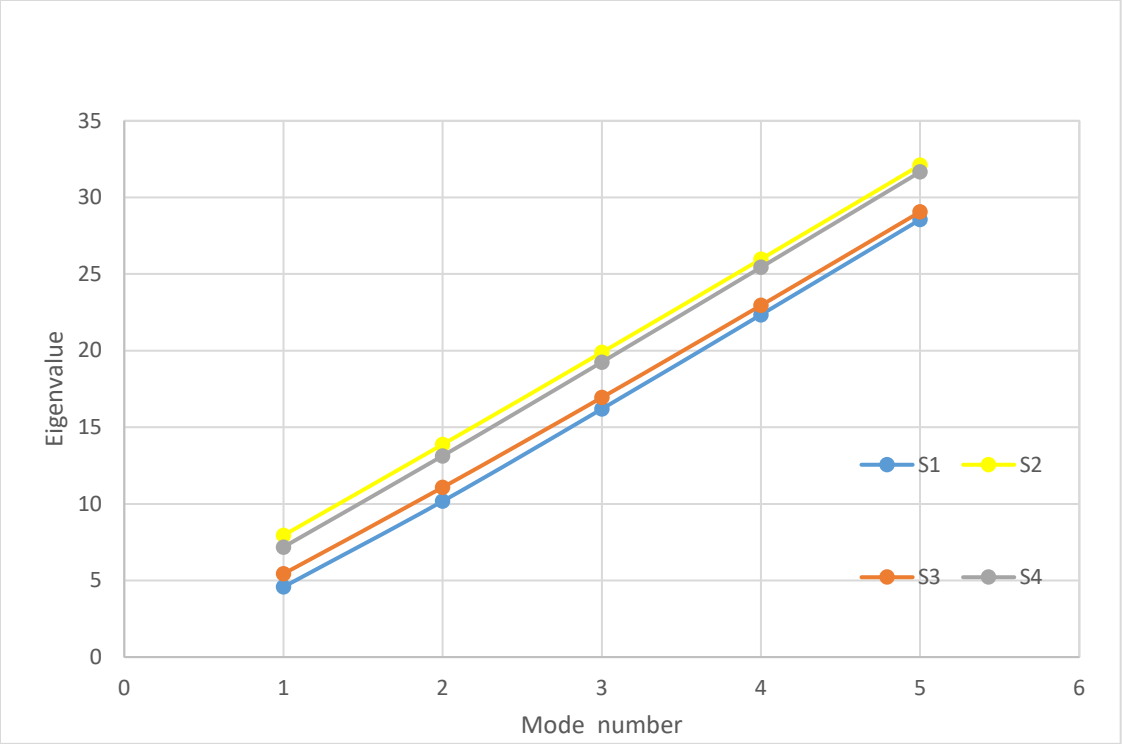

Figure 4.6: C_{2v} Frame, Eigenvalue versus Eigenmode (Analytical results)

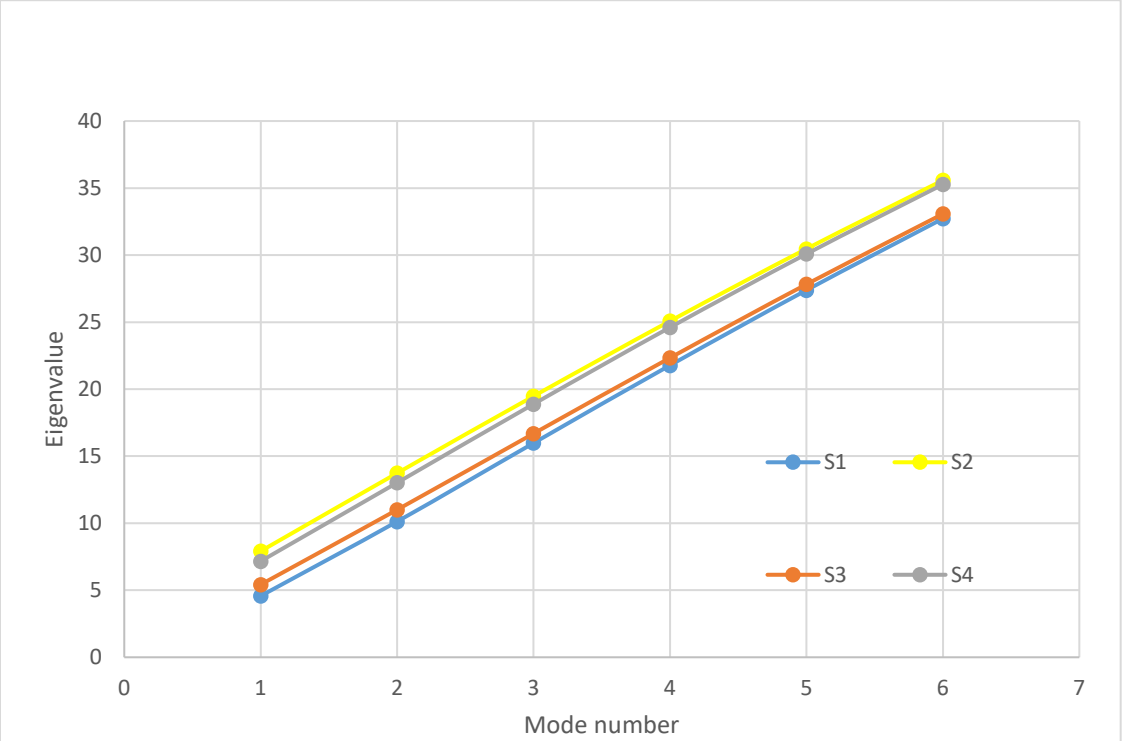

Figure 4.7: C_{2v} Frame, Eigenvalue versus Eigenmode (FEM results)

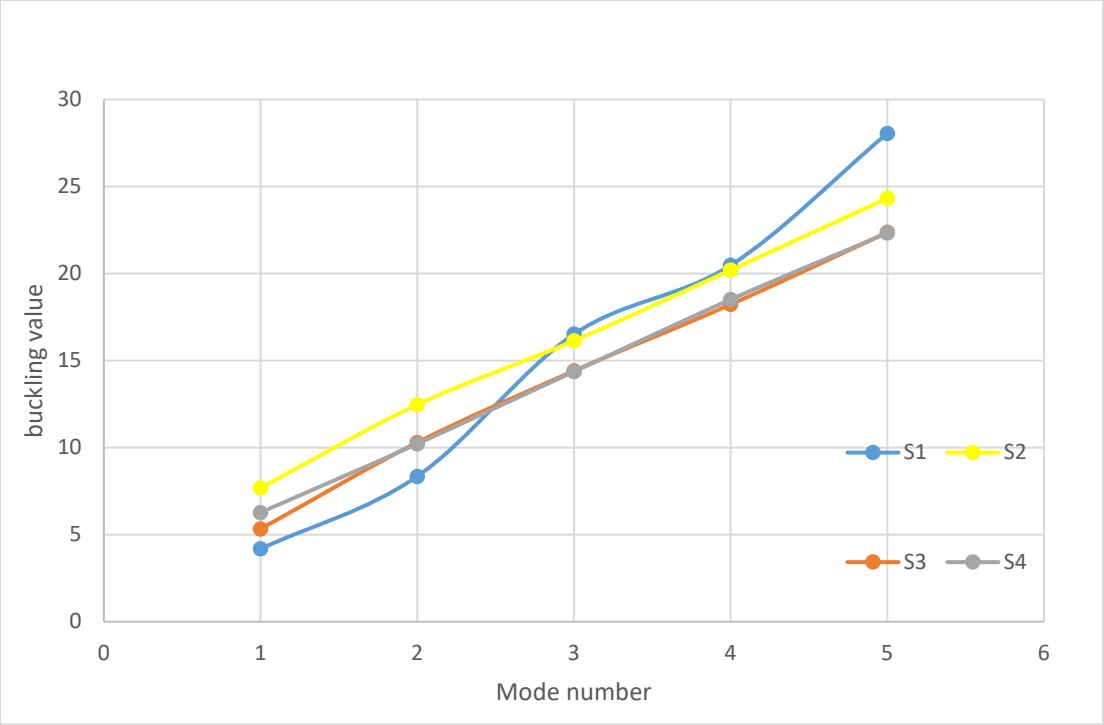

Figure 4.8: C_{2v} Frame, buckling value versus buckling mode (γ_1=1)

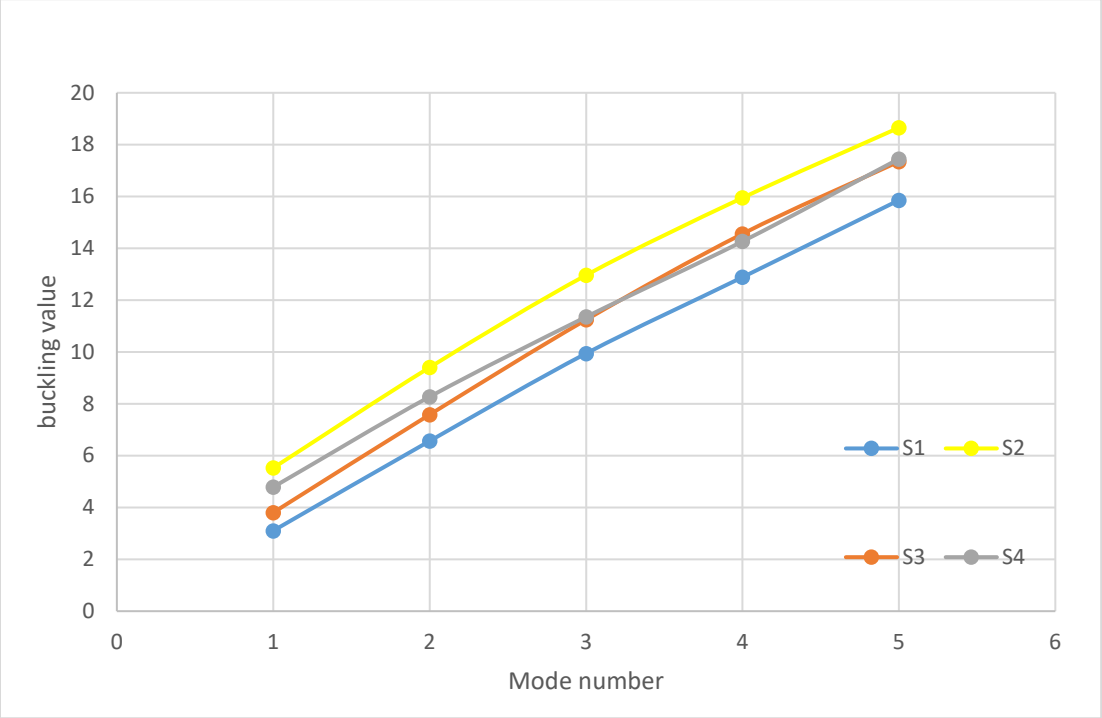

Figure 4.9: C_{2v} Frame, buckling value versus buckling mode (γ_1=2)

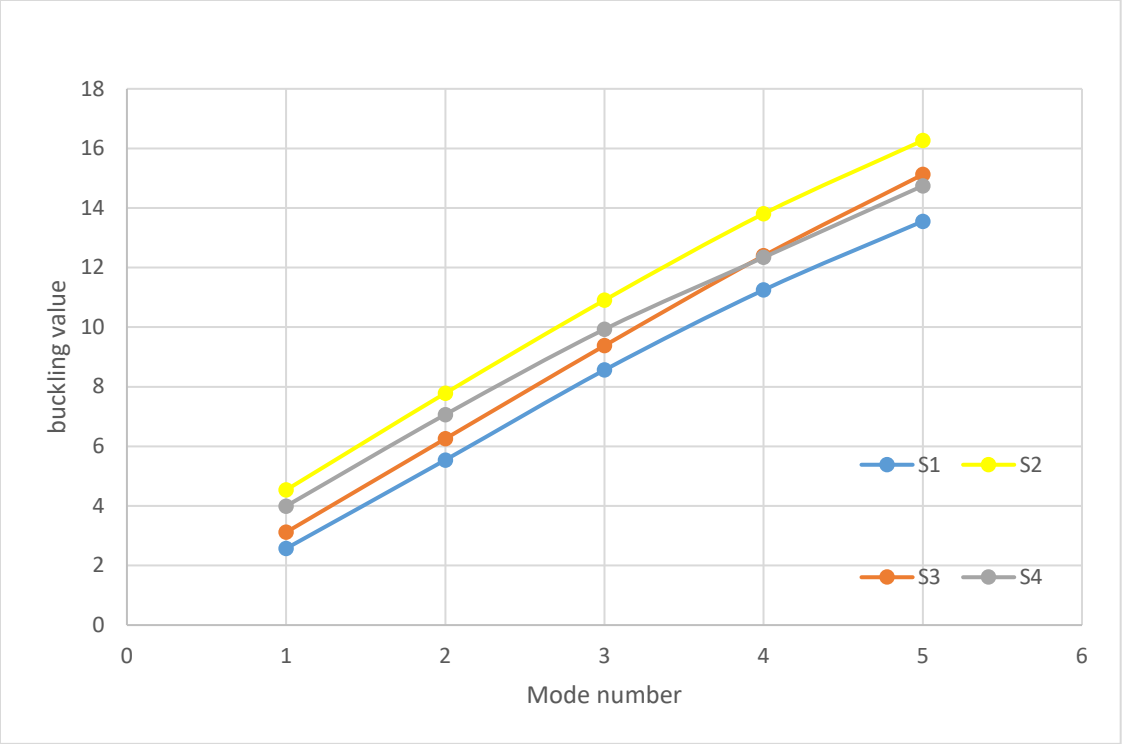

Figure 4.10: C_{2v} Frame, buckling value versus buckling mode (γ_1=3)

When buckling values for each value of γ_1 are plotted on the same graph, it is observed that increasing value of $(\gamma_1)^{-1}$, the buckling values get closer to each other as is shown in Figure *4.11*.

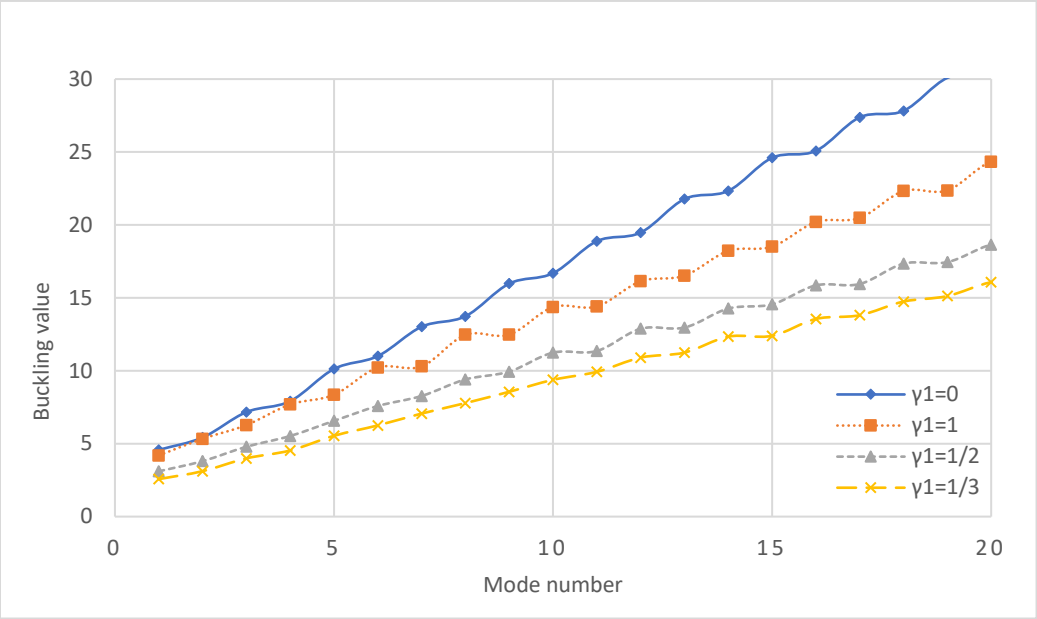

Figure 4.11: Effect of γ_1, C_{2v} loading on buckling of C_{2v} frame

The effect of a C_{1v} loading on the buckling behaviour of a C_{2v} frame was also investigated. For this investigation, $P_3 = 0$, and $\gamma_2 = P_2/P_1$ was varied from *2* to *8*. For all values of γ_2, a linear eigenvalue analysis of the frame in Abaqus revealed that the symmetries of the buckling modes were C_{1v} or C_1 symmetric. Essentially, the frame displayed the buckling behaviour of a C_{1v} symmetric frame. For each value of γ_2, fifty buckling values were analysed, and no common pattern in terms of the order of emergence of symmetries of buckling modes was apparent for different values of γ. Samples of the buckling mode symmetries for the first ten buckling values are shown in Table *4.9*.

As was the case with C_{2v} loads, it was observed that with the increasing value of γ, the buckling was smaller and closer to each other. However, unlike the case of C_{2v} loads, for all the ranges of γ investigated no repeating buckling values were produced.

Table 4.9:Buckling mode pattern for C_{1v} loads

No	γ=2		γ=3		γ=4		γ=5	
	λ_{cr}		λ_{cr}		λ_{cr}		λ_{cr}	
1	3.456	C^x_{1v}	2.842	C^x_{1v}	2.467	C^x_{1v}	2.209	C^x_{1v}
2	5.062	C^x_{1v}	4.333	C_1	3.756	C_1	3.362	C_1
3	5.293	C_1	4.982	C^x_{1v}	4.841	C^x_{1v}	4.540	C^x_{1v}
4	7.463	C^x_{1v}	6.157	C^x_{1v}	5.472	C^x_{1v}	5.207	C^x_{1v}
5	7.555	C_1	7.358	C_1	6.605	C_1	5.934	C_1
6	9.477	C_1	7.924	C_1	7.629	C_1	7.292	C^x_{1v}
7	10.508	C^x_{1v}	9.348	C^x_{1v}	8.135	C^x_{1v}	7.568	C_1
8	11.632	C^x_{1v}	10.644	C^x_{1v}	9.591	C_1	8.605	C_1
9	13.193	C_1	11.051	C_1	10.502	C^x_{1v}	9.786	C^x_{1v}
10	13.759	C_1	12.740	C^x_{1v}	11.129	C^x_{1v}	10.656	C^x_{1v}

4.2.2 Buckling Behaviour of C_{2v} symmetric frame (Stiffness)

The effect of stiffness on the buckling behaviour of a C_{2v} frame was also investigated using a similar approach to that used to study the effect of various loading arrangements on the buckling behaviour. This was achieved by varying the parameter β, which was defined as $\beta_1 = I_1/I_3$, and $I_1 = I_2$. The applied loading was C_{2v} symmetric, that is, $P_1 = P_2 = P_3$. A linear eigenvalue analysis of this frame was carried out for the case where β ranged from *1* to *8*. Regardless of the value of β, all the symmetries of all buckling modes were in accordance with the symmetries of the subspaces illustrated in Figure *4.3*. It was also observed that for the first three buckling values, the symmetries of each buckling mode emerged in the order shown in Table *4.10* below. Beyond the third buckling

value, no common pattern in the emergence of symmetries was apparent for the first fifty buckling modes. The symmetries of the buckling modes of the first ten buckling values are also shown in Table *4.10*.

As was observed with the study of the influence of the value of γ on the buckling value λ_{cr}, an increase in β_1, results in buckling values that are smaller and closer to each other, as shown in Figure *4.12*.

The effect of applying C_{1v} stiffness to a C_{2v} symmetric frame was also investigated. In this case, $\beta=I_2/I_1$, $I_1=I_3$ and $P_1=P_2=P_3$. In this stiffness arrangement, the frame only has one vertical plane of reflection symmetry, σ_x, making it C_{1v} symmetric. A linear eigenvalue analysis of this frame confirmed that all the buckling modes had symmetries that were C_1 or C^x_{1v} symmetric. Further, the first buckling mode was C_{1v} symmetric regardless of the value of β. However, no common pattern was apparent beyond the first buckling mode as shown in Table *4.11*.

Table 4.10: Buckling mode patterns for C_{2v} stiffness

No	β_1=1	λ_{cr}	β_1=2	λ_{cr}	β_1=3	λ_{cr}	β_1=4	λ_{cr}	β_1=5	λ_{cr}	β_1=6	λ_{cr}
1	C_{2v}	4.2	C_{2v}	3.6	C_{2v}	3.3	C_{2v}	3.1	C_{2v}	3.0	C_{2v}	2.9
2	C^x_{1v}	5.3	C^x_{1v}	4.7	C^x_{1v}	4.3	C^x_{1v}	4.1	C^x_{1v}	3.9	C^x_{1v}	3.7
3	C^y_{1v}	6.3	C^y_{1v}	5.6	C^y_{1v}	5.2	C^y_{1v}	4.9	C^y_{1v}	4.6	C^y_{1v}	4.4
4	C_2	7.7	C_2	7.0	C_2	6.6	C_{2v}	6.3	C_{2v}	5.8	C_{2v}	5.4
5	C_{2v}	8.4	C_{2v}	7.5	C_{2v}	6.9	C_2	6.3	C_2	6.0	C_2	5.8
6	C^y_{1v}	10.3	C^y_{1v}	8.9	C^y_{1v}	8.0	C^y_{1v}	7.4	C^y_{1v}	7.0	C^y_{1v}	6.8
7	C^x_{1v}	10.3	C^x_{1v}	9.2	C^x_{1v}	8.6	C^x_{1v}	8.0	C^x_{1v}	7.5	C^x_{1v}	7.1
8	C_2	12.6	C_{2v}	10.8	C_2	9.8	C_2	9.0	C_2	8.3	C_2	7.8
9	C_2	12.6	C_2	11.0	C_{2v}	9.9	C_{2v}	9.4	C_{2v}	9.1	C_{2v}	8.8
10	C^y_{1v}	14.5	C^x_{1v}	12.6	C^x_{1v}	11.3	C^x_{1v}	10.5	C^x_{1v}	10.0	C^x_{1v}	9.7

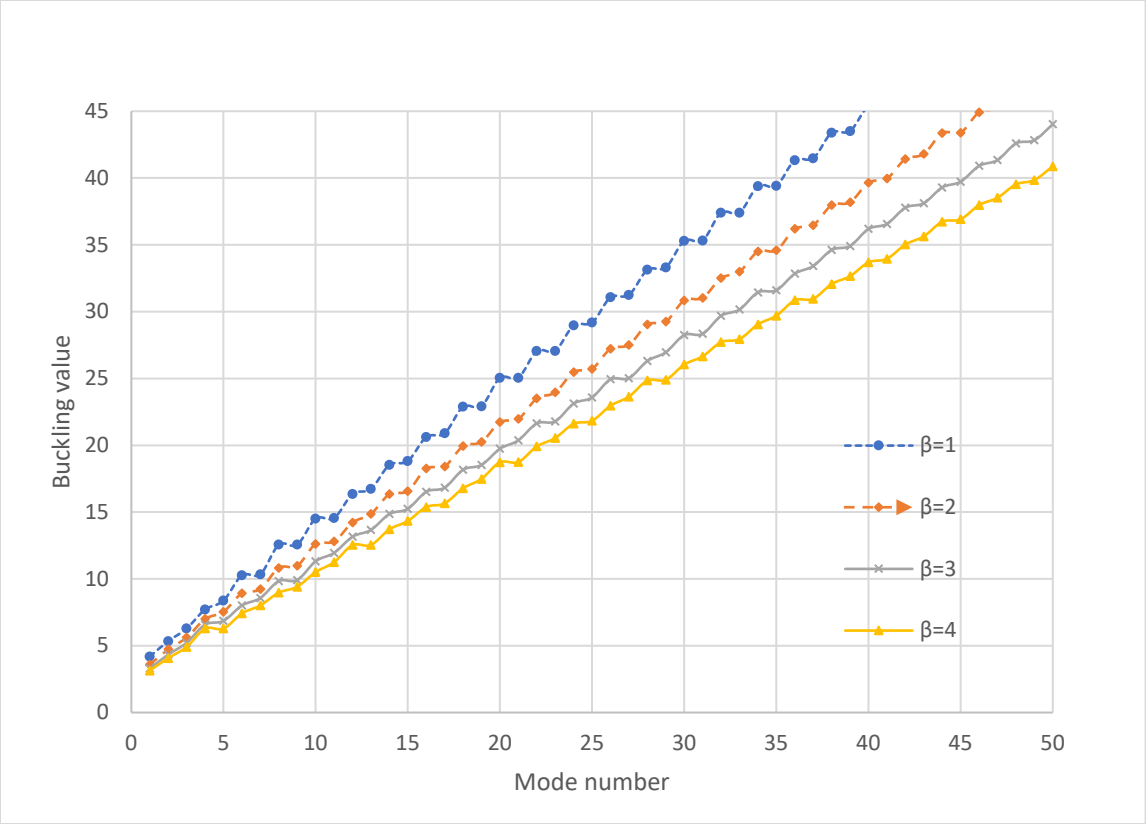

Figure 4.12: Effect of C_{2v} stiffness on C_{2v} symmetric frame ($\beta=\beta_1$)

Table 4.11: Buckling mode patterns for a C_{2v} frame with C_{1v} stiffness

No	β_2=2	λ_{cr}	β_2=3	λ_{cr}	β_2=4	λ_{cr}	β_2=5	λ_{cr}
1	C^x_{1v}	4.5	C^x_{1v}	4.6	C^x_{1v}	4.7	C^x_{1v}	4.7
2	C^x_{1v}	6.1	C^x_{1v}	6.6	C_1	7.0	C_1	7.0
3	C_1	6.8	C_1	6.9	C^x_{1v}	7.0	C^x_{1v}	7.4
4	C_1	8.9	C^x_{1v}	9.5	C^x_{1v}	9.6	C^x_{1v}	9.8
5	C^x_{1v}	9.2	C_1	9.7	C_1	10.1	C_1	10.3
6	C_1	11.3	C_1	12.0	C^x_{1v}	12.6	C^x_{1v}	12.7
7	C^x_{1v}	11.7	C^x_{1v}	12.3	C_1	12.6	C_1	13.0
8	C_1	13.8	C_1	14.3	C_1	14.6	C_1	15.0
9	C^x_{1v}	13.8	C^x_{1v}	14.7	C^x_{1v}	15.1	C^x_{1v}	15.4
10	C_1	16.0	C_1	16.6	C_1	17.0	C_1	17.3

4.3 C_{3v} Plane Frame

We now consider the buckling behaviour of a C_{3v} symmetric plane frame as shown below in Figure *4.13 (a)*, using a similar approach to the one employed for the C_{2v} plane frame previously discussed. We may gain insights on the buckling behaviour of such a frame, by obtaining the basis vectors of each subspace of a model of such a frame, as shown in Figure *4.13 (b)*.

The idempotents for the C_{3v} symmetry group are (Kaveh & Nikbakht, 2008; Zingoni, 2014).

$$P^1 = \frac{1}{6}\left(e + C_3 + C_3^{-1} + \sigma_1 + \sigma_2 + \sigma_3\right) \qquad (4.13)$$

$$P^2 = \frac{1}{6}\left(e + C_3 + C_3^{-1} - \sigma_1 - \sigma_2 - \sigma_3\right) \qquad (4.14)$$

$$P^3 = \frac{1}{3}\left(2e - C_3 - C_3^{-1}\right) \qquad (4.15)$$

$$P^3 = P^{3,1} + P^{3,2}$$

$$P^{3,1} = \frac{1}{6}\left(2e - C_3 - C_3^{-1} - \sigma_1 - \sigma_2 + 2\sigma_3\right) \qquad (4.16)$$

$$P^{3,2} = \frac{1}{6}\left(2e - C_3 - C_3^{-1} + \sigma_1 + \sigma_2 - 2\sigma_3\right) \qquad (4.17)$$

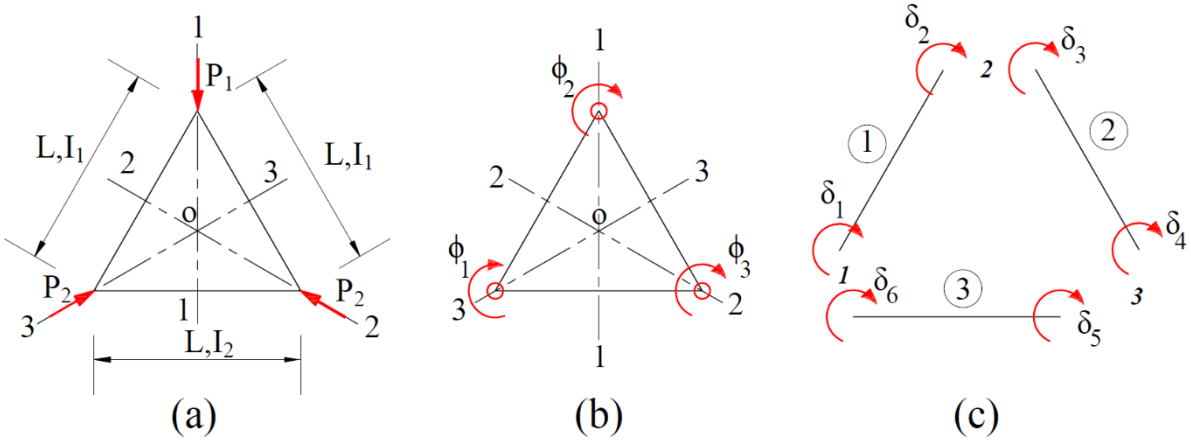

Figure 4.13: C_{3v} Symmetric frame

To obtain the basis vectors for each subspace, we apply each idempotent to each positional vector shown in Figure *4.13 (b)*.

Subspace S^1

$$P^1\phi_1 = \frac{1}{6}\left(e + C_3 + C_3^{-1} + \sigma_1 + \sigma_2 + \sigma_3\right)\phi_1 = \frac{1}{6}\left(\phi_1 + \phi_3 + \phi_2 - \phi_3 - \phi_2 - \phi_1\right) = P^1\phi_2 = P^1\phi_3 = 0$$

Therefore, subspace S^1 is a null space. However, if in addition to the rotational degrees of freedom,

there are translational degrees of freedom at the mid-height of each beam-column towards the centre of rotation O, then subspace S^1 is not a null space, and it has translational degrees of freedom towards the centre of rotation O. This would result in basis vectors that are C_{3v} symmetric.

Subspace S^2

$$P^2\phi_1 = \frac{1}{6}\left(e + C_3 + C_3^{-1} - \sigma_1 - \sigma_2 - \sigma_3\right)\phi_1$$

$$= \frac{1}{6}\left(\phi_1 + \phi_3 + \phi_2 + \phi_3 + \phi_2 + \phi_1\right) = P^2\phi_2 = P^2\phi_3$$

$$= \frac{1}{3}\left(\phi_1 + \phi_2 + \phi_3\right)$$

Therefore, the basis vectors for S^2 are:

$$\Phi_1^1 = \phi_1 + \phi_2 + \phi_3 \qquad (4.18)$$

Subspace S_3

$$P^3\phi_1 = \frac{1}{3}\left(2e - C_3 - C_3^{-1}\right)\phi_1$$

$$= \frac{1}{3}\left(2\phi_1 - \phi_3 - \phi_2\right)$$

$$P^3\phi_2 = \frac{1}{3}\left(2e - C_3 - C_3^{-1}\right)\phi_2$$

$$= \frac{1}{3}\left(2\phi_2 - \phi_1 - \phi_3\right)$$

The basis vectors of S^3 are therefore:

$$\Phi_1^3 = 2\phi_1 - \phi_2 - \phi_3 \qquad (4.19)$$

$$\Phi_2^3 = -\phi_1 + 2\phi_2 - \phi_3 \qquad (4.20)$$

Alternatively

$$P^{3,1}\phi_1 = \frac{1}{6}\left(2e - C_3 - C_3^{-1} - \sigma_1 - \sigma_2 + 2\sigma_3\right)\phi_1$$

$$= \frac{1}{6}\left(2\phi_1 - \phi_3 - \phi_2 + \phi_3 + \phi_2 - 2\phi_1\right) = \frac{1}{12}\left(2\phi_1 - 2\phi_1 - \phi_3 + \phi_3 - \phi_2 + \phi_2\right) = 0$$

$$P^{3,1}\phi_2 = \frac{1}{6}\left(2e - C_3 - C_3^{-1} - \sigma_1 - \sigma_2 + 2\sigma_3\right)\phi_2$$

$$= \frac{1}{6}\left(2\phi_2 - \phi_1 - \phi_3 + \phi_2 + \phi_1 - 2\phi_3\right) = -P^{3,1}\phi_3$$

$$= \frac{1}{6}\left(2\phi_2 + \phi_2 - \phi_1 + \phi_1 - \phi_3 - 2\phi_3\right)$$

$$= \frac{1}{6}\left(3\phi_2 - 3\phi_3\right)$$

$$= \frac{3}{6}\left(\phi_2 - \phi_3\right)$$

Therefore, the basis vectors of subspace $S^{3,1}$ is:

$$\Phi_1^{3,1} = \phi_2 - \phi_3 \qquad (4.21)$$

The sketches of these basis vectors are shown in Figure *4.14* and their symmetries are summarised in Table *4.12*. To identify the symmetry pattern of each subspace, moments must be applied in accordance with the coordinates of the basis vectors, as shown in Table *4.12*.

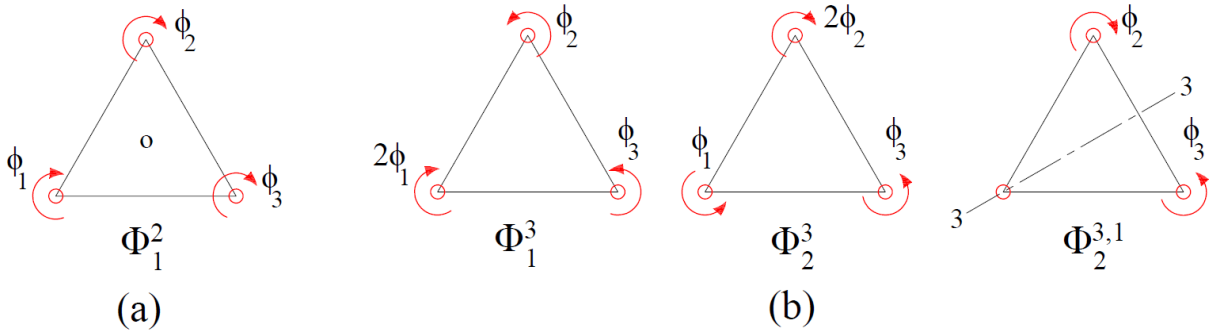

Figure 4.14:C_{3v} Basis vectors

Table 4.12: C_{3v} Basis vector symmetries

Figure	Subspace	Symmetry Group	Order (n)	Group index (n/m)	Applied moments
(a)	S^2	C_3	3	2	$\phi_1 = \phi_2 = \phi_3 = 1$
(b)	S^3	C_1	1	6	$\phi_1 = 1,\ \phi_2 = \phi_3 = -0.5$
(b)	S^3	C_1	1	6	$\phi_1 = \phi_3 = -0.5,\ \phi_2 = 1$
(b)	S^3	C_{1v}	2	3	$\phi_2 = 1,\ \phi_3 = -1$

It is important to note that the C_1 symmetry group would actually be the C_s symmetry group with order *2*, if we imagined a horizontal plane of reflection symmetry in Figure *4.13*. We would thus have a group index of *3*.

4.3.1 Buckling Behaviour of C_{3v} symmetric frame

The approach used to study the C_{3v} symmetric frame was the same as that employed for the C_{2v} symmetric frame. The C_{3v} symmetric frame was first studied analytically using the slope deflection method to determine the eigenvalues and the symmetries of their eigenmodes. The software Matlab was used to solve the resulting trigonometric equations to obtain eigenvalues from equation *4.6*. The eigenmodes were also solved for, by utilising Matlab to solve the resulting matrix linear equations when equation *4.7* was solved.

For this section of the study two load conditions were considered:

i. C_{3v} loading, with $P_1=P_2$; and
ii. C_{1v} loading with $P_1= \gamma P_2$.

For both cases, the stiffness of the frame was C_{3v} symmetric, with $I_1=I_2$. The boundary conditions load cases (i) and (ii) are shown in Figure *4.15 (b).* The boundary conditions shown in Figure *4.15* (a) only apply to load case (i).

To obtain analytical solutions for this buckling problem using a symmetry adapted slope deflection method, the frame was divided into three elements as shown in Figure *4.13 (c)* and the transformation matrices for each element are:

$$\begin{matrix} & \phi_1 & \phi_2 \end{matrix} \qquad \begin{matrix} & \phi_2 & \phi_3 \end{matrix} \qquad \begin{matrix} & \phi_3 & \phi_1 \end{matrix}$$

$$[D_1]=\begin{bmatrix} 1 & 0 \\ 0 & 1 \end{bmatrix}\begin{matrix}\delta_1 \\ \delta_2\end{matrix} \qquad [D_2]=\begin{bmatrix} 1 & 0 \\ 0 & 1 \end{bmatrix}\begin{matrix}\delta_3 \\ \delta_4\end{matrix} \qquad [D_3]=\begin{bmatrix} 1 & 0 \\ 0 & 1 \end{bmatrix}\begin{matrix}\delta_5 \\ \delta_6\end{matrix}$$

For the case of C_{3v} loading and C_{3v} stiffness, the element stiffness matrices of the C_{3v} frame ($b=l/2$) shown in Figure *4.13* are obtained by applying Equation *3.6* and these are:

$$\begin{matrix} & \phi_1 & \phi_2 \end{matrix} \qquad \begin{matrix} & \phi_2 & \phi_3 \end{matrix} \qquad \begin{matrix} & \phi_3 & \phi_1 \end{matrix}$$

$$[K_1]=\begin{bmatrix} s & sc \\ sc & s \end{bmatrix}\begin{matrix}\phi_1 \\ \phi_2\end{matrix} \qquad [K_2]=\begin{bmatrix} s & sc \\ sc & s \end{bmatrix}\begin{matrix}\phi_2 \\ \phi_3\end{matrix} \qquad [K_3]=\begin{bmatrix} s & sc \\ sc & s \end{bmatrix}\begin{matrix}\phi_3 \\ \phi_1\end{matrix}$$

The global stiffness matrix is then given as:

$$A = K_1 + K_2 + K_3 + K_4 = \frac{EI}{L}\begin{bmatrix} 2s & sc & sc \\ sc & 2s & sc \\ sc & sc & 2s \end{bmatrix} \qquad (4.22)$$

The stability functions *s* and *c* are as previously defined in Equations *4.2* and 4.3.

We can now employ the group theoretic approach to determine the symmetry adapted matrix *B* for each subspace and then employ equation *4.6* and *4.7* to determine the eigenvalues and eigenvectors respectively.

Subspace S^2

$$\begin{aligned} B^2 &= a_{11} + a_{12} + a_{13} \\ &= 2s + sc + sc \\ &= 2s + 2sc \end{aligned}$$

$$\left|B^2\right| = s + sc = s(1+c) = 0$$

Solving this trigonometric equation, we find the eigenvalues as:

$$\lambda_1 = 6.2832 = 2\pi$$

$$\lambda_n = 2n\pi$$

Solving the eigenvectors for each eigenvalue using the full space solution equation *4.7*, shows that for each eigenvalue, the eigenvector is C_3 and C_{3v} symmetric. For example, for $\lambda_1 = 6.2832$, the stability functions are now: $s = 4.2764(10)^5$ and $c = -1.0000$. Substituting Equation *4.22* into Equation 4.7 we obtain:

$$(10)^5\begin{bmatrix} 8.5527 & -4.2764 & -4.2764 \\ -4.2764 & 8.5527 & -4.2764 \\ -4.2764 & -4.2764 & 8.5527 \end{bmatrix}\begin{Bmatrix} \phi_1 \\ \phi_2 \\ \phi_3 \end{Bmatrix} = \begin{Bmatrix} 0 \\ 0 \\ 0 \end{Bmatrix}$$

Solving the above equation using Matlab we obtain:

$$\begin{Bmatrix} \phi_1 \\ \phi_2 \\ \phi_3 \end{Bmatrix} = \begin{Bmatrix} 0.5774 \\ 0.5774 \\ 0.5774 \end{Bmatrix} \text{ or } \begin{Bmatrix} \phi_1 \\ \phi_2 \\ \phi_3 \end{Bmatrix} = \begin{Bmatrix} 8.0000(10)^{-8} \\ 8.0000(10)^{-8} \\ 8.0000(10)^{-8} \end{Bmatrix}$$

The eigenvalues and eigenvectors obtained from the analytical analysis for S^2 are summarised in Table *4.13* below.

Table 4.13: C_{3v} plane frame: subspace S^2 eigenvalues and eigenvectors

λ	ϕ_1	ϕ_2	ϕ_3	symmetry group
6.2832	0.5774	0.5774	0.5774	C_3
6.2832	8.0000E-08	8.0000E-08	8.0000E-08	C_{3v}
12.5664	0.5774	0.5774	0.5774	C_3
12.5664	8.0000E-08	8.0000E-08	8.0000E-08	C_{3v}
18.8496	0.5774	0.5774	0.5774	C_3
18.8496	2.9860E-05	2.9860E-05	2.9860E-05	C_{3v}
25.1327	0.5774	0.5774	0.5774	C_3
25.1327	-3.3060E-08	-3.3060E-08	-3.3060E-08	C_{3v}

The C_{3v} eigenmode displacements shown in *Table 4.13* indicate that there is zero displacement at both ends of each member in the triangular frame. Thus, each member of the triangular frame for this type of eigenmode can be modelled as a column fixed at both ends. The buckling load of an axially loaded column fixed at both ends is well known as:

$$P_{cr} = \frac{(2n\pi)^2 EI}{l^2}$$ for n buckling modes. Substituting this buckling load into Equation *4.1* obtain:

$$\lambda = l\sqrt{\frac{(2n\pi)^2 EI}{l^2 EI}} = 2n\pi \,.$$

Thus, the eigenvalue $\lambda_n=2n\pi$ can be obtained from either subspace S^1 or subspace S^2. The eigenmodes that are C_{3v} symmetric thus belong to subspace S^1.

Subspace S^3

$$B^3 = a_{22} - a_{23}$$
$$= 2s - sc$$
$$\left|B^3\right| = s(2-c) = 0$$

Solving for eigenvalues and the eigenvectors for each eigenvalue using the full space solution equation *4.7* shows that for each eigenvalue, the eigenmode is C_1 or C_{1v} symmetric. The eigenvalues and eigenvectors obtained from the analytical analysis for S^3 are summarised in Table *4.14* below.

Table 4.14: C_{3v} plane frame: subspace S^3 eigenvalues and eigenvectors

λ	ϕ_1	ϕ_2	ϕ_3	symmetry group
3.8567	-0.4082	-0.4082	0.8165	C_1
3.8567	1.0000	-1.0000	0.0000	C_{1v}
8.1869	-0.4082	-0.4082	0.8165	C_1
8.1869	1.0000	-1.0000	0.0000	C_{1v}
10.3338	-0.4082	-0.4082	0.8165	C_1
10.3338	1.0000	-1.0000	0.0000	C_{1v}
14.5550	-0.4082	-0.4082	0.8165	C_1
14.5550	1.0000	-1.0000	0.0000	C_{1v}
16.6677	-0.4082	-0.4082	0.8165	C_1
16.6677	1.0000	-1.0000	0.0000	C_{1v}

The table below presents a summary of the results obtained from the analytical analysis.

Table 4.15: C_{3v} Eigenvalues obtained by analytical method

No	Eigenvalue	Eigenmode symmetry
1	3.857	C_1, C_{1v}
2	6.283	C_3, C_{3v}
3	8.187	C_1, C_{1v}
4	10.334	C_1, C_{1v}
5	12.566	C_3, C_{3v}
6	14.555	C_1, C_{1v}
7	16.668	C_1, C_{1v}
8	18.850	C_3, C_{3v}
9	25.133	C_3, C_{3v}
10	31.416	C_3, C_{3v}

The analytical solution shows that the lowest eigenvalue was 1.228π and its eigenmode is either C_1 or C_{1v} symmetric. This result was also reported by Timoshenko and Jere (1963); however, the symmetry of the buckling mode was not reported.

A *FEM* of a C_{3v} frame was created using Abaqus, and the first fifty eigenmodes and eigenvalues were analysed. The loading and applied boundary conditions employed for this *FEM* are shown in Figure *4.15 (a)* and *(b)*. Both boundary conditions shown in Figure *4.15* yield identical buckling

loads and modes, since they both result in a stress distribution that is C_{3v} symmetric and the frame is laterally restrained.

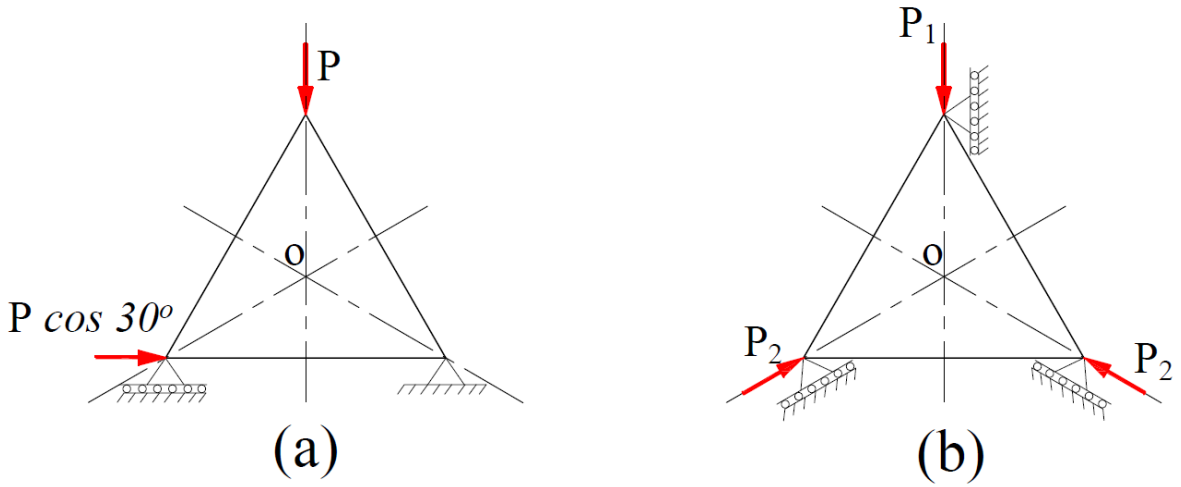

Figure 4.15: C_{3v} Frame FEM boundary conditions

The validation of the *FEM* was made by comparison with the buckling loads obtained analytically in this study. The convergence analysis shown in Figure *4.16* was based on the eigenvalues obtained from the analytical results using the symmetry adapted slope deflection method.

The symmetry of eigenmodes for each eigenvalue was also categorised, and these are shown for the first fourteen eigenvalues in Table *4.16* below. Samples of eigenmode shapes obtained from the linear eigenvalue analysis are shown in Figure *4.17*. From Tables *4.15* and *4.16,* it is clear to see that the analytical results closely agree with the *FEM* results in terms of eigenvalues and symmetry classification of eigenmodes.

From Tables *4.15* and *4.16,* we observe that the lowest eigenvalue has eigenmodes that are C_1 or C_{1v} symmetric. These two symmetry groups have group indexes of three and six, respectively. The C_3 symmetry group has the lowest group index of two, and it is not the eigenmode of the lowest eigenvalue, as was the case with the C_{2v} frame studied earlier. However, if we consider that the C_1 symmetry group can also be considered a C_s group with a group index of two, as earlier explained, then the symmetry group with the lowest index is still the symmetry group of the eigenmode for the lowest eigenvalue. Further, it can also be observed from Table *4.16* that every eigenvalue is a repeating eigenvalue. The eigenvalues with either C_1 or C_{1v} symmetric modes are group-theoretic

repeating eigenvalues and those with C_3 or C_{3v} symmetric eigenmodes are parametric repeating eigenvalues.

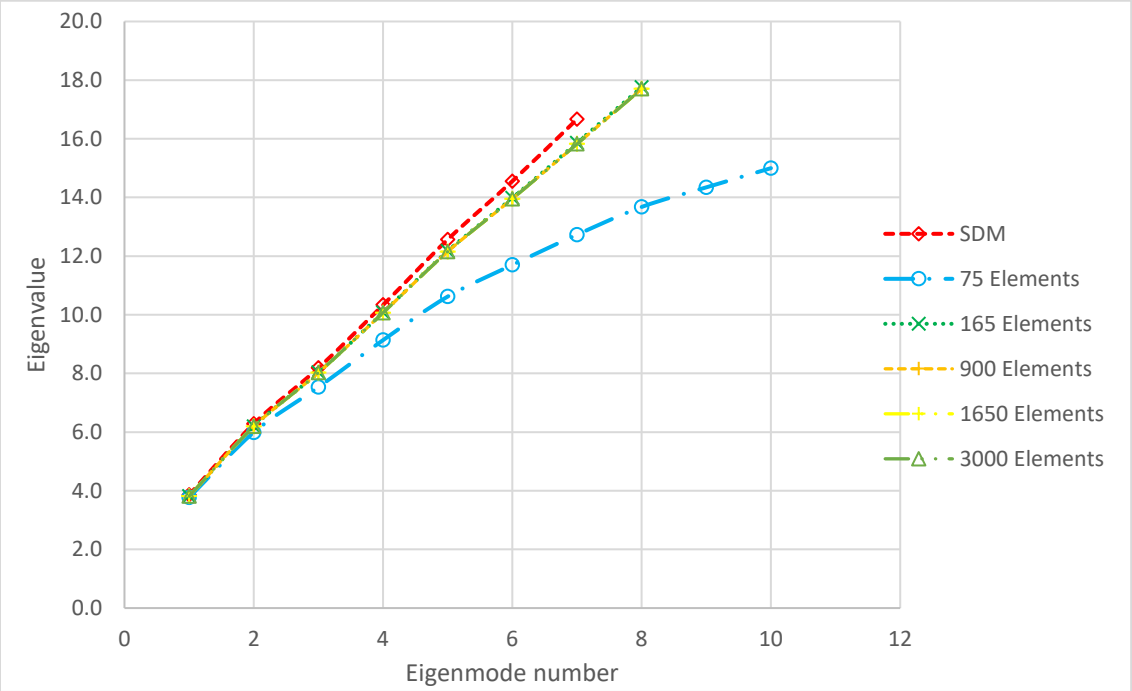

Figure 4.16: C_{3v} Plane frame convergence analysis

Table 4.16: C_{3v} Eigenvalues obtained from FEM

Number	Eigenvalue	Eigenmode symmetry
1	3.813	C_1
2	3.813	$C^1{}_{1v}$
3	6.191	C_3
4	6.191	C_3
5	8.026	C_1
6	8.026	$C^1{}_{1v}$
7	10.069	C_1
8	10.069	$C^1{}_{1v}$
9	12.154	C_{3v}
10	12.154	C_3
11	13.953	C_1
12	13.953	$C^1{}_{1v}$
13	15.822	C_1
14	15.822	$C^1{}_{1v}$

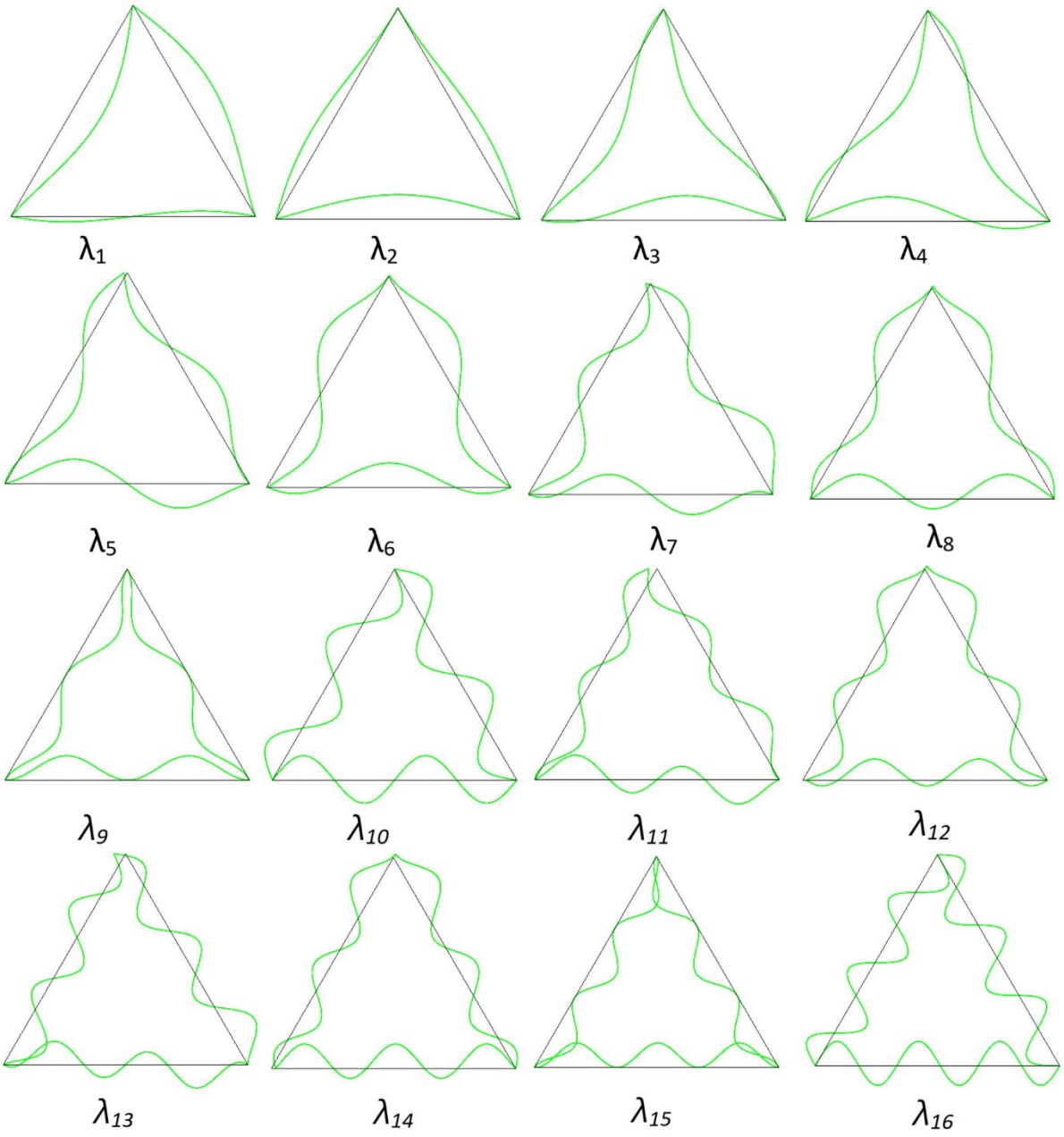

Figure 4.17: C_{3v} plane frame eigenmodes

The pattern of the emergence of symmetries of eigenmodes shown in Table *4.16* was repeating for every six eigenvalues, for all the eigenmodes of the fifty eigenvalues produced from the finite element analysis. Again, as in the case of the C_{2v} frame, the pattern of emergence of symmetries repeats by a number equal to the order of the group. Recall that the order of the C_{3v} symmetry group is six. The reason for the clear repeating pattern can be seen in Figures *4.18* and *4.19,* shown

below, of plots of eigenvalues produced from each subspace from the analytical analysis and finite element analysis. The curves do not intersect, and thus the symmetries of the eigenmodes emerge in a very clear pattern.

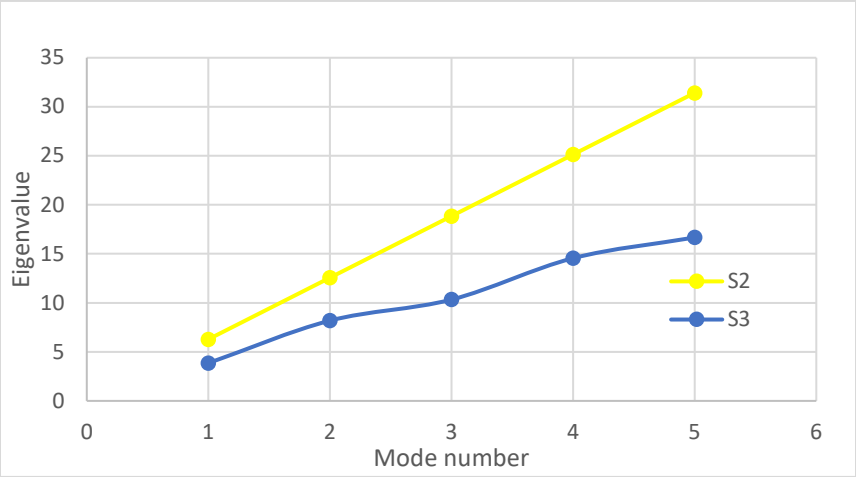

Figure 4.18:C_{3v} Frame, Eigenvalue versus Eigenmode (Analytical results)

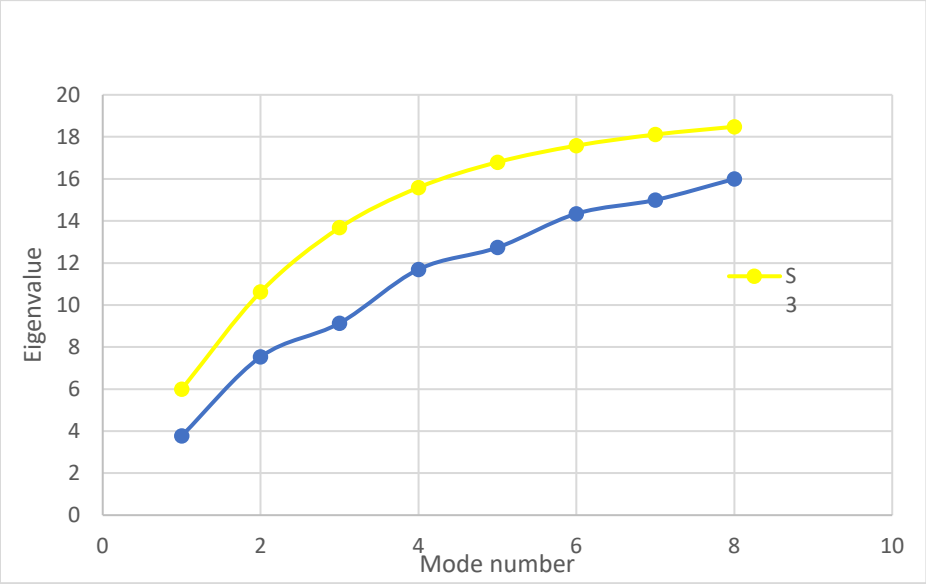

Figure 4.19: C_{3v} Frame, Eigenvalue versus Eigenmode (Abaqus results)

We now consider the effect of imposing a C_{1v} loading arrangement on a C_{3v} frame. That is, the loading arrangement is set as $P_1 = \gamma P_2$, and the stiffness as $I_1 = I_2$.

An eigenvalue analysis of such a frame showed that all buckling modes were either C_{1v} symmetric or C_1 symmetric, regardless of the value of γ. From the linear eigenvalue analysis carried out using Abaqus, the lowest buckling value had a buckling mode that was C_1 symmetric, and the second

lowest buckling value, the buckling mode was C_{1v} symmetric. This alternating pattern of C_1 and then C_{1v} was observed for the first fifty buckling values from a linear eigenvalue analysis produced from Abaqus. When the buckling values for all values of γ are plotted on the same graph, Figure *4.20*, we easily observe that an increase in γ results in more closely spaced buckling values. It should be noted that for $\gamma=3$, the linear eigenvalue analysis in Abaqus produced some negative buckling values.

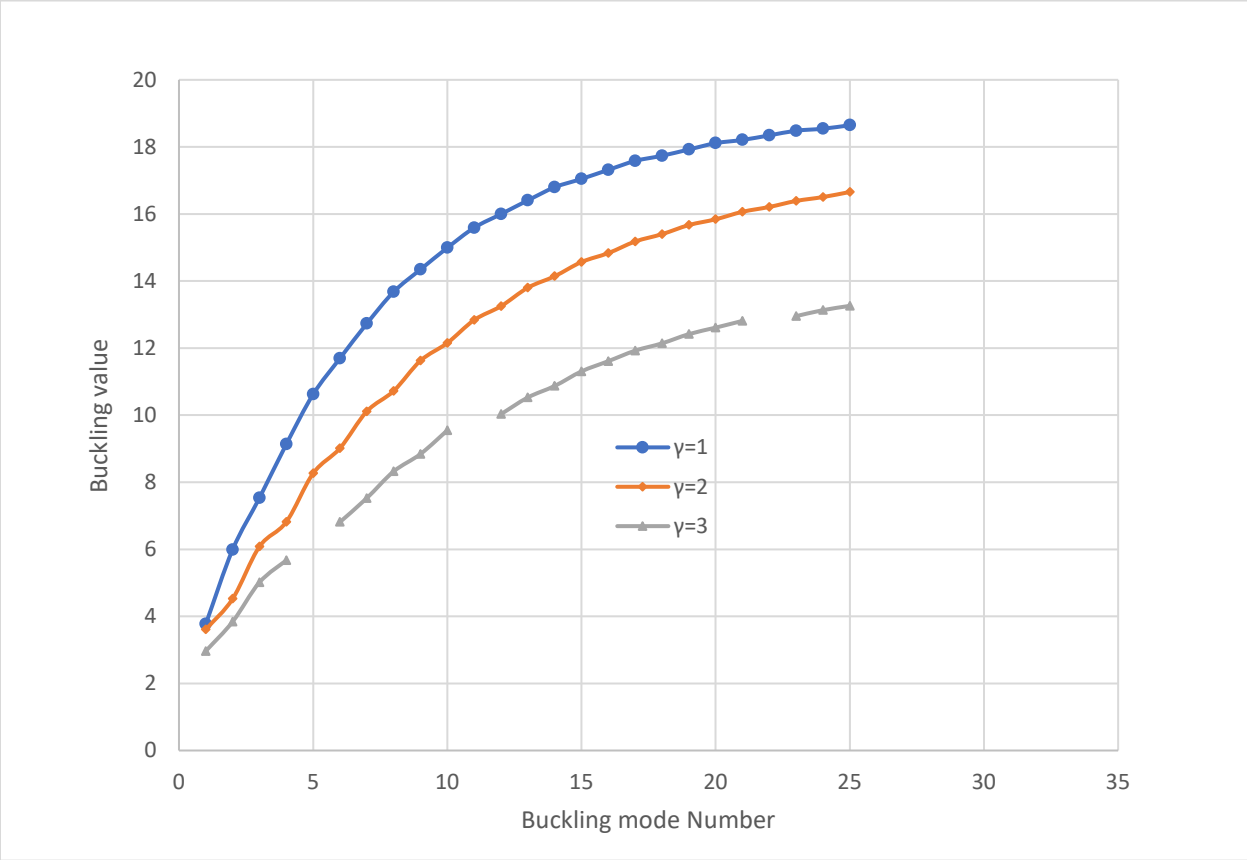

Figure 4.20: Influence of γ on Buckling load of C_{3v} Frame

A similar study was carried out by imposing a C_{1v} stiffness arrangement on the frame. For this study all the applied loadings were of the same magnitude, that is: $P_1=P_2$. A linear finite element analysis was carried out in Abaqus for values of β (I_1/I_2) ranging from *2* to *5*. The symmetries of all buckling modes were either C_1 or C_{1v} symmetric and the buckling mode of the lowest buckling value was always C_{1v} symmetric. When the buckling values for all values of β are plotted on the same graph, Figure *4.21*, we easily observe that a decrease in β results closely spaced buckling values.

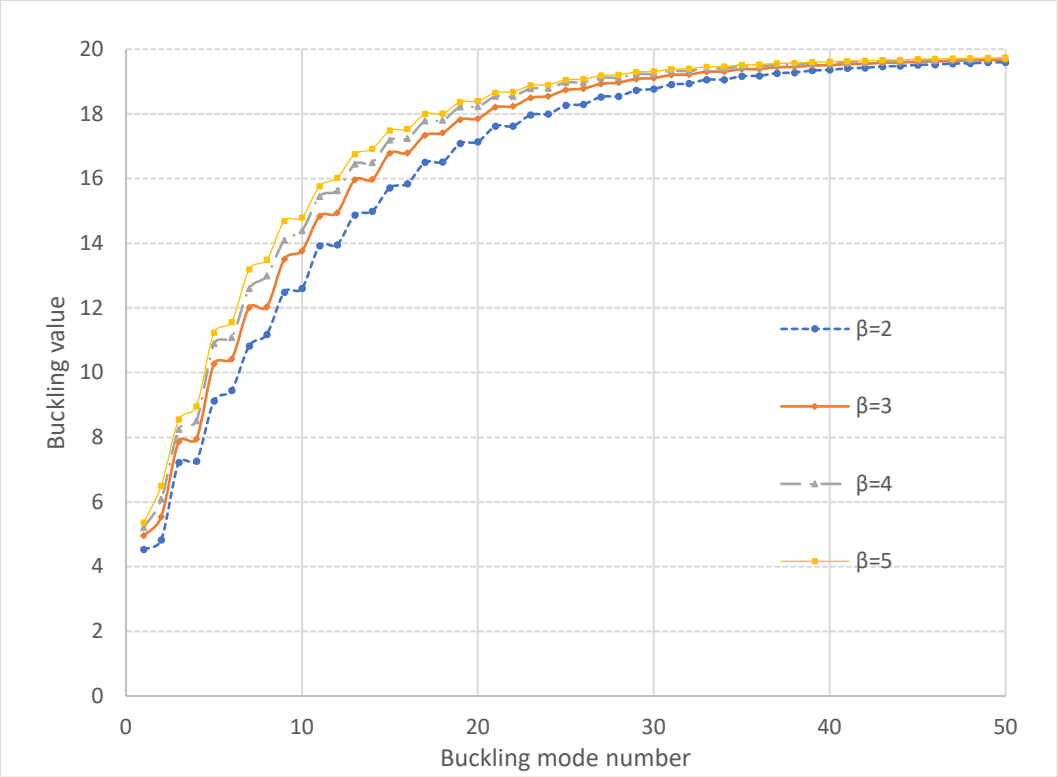

Figure 4.21: Influence of β on Buckling load of C_{3v} Frame

4.4 C_{4v} Plane Frame

We now consider the influence of symmetry on the buckling behaviour of a C_{4v} symmetry group which is shown in Figure *4.22 (a)*.

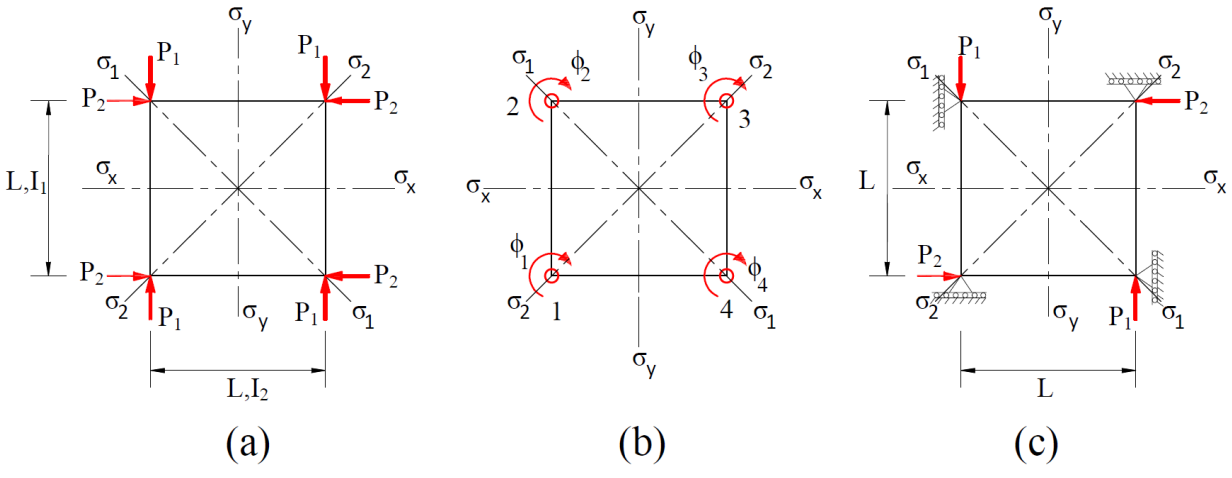

Figure 4.22: C_{4v} symmetric plane frame

The symmetry adapted basis vectors for the frame shown in Figure *4.22 (b)* can be obtained by applying idempotent equations *3.219-3.134* to the positional vectors in Figure *4.22 (b)* as outlined in Section *3.2.2.3* of this study.

Subspace S^1

Subspace S^1 is a null space; however, it should be noted that if we also consider translational degrees of freedom at the mid-point of each beam column (Figure *3.10* (b)), this subspace is C_{4v} symmetric as shown in Figure *3.11 (a)*.

Subspace S_2

The basis vector of Subspace S^2

$$\Phi_1^2 = \phi_1 + \phi_2 + \phi_3 + \phi_4 \qquad (4.23)$$

Subspace S^3

$$\Phi_1^3 = \phi_1 - \phi_2 + \phi_3 - \phi_4 \qquad (4.24)$$

Subspace S^4

Subspace S^4 is a null space; however, it should be noted that if we consider rotational degrees at the mid-point of each beam column (Figure *3.10 (b)*), subspace S^4 is C_{2v} symmetric as shown in Figure *3.11 (d)*. The reflection planes in this case are the diagonals σ_1 and σ_2 respectively.

Subspace S^5

$$\Phi_1^5 = \phi_1 - \phi_3 \qquad (4.25)$$

$$\Phi_2^5 = \phi_2 - \phi_4 \qquad (4.26)$$

$$\Phi_1^{5,1} = \phi_1 - \phi_2 - \phi_3 + \phi_4 \qquad (4.27)$$

The sketches of these basis vectors are shown in Figure *4.23* below. The symmetries for the basis vectors shown below are summarised in Table *4.17*. To identify the symmetry pattern of each subspace, unit moments must be applied in accordance with the coordinates of the basis vectors, as shown in Table *4.17*. It should be noted that, the symmetry adapted basis vectors given by equations *4.25* and *4.26* also display C_{1v} symmetry.

Table 4.17: C_{4v} Basis vector symmetries

Figure	Subspace	Symmetry Group	Order (n)	Group index (m/n)	Applied unit moments
(a)	S^2	C_4	4	2	$\phi_1=\phi_2=\phi_3=\phi_4=1$
(b)	S^3	C_{2v}	4	2	$\phi_1=\phi_3=1,\ \phi_2=\phi_4=-1$
(c)	S^5	$C^{x}{}_{1v}$	2	4	$\phi_1=\phi_4=1,\ \phi_2=\phi_3-1$

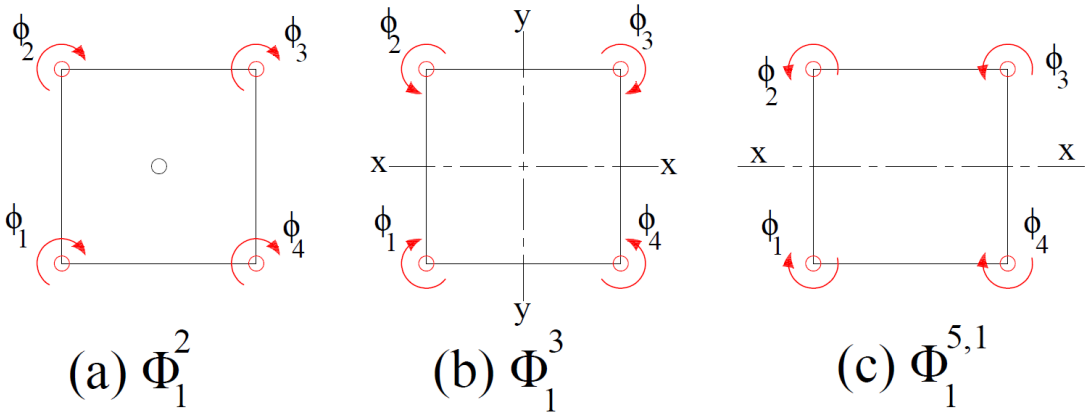

Figure 4.23: Basis vectors for subspaces of C_{4v} symmetric frame

4.4.1 Buckling Behaviour of C_{4v} symmetric frame (Loading)

For this section, two load cases were considered:

i. C_{4v} loading, $P_1=P_2$; and

ii. C_{2v} loading, $P_1=\gamma P_2$

For both load cases, the stiffness of the frame was C_{4v} symmetric, i.e. $I_1=I_2$.

As in the previous frames considered so far, the C_{4v} symmetric frame was first studied analytically using the symmetry adapted slope deflection method to determine the eigenvalues and the symmetries of their eigenmodes. The *FEM* created in Abaqus was validated using these analytical results, and the results from the *FEMs* were used to further investigate the buckling behaviour.

Supposing we are considering the C_{4v} loading described above, using the approach demonstrated for the C_{2v} and C_{3v} frames, respectively, the stability stiffness matrix of the C_{4v} frame shown in Figure *4.22 (b)* can be written as:

$$A = \frac{EI}{L}\begin{bmatrix} 2s & sc & 0 & sc \\ sc & 2s & sc & 0 \\ 0 & sc & 2s & sc \\ sc & 0 & sc & 2s \end{bmatrix} \qquad (4.28)$$

We can now employ the group theoretic approach to determine the symmetry adapted matrix *B* for each subspace and then employ Equations *4.6* and *4.7* to determine the eigenvalues and eigenvectors, respectively.

Subspace S^2

$$\begin{aligned} B^2 &= a_{11} + a_{12} + a_{13} + a_{14} + a_{15} \\ &= 2s + sc + 0 + 0 + sc \\ &= 2s + 2sc \\ \left|B^2\right| &= s + sc = s(1+c) = 0 \end{aligned}$$

Solving this trigonometric equation we find the eigenvalues as:

$$\lambda_1 = 6.2832 = 2\pi$$
$$\lambda_n = 2n\pi$$

Solving the eigenvectors for each eigenvalue using the full space solution equation 4.7, shows that for each eigenvalue the eigenvector is C_4 and C_{4v} symmetric. The eigenvalues and eigenvectors obtained from the analytical analysis for S^2 are summarised in Table *4.18* below.

Table 4.18: C_{4v} plane frame: subspace S^2 eigenvalues and eigenvectors

λ	ϕ_1	ϕ_2	ϕ_3	ϕ_4	symmetry group
6.2832	0.5000	0.5000	0.5000	0.5000	C_4
6.2832	-5.0000E-08	-5.0000E-08	-5.0000E-08	-5.0000E-08	C_{4v}
12.5664	0.5000	0.5000	0.5000	0.5000	C_4
12.5664	-5.0000E-08	-5.0000E-08	-5.0000E-08	-5.0000E-08	C_{4v}
18.8496	0.5000	0.5000	0.5000	0.5000	C_4
18.8496	-5.0000E-08	-5.0000E-08	-5.0000E-08	-5.0000E-08	C_4
25.1327	0.5000	0.5000	0.5000	0.5000	C_4
25.1327	-2.6360E-07	-2.6360E-07	-2.6360E-07	-2.6360E-07	C_{4v}

It should be noted that, though the numerical solution to Equation *4.7* indicates the presence of C_{4v} modes in subspace S^2, this is not actually the case. As shown for the C_{3v} frame problem, the zero displacements in Table 4.*18* indicate that the C_{4v} modes are actually produced in subspace S^1. Recall that it is subspace S^1 that has zero basis vectors at the vertices. Furthermore, from Figure *3.11* (a), we observe that Subspace S^1 is C_{4v} symmetric, with zero rotational displacements at the vertices and mid-point of every member. Also, there are non-zero lateral displacements at mid-points of every member.

Subspace S^3

$$B^3 = a_{11} - a_{12} + a_{13} - a_{14}$$
$$= 2s - sc + 0 - sc$$
$$= 2s - 2sc$$
$$\left|B^3\right| = 2s(1-c) = 0$$
$$\lambda_1 = 3.1416 = \pi$$
$$\lambda_n = (2n-1)\pi$$

Solving the eigenvectors for each eigenvalue using the full space solution equation 4.7, shows that for each eigenvalue the eigenvector is C_{2v} symmetric. The eigenvalues and eigenvectors obtained from the analytical analysis for S^3 are summarised in Table *4.19* below.

Table 4.19: C_{4v} plane frame: subspace S^3 eigenvalues and eigenvectors

λ	ϕ_1	ϕ_2	ϕ_3	ϕ_4	symmetry group
3.1416	-0.5000	0.5000	-0.5000	0.5000	C_{2v}
9.4248	-0.5000	0.5000	-0.5000	0.5000	C_{2v}
15.7080	-0.5000	0.5000	-0.5000	0.5000	C_{2v}
21.9911	-0.5000	0.5000	-0.5000	0.5000	C_{2v}
28.2743	-0.5000	0.5000	-0.5000	0.5000	C_{2v}

Subspace $S^{5,1}$

$$B^{5,1} = a_{11} - a_{12} - a_{13} + a_{14}$$
$$= 2s - sc - 0 + sc$$
$$\left|B^{5,1}\right| = s = 0$$
$$\lambda_1 = 4.4934$$
$$\lambda_n \approx 3.1796n + 1.3433$$

Solving for the eigenvectors for each eigenvalue using the full space solution equation *4.7*, shows that for each eigenvalue the eigenvector is C_{1v} symmetric.

Table 4.20: C_{4v} plane frame: subspace $S^{5,1}$ eigenvalues and eigenvectors

λ	ϕ_1	ϕ_2	ϕ_3	ϕ_4	symmetry group
4.4934	0.0000	-0.7071	0.0000	0.7071	C^2_{1v}
7.7253	0.7071	0.0000	-0.7071	0.0000	C^1_{1v}
10.9041	0.0000	-0.7071	0.0000	0.7071	C^2_{1v}
14.0662	0.0000	-0.7071	0.0000	0.7071	C^2_{1v}

Subspace S^4

As shown earlier, subspace S^4 is a null space if the model shown in Figure *4.22 (a)* is used. However, if the model shown in Figure *3.10 (b)* is used, S^4 is C_{2v} symmetric with rotational degrees of freedom at the midpoints of every member shown in Figure 3.*11 (d)*. Therefore, the problem of the buckling modes for subspace S^4 may be modelled as a column fixed at both with lateral restraint at the midspan as an approximate case.

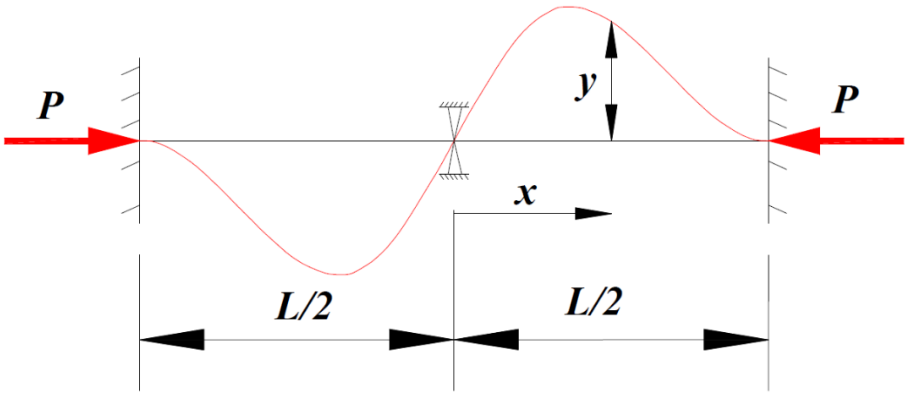

Figure 4.24: C_{4v} plane frame Subspace S^4 buckling model

The general differential equation that governs the deflection of such a column is given by (Chajes, 1974):

$$\left(y''\right)''+\lambda^2 y''=0$$

Where

$$\lambda^2 = \frac{P}{EI}$$

The solution is given by:

$$y = A + Bx + C\sin\lambda x + D\cos\lambda x$$

Applying the following boundary Equations:

$$y(0) = 0$$
$$y''(0) = \frac{-M_o}{EI}$$
$$y(L/2) = 0$$
$$y'(L/2) = 0$$

Where M_o is the internal moment at the midspan of the column

The resulting linear equations can be solved using Crammers Rule, that is:

$$\phi_i = \frac{D_i}{D_n}$$

Where:

D_n is the determinant of the left-hand matrix, and D_i is the matrix obtained when the right-hand side replaces the corresponding ϕ_i. The critical state is obtained when ϕ_i becomes very large, and this occurs when the determinant of D_n is equated to zero. Equating the determinant of D_n to zero, we obtain the characteristic equation as:

$$|D_n| = 0 = 2\tan\frac{\lambda l}{2} = \lambda l$$

Solving this characteristic equation, we obtain the lowest and n eigenvalues as:

$$\lambda_1 = 8.9868 = 2.8606\pi$$
$$\lambda_n = (2.0212n + 0.8622)\pi$$

The table below presents a summary of the results obtained from the analytical analysis.

Table 4.21: C_{4v} Eigenvalues obtained by analytical method

No	Eigenvalue	Eigenmode symmetry
1	3.142	C_{2v}
2	4.493	C_{1v}
3	6.283	C_4, C_{4v}
4	7.725	C_{1v}
5	8.987	C_{2v}
6	9.425	C_{2v}
7	10.904	C_{1v}
8	12.566	C_4, C_{4v}
9	14.066	C_{1v}
10	15.451	C_{2v}
11	15.708	C_{2v}
12	17.221	C_{1v}
13	18.850	C_4, C_{4v}
14	21.808	C_{2v}

The analytical solution shows that the lowest eigenvalue is equal to π and its eigenmode is C_{2v} symmetric. This result is also reported in literature (Timošenko & Gere, 1963).

A *FEM* of a C_{4v} frame was created using Abaqus, and the first fifty eigenmodes and eigenvalues were produced. The boundary conditions applied to the *FEM* are shown in Figure *4.22 (c).* The convergence analysis (Figure *4.25*) was based on the analytical results of buckling loads obtained from the symmetry adapted slope deflection for C_{4v} loading and stiffness. Samples of the produced eigenmodes are shown in *Figure 4.26*.

The symmetry of eigenmodes for each eigenvalue was also categorised, and these are shown for the first fourteen eigenvalues in Table *4.22*. It is clear that the eigenvalues and eigenmode symmetry classification obtained from the finite element analysis agree with the results obtained from the analytical solution.

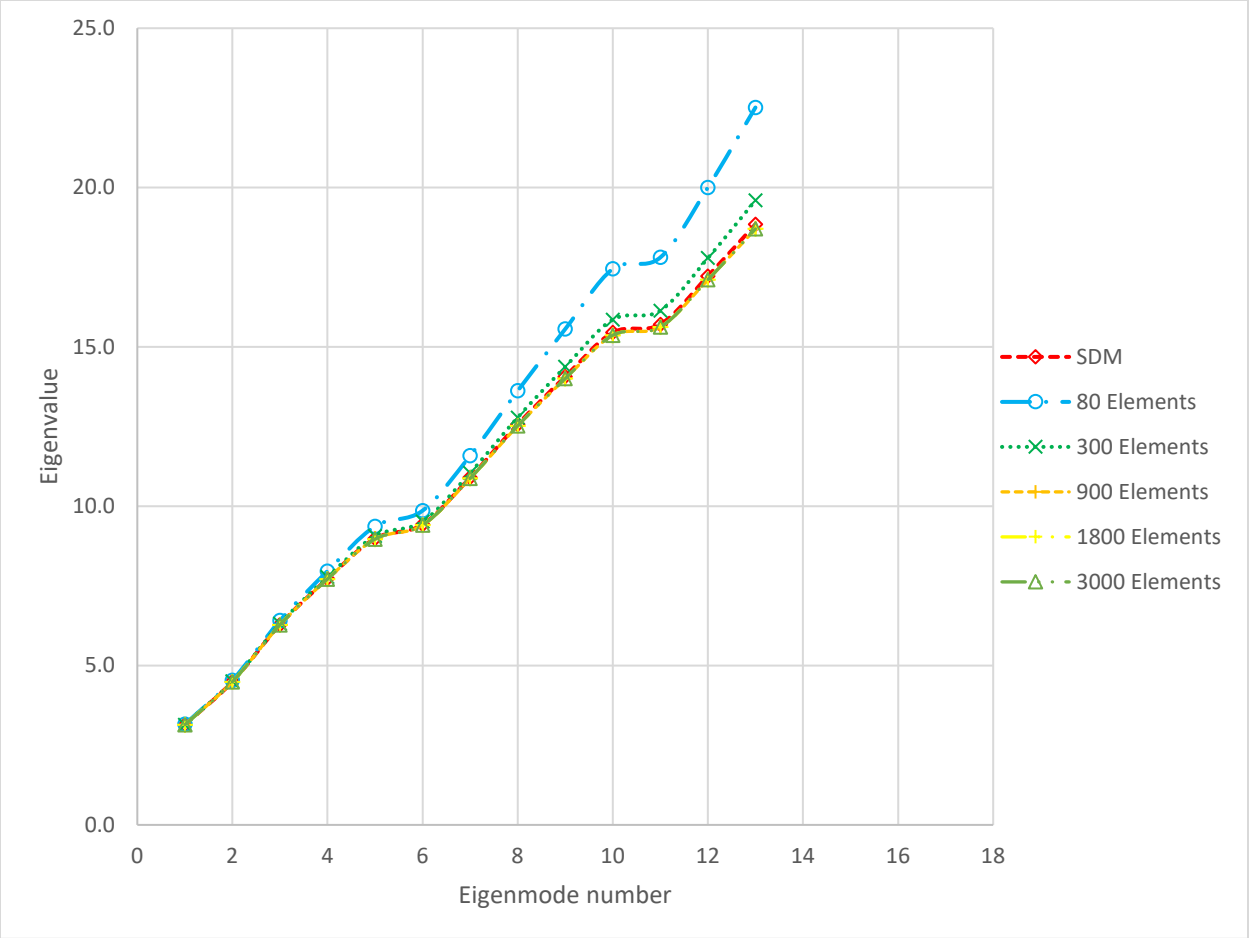

Figure 4.25: C_{4v} plane frame FEM convergence analysis

It is observed from Tables *4.22* and *4.21* that the lowest eigenvalue has an eigenmode with C_{2v} symmetry. The C_{2v} and C_4 symmetry groups have the lowest group index in Table *4.17*. The lowest eigenvalue has an eigenmode that is C_{nv} symmetric with the lowest index. Subsequent eigenvalues have eigenmodes belonging to C_{nv} symmetry groups of higher group index. It should be noted that the group-theoretic repeating eigenvalues have C_{1v} symmetric eigenmodes. On the other hand, parametric repeating eigenvalues have C_4 or C_{4v} symmetric eigenmodes. It is worth noting that the C_{2v} symmetric eigenmode for the eighth eigenvalue had diagonal lines of symmetry as opposed to the eigenmode for the first eigenvalue with the *x,* and *y* axes as the lines of symmetry.

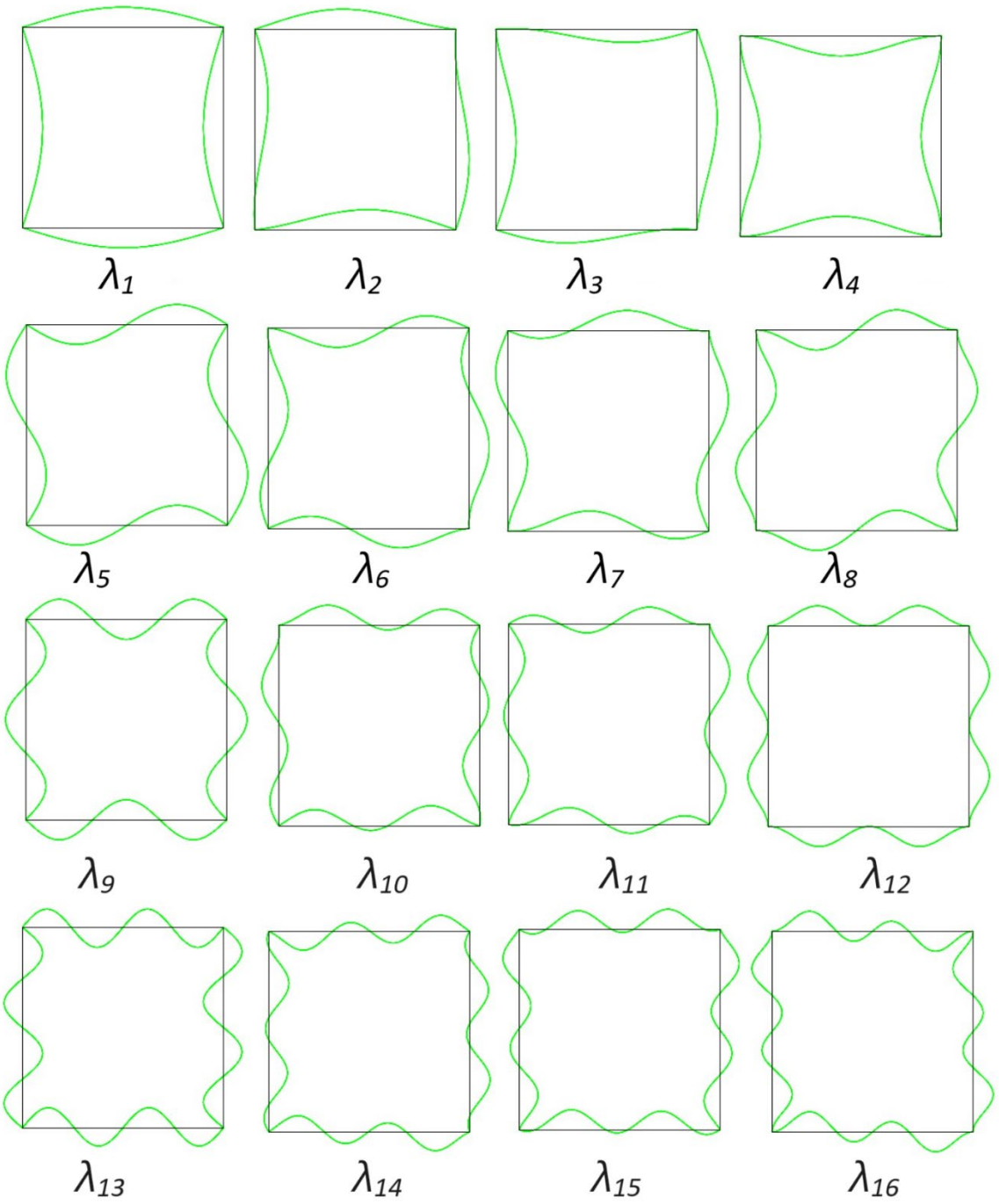

Figure 4.26: C_{4v} plane frame eigenmodes

The pattern of the emergence of symmetries of eigenmodes shown in Table *4.22* was repeating for every eighth eigenvalue for the first fifty eigenvalues produced from the finite element analysis. The reason for this clear repeating pattern can be seen in Figure *4.27,* shown below of plots of

eigenvalues produced from each subspace from the analytical analysis. The curves intersect at only one point, and thus the symmetries of the eigenmodes emerge in a very clear pattern.

Table 4.22: C_{4v} Eigenvalues obtained from FEM model

Number	Eigenvalue	Eigenmode symmetry
1	3.141	C_{2v}
2	4.492	C^1_{1v}
3	4.492	C^2_{1v}
4	6.278	C_{4v}
5	6.278	C_4
6	7.715	C^2_{1v}
7	7.715	C^1_{1v}
8	8.969	C_{2v}
9	9.407	C_{2v}
10	10.875	C^1_{1v}
11	10.875	C^2_{1v}
12	12.523	C_4
13	12.523	C_{4v}
14	14.004	C^2_{1v}

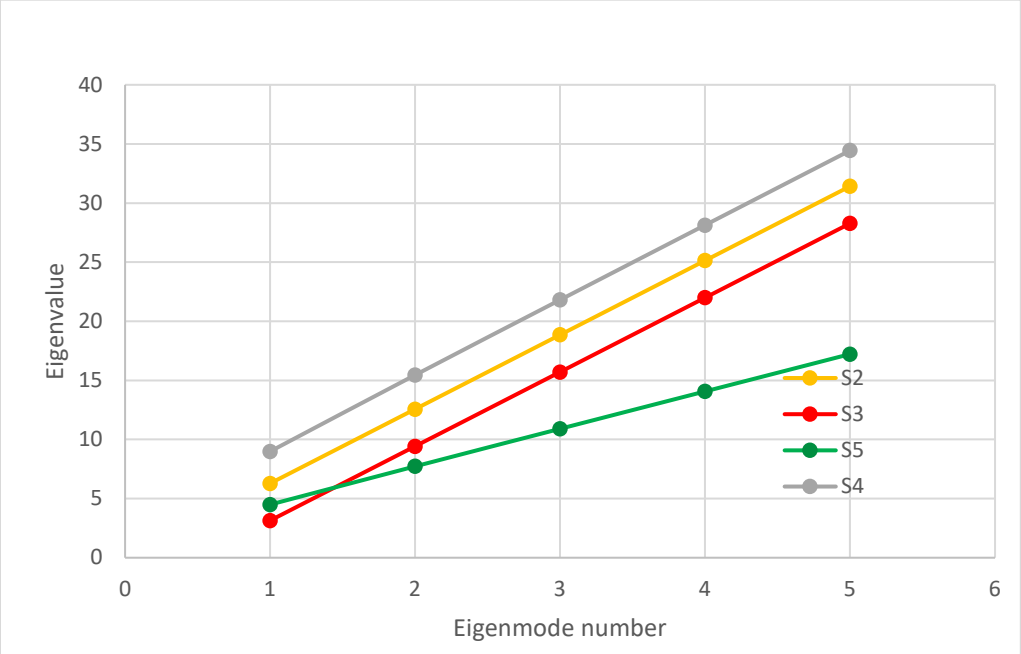

Figure 4.27:C_{4v} Frame, Eigenvalue versus Eigenmode number for each symmetry group

After the *FEM* was validated using analytical results, it was then used to study the effect of C_{2v} loading on the buckling behaviour of a C_{4v} frame. Recall the loading and stiffness arrangement for this case: $P_1=\gamma P_2$ and $I_1=I_2$.

Different load ratios of γ (P_1/P_2) were investigated, and in all cases, all buckling mode symmetries were in accordance with the symmetries of the C_{2v} frame studied earlier. It was also observed that for all the values of γ (*2* to *4*) investigated, the pattern in the emergence of buckling modes was the same for the first seven buckling values, as shown in Table *4.23* below. It was, however, also observed that, unlike the case of C_{4v} loading, the C_{2v} loading case does not show a clear pattern in the repeating sequence of emergence of buckling modes for values of γ investigated. The reason why this is the case becomes apparent when we plot the buckling values for each separate buckling mode symmetry. For example, in the case where $\gamma=2$ and $\gamma=3$ as shown in Figures *4.28* and *4.29* respectively, we observe that the curves for the buckling loads of C^x_{1v} (S^3) and C^y_{1v} (S^4) intersect at several points. As a result, no repeatable sequence in the emergence of buckling mode symmetries is observed. This behaviour was also observed in the other case, where $\gamma=4$. Another observation was that when buckling loads are arranged by buckling mode symmetry for $\gamma\geq2$, the buckling loads for C_2 buckling modes (S^2) and C_{2v} buckling modes (S^1) form the upper and lower bounds, respectively, of the buckling loads, as shown in Figures *4.28* and *4.29*. This means that buckling values with C_2 and C_{2v} symmetric buckling modes form the higher and lower bounds for the buckling loads. When the buckling loads for all values of γ are plotted on the same graph, Figure *4.30*, we easily observe that an increase in γ results in more closely spaced buckling values.

Table 4.23:Buckling behaviour of C_{4v} frame, with C_{2v} loading

No	γ=1		γ=2		γ=3		γ=4	
	λ_{cr}	Symmetry	λ_{cr}	Symmetry	λ_{cr}	Symmetry	λ_{cr}	Symmetry
1	3.141	C_{2v}	2.531	C_{2v}	2.159	C_{2v}	1.910	C_{2v}
2	4.492	$C_{1v,1}$	3.339	$C_{1v,x}$	2.765	$C_{1v,x}$	2.410	$C_{1v,x}$
3	4.492	$C_{1v,2}$	3.967	$C_{1v,y}$	3.500	$C_{1v,y}$	3.140	$C_{1v,y}$
4	6.278	C_{4v}	4.947	C_2	4.143	C_2	3.627	C_2
5	6.278	C_4	5.328	C_{2v}	4.790	C_{2v}	4.367	C_{2v}
6	7.715	$C_{1v,2}$	6.310	$C_{1v,y}$	5.628	$C_{1v,x}$	4.984	$C_{1v,x}$
7	7.715	$C_{1v,1}$	6.524	$C_{1v,x}$	5.741	$C_{1v,y}$	5.370	$C_{1v,y}$
8	8.969	C_{2v}	7.649	C_{2v}	6.764	C_{2v}	6.265	C_2

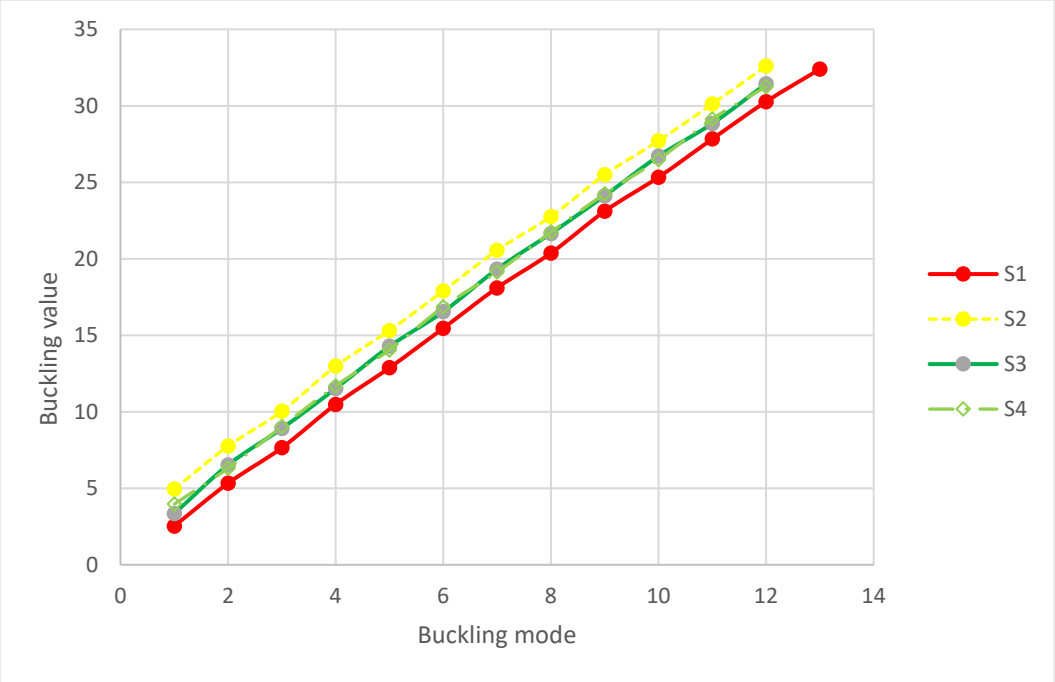

Figure 4.28: C_{2v} loads (γ=2), Buckling value versus buckling mode number for each symmetry group

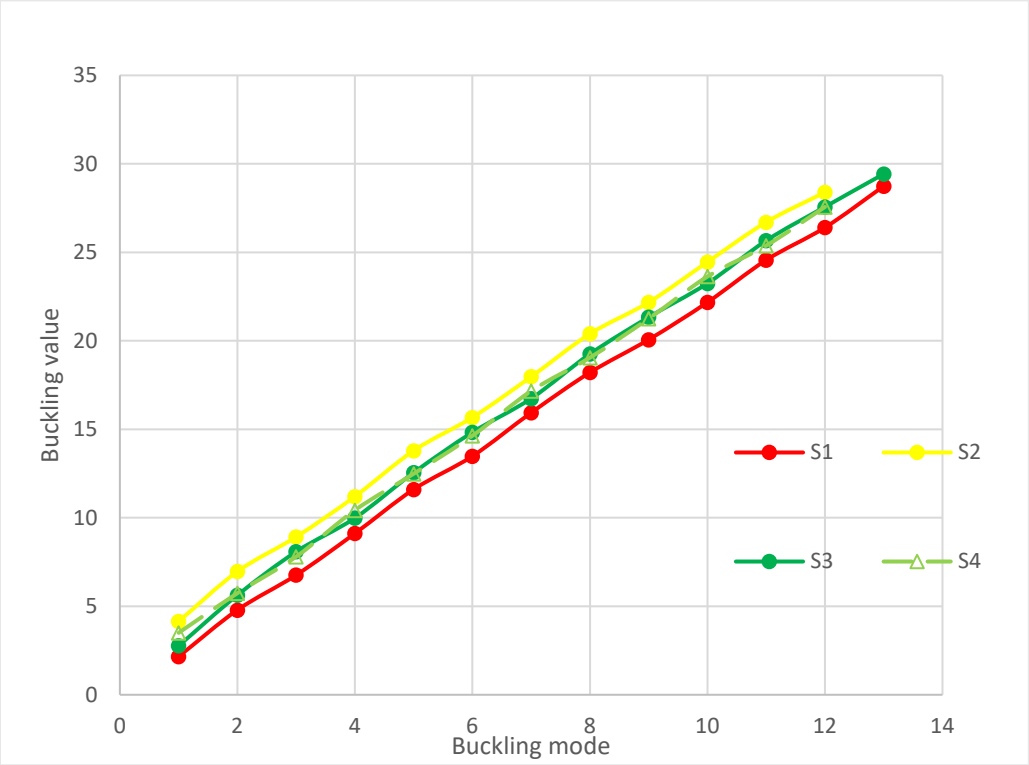

Figure 4.29:C_{2v} loads (γ=3), Buckling value versus buckling mode number for each symmetry group

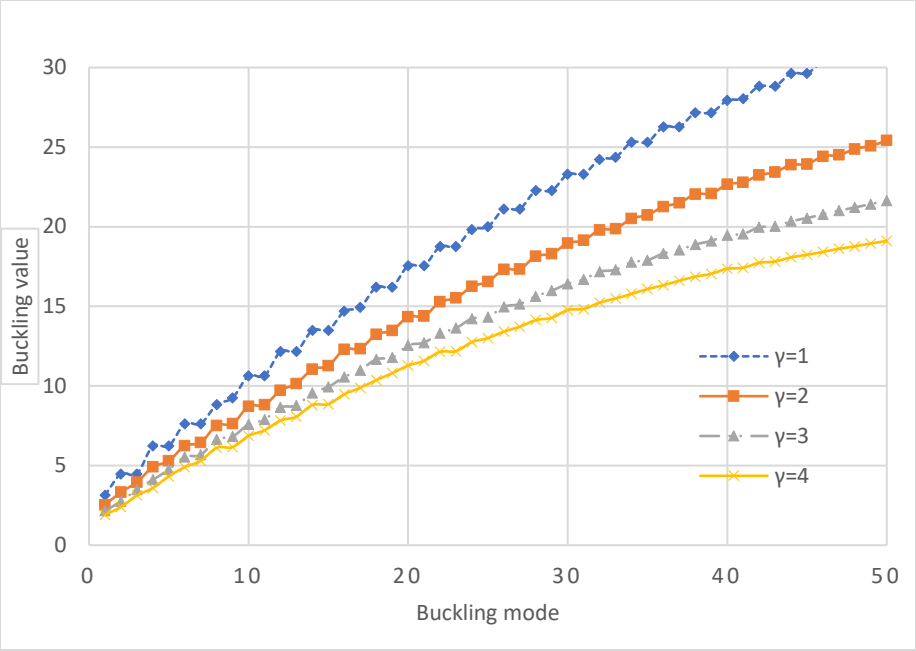

Figure 4.30: Influence of γ on Buckling load of C_{4v} Frame

4.4.2 Buckling Behaviour of C_{4v} symmetric frame with C_{2v} stiffness

The C_{4v} frame shown in Figure *4.22* for this section of the study was subjected to C_{4v} loading, with C_{2v} stiffness ($I_1=\beta I_2$). The buckling behaviour was then investigated using a linear eigenvalue analysis in Abaqus. Different ratios of β were investigated, and in all cases, all buckling mode symmetries were in accordance with the symmetries of the C_{2v} symmetric frame presented in Section *4.2* of this study. It was also observed that for all the values of β *(2 to 4)* investigated, the pattern in the emergence of buckling modes was the same for the first seven buckling values, as shown in Table *4.24* below. Beyond the seventh buckling value, no clear pattern in the emergence of symmetry groups of buckling modes was apparent. This observation can be easily explained when the buckling values are graphed by the symmetry group or subspace, as shown in Figure *4.31* for the case where $\beta=2$. From Figure *4.31*, we can easily observe that the plots for the C^x_{1v} (S^3) and C^y_{1v} (S^4) symmetry groups intersect at several points, and thus no clear sequence in the emergence of symmetry groups was observed. This behaviour was also observed for the case where $\beta=3$ and $\beta=4$. Another observation made was that the buckling values for the C_{2v} and C_2 symmetry groups form the lower and upper bound values, respectively. This was also the case for $\beta=3$ and $\beta=4$. Further, when the buckling loads for all values of β are plotted on the same graph, Figure *4.32*, we easily observe that an increase in β results in less closely spaced buckling values.

Table 4.24: C_{4v} Frame with C_{2v} Stiffness

No	β=1		β=2		β=3		β=4	
	λ_{cr}	symmetry	λ_{cr}	symmetry	λ_{cr}	symmetry	λ_{cr}	symmetry
1	3.141	C_{2v}	3.786	C_{2v}	4.250	C_{2v}	4.600	C_{2v}
2	4.492	C^2_{1v}	5.223	C^x_{1v}	5.554	C^x_{1v}	5.733	C^x_{1v}
3	4.492	C^1_{1v}	5.301	C^y_{1v}	5.847	C^y_{1v}	6.280	C^y_{1v}
4	6.278	C_{4v}	7.179	C_{2v}	7.616	C_{2v}	7.958	C_{2v}
5	6.278	C_4	7.334	C_2	7.850	C_2	8.135	C_2
6	7.715	C^1_{1v}	8.938	C^y_{1v}	9.476	C^y_{1v}	9.810	C^y_{1v}
7	7.715	C^2_{1v}	9.138	C^x_{1v}	10.100	C^x_{1v}	10.763	C^x_{1v}
8	8.969	C_{2v}	10.562	C_2	11.656	C_2	12.528	C_{2v}
9	9.407	C_{2v}	11.216	C_{2v}	12.101	C_{2v}	12.534	C_2
10	10.875	C^1_{1v}	12.574	C^x_{1v}	13.414	C^x_{1vx}	14.125	C^x_{1v}

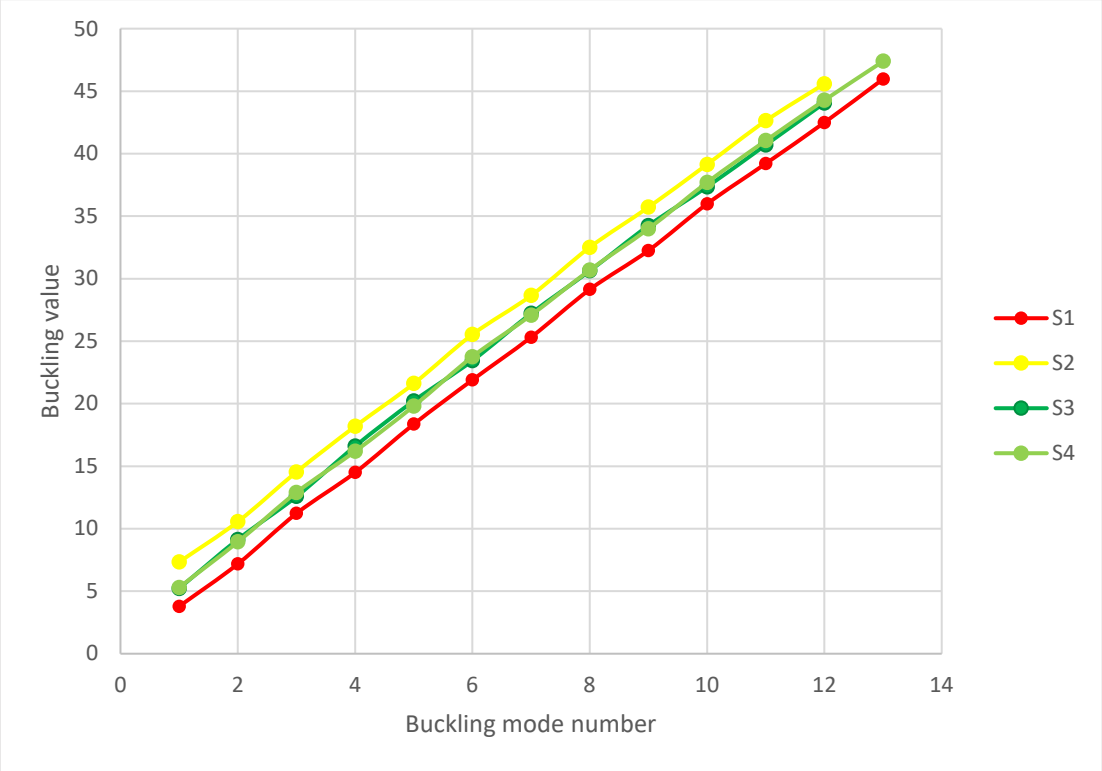

Figure 4.31: Buckling values by symmetry group for β=2 for a C_{4v} frame

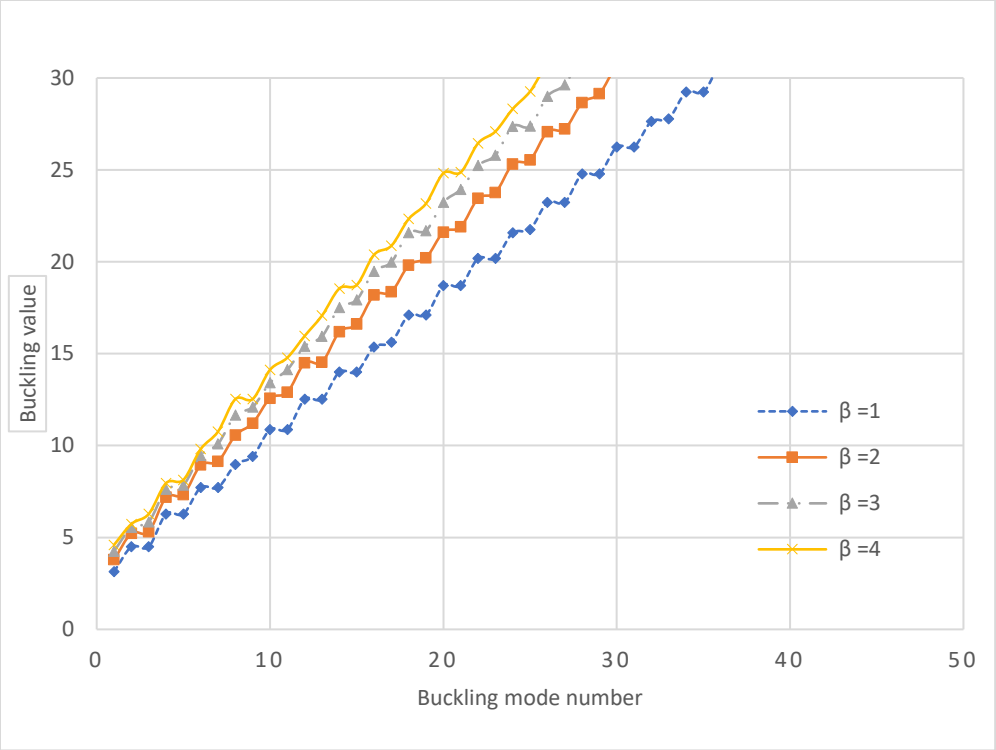

Figure 4.32: Influence of β on Buckling load of C_{4v} Frame

4.5 Plane Frames with C_{5v} symmetry

We now consider the buckling behaviour of a C_{5v} symmetric frame as shown in Figure *4.33 (a)* below.

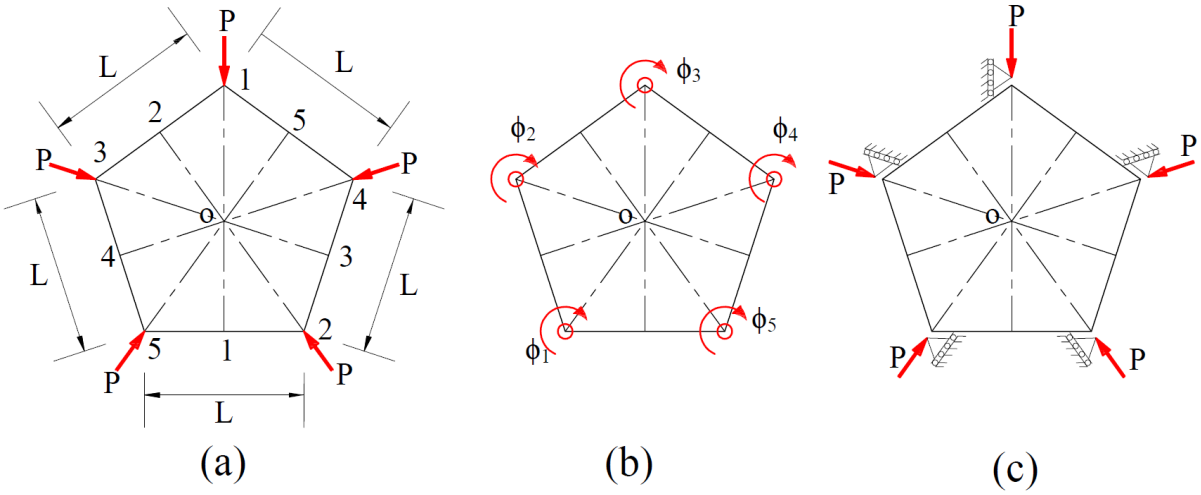

Figure 4.33: C_{5v} symmetric frame

The idempotents for this symmetry group are given as:

$$P^1 = \frac{1}{10}\left(e + C_5 + C_5^{-1} + C_5^2 + C_5^{-2} + \sigma_1 + \sigma_2 + \sigma_3 + \sigma_4 + \sigma_5\right) \qquad (4.29)$$

$$P^2 = \frac{1}{10}\left(e + C_5 + C_5^{-1} + C_5^2 + C_5^{-2} - \sigma_1 - \sigma_2 - \sigma_3 - \sigma_4 - \sigma_5\right) \qquad (4.30)$$

$$P^3 = \frac{1}{5}\left(2e + 0.6180C_5 + 0.6180C_5^{-1} - 1.6180C_5^2 - 1.6180C_5^{-2}\right) \qquad (4.31)$$

$$P^3 = P^{3,1} + P^{3,2}$$

$$P^{3,1} = \frac{1}{10}\begin{pmatrix} e + 0.3090C_5 + 0.3090C_5^{-1} - 0.8090C_5^2 - 0.8090C_5^{-2} \\ +\sigma_1 + 0.3090\sigma_2 - 0.8090\sigma_3 - 0.8090\sigma_4 + 0.3090\sigma_5 \end{pmatrix} \qquad (4.32)$$

$$P^{3,2} = \frac{1}{10}\begin{pmatrix} e + 0.3090C_5 + 0.3090C_5^{-1} - 0.8090C_5^2 - 0.8090C_5^{-2} \\ -\sigma_1 - 0.3090\sigma_2 + 0.8090\sigma_3 + 0.8090\sigma_4 - 0.3090\sigma_5 \end{pmatrix} \qquad (4.33)$$

$$P^4 = \frac{1}{5}\left(2e - 1.6180C_5 - 1.6180C_5^{-1} + 0.6180C_5^2 + 0.6180C_5^{-2}\right) \qquad (4.34)$$

$$P^4 = P^{4,1} + P^{4,2}$$

$$P^{4,1} = \frac{1}{10}\begin{pmatrix} e - 0.8090C_5 - 0.8090C_5^{-1} + 0.3090C_5^2 + 0.3090C_5^{-2} \\ +\sigma_1 - 0.8090\sigma_2 + 0.3090\sigma_3 + 0.3090\sigma_4 - 0.8090\sigma_5 \end{pmatrix} \qquad (4.35)$$

$$P^{4,2} = \frac{1}{10}\begin{pmatrix} e - 0.8090C_5 - 0.8090C_5^{-1} + 0.3090C_5^2 + 0.3090C_5^{-2} \\ -\sigma_1 + 0.8090\sigma_2 - 0.3090\sigma_3 - 0.3090\sigma_4 + 0.8090\sigma_5 \end{pmatrix} \qquad (4.36)$$

To obtain the basis vectors for each subspace we apply each idempotent to each positional vector shown in Figure *4.33 (b).*

Subspace S^1

$$P^1\phi_1 = \frac{1}{10}\left(e + C_5 + C_5^{-1} + C_5^2 + C_5^{-2} + \sigma_1 + \sigma_2 + \sigma_3 + \sigma_4 + \sigma_5\right)\phi_1$$

$$= \frac{1}{10}\left(\phi_1 + \phi_5 + \phi_2 + \phi_4 + \phi_3 - \phi_5 - \phi_4 - \phi_3 - \phi_2 - \phi_1\right) = P^1\phi_5 = P^1\phi_2 = P^1\phi_4 = P^1\phi_3$$

$$= \frac{1}{10}\left(\phi_1 - \phi_1 + \phi_5 - \phi_5 + \phi_2 - \phi_2 + \phi_4 - \phi_4 + \phi_3 - \phi_3\right) = 0$$

Therefore, this subspace is a null subspace. However, it should be noted that if we also consider translational degrees of freedom at mid-length of each beam column towards the centre of rotation, this subspace is C_{5v} symmetric.

Subspace S^2

$$P^2\phi_1 = \frac{1}{10}\left(e + C_5 + C_5^{-1} + C_5^2 + C_5^{-2} - \sigma_1 - \sigma_2 - \sigma_3 - \sigma_4 - \sigma_5\right)\phi_1$$

$$= \frac{1}{10}\left(\phi_1 + \phi_5 + \phi_2 + \phi_4 + \phi_3 + \phi_5 + \phi_4 + \phi_3 + \phi_2 + \phi_1\right) = P^2\phi_5 = P^2\phi_2 = P^2\phi_4 = P^2\phi_3$$

$$= \frac{1}{10}\left(\phi_1 + \phi_1 + \phi_5 + \phi_5 + \phi_2 + \phi_2 + \phi_4 + \phi_4 + \phi_3 + \phi_3\right)$$

$$= \frac{1}{5}\left(\phi_1 + \phi_5 + \phi_2 + \phi_4 + \phi_3\right)$$

$$\Phi_1^2 = \phi_1 + \phi_2 + \phi_3 + \phi_4 + \phi_5$$

The basis vectors of subspace S^2 are therefore:

$$\Phi_1^2 = \phi_1 + \phi_2 + \phi_3 + \phi_4 + \phi_5 \qquad (4.37)$$

Subspace S^3

$$P^3\phi_1 = \frac{1}{5}\left(2e + 0.6180C_5 + 0.6180C_5^{-1} - 1.6180C_5^2 - 1.6180C_5^{-2}\right)\phi_1$$

$$= \frac{1}{10}\left(2\phi_1 + 0.6180\phi_5 + 0.6180\phi_2 - 1.6180\phi_4 - 1.6180\phi_3\right) = P^3\phi_5 = P^3\phi_2 = P^3\phi_4 = P^3\phi_3$$

$$= \frac{1}{10}\left(2\phi_1 + 0.6180\phi_5 + 0.6180\phi_2 - 1.6180\phi_4 - 1.6180\phi_3\right)$$

$$\Phi_1^3 = 2\phi_1 + 0.6180\phi_2 - 1.6180\phi_3 - 1.6180\phi_4 + 0.6180\phi_5$$

$$\Phi_1^3 = \frac{1}{2}\left(\phi_1 + 0.3090\phi_2 - 0.8090\phi_3 - 0.8090\phi_4 + 0.3090\phi_5\right)$$

$$P_3\phi_2 = \frac{1}{5}\left(2e + 0.6180C_5 + 0.6180C_5^{-1} - 1.6180C_5^2 - 1.6180C_5^{-2}\right)\phi_2$$

$$= \frac{1}{10}\left(2\phi_2 + 0.6180\phi_1 + 0.6180\phi_3 - 1.6180\phi_5 - 1.6180\phi_4\right) = P_1\phi_1 = P_1\phi_3 = P_1\phi_5 = P_1\phi_4$$

$$= \frac{1}{10}\left(0.6180\phi_1 + 2\phi_2 + 0.6180\phi_3 - 1.6180\phi_4 - 1.6180\phi_5\right)$$

$$\Phi_2^3 = 0.6180\phi_1 + 2\phi_2 + 0.6180\phi_3 - 1.6180\phi_4 - 1.6180\phi_5$$

$$\Phi_2^3 = \frac{1}{2}\left(0.3090\phi_1 + \phi_2 + 0.3090\phi_3 - 0.8090\phi_4 - 0.8090\phi_5\right)$$

Subspace $S^{3,1}$

$$P_{3,1}\phi_1 = \frac{1}{10}\begin{pmatrix} e + 0.3090C_5 + 0.3090C_5^{-1} - 0.8090C_5^2 - 0.8090C_5^{-2} \\ +\sigma_1 + 0.3090\sigma_2 - 0.8090\sigma_3 - 0.8090\sigma_4 + 0.3090\sigma_5 \end{pmatrix}\phi_1$$

$$= \frac{1}{10}\begin{pmatrix} \phi_1 + 0.3090\phi_5 + 0.3090\phi_2 - 0.8090\phi_4 - 0.8090\phi_3 \\ -\phi_5 - 0.3090\phi_4 + 0.8090\phi_3 + 0.8090\phi_2 - 0.3090\phi_1 \end{pmatrix}$$

$$= \frac{1}{10}\begin{pmatrix} \phi_1 - 0.3090\phi_1 + 0.3090\phi_5 - \phi_5 + 0.3090\phi_2 + 0.8090\phi_2 \\ -0.8090\phi_4 - 0.3090\phi_4 - 0.8090\phi_3 + 0.8090\phi_3 \end{pmatrix}$$

$$= \frac{1}{10}\left(0.6910\phi_1 - 0.6910\phi_5 + 1.1180\phi_2 - 1.1180\phi_4\right)$$

$$\Phi_1^{3,1} = 0.6910\phi_1 + 1.1180\phi_2 - 1.1180\phi_4 - 0.6910\phi_5 = \frac{1}{1.1180}\left(0.6181\phi_1 + \phi_2 - \phi_4 - 0.6181\phi_5\right)$$

The basis vectors of subspace S^3 are therefore:

$$\Phi_1^3 = 2\phi_1 + 0.6180\phi_2 - 1.6180\phi_3 - 1.6180\phi_4 + 0.6180\phi_5 \qquad (4.38)$$

$$\Phi_2^3 = 0.6180\phi_1 + 2\phi_2 + 0.6180\phi_3 - 1.6180\phi_4 - 1.6180\phi_5 \qquad (4.39)$$

$$\Phi_1^{3,1} = 0.6910\phi_1 + 1.1180\phi_2 - 1.1180\phi_4 - 0.6910\phi_5 \qquad (4.40)$$

Subspace S^4

$$P^4\phi_1 = \frac{1}{5}\left(2e - 1.6180C_5 - 1.6180C_5^{-1} + 0.6180C_5^2 + 0.6180C_5^{-2}\right)\phi_1$$

$$= \frac{1}{5}\left(2\phi_1 - 1.6180\phi_5 - 1.6180\phi_2 + 0.6180\phi_4 + 0.6180\phi_3\right)$$

$$= \frac{1}{5}\left(2\phi_1 - 1.6180\phi_2 + 0.6180\phi_3 + 0.6180\phi_4 - 1.6180\phi_5\right)$$

$$\Phi_1^4 = 2\phi_1 - 1.6180\phi_2 + 0.6180\phi_3 + 0.6180\phi_4 - 1.6180\phi_5$$

$$\Phi_1^4 = \frac{1}{2}\left(\phi_1 - 0.8090\phi_2 + 0.3090\phi_3 + 0.3090\phi_4 - 0.8090\phi_5\right)$$

$$P^4\phi_2 = \frac{1}{5}\left(2e - 1.6180C_5 - 1.6180C_5^{-1} + 0.6180C_5^2 + 0.6180C_5^{-2}\right)\phi_2$$

$$= \frac{1}{5}\left(2\phi_2 - 1.6180\phi_1 - 1.6180\phi_3 + 0.6180\phi_5 + 0.6180\phi_4\right)$$

$$= \frac{1}{5}\left(2\phi_2 - 1.6180\phi_1 - 1.6180\phi_3 + 0.6180\phi_5 + 0.6180\phi_4\right)$$

$$\Phi_2^4 = -1.6180\phi_1 + 2\phi_2 - 1.6180\phi_3 + 0.6180\phi_4 + 0.6180\phi_5$$

$$\Phi_2^4 = \frac{1}{2}\left(-0.8090\phi_1 + \phi_2 - 0.8090\phi_3 + 0.3090\phi_4 + 0.3090\phi_5\right)$$

Subspace $S^{4,1}$

$$P^{4,1}\phi_1 = \frac{1}{10}\begin{pmatrix} e - 0.8090C_5 - 0.8090C_5^{-1} + 0.3090C_5^2 + 0.3090C_5^{-2} \\ +\sigma_1 - 0.8090\sigma_2 + 0.3090\sigma_3 + 0.3090\sigma_4 - 0.8090\sigma_5 \end{pmatrix}\phi_1$$

$$= \frac{1}{10}\begin{pmatrix} \phi_1 - 0.8090\phi_5 - 0.8090\phi_2 + 0.3090\phi_4 + 0.3090\phi_3 \\ -\phi_5 + 0.8090\phi_4 - 0.3090\phi_3 - 0.3090\phi_2 + 0.8090\phi_1 \end{pmatrix}$$

$$= \frac{1}{10}\begin{pmatrix} \phi_1 + 0.8090\phi_1 - 0.8090\phi_2 - 0.3090\phi_2 + 0.3090\phi_3 - 0.3090\phi_3 \\ -\phi_5 - 0.8090\phi_5 + 0.8090\phi_4 + 0.3090\phi_4 \end{pmatrix}$$

$$= \frac{1}{10}\left(1.8090\phi_1 - 1.1180\phi_2 + 1.1180\phi_4 - 1.8090\phi_5\right)$$

$$\Phi_1^{4,1} = 1.8090\phi_1 - 1.1180\phi_2 + 1.1180\phi_4 - 1.8090\phi_5$$

$$\Phi_1^{4,1} = \frac{1}{1.8090}\left(\phi_1 - 0.6180\phi_2 + 0.6180\phi_4 - \phi_5\right)$$

The basis vectors of subspace S^4 are therefore:

$$\Phi_1^4 = 2\phi_1 - 1.6180\phi_2 + 0.6180\phi_3 + 0.6180\phi_4 - 1.6180\phi_5 \qquad (4.41)$$

$$\Phi_2^4 = -1.6180\phi_1 + 2\phi_2 - 1.6180\phi_3 + 0.6180\phi_4 + 0.6180\phi_5 \qquad (4.42)$$

$$\Phi_1^{4,1} = 1.8090\phi_1 - 1.1180\phi_2 + 1.1180\phi_4 - 1.8090\phi_5 \qquad (4.43)$$

The sketches of these basis vectors are shown in Figure *4.34* below, and the symmetries of the basis vectors are summarised in Table *4.25* below. To correctly identify the symmetry of each subspace unit, moments must be applied to the basis vectors as given in Table *4.25*.

Table 4.25: C_{5v} Basis vector symmetries

Figure	Subspace	Symmetry Group	order (n)	index (m/n)	Applied unit moments
(a)	S^2	C_5	5	2	$\phi_1 = \phi_2 = \phi_3 = \phi_4 = \phi_5 = 1$
(b)	S^3	C_1	1	10	$\phi_1 = 1,\ \phi_2 = 0.3090,\ \phi_3 = -0.8090$ $\phi_4 = -0.8090,\ \phi_5 = 0.3090$
(b)	S^3	C_1	1	10	$\phi_1 = 0.3090,\ \phi_2 = 1,\ \phi_3 = 0.3090$ $\phi_4 = -0.8090,\ \phi_5 = -0.8090$
(b)	S^3	C_{1v}	2	5	$\phi_1 = 0.6181,\ \phi_5 = -0.6181,\ \phi_2 = 1,\ \phi_4 = -1$
(c)	S^4	C_1	1	10	$\phi_1 = 1,\ \phi_2 = -0.8090,\ \phi_3 = 0.3090,$ $\phi_4 = 0.3090,\ \phi_5 = -0.8090$
(c)	S^4	C_1	1	10	$\phi_1 = -0.8090,\ \phi_2 = 1,\ \phi_3 = -0.8090$ $\phi_4 = 0.3090,\ \phi_5 = 0.3090$
(c)	S^4	C_{1v}	2	5	$\phi_1 = 1,\ \phi_2 = -0.6180,\ \phi_4 = 0.6180,\ \phi_5 = -1$

4.5.1 Buckling Behaviour of C_{5v} symmetric frame

The C_{5v} symmetric frame was first studied analytically using the slope deflection method to determine the eigenvalues and the symmetries of their eigenmodes. The software Matlab was used to solve trigonometric equations to obtain eigenvalues from equation *4.6*. The eigenmodes were also solved by utilising Matlab to solve the resulting matrix linear equations from the implementation of equation *4.7*.

Following the procedure previously shown for the C_{3v} plane frame, the stiffness matrix of the C_{5v} frame shown in Figure *4.33 (b)* can be written as:

$$K = \frac{EI}{L}\begin{bmatrix} 2s & sc & 0 & 0 & sc \\ sc & 2s & sc & 0 & 0 \\ 0 & sc & 2s & sc & 0 \\ 0 & 0 & sc & 2s & sc \\ sc & 0 & 0 & sc & 2s \end{bmatrix} \qquad (4.44)$$

We can now employ the group theoretic approach to determine the symmetry adapted matrix B for each subspace and determine the eigenvalues and eigenvectors, respectively.

Subspace S^2

$$\begin{aligned} B^2 &= a_{11} + a_{12} + a_{13} + a_{14} + a_{15} \\ &= 2s + sc + 0 + 0 + sc \\ &= 2s + 2sc \\ \left|B^2\right| &= s + sc = s(1+c) = 0 \end{aligned}$$

Solving this trigonometric equation, we find the eigenvalues as:

$$\lambda_1 = 6.2832$$
$$\lambda_n = 2n\pi$$

Solving the eigenvectors for each eigenvalue using the full space solution equation 4.7 shows that for each eigenvalue, the eigenvector is C_5 and C_{5v} symmetric. The eigenvalues and eigenvectors obtained from the analytical analysis for S^2 are summarised in Table *4.26* below.

Table 4.26: C_{5v} subspace S^2 eigenvalues and eigenvectors

λ	ϕ_1	ϕ_2	ϕ_3	ϕ_4	ϕ_5	symmetry group
6.2714	0.1329	0.1329	0.1329	0.1329	0.1329	C_5
6.2714	0.8333E-7	0.8333E-7	0.8333E-7	0.8333E-7	0.8333E-7	C_{5v}
12.4720	0.1329	0.1329	0.1329	0.1329	0.1329	C_5
12.4720	0.8333E-7	0.8333E-7	0.8333E-7	0.8333E-7	0.8333E-7	C_{5v}
18.5358	0.0863	0.0863	0.0863	0.0863	0.0863	C_5
18.5358	0.6250E-7	0.6250E-7	0.6250E-7	0.6250E-7	0.6250E-7	C_{5v}
24.4031	0.1250	0.1250	0.1250	0.1250	0.1250	C_5
24.4031	0.1250E-6	0.1250E-6	0.1250E-6	0.1250E-6	0.1250E-6	C_{5v}

It's worth noting that the numerical solution to Equation *4.7* reveals that the C_{5v} symmetric modes pertain to subspace S^2. However, contrary to this finding, the C_{5v} symmetric modes are actually associated with subspace S^1. This discrepancy mirrors the explanation provided for the C_{3v} frame problem, where the zero displacements listed in Table *4.26* suggest that the C_{5v} modes emerge from subspace S^1. It's important to recall that subspace S^1 features zero basis vectors at the vertices. Consequently, the buckling problem for this mode can be effectively modelled as the buckling of a column fixed at both ends.

Subspace S^3

$$B^{3,1} = a_{11} + \left(\frac{1.1180}{0.6910}\right)a_{12} - \left(\frac{1.1180}{0.6910}\right)a_{14} - a_{15}$$

$$= a_{11} + \left(1 + 2\cos\frac{2\pi}{5}\right)a_{12} - \left(1 + 2\cos\frac{2\pi}{5}\right)a_{14} - a_{15}$$

$$= 2s + \left(1 + 2\cos\frac{2\pi}{5}\right)sc - \left(1 + 2\cos\frac{2\pi}{5}\right)0 - sc$$

$$= 2s + sc + 2sc\left(\cos\frac{2\pi}{5}\right) - sc$$

$$= 2s + 2sc\left(\cos\frac{2\pi}{5}\right)$$

$$\left|B^{3,1}\right| = 2s\left(1 + c\left(\cos\frac{2\pi}{5}\right)\right) = 0$$

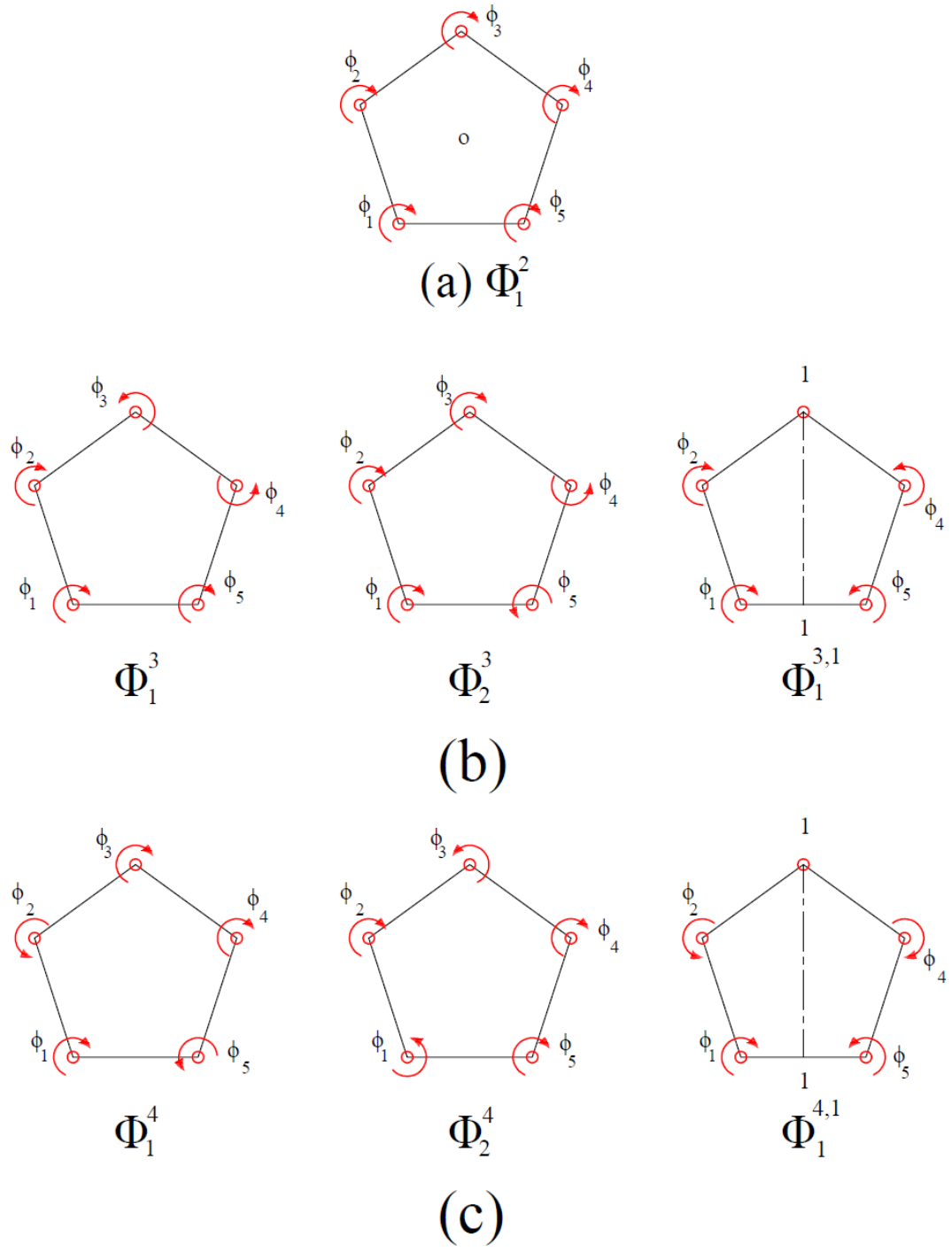

Figure 4.34:C_{5v} symmetric frame basis vectors

Solving for the eigenvalues and respective eigenvectors for subspace S^3 shows that for each eigenvalue, the eigenmode is C_1 or C_{1v} symmetric. The eigenvalues and eigenvectors obtained from the analytical analysis for S^3 are summarised in Table *4.27* below.

Table 4.27: C_{5v} plane frame: subspace S^3 eigenvalues and eigenvectors

λ	ϕ_1	ϕ_2	ϕ_3	ϕ_4	ϕ_5	symmetry group
4.8828	1.0000	0.6181	-0.6181	-1.0000	0.0000	C^2_{1v}
4.8828	-0.8091	0.3090	1.0000	0.3090	-0.8091	C_1
7.4487	1.0000	0.6180	-0.6180	-1.0000	0.0000	C^2_{1v}
7.4487	-1.0000	0.3820	1.2361	0.3820	-1.0000	C_1
11.2478	1.0000	0.6181	-0.6181	-1.0000	0.0000	C^2_{1v}
11.2478	-1.0000	0.3820	1.2361	0.3820	-1.0000	C_1
13.7733	-1.0000	-0.6180	0.6180	1.0000	0.0000	C^2_{1v}
13.7733	1.0000	-0.3820	-1.2361	-0.3820	1.0000	C_1

Subspace S^4

$$B^{4,1} = a_{11} - \left(\frac{1.1180}{1.8090}\right)a_{12} + \left(\frac{1.1180}{1.8090}\right)a_{14} - a_{15}$$

$$= a_{11} - \left(2\cos\frac{2\pi}{5}\right)a_{12} - \left(2\cos\frac{2\pi}{5}\right)a_{14} - a_{15}$$

$$= 2s - \left(2\cos\frac{2\pi}{5}\right)sc - \left(2\cos\frac{2\pi}{5}\right)0 - sc$$

$$= 2s - \left(2\cos\frac{2\pi}{5}\right)sc - sc$$

$$= s\left(2 - c\left(2\cos\frac{2\pi}{5} + 1\right)\right)$$

$$\left|B^{4,1}\right| = s\left(2 - c\left(2\cos\frac{2\pi}{5} + 1\right)\right) = 0$$

Solving for the eigenvalues and respective eigenvectors shows that for each eigenvalue, the eigenmode is C_1 or C_{1v} symmetric. The eigenvalues and eigenvectors obtained from the analytical analysis for S^4 are summarised in Table *4.28* below.

The analytical results obtained from the symmetry adapted slope deflection method are summarised in Table *4.29.* The analytical solution shows that the lowest eigenvalue $\lambda_1 = 1.092\pi$ and its eigenmode is either C_1 or C_{1v} symmetric. However, Timošenko and Gere (1963) report that the lowest eigenvalue as $\lambda_1 = 0.8\pi$ and the eigenmode is not reported.

Table 4.28: C_{5v} plane frame: subspace S^4 eigenvalues and eigenvectors

λ	ϕ_1	ϕ_2	ϕ_3	ϕ_4	ϕ_5	symmetry group
3.4296	-1.0000	1.6180	-1.6180	1.0000	0.0000	C^2_{1v}
3.4296	-0.3090	0.8090	-1.0000	0.8090	-0.3090	C_1
8.5590	-0.6181	1.0000	-1.0000	0.6181	0.0000	C^2_{1v}
8.5590	-0.3090	0.8090	-1.0000	0.8090	-0.3090	C_1
9.8944	-0.6180	1.0000	-1.0000	0.6180	0.0000	C^2_{1v}
9.8944	-0.3090	0.8090	-1.0000	0.8090	-0.3090	C_1
14.9493	-0.6180	1.0000	-1.0000	0.6180	0.0000	C^2_{1v}
14.9493	-0.3090	0.8091	-1.0000	0.8091	-0.3090	C_1

Table 4.29: C_{5v} Eigenvalues obtained by analytical method

No	Eigenvalue	Eigenmode symmetry
1	3.430	C_{1v}, C_1
2	4.883	C_{1v}, C_1
3	6.283	C_5, C_{5v}
4	7.449	C_{1v}, C_1
5	8.559	C_{1v}, C_1
6	9.894	C_{1v}, C_1
7	11.248	C_{1v}, C_1
8	12.566	C_5, C_{5v}
9	13.773	C_{1v}, C_1
10	14.949	C_{1v}, C_1
11	16.234	C_{1v}, C_1
12	17.553	C_{1v}, C_1
13	18.850	C_5, C_{5v}
14	20.072	C_{1v}, C_1

A *FEM* of a C_{5v} frame was created using Abaqus, and the first fifty eigenmodes and eigenvalues were analysed. The boundary conditions applied for the *FEM* are shown in Figure *4.33 (c)*. The convergence analysis was made by comparing the eigenvalues obtained from the analytical analysis with those obtained from the FEM (see Figure *4.35*).

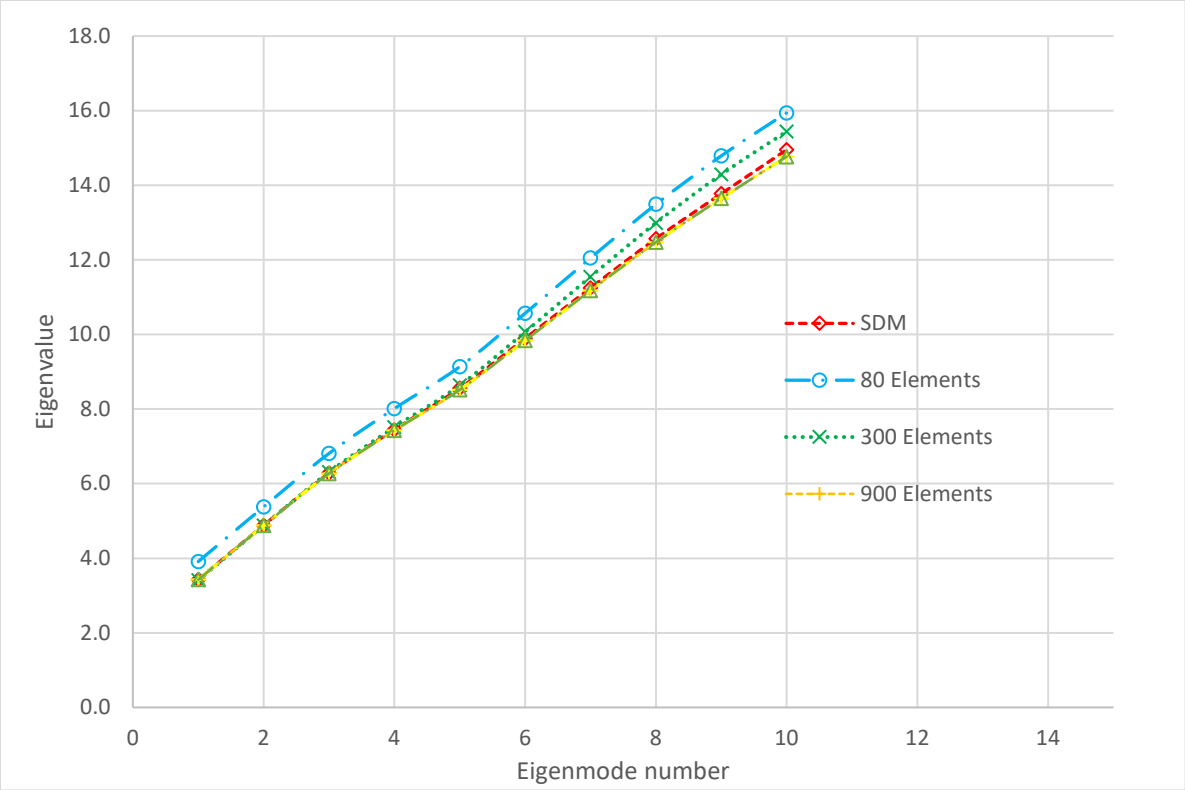

Figure 4.35: C_{5v} Plane frame convergence analysis

The symmetry of eigenmodes for each eigenvalue was also categorised, and these are shown for the first fourteen eigenvalues in Table *4.30*. Sample images of the eigenmodes are shown in Figure *4.36*. It is clear from Tables *4.29* and *4.35* that the results obtained from the finite element analysis agree with the results obtained from the analytical solution in terms of magnitude of eigenvalues and symmetry classification of eigenmode. From Table *4.30*, we observe that group-theoretic repeating eigenvalues have C_1 symmetric eigenmodes. The parametric repeating eigenvalues have eigenmodes that are either C_5 or C_{5v} symmetric. Alternatively, when the group index is five, we have a group theoretic repeating eigenvalue. When the group index is two, we have parametric repeating eigenvalues.

Further, the sequence of eigenmode symmetries shown in Table *4.30* was repeating for every ten eigenvalues, and ten is the group order for the C_{5v} symmetry group. When the results for the eigenvalues obtained from the analytical results are plotted for each subspace, as shown in Figure *4.37* below, it is observed that the curves for subspaces S^3 and S^4 intersect at several points at regular intervals.

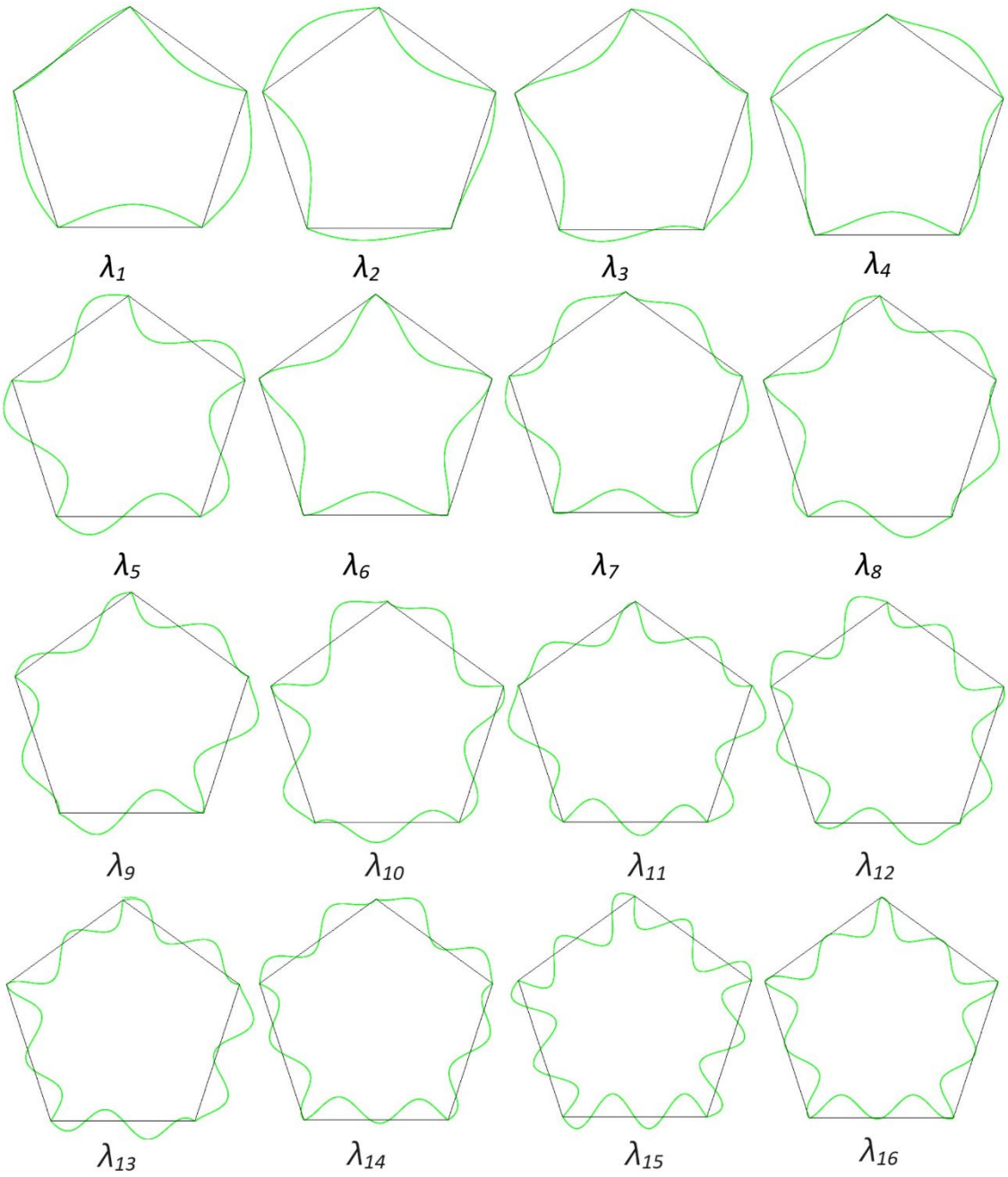

Figure 4.36: C_{5v} plane frame sample Eigenmodes

Table 4.30: C_{5v} Eigenvalues obtained from FEM model

Number	Eigenvalue	Eigenmode symmetry
1	3.426	C_1
2	3.426	C_1
3	4.877	C_1
4	4.877	C_1
5	6.271	C_5
6	6.271	C_{5v}
7	7.428	C_1
8	7.428	C_1
9	8.515	C_1
10	8.515	C_1
11	9.839	C_1
12	9.839	C_1
13	11.179	C_1
14	11.179	C_1

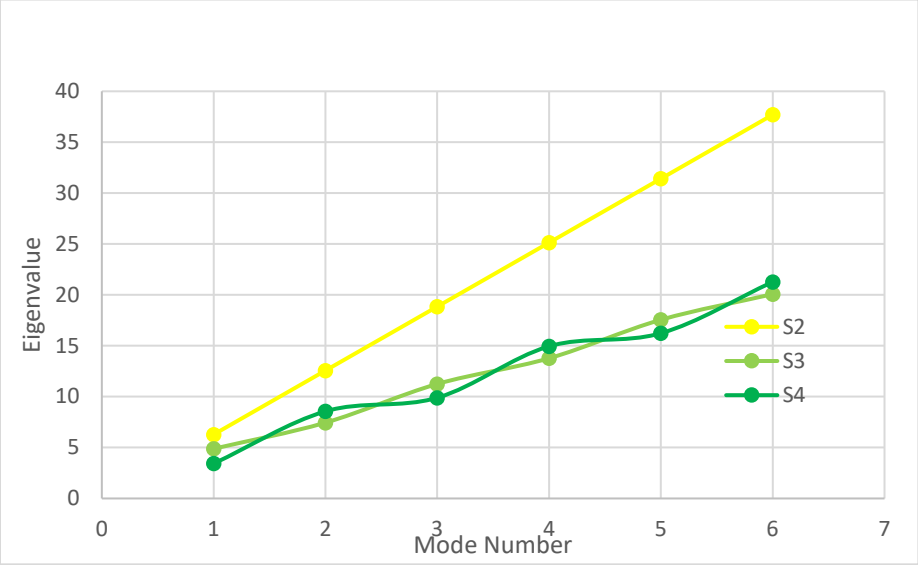

Figure 4.37:C_{5v} Frame, Eigenvalue versus Eigenmode (Analytical results)

4.6 Plane Frames with C_{6v} symmetry

We now consider a C_{6v} symmetric frame as shown in Figure *4.38* below.

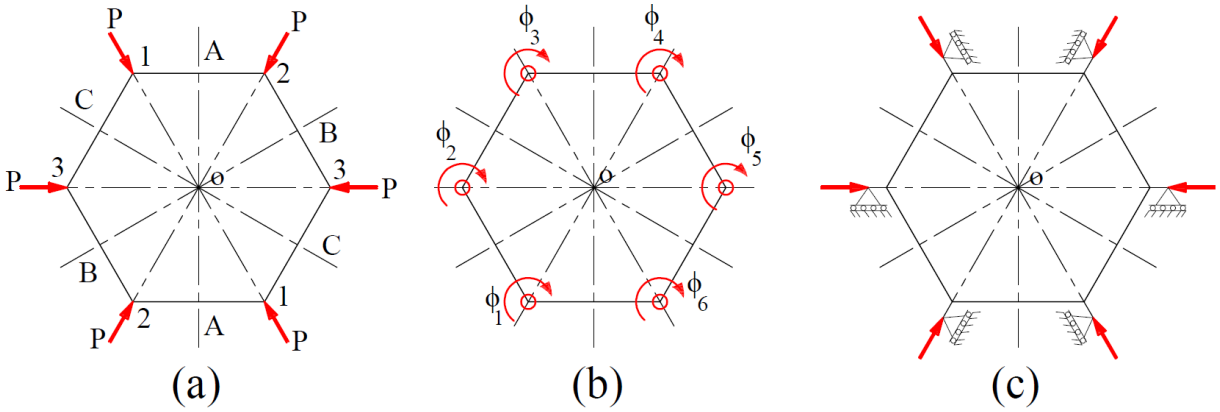

Figure 4.38: C_{6v} Symmetric Frame

The idempotents are given as:

$$P^1 = \frac{1}{12}\left(e + C_6 + C_6^{-1} + C_3 + C_3^{-1} + C_2 + \sigma_A + \sigma_B + \sigma_C + \sigma_1 + \sigma_2 + \sigma_3\right) \qquad (4.45)$$

$$P^2 = \frac{1}{12}\left(e + C_6 + C_6^{-1} + C_3 + C_3^{-1} + C_2 - \sigma_A - \sigma_B - \sigma_C - \sigma_1 - \sigma_2 - \sigma_3\right) \qquad (4.46)$$

$$P^3 = \frac{1}{12}\left(e - C_6 - C_6^{-1} + C_3 + C_3^{-1} - C_2 + \sigma_A + \sigma_B + \sigma_C - \sigma_1 - \sigma_2 - \sigma_3\right) \qquad (4.47)$$

$$P^4 = \frac{1}{12}\left(e - C_6 - C_6^{-1} + C_3 + C_3^{-1} - C_2 - \sigma_A - \sigma_B - \sigma_C + \sigma_1 + \sigma_2 + \sigma_3\right) \qquad (4.48)$$

$$P^5 = \frac{1}{6}\left(2e + C_6 + C_6^{-1} - C_3 - C_3^{-1} - 2C_2\right) \qquad (4.49)$$

$$P^5 = P^{5,1} + P^{5,2}$$

$$P_{5,1} = \frac{1}{6}\left(e + \frac{1}{2}C_6 + \frac{1}{2}C_6^{-1} - \frac{1}{2}C_3 - \frac{1}{2}C_3^{-1} - C_2 - \sigma_A + \frac{1}{2}\sigma_B + \frac{1}{2}\sigma_C - \frac{1}{2}\sigma_1 - \frac{1}{2}\sigma_2 + \sigma_3\right) \qquad (4.50)$$

$$P_{5,2} = \frac{1}{6}\left(e + \frac{1}{2}C_6 + \frac{1}{2}C_6^{-1} - \frac{1}{2}C_3 - \frac{1}{2}C_3^{-1} - C_2 + \sigma_A - \frac{1}{2}\sigma_B - \frac{1}{2}\sigma_C + \frac{1}{2}\sigma_1 + \frac{1}{2}\sigma_2 - \sigma_3\right) \qquad (4.51)$$

$$P_6 = \frac{1}{6}\left(2e - C_6 - C_6^{-1} - C_3 - C_3^{-1} + 2C_2\right) \qquad (4.52)$$

$$P_6 = P_{6,1} + P_{6,2}$$

$$P_{6,1} = \frac{1}{6}\left(e - \frac{1}{2}C_6 - \frac{1}{2}C_6^{-1} - \frac{1}{2}C_3 - \frac{1}{2}C_3^{-1} + C_2 + \sigma_A - \frac{1}{2}\sigma_B - \frac{1}{2}\sigma_C - \frac{1}{2}\sigma_1 - \frac{1}{2}\sigma_2 + \sigma_3 \right) \qquad (4.53)$$

$$P_{6,2} = \frac{1}{6}\left(e - \frac{1}{2}C_6 - \frac{1}{2}C_6^{-1} - \frac{1}{2}C_3 - \frac{1}{2}C_3^{-1} + C_2 - \sigma_A + \frac{1}{2}\sigma_B + \frac{1}{2}\sigma_C + \frac{1}{2}\sigma_1 + \frac{1}{2}\sigma_2 - \sigma_3 \right) \qquad (4.54)$$

To obtain the basis vectors for each subspace, we apply each idempotent to each positional vector shown in Figure *4.38 (b)*.

Subspace S^1

$$P^1\phi_1 = \frac{1}{12}\left(e + C_6 + C_6^{-1} + C_3 + C_3^{-1} + C_2 + \sigma_A + \sigma_B + \sigma_C + \sigma_1 + \sigma_2 + \sigma_3\right)\phi_1$$

$$= \frac{1}{12}\left(\phi_1 + \phi_6 + \phi_2 + \phi_5 + \phi_3 + \phi_4 - \phi_6 - \phi_2 - \phi_4 - \phi_5 - \phi_1 - \phi_3\right) = P^1\phi_6 = P^1\phi_2 = P^1\phi_5 = P^1\phi_3 = P^1\phi_4$$

$$= \frac{1}{12}\left(\phi_1 - \phi_1 + \phi_2 - \phi_2 + \phi_3 - \phi_3 + \phi_4 - \phi_4 + \phi_5 - \phi_5 + \phi_6 - \phi_6\right) = 0$$

Therefore, subspace S^1 is a null space. However, this subspace is actually C_{6v} symmetric when translational degrees of freedom towards the centre of rotation are considered.

Subspace S^2

$$P^2\phi_1 = \frac{1}{6}\left(e + C_6 + C_6^{-1} + C_3 + C_3^{-1} + C_2 - \sigma_A - \sigma_B - \sigma_C - \sigma_1 - \sigma_2 - \sigma_3\right)\phi_1$$

$$= \frac{1}{6}\left(\phi_1 + \phi_6 + \phi_2 + \phi_5 + \phi_3 + \phi_4 + \phi_6 + \phi_2 + \phi_4 + \phi_5 + \phi_1 + \phi_3\right) = P^2\phi_6 = P^2\phi_2 = P^2\phi_5 = P^2\phi_3 = P^2\phi_4$$

$$= \frac{1}{6}\left(\phi_1 + \phi_1 + \phi_2 + \phi_2 + \phi_3 + \phi_3 + \phi_4 + \phi_4 + \phi_5 + \phi_5 + \phi_6 + \phi_6\right)$$

$$= \frac{1}{3}\left(\phi_1 + \phi_2 + \phi_3 + \phi_4 + \phi_5 + \phi_6\right)$$

The basis vector of subspace S^2 is therefore:

$$\Phi_1^2 = \phi_1 + \phi_2 + \phi_3 + \phi_4 + \phi_5 + \phi_6 \qquad (4.55)$$

Subspace S^3

$$P^3\phi_1 = \frac{1}{6}\left(e - C_6 - C_6^{-1} + C_3 + C_3^{-1} - C_2 + \sigma_A + \sigma_B + \sigma_C - \sigma_1 - \sigma_2 - \sigma_3\right)\phi_1$$

$$= \frac{1}{6}\left(\phi_1 - \phi_6 - \phi_2 + \phi_5 + \phi_3 - \phi_4 - \phi_6 - \phi_2 - \phi_4 + \phi_5 + \phi_1 + \phi_3\right) = -P^3\phi_6 = -P^3\phi_2 = P^3\phi_5 = P^3\phi_3 = -P^3\phi_4$$

$$= \frac{1}{6}\left(\phi_1 + \phi_1 - \phi_2 - \phi_2 + \phi_3 + \phi_3 - \phi_4 - \phi_4 + \phi_5 + \phi_5 - \phi_6 - \phi_6\right)$$

$$= \frac{1}{3}\left(\phi_1 - \phi_2 + \phi_3 - \phi_4 + \phi_5 - \phi_6\right)$$

The basis vector of subspace S^3 is therefore:

$$\Phi_1^3 = \phi_1 - \phi_2 + \phi_3 - \phi_4 + \phi_5 - \phi_6 \qquad (4.56)$$

Subspace S^4

$$P^4\phi_1 = \frac{1}{6}\left(e - C_6 - C_6^{-1} + C_3 + C_3^{-1} - C_2 - \sigma_A - \sigma_B - \sigma_C + \sigma_1 + \sigma_2 + \sigma_3\right)\phi_1$$

$$= \frac{1}{6}\left(\phi_1 - \phi_6 - \phi_2 + \phi_5 + \phi_3 - \phi_4 + \phi_6 + \phi_2 + \phi_4 - \phi_5 - \phi_1 - \phi_3\right) = -P^4\phi_6 = -P^4\phi_2 = P^4\phi_5 = P^4\phi_3 = -P^4\phi_4$$

$$= \frac{1}{6}\left(\phi_1 - \phi_1 - \phi_2 + \phi_2 + \phi_3 - \phi_3 - \phi_4 + \phi_4 + \phi_5 - \phi_5 - \phi_6 + \phi_6\right) = 0$$

Therefore, subspace S^4 is a null space.

Subspace S^5

$$P^5\phi_1 = \frac{1}{6}\left(2e + C_6 + C_6^{-1} - C_3 - C_3^{-1} - 2C_2\right)\phi_1$$

$$= \frac{1}{6}\left(2\phi_1 + \phi_6 + \phi_2 - \phi_5 - \phi_3 - 2\phi_4\right)$$

$$P^5\phi_2 = \frac{1}{6}\left(2e + C_6 + C_6^{-1} - C_3 - C_3^{-1} - 2C_2\right)\phi_2$$

$$= \frac{1}{6}\left(2\phi_2 + \phi_1 + \phi_3 - \phi_6 - \phi_4 - 2\phi_5\right) = P^5\phi_2 = P^5\phi_1 = P^5\phi_3 = -P^5\phi_6 = -P^5\phi_4$$

The basis vectors of subspace S^5 are therefore:

$$\Phi_1^5 = 2\phi_1 + \phi_2 - \phi_3 - 2\phi_4 - \phi_5 + \phi_6 \qquad (4.57)$$

$$\Phi_2^5 = \phi_1 + 2\phi_2 + \phi_3 - \phi_4 - 2\phi_5 - \phi_6 \qquad (4.58)$$

Alternatively

Subspace $S^{5,1}$

$$P_{5,1} = \frac{1}{12}\left(e + \frac{1}{2}C_6 + \frac{1}{2}C_6^{-1} - \frac{1}{2}C_3 - \frac{1}{2}C_3^{-1} - C_2 - \sigma_A + \frac{1}{2}\sigma_B + \frac{1}{2}\sigma_C - \frac{1}{2}\sigma_1 - \frac{1}{2}\sigma_2 + \sigma_3\right)$$

$$P^{5,1}\phi_1 = \frac{1}{6}\left(e + \frac{1}{2}C_6 + \frac{1}{2}C_6^{-1} - \frac{1}{2}C_3 - \frac{1}{2}C_3^{-1} - C_2 - \sigma_A + \frac{1}{2}\sigma_B + \frac{1}{2}\sigma_C - \frac{1}{2}\sigma_1 - \frac{1}{2}\sigma_2 + \sigma_3 \right)\phi_1$$

$$= \frac{1}{6}\left(\phi_1 + \frac{1}{2}\phi_6 + \frac{1}{2}\phi_2 - \frac{1}{2}\phi_5 - \frac{1}{2}\phi_3 - \phi_4 + \phi_6 - \frac{1}{2}\phi_2 - \frac{1}{2}\phi_4 + \frac{1}{2}\phi_5 + \frac{1}{2}\phi_1 - \phi_3 \right)$$

$$= P^{5,1}\phi_6 = P^{5,1}\phi_2 = P^{5,1}\phi_5 = P^{5,1}\phi_3 = P^{5,1}\phi_4$$

$$= \frac{1}{6}\left(\phi_1 + \frac{1}{2}\phi_1 + \frac{1}{2}\phi_2 - \frac{1}{2}\phi_2 - \frac{1}{2}\phi_3 - \phi_3 - \phi_4 - \frac{1}{2}\phi_4 - \frac{1}{2}\phi_5 + \frac{1}{2}\phi_5 + \phi_6 + \frac{1}{2}\phi_6 \right)$$

$$= \frac{1}{6}\left(\frac{3}{2}\phi_1 - \frac{3}{2}\phi_3 - \frac{3}{2}\phi_4 + \frac{3}{2}\phi_6 \right)$$

The basis vector for subspace $S^{5,1}$ is therefore:

$$\Phi_1^{5,1} = \phi_1 - \phi_3 - \phi_4 + \phi_6 \qquad (4.59)$$

Subspace S^6

$$P^6\phi_1 = \frac{1}{6}\left(2e - C_6 - C_6^{-1} - C_3 - C_3^{-1} + 2C_2\right)\phi_1 = \frac{1}{6}\left(2\phi_1 - \phi_6 - \phi_2 - \phi_5 - \phi_3 + 2\phi_4\right)$$

$$P^6\phi_2 = \frac{1}{6}\left(2e - C_6 - C_6^{-1} - C_3 - C_3^{-1} + 2C_2\right)\phi_2 = \frac{1}{6}\left(2\phi_2 - \phi_1 - \phi_3 - \phi_6 - \phi_4 + 2\phi_5\right)$$

The basis vectors of S^6 are therefore:

$$\Phi_1 = 2\phi_1 - \phi_2 - \phi_3 + 2\phi_4 - \phi_5 - \phi_6 \qquad (4.60)$$

$$\Phi_2 = -\phi_1 + 2\phi_2 - \phi_3 - \phi_4 + 2\phi_5 - \phi_6 \qquad (4.61)$$

Alternatively

Subspace $S^{6,1}$

$$P^{6,1}\phi_1 = \frac{1}{6}\left(e - \frac{1}{2}C_6 - \frac{1}{2}C_6^{-1} - \frac{1}{2}C_3 - \frac{1}{2}C_3^{-1} + C_2 + \sigma_A - \frac{1}{2}\sigma_B - \frac{1}{2}\sigma_C - \frac{1}{2}\sigma_1 - \frac{1}{2}\sigma_2 + \sigma_3 \right)\phi_1$$

$$= \frac{1}{6}\left(\phi_1 - \frac{1}{2}\phi_6 - \frac{1}{2}\phi_2 - \frac{1}{2}\phi_5 - \frac{1}{2}\phi_3 + \phi_4 - \phi_6 + \frac{1}{2}\phi_2 + \frac{1}{2}\phi_4 + \frac{1}{2}\phi_5 + \frac{1}{2}\phi_1 - \phi_3 \right)$$

$$= \frac{1}{6}\left(\phi_1 + \frac{1}{2}\phi_1 - \frac{1}{2}\phi_2 + \frac{1}{2}\phi_2 - \frac{1}{2}\phi_3 - \phi_3 + \phi_4 + \frac{1}{2}\phi_4 - \frac{1}{2}\phi_5 + \frac{1}{2}\phi_5 - \frac{1}{2}\phi_6 - \phi_6 \right)$$

$$= \frac{1}{6}\left(\frac{3}{2}\phi_1 - \frac{3}{2}\phi_3 + \frac{3}{2}\phi_4 - \frac{3}{2}\phi_6 \right)$$

The basis vector for subspace $S^{6,1}$ is therefore:

$$\Phi_1^{6,1} = \phi_1 - \phi_3 + \phi_4 - \phi_6 \qquad (4.62)$$

The sketches of these basis vectors are shown in Figure *4.39* and their symmetries are summarised in Table *4.31*. It is important to note that the sketch of subspace S^3 basis vectors shown in Figure *4.39 (b)* are also compatible with C_3 symmetry. To identity the symmetries of the basis vectors shown in Figure *4.39*, unit moments must be applied has shown in Table *4.31*.

Table 4.31 C_{6v} Basis vector symmetries

Figure	Subspace	Symmetry Group	order	index	Applied unit moments
(a)	S^2	C_6	6	2	$\phi_1=\phi_2=\phi_3=\phi_4=\phi_5=\phi_6=1$
(b)	S^3	C_{3v}	6	2	$\phi_1=\phi_3=\phi_5=1,\ \phi_2=\phi_4=\phi_6=-1$
(c)	S^5	C_{1v}	2	6	$\phi_1=1,\ \phi_4=-1,\ \phi_2=\phi_6=0.5,\ \phi_3=\phi_5=-0.5$
(c)	S^5	C_{1v}	2	6	$\phi_1=\phi_3=0.5,\ \phi_2=1,\ \phi_4=\phi_6=-0.5,\ \phi_5=-1$
(c)	$S^{5,1}$	C_{1v}	2	6	$\phi_1=\phi_6=1,\ \phi_3=\phi_4=-1$
(d)	S^6	C_2	2	6	$\phi_1=\phi_4=1,\ \phi_2=\phi_3=\phi_5=\phi_6=-0.5$
(d)	S^6	C_2	2	6	$\phi_2=\phi_5=1,\ \phi_1=\phi_3=\phi_4=\phi_6=-0.5$
(d)	$S^{6,1}$	C_{2v}	4	3	$\phi_1=\phi_4=1,\ \phi_3=\phi_6=-1$

4.6.1 Buckling Behaviour of C_{6v} symmetric frame

The buckling behaviour of the C_{6v} symmetric frame was studied under three different load arrangements: C_{6v}, C_{3v} and C_{2v}. For all load arrangements, the stiffness of the frame was C_{6v}.

4.6.1.1 Buckling Behaviour of C_{6v} symmetric frame with C_{6v} loading

For the C_{6v} load arrangement, the frame was first studied analytically using the slope deflection method to determine the eigenvalues and the symmetries of their eigenmodes. The software Matlab was used to solve the resulting trigonometric equations to obtain eigenvalues from equation *4.6*. The eigenmodes were also solved by utilising Matlab to solve the resulting matrix linear equations when equation *4.7* was implemented.

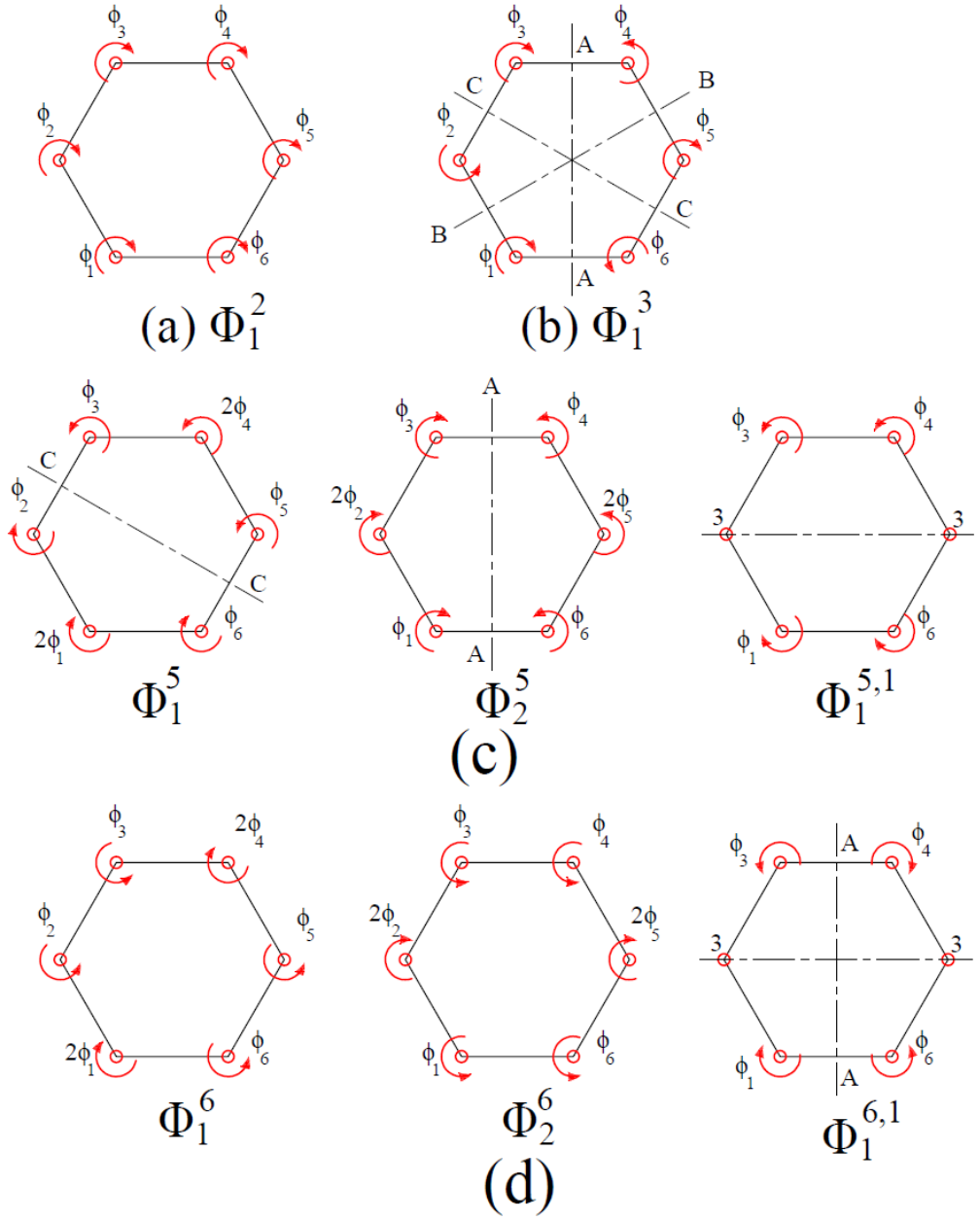

Figure 4.39:Basis vectors of C_{6v} symmetric frame

Using the approach applied for the C_{2v} and C_{3v} plane frames previously presented, the stiffness matrix of the C_{6v} frame shown in Figure *4.38 (b)* can be written as:

$$K = \frac{EI}{L}\begin{bmatrix} 2s & sc & 0 & 0 & 0 & sc \\ sc & 2s & sc & 0 & 0 & 0 \\ 0 & sc & 2s & sc & 0 & 0 \\ 0 & 0 & sc & 2s & sc & 0 \\ 0 & 0 & 0 & sc & 2s & sc \\ sc & 0 & 0 & 0 & sc & 2s \end{bmatrix} \qquad (4.63)$$

We now employ the group theoretic approach to determine the symmetry adapted matrix B for each subspace and then determine the eigenvalues and eigenvectors, respectively.

Subspace S^2

$$\begin{aligned} B^2 &= a_{11} + a_{12} + a_{13} + a_{14} + a_{15} + a_{16} \\ &= 2s + sc + 0 + 0 + 0 + sc \\ &= 2s + 2sc \\ \left|B^2\right| &= s + sc = s(1+c) = 0 \end{aligned}$$

Solving this trigonometric equation, we find the eigenvalues as:

$$\lambda_1 = 6.2832$$
$$\lambda_n = 2n\pi$$

Solving the eigenvectors for each eigenvalue using the full space solution equation *4.7*, shows that for each eigenvalue the eigenvector is C_6 and C_{6v} symmetric. The eigenvalues and eigenvectors obtained from the analytical analysis for S^2 are summarised in Table *4.32* below.

Table 4.32: C_{6v} plane frame: subspace S^2 eigenvalues and eigenvectors

λ	ϕ_1	ϕ_2	ϕ_3	ϕ_4	ϕ_5	ϕ_6	symmetry group
6.2832	-0.1354	-0.1354	-0.1354	-0.1354	-0.1354	-0.1354	C_6
6.2832	-0.3571E-7	-0.3571E-7	-0.3571E-7	-0.3571E-7	-0.3571E-7	-0.3571E-7	C_{6v}
12.5664	-0.1354	-0.1354	-0.1354	-0.1354	-0.1354	-0.1354	C_6
12.5664	-0.3571E-7	-0.3571E-7	-0.3571E-7	-0.3571E-7	-0.3571E-7	-0.3571E-7	C_{6v}
18.8496	-0.0874	-0.0874	-0.0874	-0.0874	-0.0874	-0.0874	C_6
18.8496	-0.5000E-7	-0.5000E-7	-0.5000E-7	-0.5000E-7	-0.5000E-7	-0.5000E-7	C_{6v}
25.1327	-0.0923	-0.0923	-0.0923	-0.0923	-0.0923	-0.0923	C_6
25.1327	-0.5000E-7	-0.5000E-7	-0.5000E-7	-0.5000E-7	-0.5000E-7	-0.5000E-7	C_{6v}

It can be observed from Table *4.32* that the numerical solution to Equation *4.7* indicates the existence of C_{6v} eigenmodes in subspace S^2. It should be noted that these eigenmodes belong to subspace S^1, as previously explained for the C_{3v}, C_{4v}, and C_{5v} frames.

Subspace S^3

$$B^3 = a_{11} - a_{12} + a_{13} - a_{14} + a_{15} - a_{16}$$
$$= 2s - sc + 0 - 0 + 0 - sc$$
$$= 2s - 2sc$$
$$\left|B^3\right| = s - sc = s(1-c) = 0$$
$$\lambda_1 = 3.1416$$
$$\lambda_n = \pi(2n-1)$$

Solving the eigenvectors for each eigenvalue using the full space solution equation *4.7* shows that for each eigenvalue, the eigenvector is C_{3v} symmetric. The eigenvalues and eigenvectors obtained from the analytical analysis for S^3 are summarised in Table *4.33* below.

Table 4.33: C_{6v} plane frame: subspace S^3 eigenvalues and eigenvectors

λ	ϕ_1	ϕ_2	ϕ_3	ϕ_4	ϕ_5	ϕ_6	symmetry group
3.1416	-1.0000	1.0000	-1.0000	1.0000	-1.0000	1.0000	C_{3v}
9.4248	-1.0000	1.0000	-1.0000	1.0000	-1.0000	1.0000	C_{3v}
15.7080	-1.0000	1.0000	-1.0000	1.0000	-1.0000	1.0000	C_{3v}
21.9911	-1.0000	1.0000	-1.0000	1.0000	-1.0000	1.0000	C_{3v}

It should be noted that the symmetries of eigenmodes in Table *4.33* are classified as C_{3v} and not C_3, because C_{3v} symmetry is of higher order than C_3 symmetry.

Subspace S^5

$$B^{5,1} = a_{11} - a_{13} - a_{14} + a_{16}$$
$$= 2s - 0 - 0 + 0 + 0 + sc$$
$$= 2s + sc$$
$$\left|B^{5,1}\right| = 2s + sc = s(2+c) = 0$$

Solving for the eigenvalues and respective eigenvector, shows that for each eigenvalue the eigenvector is C_{1v} symmetric. The eigenvalues and eigenvectors obtained from the analytical analysis for S^5 are summarised in Table *4.34* below.

Table 4.34: C_{6v} plane frame: subspace S^5 eigenvalues and eigenvectors

λ	ϕ_1	ϕ_2	ϕ_3	ϕ_4	ϕ_5	ϕ_6	symmetry group
5.1362	-1.0000	-0.5000	0.5000	1.0000	0.5000	-0.5000	$C^{C}{}_{1v}$
5.1362	0.0000	-1.0000	-1.0000	0.0000	1.0000	1.0000	$C^{2}{}_{1v}$
7.2630	-1.0000	-0.5000	0.5000	1.0000	0.5000	-0.5000	$C^{C}{}_{1v}$
7.2630	0.0000	-1.0000	-1.0000	0.0000	1.0000	1.0000	$C^{2}{}_{1v}$
11.4751	1.0000	0.5000	-0.5000	-1.0000	-0.5000	0.5000	$C^{C}{}_{1v}$
11.4751	0.0000	1.0000	1.0000	0.0000	-1.0000	-1.0000	$C^{2}{}_{1v}$
13.5771	-1.0000	-0.5000	0.5000	1.0000	0.5000	-0.5000	$C^{C}{}_{1v}$
13.5771	0.0000	-1.0000	-1.0000	0.0000	1.0000	1.0000	$C^{2}{}_{1v}$

Subspace S^6

$$B^{6,1} = a_{11} - a_{13} + a_{14} - a_{16}$$
$$= 2s - 0 + 0 - sc$$
$$= 2s - sc$$
$$\left|B^{6,1}\right| = 2s - sc = s\left(2 - c\right) = 0$$

Solving the eigenvalues and respective eigenvectors, shows that for each eigenvalue the eigenvector is C_{2v} symmetric or C_2 symmetric. The eigenvalues and eigenvectors obtained from the analytical analysis for S^6 are summarised in Table *4.35* below.

Table 4.35: C_{6v} plane frame: subspace S^6 eigenvalues and eigenvectors

λ	ϕ_1	ϕ_2	ϕ_3	ϕ_4	ϕ_5	ϕ_6	symmetry group
3.8567	1.0000	-0.5000	-0.5000	1.0000	-0.5000	-0.5000	C_2
3.8567	1.0000	0.0000	-1.0000	1.0000	0.0000	-1.0000	C_{2v}
8.1869	1.0000	-0.5000	-0.5000	1.0000	-0.5000	-0.5000	C_2
8.1869	1.0000	0.0000	-1.0000	1.0000	0.0000	-1.0000	C_{2v}
10.3338	1.0000	-0.5000	-0.5000	1.0000	-0.5000	-0.5000	C_2
10.3338	1.0000	0.0000	-1.0000	1.0000	0.0000	-1.0000	C_{2v}
14.5550	1.0000	-0.5000	-0.5000	1.0000	-0.5000	-0.5000	C_2
14.5550	1.0000	0.0000	-1.0000	1.0000	0.0000	-1.0000	C_{2v}

The table below presents a summary of the results obtained from the analytical analysis.

Table 4.36: C_{6v} Eigenvalues obtained by analytical method

No	Eigenvalue	Eigenmode symmetry
1	3.142	C_{3v}
2	3.857	C_{2v}, C_2
3	5.136	C_{1v}
4	6.283	C_6, C_{6v}
5	7.263	C_{1v}
6	8.187	C_{2v}, C_2
7	9.425	C_{3v},
8	10.334	C_{2v}, C_2
9	11.475	C_{1v}
10	12.566	C_6, C_{6v}
11	13.577	C_{1v}
12	14.555	C_{2v}, C_2
13	15.708	C_{3v},
14	16.668	C_{2v}, C_2

The analytical solution shows that the lowest eigenvalue is $\lambda_1=\pi$ and its eigenmode is C_{3v} symmetric. However, Mises and Ratzersdorfer (1926) report that the lowest eigenvalue is $\lambda_1=2/3\pi$ and the eigenmode is not reported.

A *FEM* of a C_{6v} frame with C_{6v} loading was created using Abaqus, and the first fifty eigenmodes and eigenvalues were produced. The boundary conditions applied to the *FEM* model in Abaqus are shown in Figure *4.38 (c)*. The results of the convergence analysis, based on analytical results, are shown in Figure *4.40*. The symmetry of eigenmodes for each eigenvalue from *FEM* was categorised, and these are shown for the first fourteen eigenvalues in Table *4.37* below. Samples of eigenmodes produced are shown in Figure *4.41*.

The results obtained from the finite element analysis agree with the results obtained from the analytical solution in terms of the magnitude of the eigenvalue and the symmetry classification of the eigenmode. It can also be observed from Tables *4.36* and *4.37* that the lowest eigenvalue has an eigenmode with the symmetry of the subgroups of C_{6v} with the highest order. The subgroup for C_{6v} with the highest order is the C_{3v} symmetry group. Further group-theoretic repeating eigenvalues have a group index greater than two. In particular, for C_{2v} and C_{1v} symmetric eigenmodes, the group index is three and six, respectively. For the parametric repeating eigenvalues, the group index for the eigenmodes was two for the C_6 symmetric eigenmodes.

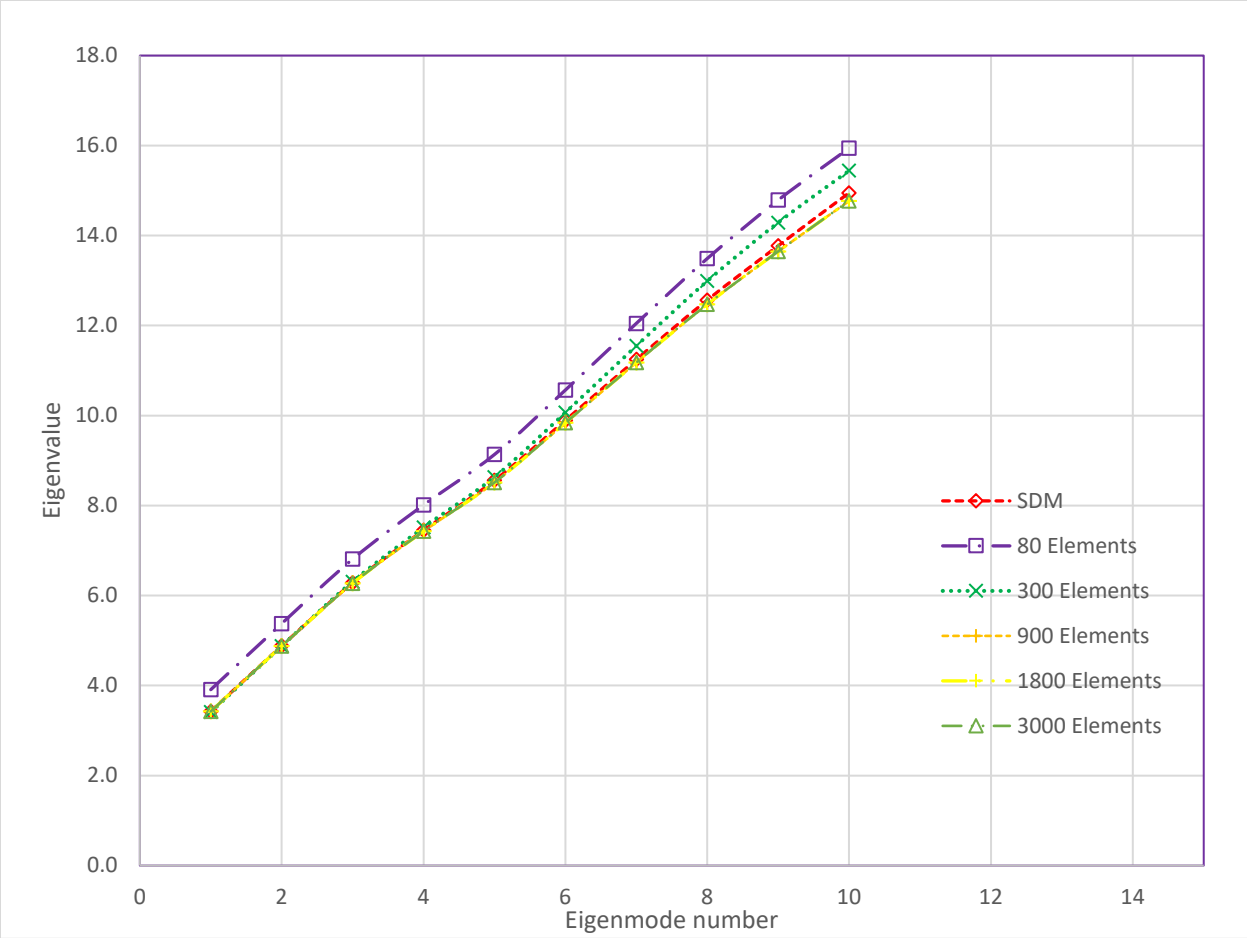

Figure 4.40:C_{6v} plane frame convergence analysis

The pattern shown in Table *4.37* was found to repeat every twelve eigenvalues. Recall that twelve is the order of the C_{6v} symmetry group. If we plot separately the eigenvalues produced from each subspace from the analytical results as shown in Figure *4.42* below, we observe that the curves for subspaces S^2 and S^3 do not intersect with other curves, while those of S^5 and S^6 regularly intersect at several points. Thus, from the first fifty eigenvalues studied, a repeating pattern of eigenmodes was observed.

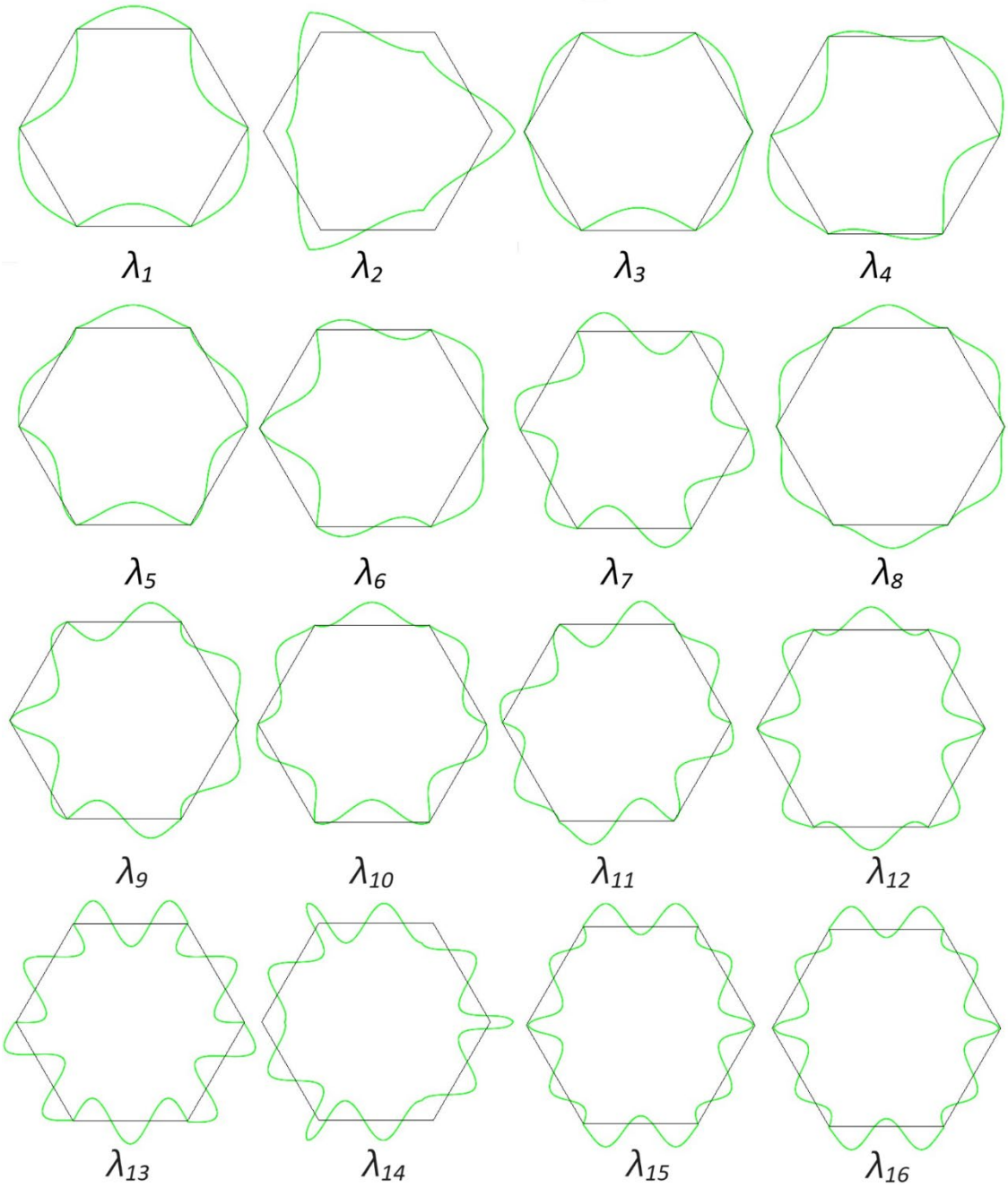

Figure 4.41: C_{6v} plane frame sample eigenmodes

Table 4.37: C_{6v} Eigenvalues obtained from FEM model

Number	Eigenvalue	Eigenmode symmetry
1	3.137	C_{3v}
2	3.170	C_{3v}
3	3.844	C_{2v}
4	3.844	C_2
5	5.116	$C^A{}_{1v}$
6	5.116	$C^3{}_{1v}$
7	6.248	C_6
8	6.248	C_{6v}
9	7.208	$C^3{}_{1v}$
10	7.208	$C^A{}_{1v}$
11	8.094	C_2
12	8.094	C_{2v}
13	9.308	C_{3v}
14	9.309	C_{3v}

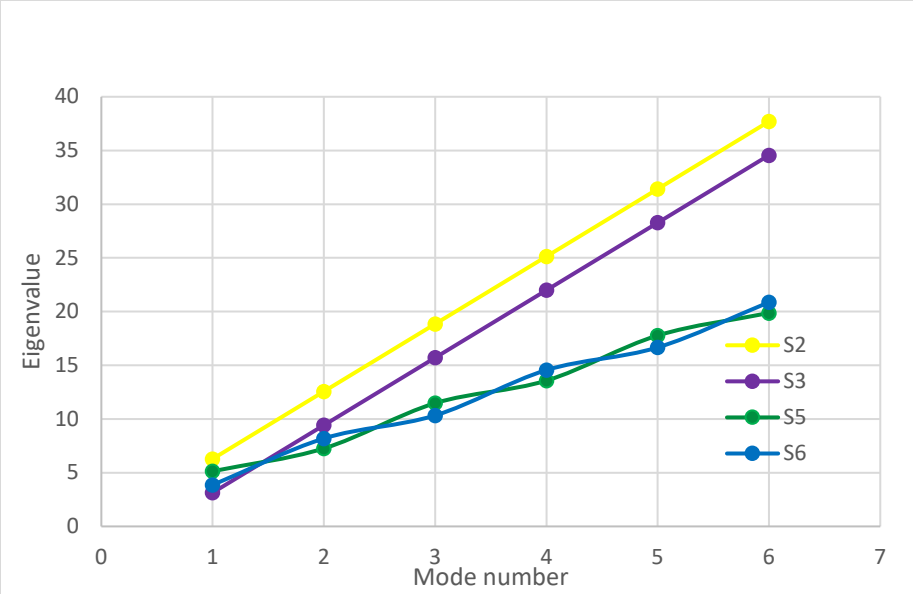

Figure 4.42:C_{6v} Frame Eigenvalues by subspace

4.6.1.2 Buckling Behaviour of C_{6v} symmetric frame with C_{3v} loading

We now consider the buckling behaviour of a C_{6v} symmetric frame subjected to a C_{3v} load arrangement as shown in Figure *4.43 (a)* below.

The basis vectors for this problem can be obtained based on the results obtained from the C_{3v} frame problem.

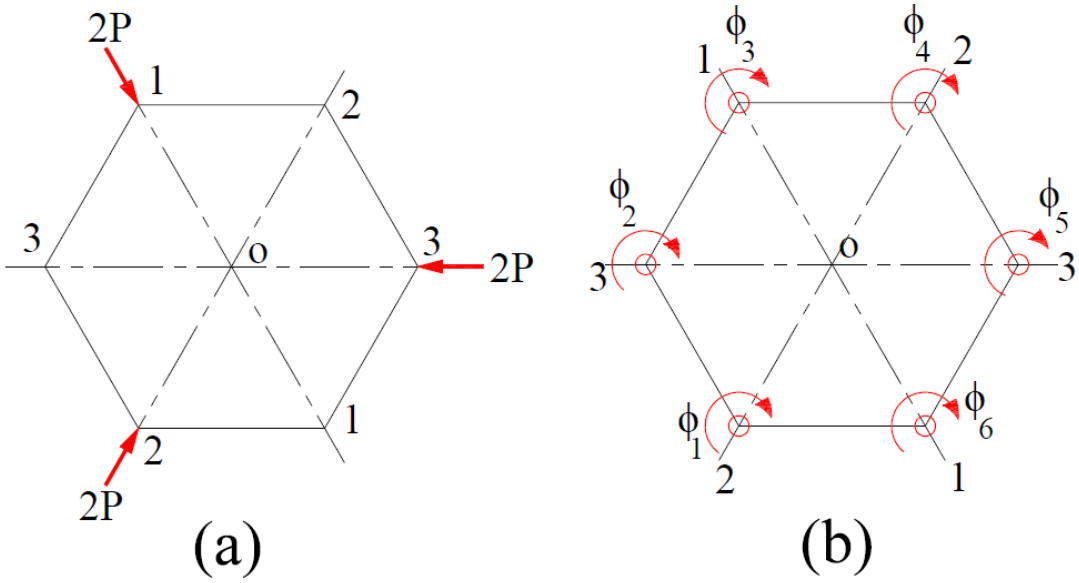

Figure 4.43: C_{6v} symmetric frame with C_{3v} loading

Subspace S^1

Null subspace

Subspace S^2

$$\Phi_1^2 = \phi_1 + \phi_3 + \phi_5 \qquad (4.64)$$

$$\Phi_2^2 = \phi_2 + \phi_4 + \phi_6 \qquad (4.65)$$

Subspace S^3

$$\Phi_1^3 = 2\phi_1 - \phi_3 - \phi_5 \qquad (4.66)$$

$$\Phi_1 = 2\phi_2 - \phi_4 - \phi_6 \qquad (4.67)$$

Subspace $S^{3,1}$

$$\Phi_1 = \phi_1 - \phi_3 \qquad (4.68)$$

$$\Phi_2 = \phi_4 - \phi_6 \qquad (4.69)$$

The sketches of these basis vectors are shown in Figure *4.42* below, and the symmetries for basis vectors are summarised in Table *4.39* below. To identify the symmetry group of the basis vectors, unit moments should be applied, as shown in Table *4.38*.

Table 4.38: Basis vector symmetries for C_{6v} frame with C_{3v} loading

Figure	Subspace	Symmetry Group	Applied unit moments
(a)	S^2	C_3	$\phi_1+\phi_3+\phi_5=1$ $\phi_2+\phi_4+\phi_6=1$
(b)	$S^{3,1}$	C_{1v}	$\phi_1=1,\ \ \phi_3=-1$ $\phi_4=1,\ \ \phi_6=-1$

As was the case for C_{6v} loading, the analytical solution for the C_{3v} loading case can be similarly obtained. The stability matrix for the C_{6v} with C_{3v} loading is given as shown in equation *4.63*. We can then employ the group theoretic approach to determine the symmetry adapted matrix B for each subspace and then employ Equations *4.6* and *4.7* to determine the eigenvalues and eigenvectors, respectively.

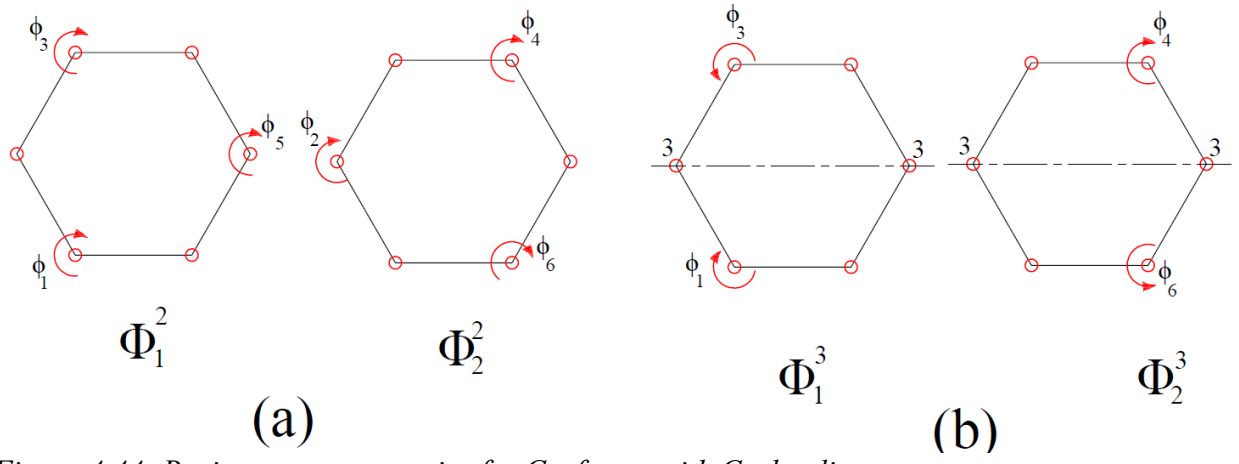

Figure 4.44: Basis vector symmetries for C_{6v} frame with C_{3v} loading

Subspace S^2

$$B^2=\begin{bmatrix} b_{11} & b_{12} \\ b_{21} & b_{22} \end{bmatrix}$$

$$b_{11}=a_{11}+a_{13}+a_{15}=2s$$

$$b_{12}=a_{12}+a_{14}+a_{16}=sc+sc=2sc$$

$$b_{22}=a_{22}+a_{24}+a_{26}=2s$$

$$b_{21}=a_{21}+a_{23}+a_{25}=sc+sc=2sc$$

$$B^2 = \begin{bmatrix} 2s & 2sc \\ 2sc & 2s \end{bmatrix}$$
$$\left|B^2\right| = s^2 - s^2c^2 = \left(s + sc\right)\left(s - sc\right) = 0$$

Solving the first trigonometric equation *s+sc=0* we obtain:

$$\lambda_1 = 6.2832$$
$$\lambda_n = 2n\pi$$

Solving the eigenvectors for each eigenvalue using the full space solution equation *4.7* shows that for each eigenvalue, the eigenvector is C_6 and C_{6v} symmetric. The same result is obtained if we compute for eigenvectors using the symmetry adapted matrix B^2.

Solving the second trigonometric equation *s-sc=0* we obtain:

$$\lambda_1 = 3.1416$$
$$\lambda_n = \pi\left(2n - 1\right)$$

Solving the eigenvectors for each eigenvalue using the full space solution equation *4.7* shows that for each eigenvalue, the eigenvector is C_{3v} symmetric. However, if we compute eigenvectors using the symmetry adapted matrix B^2, the eigenvectors are C_3 symmetric.

Subspace $S^{3,1}$

$$B^3 = \begin{bmatrix} b_{11} & b_{12} \\ b_{21} & b_{22} \end{bmatrix}$$
$$b_{11} = a_{11} - a_{13} = 2s$$
$$b_{12} = a_{14} - a_{16} = -sc$$
$$b_{22} = a_{44} - a_{46} = 2s$$
$$b_{21} = a_{41} - a_{43} = -sc$$
$$B^3 = \begin{bmatrix} 2s & -sc \\ -sc & 2s \end{bmatrix}$$
$$\left|B^3\right| = 4s^2 - s^2c^2 = s^2\left(2^2 - c^2\right) = s^2\left(2 + c\right)\left(2 - c\right) = 0$$

From the first trigonometric equation *2-c=0*, we obtain:

$$\lambda_1 = 3.8567$$

Solving the eigenvectors for each eigenvalue using the full space solution equation *4.7* shows that for each eigenvalue, the eigenmode is C_{2v} symmetric or C_2 symmetric. However, if we compute eigenvectors using the symmetry adapted matrix B^3, the eigenmodes are only C_{2v} symmetric.

Now, solving the second trigonometric equation $2+c=0$, we obtain:

$$\lambda_1 = 5.1362$$

Solving the eigenvectors for each eigenvalue using the full space solution equation *4.7*, shows that for each eigenvalue the eigenmode is C_{1v} symmetric. The same result is obtained when eigenvectors are computed using the symmetry adapted matrix B^3.

Solving the eigenvectors for each eigenvalue using the full space solution equation *4.7* shows that for each eigenvalue, the eigenmode is C_{1v} symmetric. The same result is obtained when eigenvectors are computed using the symmetry adapted matrix B^3.

The summary of the results obtained from the analytical analysis is shown in Table *4.39*. These results are identical to those obtained for C_{6v} loading and summarised in Table *4.37*.

Table 4.39: C_{6v} Frame C_{3v} loading Analytical Results

No	Eigenvalue	Eigenmode symmetry
1	3.142	C_{3v}, C_3
2	3.857	C_{2v}, C_2
3	5.136	C_{1v}
4	6.283	C_{6v}, C_6
5	7.263	C_{1v}
6	8.187	C_{2v}, C_2
7	9.425	C_{3v}, C_3
8	10.334	C_{2v}, C_2
9	11.475	C_{1v}
10	12.566	C_{6v}, C_6
11	13.577	C_{1v}
12	14.555	C_{2v}, C_2
13	15.708	C_{3v}, C_3
14	16.668	C_{2v}, C_2

A *FEM* of a C_{6v} frame with C_{3v} loading and with the same support conditions used for the C_{6v} loading case was created using Abaqus. A linear eigenvalue analysis was carried out. The results

are summarised in Table *4.40* below. The buckling behaviour observed was similar to that observed for C_{6v} loading. However, it can be observed from Table *4.40* that the eigenmode for the lowest eigenvalue was C_3 symmetric, while that for the case of C_{6v} loading was C_{3v} symmetric. It should be noted that a C_{3v} eigenmode for the lowest eigenvalue is still possible. Whether the eigenmode is C_{3v} or C_3, is dependent on the numerical method used to compute the eigenmodes. This is because both eigenmodes are produced from the same subspace.

Table 4.40:C_{6v} frame C_{3v} loading FEM Results

Number	Eigenvalue	Eigenmode symmetry
1	3.137	C_3
2	3.170	C_3
3	3.844	C_{2v}
4	3.844	C_2
5	5.116	$C^{A}{}_{1v}$
6	5.116	$C^{3}{}_{1v}$
7	6.248	C_6
8	6.248	C_{6v}
9	7.208	$C^{3}{}_{1v}$
10	7.208	$C^{A}{}_{1v}$
11	8.094	C_2
12	8.094	C_{2v}
13	9.308	C_{3v}
14	9.309	C_3

The eigenmodes produced from the C_{6v} frame with C_{3v} loading produced eigenmodes whose symmetries are not all in accordance with the symmetries listed in Table *4.38* and sketched in Figure *4.44*. However, careful examination of the basis vectors shown in Figure *4.44* reveals why the buckling behaviour was still the same as that for the frame with C_{6v} loading. The basis vectors of subspace S^2 when sketched on one single frame are compatible with C_6 , C_{3v} and C_3 symmetry. For C_{3v} and C_3 symmetry, this is possible if we rearrange the basis vector equation *4.65* as follows:

$$\Phi_2^2 = -\phi_2 - \phi_4 - \phi_6 \qquad (4.70)$$

Similarly, sketching the basis vectors of subspace $S^{3,1}$ on one single frame reveals a symmetry pattern compatible with C_{2v} and C_2 symmetry.

4.6.1.3 Buckling Behaviour of C_{6v} symmetric frame with C_{2v} loading

We now consider the buckling behaviour of a C_{6v} symmetric frame subjected to a C_{2v} load arrangement, as shown in Figure *4.45* below. This frame was studied by means of a *FEM* in Abaqus only. A linear eigenvalue analysis of the model was carried out, and the symmetries of buckling modes for the first fifty buckling values were categorised. Table *4.41* below presents a summary of the results obtained from the *FEM*.

The sequence of buckling mode symmetries shown in Table *4.41* from the 5th to the 8th buckling value was repeating for all the other buckling modes studied. It was also observed that the symmetries of buckling modes produced for the case of a C_{6v} frame with C_{2v} loading were the same as those produced for the case of a C_{2v} frame with C_{2v} loading.

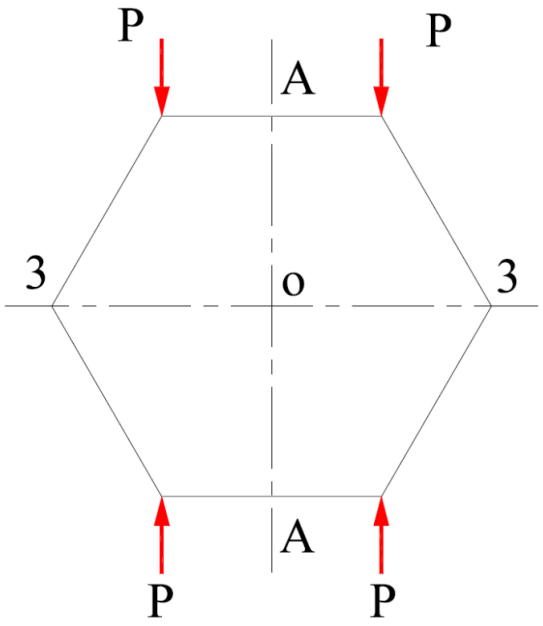

Figure 4.45: C_{6v} Frame with C_{2v} loading

Table 4.41: C_{6v} Frame C_{2v} loading

No	Buckling value	Buckling mode symmetry
1	2.458	C_{2v}
2	3.371	C_2
3	3.851	C^{A}_{1v}
4	4.071	C^{3}_{1v}
5	5.444	C_{2v}
6	5.972	C^{3}_{1v}
7	6.710	C_2
8	7.008	C^{A}_{1v}
9	8.610	C_{2v}
10	9.284	C^{3}_{1v}
11	9.987	C_2
12	10.193	C^{A}_{1v}
13	11.774	C_{2v}
14	12.056	C^{3}_{1v}

4.7 Plane Frames with C_{8v} symmetry

The C_{8v} symmetry group is the symmetry of an eight-sided polygon. This symmetry group has a group order of sixteen, and the symmetry elements are presented in Table *2.1.* The subgroups of this symmetry group are presented in Table *4.42* (Altmann & Herzig, 2011).

Table 4.42:Subgroups, C_{8v} symmetry group

Subgroup	order (n)	index (m/n)
C_8	8	2
C_{4v}	8	2
C_4	4	4
C_{2v}	4	4
C_2	2	8
C_1	1	16

The buckling behaviour of a C_{8v} symmetric frame with three different load arrangements was studied. These load arrangements included: C_{8v}, C_{4v} and C_{2v} load arrangements, as shown in Figure *4.46*. The arrangement of the stiffness for all three load arrangements was C_{8v}.

A linear *FEM* of a C_{8v} symmetric frame was created and modelled in Abaqus. The mesh density chosen for this frame was based on that used for the C_{6v} plane frame presented earlier. For each load arrangement, a linear eigenvalue analysis was carried out, and the symmetry of the buckling mode for each buckling value was categorised. The symmetries of the first fifty buckling values were studied, and the findings for the first fourteen buckling values are presented in Table *4.43* below. Sample images of the buckling modes produced from the linear eigenvalue analysis are shown in Figure *4.47* for the case of C_{8v} loading.

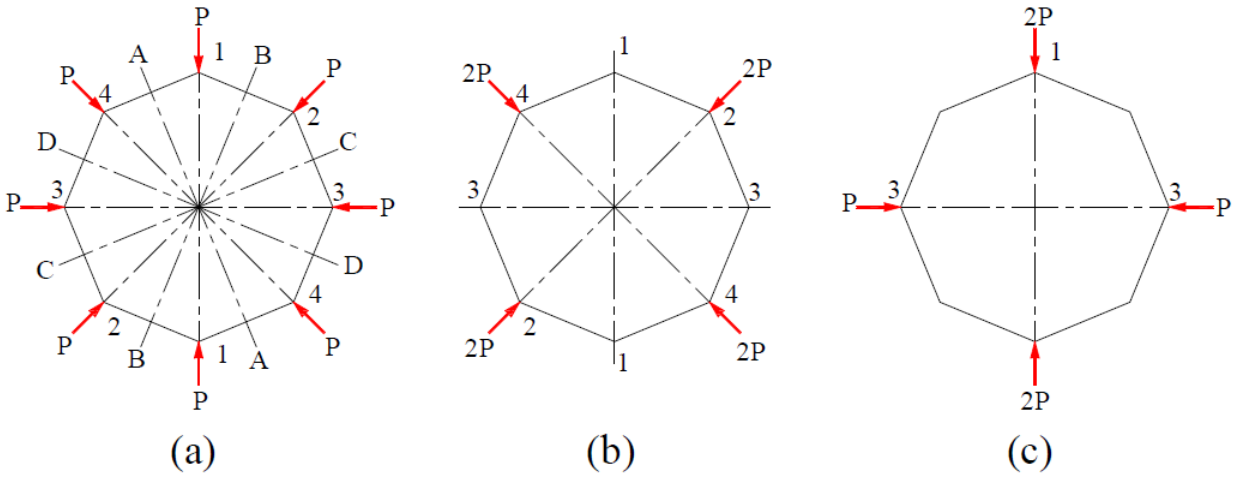

Figure 4.46: C_{8v} symmetric frame (a) C_{8v} loading (b) C_{4v} loading (c) C_{2v} loading

From Table *4.43,* we can observe that the buckling behaviour of a C_{8v} frame with C_{8v} loading is the same as that with C_{4v} loading. Further, we notice that in both cases, the lowest buckling value is C_{4v} symmetric. On the other hand, when a C_{2v} load arrangement is applied to the frame, the buckling mode with the lowest buckling value is C_{2v} symmetric. The pattern of symmetry shown in Table *4.43* was repeating for every sixteenth buckling value for C_{8v} and C_{4v} loading arrangements. For the C_{2v} loading arrangement, the pattern of symmetries observed from the fourth buckling value was repeating for every fourth buckling value. When the group index for the symmetry for each buckling mode is considered, the following is observed:

- The C_{nv} buckling mode with the lowest index was the buckling mode with the lowest eigenvalue; and

- C_8 and C_2 eigenmodes for the C_{8v} and C_{2v} load arrangements, respectively, both have buckling modes with a group index of *2*.

When the results for the C_{8v} load arrangements are plotted on a graph of buckling values against buckling mode symmetry, as shown in Figure *4.48,* we observe the following:

- Buckling values whose buckling modes are C_8 symmetric form the higher bound values;
- buckling values whose buckling modes are C_{2v} symmetric form a lower bound of buckling values with respect to the C_8 and C_{2v} symmetric buckling modes, respectively; and
- buckling values with C_{1v} symmetric buckling modes form lower bound values.

Table 4.43: C_{8v} Frame buckling behaviour

Loading	(a) C_{8v}		(b) C_{4v}		(c) C_{2v}	
No	λ_{cr}	symmetry	λ_{cr}	symmetry	λ_{cr}	symmetry
1	2.741	C_{4v}	2.736	C_{4v}	1.587	C_{2v}
2	2.742	C_{4v}	2.737	C_{4v}	2.343	$C^3{}_{1v}$
3	3.093	$C^3{}_{1v}$	3.080	$C^3{}_{1v}$	2.418	$C^1{}_{1v}$
4	3.121	$C^1{}_{1v}$	3.122	$C^1{}_{1v}$	3.154	C_{2v}
5	3.917	C_{2v}	3.907	C_{2v}	3.202	C_{2v}
6	3.919	C_{2v}	3.913	C_{2v}	3.947	$C^1{}_{1v}$
7	4.733	$C^1{}_{1v}$	4.722	$C^1{}_{1v}$	4.010	$C^3{}_{1v}$
8	4.754	$C^3{}_{1v}$	4.746	$C^3{}_{1v}$	4.592	C_2
9	5.456	C_8	5.443	C_8	4.747	C_{2v}
10	5.475	C_{8v}	5.465	C_{8v}	5.444	$C^3{}_{1v}$
11	6.105	$C^3{}_{1v}$	6.090	$C^3{}_{1v}$	5.552	$C^1{}_{1v}$
12	6.109	$C^1{}_{1v}$	6.099	$C^1{}_{1v}$	6.282	C_2
13	6.696	$C^1{}_{1v}$	6.678	$C^1{}_{1v}$	6.371	C_{2v}
14	6.698	$C^4{}_{1v}$	6.686	$C^4{}_{1v}$	7.056	$C^1{}_{1v}$
15	7.212	$C^1{}_{1v}$	7.193	$C^1{}_{1v}$	7.122	$C^3$1v
16	7.271	$C^3{}_{1v}$	7.262	$C^3{}_{1v}$	7.838	C_2

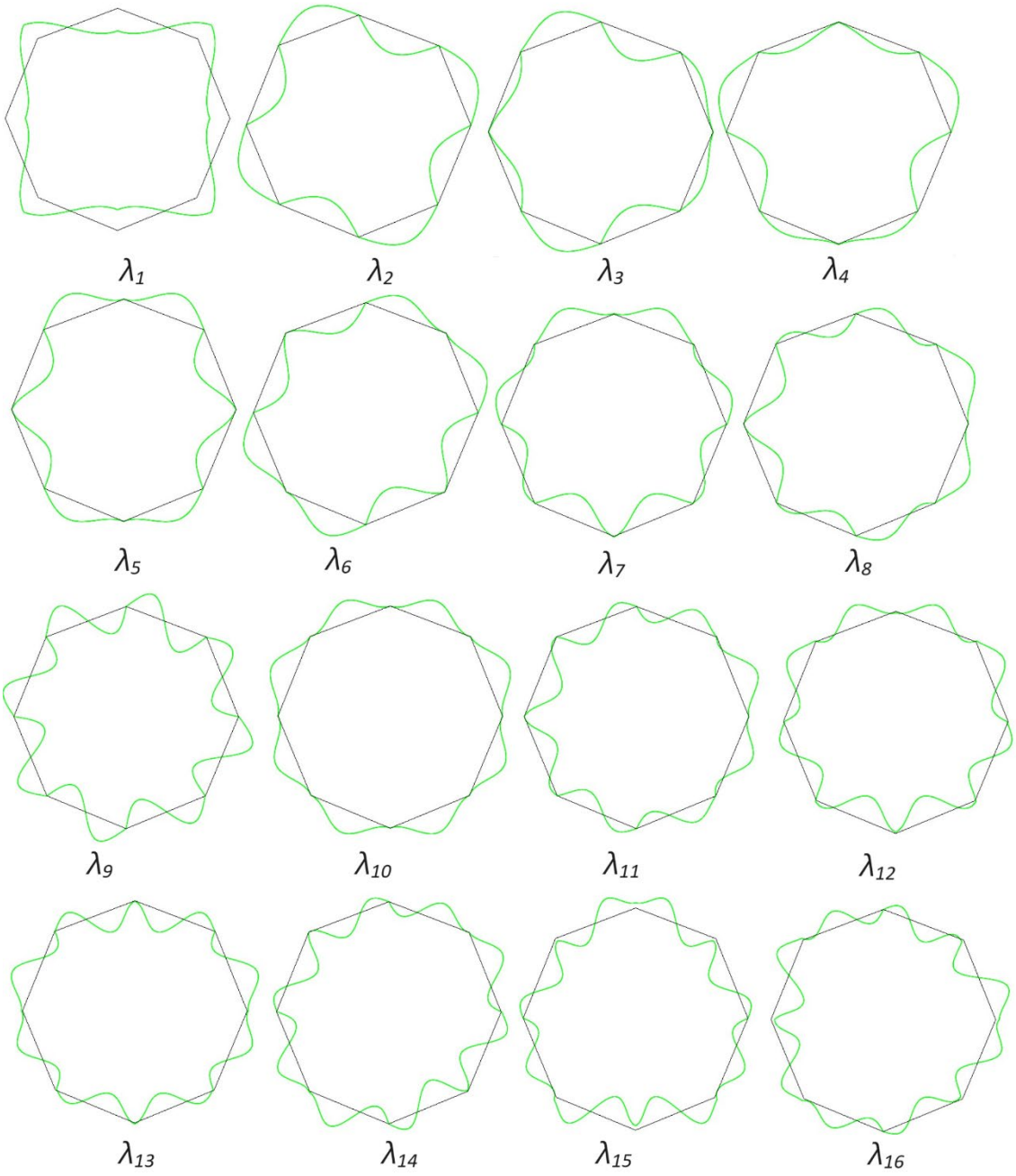

Figure 4.47: C_{8v} plane frame eigenmodes

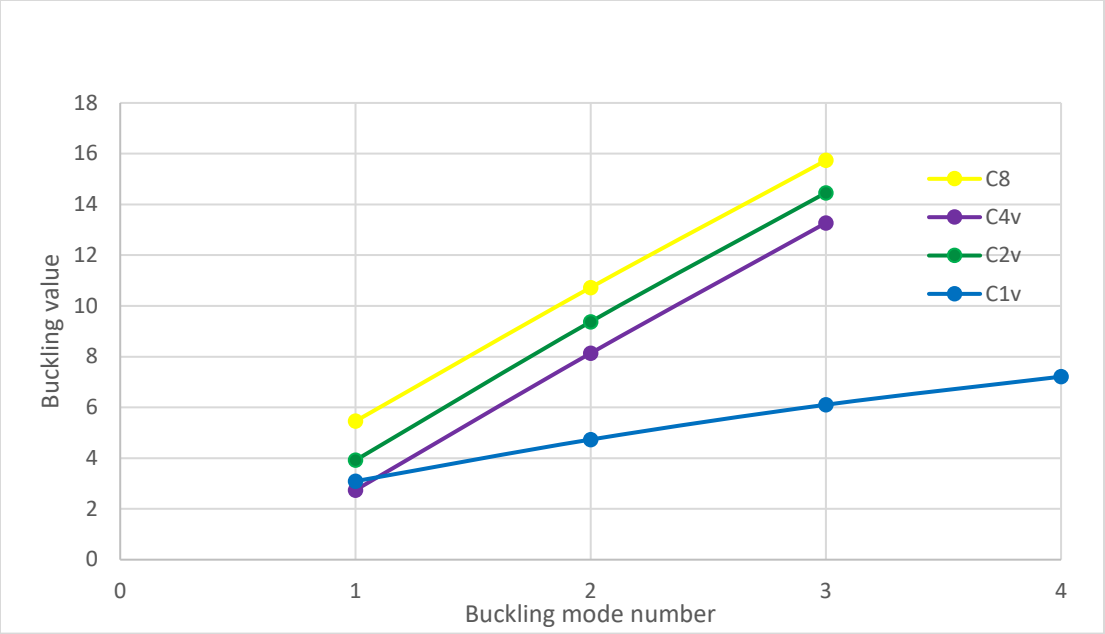

Figure 4.48: C_{8v} Eigenvalues by symmetry of eigenmode

4.8 Influence of symmetry on the stability behaviour of Plane frames

This part of the study sought to investigate the influence of symmetry on the stability behaviour of plane frames. Stability behaviour was studied in terms of symmetries of eigenmodes produced from a linear eigenvalue analysis. From five of the six types of point group symmetries considered in this study, we have seen that it is possible to deduce the possible symmetries of eigenmodes produced from a linear eigenvalue analysis of plane C_{nv} symmetric frames by merely determining the basis vectors of models of such frames. Upon application of the idempotents of applicable symmetry groups to such a model, we then obtain the basis vectors of the frame. The symmetries of such basis vectors are the possible symmetries of the eigenmodes. The symmetries of such basis vectors are the subgroups of the group. From the symmetry adapted basis vectors analytically determined in this study, only the C_{3v} and C_{5v} symmetry groups displayed the C_1 symmetry group. From the linear eigenvalue analysis carried out in this study, only the C_{3v} and C_{5v} symmetric frames displayed C_1 symmetric eigenmodes. The only other exception was the case where a frame is subjected to C_{1v} loading or the frame is constructed in such a way that the stiffness of the frame is C_{1v} symmetric. It was also observed that for a C_{4v} and C_{8v} symmetric frames, no C_2 symmetric eigenmodes were produced. This is despite the fact that the C_2 symmetric group is a subgroup of both the C_{4v} and C_{8v} symmetry groups.

A question that may arise in a linear eigenvalue analysis of symmetric frames is the order of emergence of symmetries of eigenmodes produced from an eigenvalue analysis for a frame that is C_{nv} symmetric in terms of geometry, stiffness, and load arrangement. For the point group symmetries considered in this study, it was observed that the symmetry of the eigenmode for the lowest eigenvalue, was always that of the subgroup with the highest order of symmetry. However, for the C_{2v} symmetry group, it was observed that the symmetry of the eigenmode for the lowest eigenvalue was C_{2v}. Another observation for C_{nv} symmetry groups was that the order of emergence of symmetries was from the subgroup with the highest order of elements to that with the lowest order of elements. This kind of behaviour has also been observed in studies tracing the equilibrium paths C_{nv} of lattice domes (Healey, 1985; Ikeda et al., 1986b; Ikeda et al., 1986a; Ikeda & Torii, 1987a; Ikeda & Torii, 1987b; Healey, 1988; Ikeda et al., 1991; Ikeda & Murota, 1991).

It should also be noted that whenever a C_{nv} frame produced a C_{nv} eigenmode, this eigenmode was produced with a repeating eigenvalue whose other eigenmode was C_n symmetric. This was the case for all C_{nv} point group symmetries except for the C_{2v} group. This kind of behaviour can be noted from the results presented in Tables *4.16*, *4.22*, *4.30*, *4.37,* and *4.43* (a). It was further observed that when eigenvalues are arranged by symmetries of their eigenmodes, the highest order C_n subgroup always forms the upper bound values of buckling loads for a C_{nv} symmetric frame when compared to eigenvalues with $C_{nv/2}$ symmetric eigenmodes.

In cases where the geometry of the frame is C_{nv} symmetric and either the loading or stiffness is of a lower order symmetry group, the buckling behaviour was as such of a frame that had a symmetry of lower order. For example, C_{4v} symmetric frame with C_{2v} loading and C_{4v} stiffness displayed the buckling behaviour of a C_{2v} symmetric frame with C_{2v} stiffness and loading. Similarly, a C_{4v} frame with C_{2v} stiffness and C_{4v} loading displayed the buckling behaviour of a C_{2v} frame with C_{2v} loading and stiffness. However, it was noted that when a C_{6v} symmetric frame with C_{6v} stiffness was subjected to C_{3v} loading, the buckling behaviour of such a frame was still the same as that of a C_{6v} symmetric frame with C_{6v} stiffness and loading. Similarly, a C_{8v} symmetric frame with C_{8v} stiffness and C_{4v} loading displayed the buckling behaviour of a C_{8v} symmetric frame with C_{8v} stiffness and loading. If we consider a $C_{nv/2}$ frame inscribed by a C_{nv} frame as shown in Figure *4.49*, it is easy to see that when a C_{nv} symmetric frame is subjected to $C_{nv/2}$ loading, the resulting stress distribution will always be C_{nv}, as long as the stiffness is C_{nv} symmetric, and $n/2$ is even.

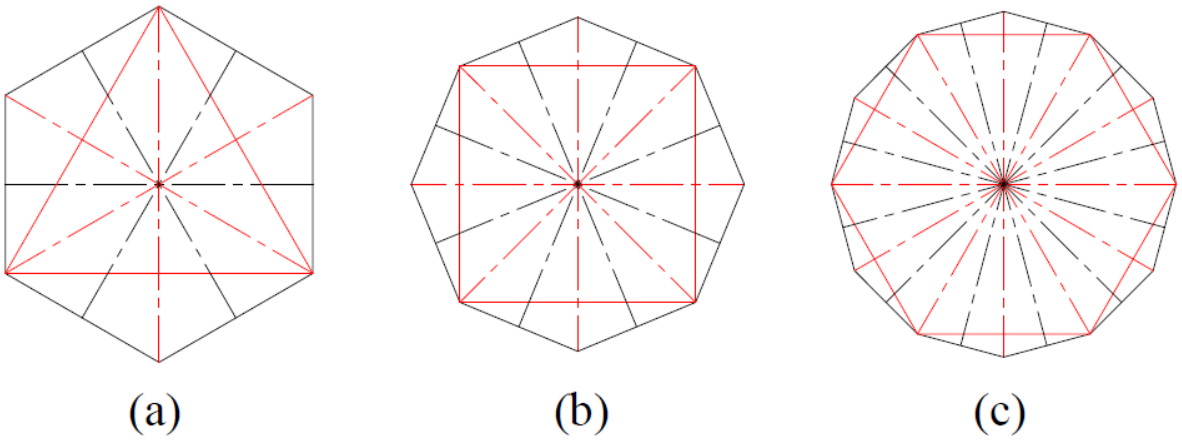

Figure 4.49: $C_{nv/2}$ frame inscribed in C_{nv} Frame

When the group index is used to classify the symmetry of the eigenmodes, two observations were made for C_{nv} symmetric frames with n greater than two:

- When the group index is greater than two, then the respective eigenvalue is a repeating eigenvalue; and
- when the group index is equal to two, then the respective eigenvalue is non-repeating.

From the forgoing discussion, we can conclude that for a plane frame that is C_{nv} symmetric in terms of stiffness and loading, the following buckling behaviour will be displayed for $n \geq 3$:

1. The lowest buckling load will have an eigenmode with the symmetry of a subgroup of C_{nv} with the highest order of elements;
2. the order of emergence of symmetries for eigenmodes of higher eigenvalues will be from the subgroups of C_{nv} with the highest order of elements to those with the lowest order of elements, and it repeats every $2n$ eigenvalue;
3. the eigenvalues whose eigenmodes have the C_n symmetries form the higher bound eigenvalues in relation to eigenmodes with $C_{(n/2)v}$ symmetry;
4. plane frames that are C_{nv} symmetric in terms of stiffness subjected to a loading arrangement symmetric to a subgroup of C_{nv}, display the buckling behaviour of a frame that is symmetric to that particular subgroup in terms of stiffness and loading; and

5. plane frames that are C_{nv} symmetric in terms of loading and subjected to $C_{nv/2}$ loading display the buckling behaviour of a plane frame symmetric to C_{nv} with respect to loading and stiffness for cases where $n/2$ is even.

4.9 Summary and concluding remarks

The main findings of this chapter were the analytical tools developed for the buckling analysis of plane frames and the findings on the influence of symmetry on the buckling behaviour of plane frames.

Through several examples, it was demonstrated how the conventional slope deflection method can be adapted using the group theoretic approach in the buckling analysis of plane frames. It was observed that this symmetry adapted slope deflection method reduced the computational method required to compute eigenvalues when compared with the conventional approach. Furthermore, while eigenvectors were computed using the conventional approach, the group theoretic approach developed in this study can also be used to compute the eigenvectors, which would result in less computational effort than the conventional approach.

The buckling behaviour of C_{nv} plane frames subjected to C_{nv} stiffness and loading was studied using both the analytical and finite element method approaches. When the buckling behaviour is described in terms of the eigenmodes produced, it was found that the symmetry of the eigenmodes produced were subgroups of the applicable C_{nv} group. The symmetry of the eigenmode for the lowest eigenvalue was found to be the symmetry subgroup with the highest order of elements. The order of emergence of symmetries for eigenmodes for higher eigenvalues was from the subgroup with the highest order of elements to that with the lowest order of elements. The emergence of these symmetries was found to be repeating for every $2n$ eigenvalues.

In cases where either the applied loading or stiffness for a C_{nv} frame was a subgroup of C_{nv}, the observed buckling behaviour could be explained by making reference to the applicable subgroup and its own subgroups. The lower order of symmetry was introduced by changing the load ratio γ. This was the ratio of loads among the members. When this ratio was equal to unity, the applied load was C_{nv}, and when it was not equal to unity, the applied load was a subgroup of the applicable C_{nv} symmetry group. Similarly, a lower order of symmetry in stiffness was introduced by adjusting the ratio of stiffness between members (β). For both cases of either introducing a

lower symmetry order of either stiffness or loading, it was observed that the symmetries of eigenmodes that emerged from a linear eigenvalue analysis were subgroups of the applicable subgroup. It was observed that the emergence of symmetries of eigenvalues was, for the most part, not repeating for the first fifty eigenvalues investigated. It was also observed that when the buckling loads for all values of γ are plotted on the same graph, an increase in γ results in more closely spaced buckling values. Similarly, it was observed that an increase in β results in less closely spaced buckling values.

Chapter 5

5. Influence of symmetry on the stability behaviour of C_{nv} space symmetric frames

5.1 Introduction

In this part of the study, we attempt to establish the influence of symmetry on the stability behaviour of C_{nv} symmetric space frames of the type shown in Figure *1.2*. Plane frames symmetric to five point-group symmetries were investigated, and these are: C_{2v}, C_{3v}, C_{4v}, C_{5v}, and C_{6v}. The approximate values of the buckling loads were obtained using the slope deflection method. These analytical results were subsequently used to validate *FEMs* created in the software Abaqus. The models created in Abaqus were created from a circular hollow section with an outer diameter of *52 mm*, a thickness of *6 mm,* and a length of *2 m*. The material properties of the cross-section were as follows: modulus of elasticity *E=200 MPa* and Poisson's ratio *v=0.3*. The beam elements used for the model were *B31* two-node linear elements. The mesh refinement was validated using the results obtained from the approximate results.

5.2 C_{2v} symmetric space frame

The space frame shown in Figure *1.2 (a)* is a laterally unrestrained C_{2v} symmetric frame. We consider the frame with C_{2v} stiffness and loading as shown in Figure *1.2 (a)*, with dimensions $a=c=l=2\ m$ and $b=l/2$.

5.2.1 Buckling behaviour of C_{2v} symmetric frame

We begin to study this problem by obtaining the buckling values for two types of buckling modes:

i. C^{y}_{1v} sway buckling mode of the type shown in Figure *5.4* for the first buckling mode λ_{cr1}; and
ii. C_{2v} non-sway buckling mode of the type shown in Figure *5.4* for the fourth buckling mode λ_{cr4}.

The analytical solution for buckling values for C^{y}_{1v} (i) and C_{2v} (ii) symmetric buckling modes can be easily obtained if the C_{2v} space frame shown in Figure *1.2 (a)* is modelled as two separate independent plane frames with a height of *2m* and length as *2m* as shown in Figure *5.1*.

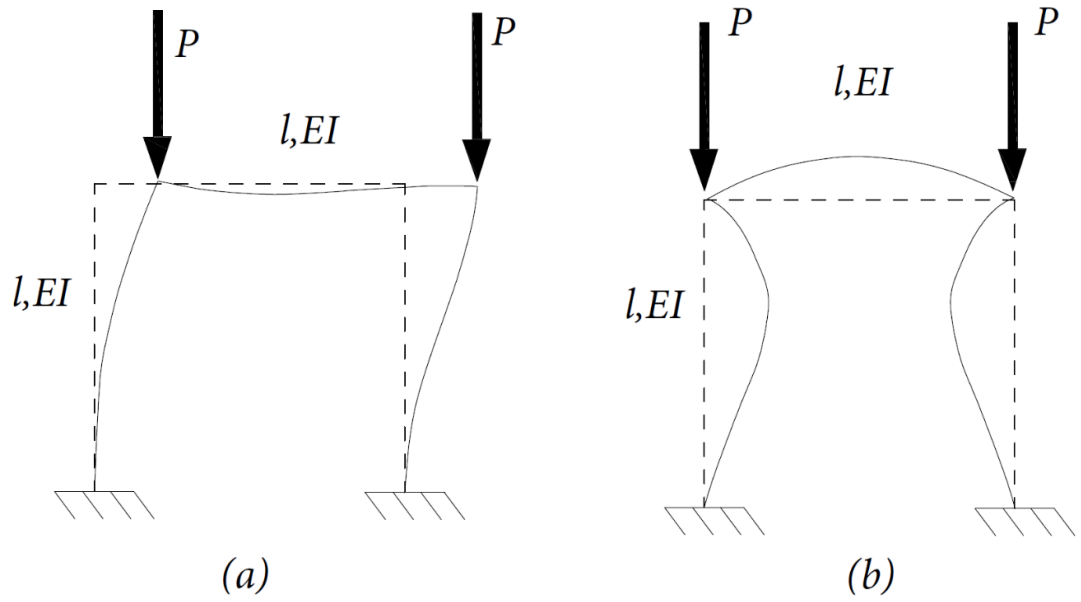

Figure 5.1: (a) C^{y}_{1v} sway buckling mode, (b) C_{2v} non-sway buckling mode

The characteristic equation for the buckling mode shown in Figure *5.1 (a)* has been derived using the *SDM* by Chajes (1974) as:

$$\frac{\tan(\lambda_{cr} l)}{\lambda_{cr} l} + \frac{1}{6} = 0 \qquad (5.1)$$

where λ is as defined in equation 4.4.

Equation *5.1* was solved using Matlab, and the results are summarised in Figure *5.2*.

The characteristic equation for the buckling mode shown in Figure *5.1 (b)* has also been derived using the *SDM* and is given as (Chajes, 1974):

$$\lambda_{cr} l \sin \lambda_{cr} l + 4 \cos \lambda_{cr} l + (\lambda_{cr} l)^2 \cos \lambda_{cr} l = 4 \qquad (5.2)$$

Equation *5.2* was also solved using Matlab and the results are summarised in Figure *5.2* and compared with the results obtained from the *FEM* in Abaqus. The *FEM* results were obtained by carrying out a linear eigenvalue analysis in Abaqus for the first fifty buckling values.

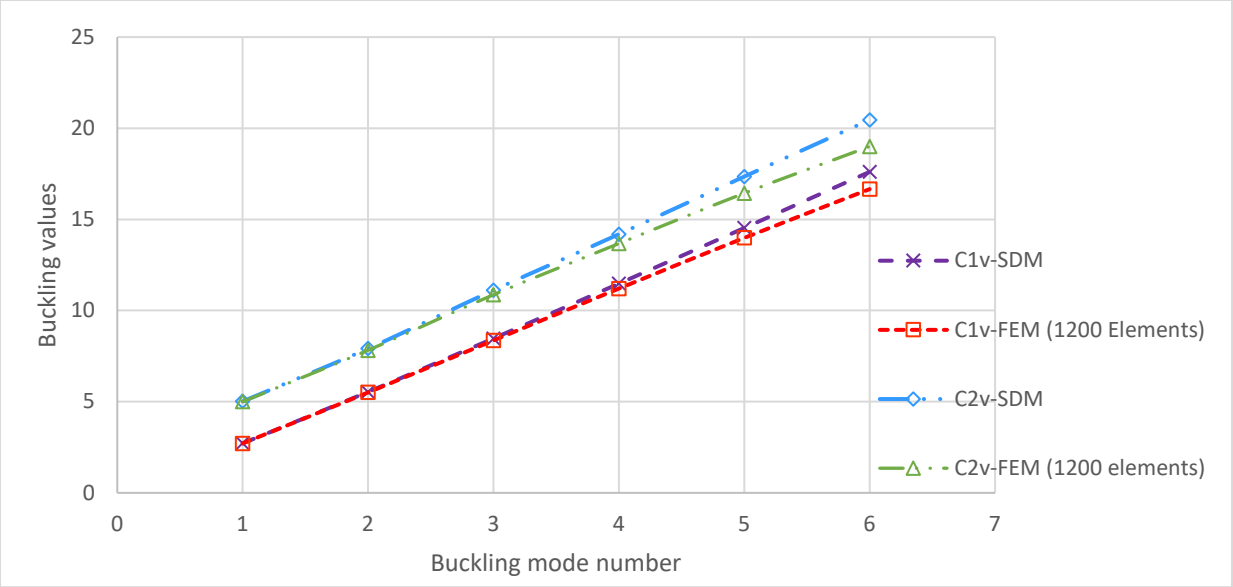

Figure 5.2: C_{2v} space frame comparison of FEM and analytical results

The boundary conditions applied to the *FEM* created in Abaqus were as shown in Figure *1.2 (a)*. The convergence analysis of the *FEM* model is shown in Figure *5.3*. The convergence analysis was based on comparison with results obtained from the analytical analysis of buckling values with C^{y}_{1v} and C_{2v} buckling modes.

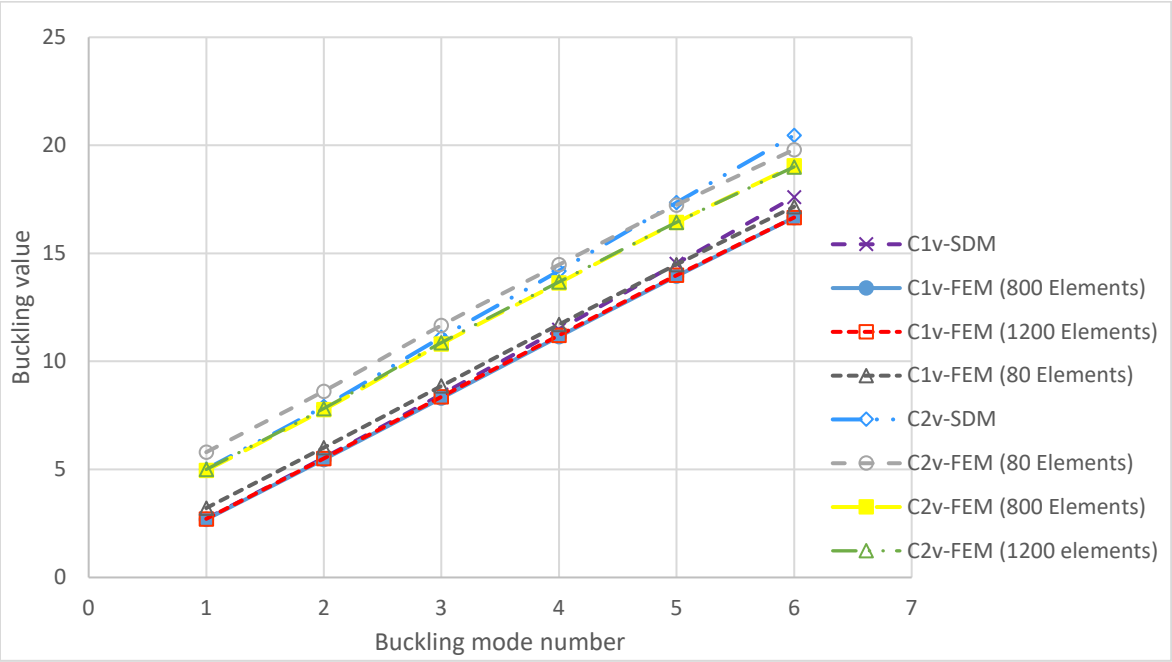

Figure 5.3: C_{2v} space frame convergence analysis

The minimum and maximum percent error with reference to the analytical solution was *0.1%* and *5.7%* respectively for the C^{y}_{1v} sway buckling mode. On the other hand, the minimum and maximum percent error with reference to the analytical solution was *0.4%* and *7.12%* for the C_{2v} non-sway buckling mode.

A linear eigenvalue analysis was carried out in Abaqus for the first fifty buckling values. The symmetry of the buckling modes for the first fifty buckling values was categorised, and the results for the first fourteen buckling values are presented in Table *5.1,* and samples of the buckling modes are shown in Figure *5.4*. The buckling mode for the lowest buckling value `was C_{1v} rather than C_{2v} and no repeatable sequence of buckling modes was observed from the results obtained for this frame. The reason for this behaviour is apparent when plots are made of buckling values versus buckling mode numbers for each symmetry group of the buckling mode, as shown in Figure *5.5*. The general trend of each curve is different, and thus there is no common pattern in the emergence in symmetry patterns of the buckling modes.

From the results obtained from this *FEM* study, we observe that the buckling mode with the lowest buckling value for sway modes is C_{1v}. Subsequent higher buckling values have buckling modes whose order of symmetry, *n*, is proceeding from a lower order to a higher order. On the other hand, the lowest buckling value for non-sway modes is C_{2v} symmetric.

Table 5.1: C_{2v} Space Frame Buckling values and Buckling mode symmetries

Number	Buckling value	Buckling mode symmetry	Sway/Non-sway
1	2.713	C^{y}_{1v}	Sway
2	2.895	C^{x}_{1v}	sway
3	3.222	C_2	Twisting
4	4.998	C_{2v}	Non-sway
5	5.305	C_{2v}	Non-sway
6	5.420	C^{x}_{1v}	Non-sway
7	5.462	$C^{y}1_{v}$	Non-sway
8	5.508	C^{y}_{1v}	Sway
9	5.684	C_2	Non-sway
10	5.786	C^{x}_{1v}	Non-sway
11	5.830	C_2	Non-sway
12	7.620	C_2	Twisting
13	7.822	C_{2v}	Non-sway
14	7.972	C_{2v}	Non-sway

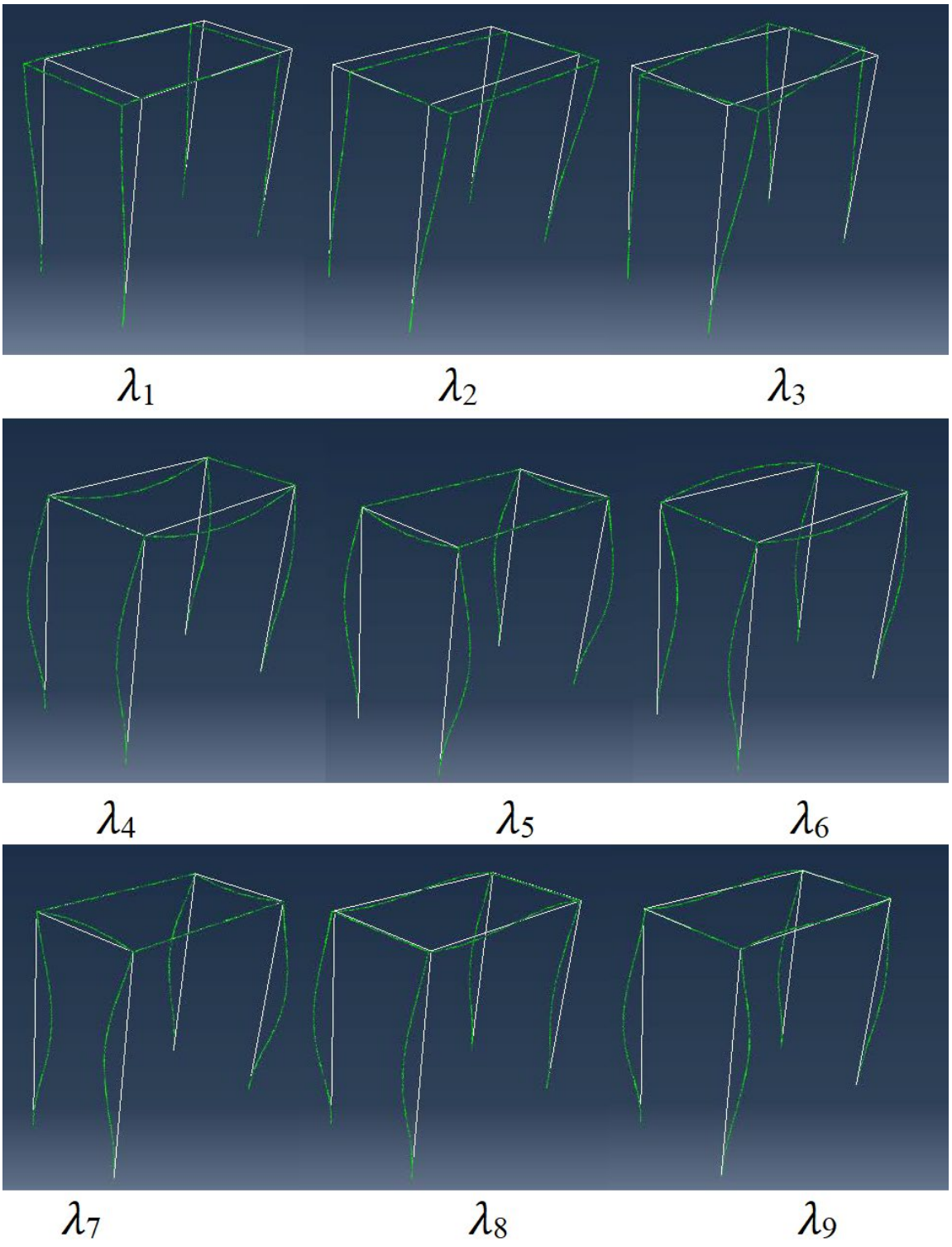

Figure 5.4:C_{2v} space frame Buckling modes

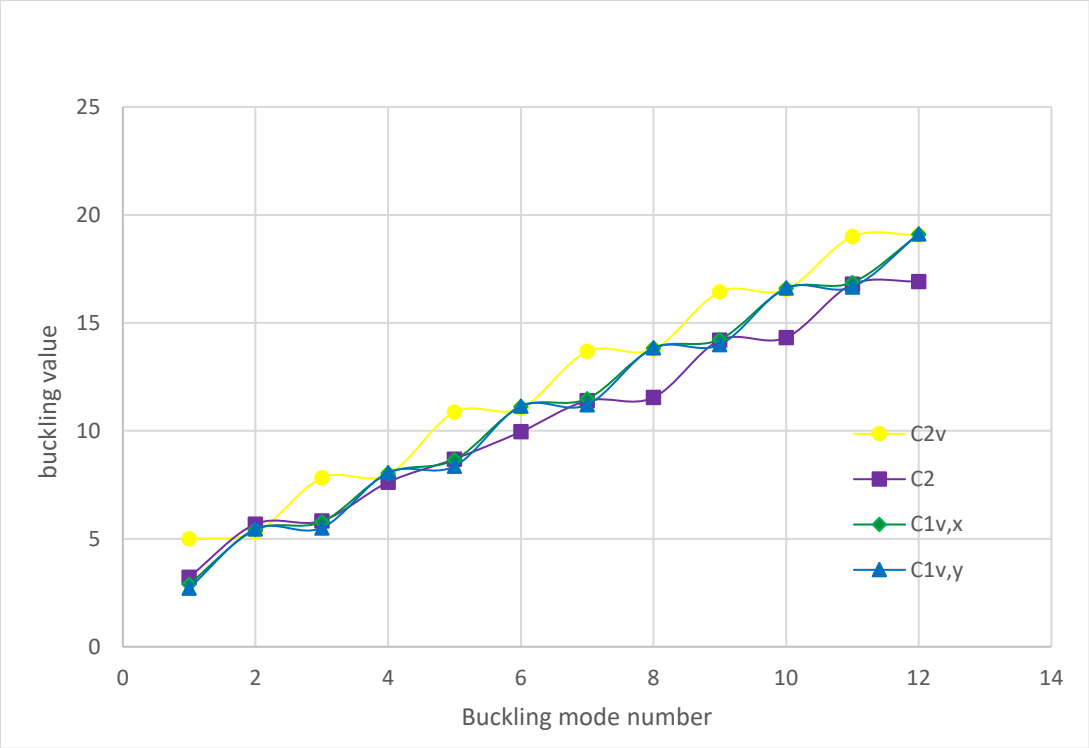

Figure 5.5: C_{2v} Space Frame, Buckling value versus Buckling mode

5.3 C_{3v} symmetric space frame

The space frame shown in Figure *1.2 (b)* is a laterally unrestrained C_{3v} symmetric frame. The frame studied was constructed with C_{3v} stiffness and loading as shown in Figure *1.2 (b)*, with dimensions $b=c=l=2\ m$.

5.3.1 Buckling behaviour of C_{3v} symmetric frame

A *FEM* of the space frame was created in Abaqus, and the boundary conditions applied were as shown in Figure *1.2 b*. The selected mesh density used was the same as that used for the C_{2v} symmetric space frame previously presented. A linear eigenvalue analysis was then carried out for the first fifty buckling values. The symmetry patterns of the buckling modes for the first fifty buckling values were categorised, and the results for the first fourteen buckling values are presented in Table *5.2,* and samples of the buckling modes produced are shown in Figure *5.6*. As in the case for the C_{2v} space frame presented earlier, it was observed that the lowest buckling value had C_{1v} symmetric buckling mode which was a sway mode. The lowest buckling value for a non-sway mode produced a C_{3v} symmetric buckling mode. Further, every repeating buckling value

produced either a C_{1v} or C_1 symmetric buckling mode. Non-repeating buckling values produced buckling modes that were C_{3v} and C_3 symmetric.

Unlike the C_{2v} space frame earlier presented, the C_{3v} space frame produced a repeatable sequence of buckling mode symmetries for every six buckling values, beginning at the fifth buckling value. When plots are made of buckling values versus buckling mode numbers for each symmetry group of the buckling mode, as shown in Figure *5.7*, it was observed that the curves do not intersect at several points. This is the reason why the repeatable sequence of buckling mode symmetries is observed.

Table 5.2: C_{3v} Space frame buckling values and buckling mode symmetries

Number	Buckling value	Buckling mode symmetry	Sway/Non-sway
1	2.631	$C^1{}_{1v}$	sway
2	2.631	C_1	sway
3	3.004	C_3	Twisting
4	5.012	$C^1{}_{1v}$	sway
5	5.012	C_1	sway
6	5.170	C_{3v}	non-sway
7	5.455	C_3	Twisting
8	5.644	C_1	non-sway
9	5.644	$C^1{}_{1v}$	non-sway
10	7.858	$C^1{}_{1v}$	sway
11	7.858	C_1	sway
12	7.901	C_{3v}	non-sway
13	8.319	C_3	Twisting
14	8.414	C_1	sway

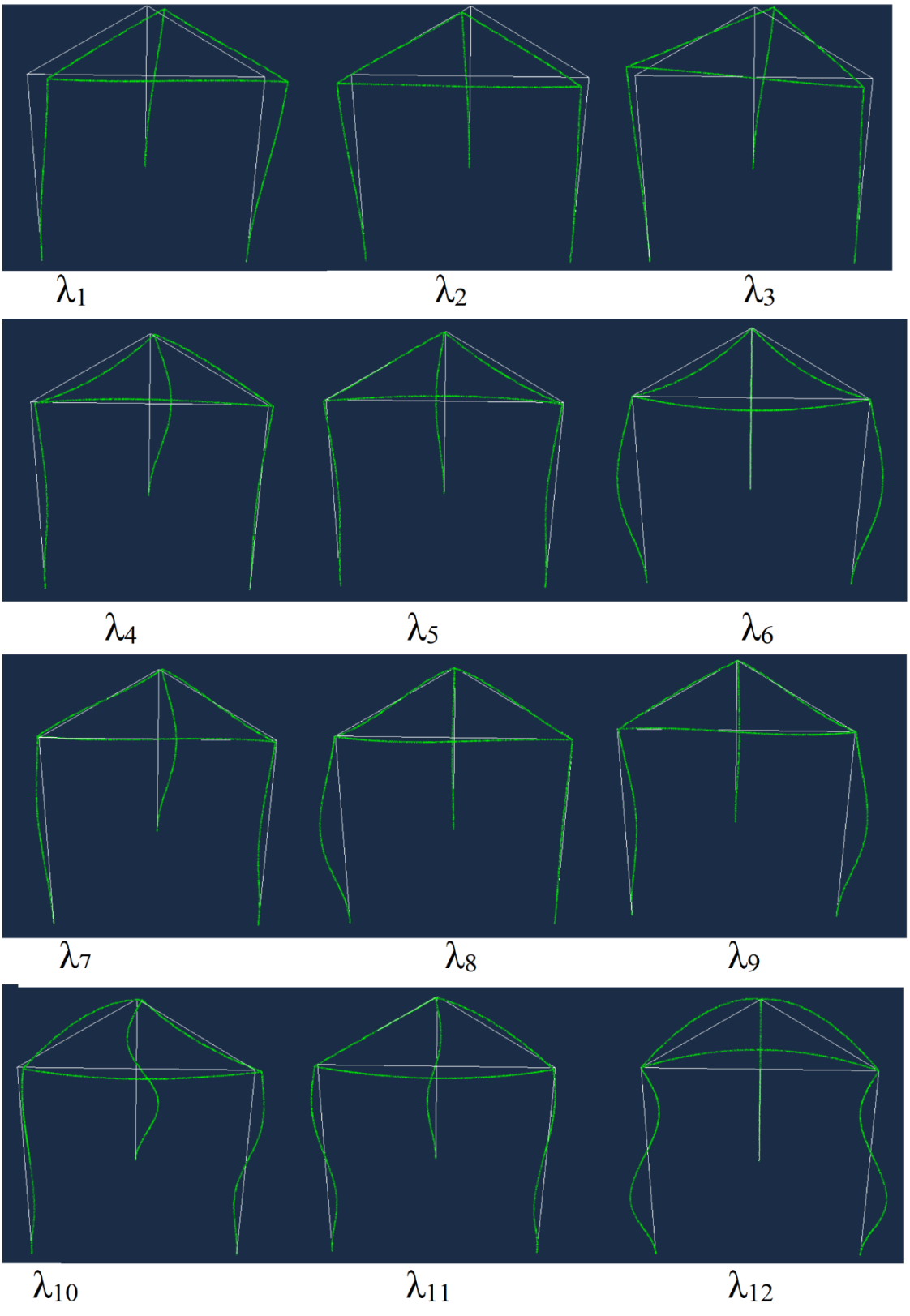

Figure 5.6: C_{3v} space frame buckling modes

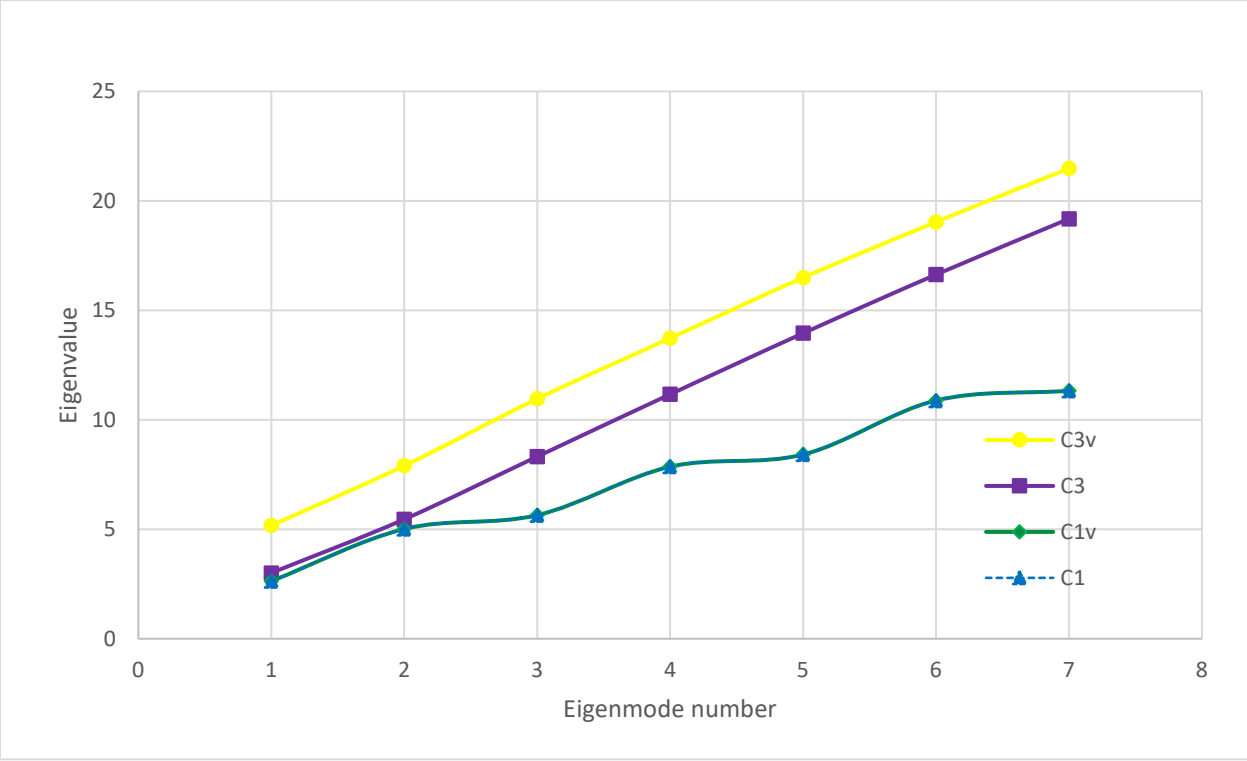

Figure 5.7 C_{3v} Space Frame, Buckling value versus Buckling mode

5.4 C_{4v} symmetric space frame

The space frame shown in Figure *1.2 (c)* is a laterally unrestrained C_{4v} symmetric frame, and the results for its buckling behaviour are presented in this section. The frame studied was constructed with C_{4v} stiffness and loading as shown in Figure *1.2 (c)*, with dimensions $b=c=l=2\ m$.

5.4.1 Buckling behaviour of C_{4v} symmetric frame

The FEM model was created with the applied boundary conditions as shown in Figure *1.2 (c).* The analytical results used to validate the *FEM* in this section were the same as those used for the C_{2v} symmetric frame previously discussed.

The results obtained in section *5.2.1* are again used here for the following types of modes:

i. $C^{y}{}_{1v}$ sway buckling mode of the kind shown in Figure *5.10* for the first buckling mode λ_{cr1}; and
ii. C_{2v} non-sway buckling mode of the kind shown in Figure *5.10* for the fourth buckling mode λ_{cr4}.

The convergence analysis for this frame is shown in Figure *5.8*. The results obtained from the analytical model in section *5.2.1* were used as the basis of the convergence analysis.

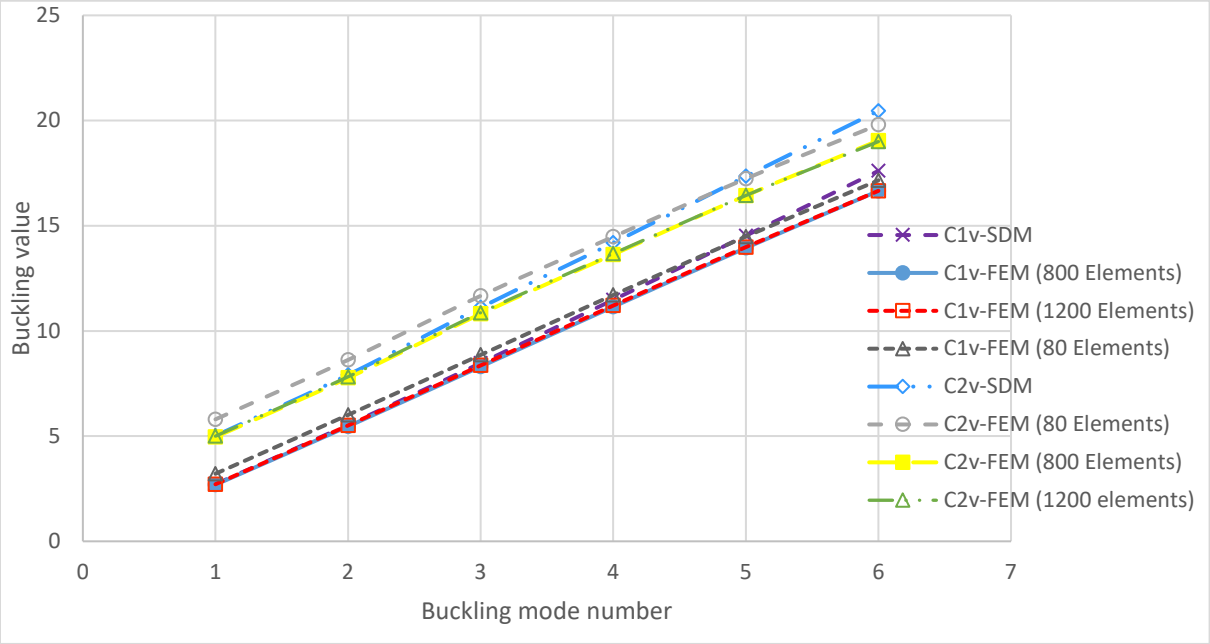

Figure 5.8: C_{4v} space frame convergence analysis

For clarity, the results of the buckling values for the two types of buckling modes listed above are plotted on the same graph as the *FEM* results obtained in Abaqus for the optimum mesh density, as shown in Figure *5.9*. The minimum and maximum percent error with reference to the analytical solution were *0.1%* and *5.3%,* respectively, for the $C^{y}{}_{1v}$ sway buckling mode. On the other hand, the minimum and maximum percent error with reference to the analytical solution were *0.4%* and *7.12%*, respectively, for the C_{2v} non-sway buckling mode.

A linear eigenvalue analysis was carried out in Abaqus for the first fifty buckling values. The symmetry of the buckling modes was categorised for each buckling value, and the results for the first fourteen buckling values are presented in Table *5.3* and Figure *5.10*. Again, as was the case for all C_{nv} space frames studied so far, the lowest buckling value produces a C_{1v} symmetric sway buckling mode. The lowest buckling value for a non-sway mode produced a C_{2v} symmetric buckling mode. Further, every buckling value is a repeating buckling value, except for buckling values that produce C_4 symmetric buckling modes. The pattern of emergence of buckling modes shown in Table *5.3*, from the fourth buckling value, was repeating for every eight buckling values.

This buckling behaviour is similar to the buckling behaviour of the C_{4v} plane frame, which was discussed in Section *4.4* of this study.

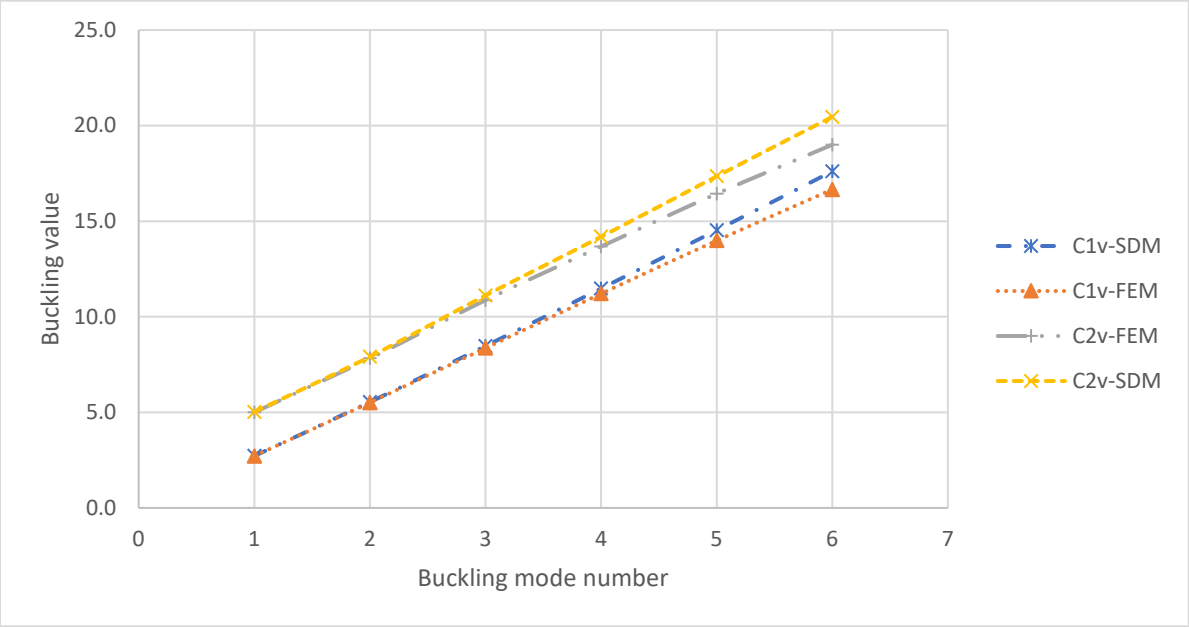

Figure 5.9: C_{4v} comparison of FEM and analytical results

Table 5.3: C_{4v} Space Frame buckling values and buckling mode symmetries

Number	Buckling value	Buckling mode symmetry	Sway or Non-sway
1	2.713	C^{y}_{1v}	sway
2	2.713	C^{x}_{1v}	sway
3	3.001	C_4	twisting
4	4.998	C_{2v}	non-sway
5	4.998	C_{2v}	non-sway
6	5.230	C_{2v}	twisting
7	5.246	C^{y}_{1v}	non-sway
8	5.246	C^{x}_{1v}	non-sway
9	5.508	C^{y}_{1v}	sway
10	5.508	C^{x}_{1v}	non-sway
11	5.610	C_4	non-sway
12	5.636	C_{2v}	twisting
13	7.822	C_{2v}	non-sway
14	7.822	C_{2v}	non-sway

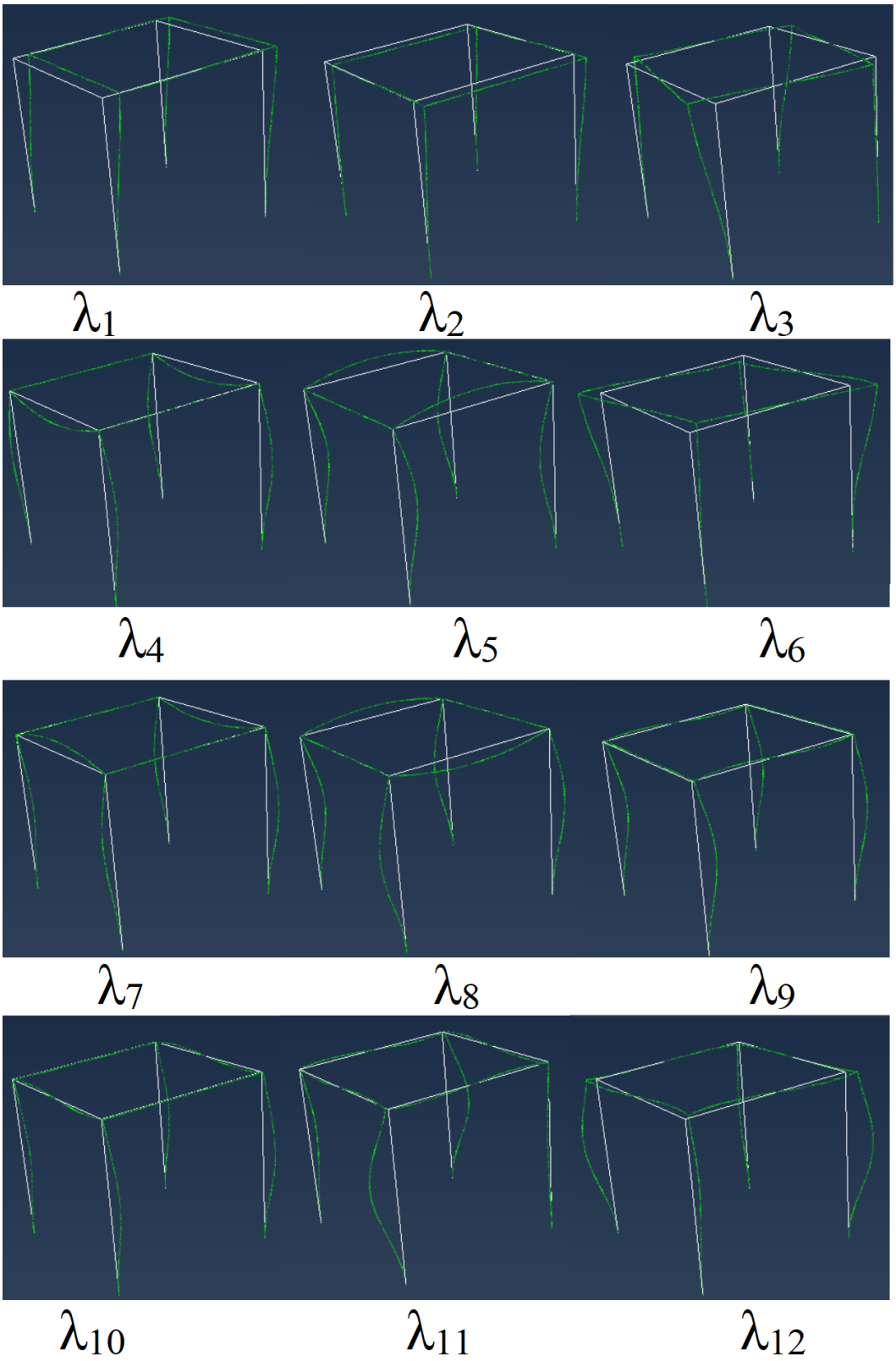

Figure 5.10: C_{4v} space frame buckling modes

5.5 C_{6v} symmetric space frame

The space frame shown in Figure *1.2 (d)* is a laterally unrestrained C_{6v} symmetric frame, and the results for its buckling behaviour are presented in this section. The frame studied was constructed with C_{6v} stiffness and loading as shown in Figure *1.2 (d)*, with dimensions $b=c=l=2\ m$.

5.5.1 Buckling behaviour of C_{6v} symmetric frame

A *FEM* was created in Abaqus, and the boundary conditions shown in Figure *1.2 (d)* were applied. A linear eigenvalue analysis was carried out in Abaqus for the first fifty buckling values. The convergence analysis for this frame is shown in Figure *5.11*. The optimum mesh density was determined when subsequent increments in the mesh density did not result in a change in the magnitude of the buckling values when compared to the buckling values produced from a *FEM* with a lower mesh density.

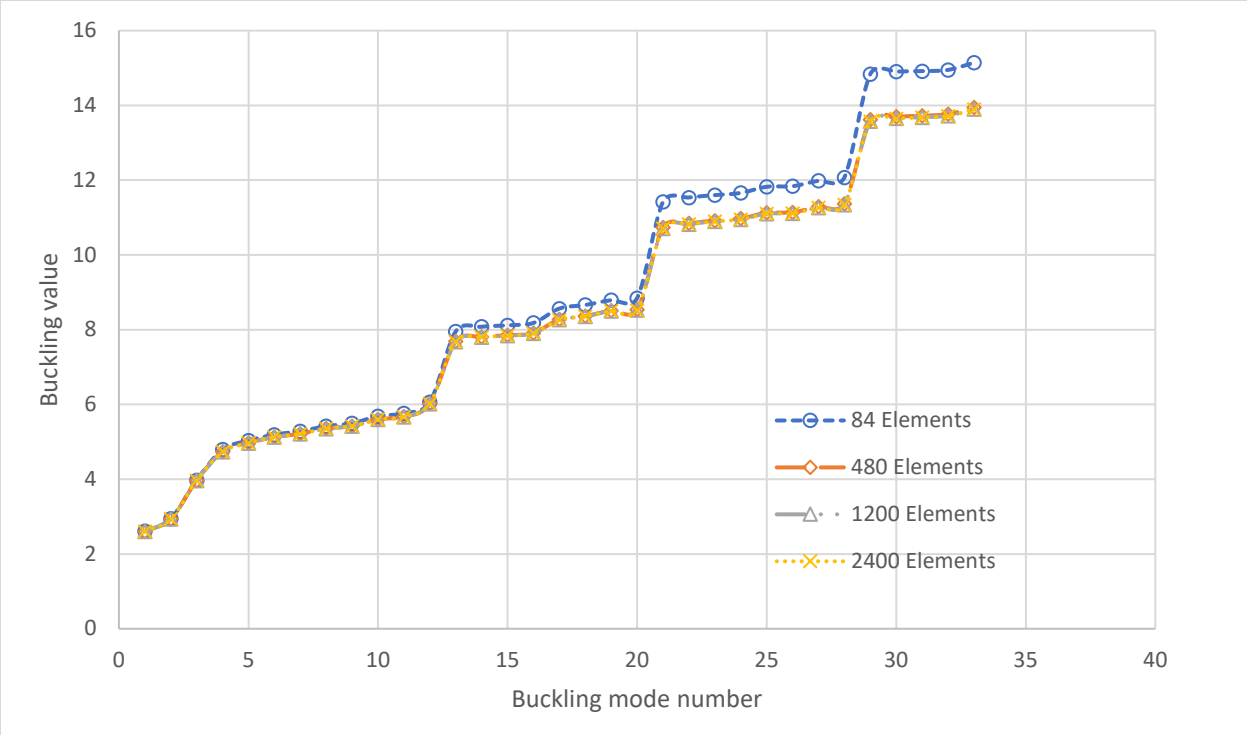

Figure 5.11: C_{6v} space frame convergence analysis

The symmetry of the buckling mode produced by each buckling value from a linear eigenvalue analysis was categorised, and a sample of the results is shown in Table *5.4*. Samples of the buckling modes produced from the buckling value analysis are shown in Figure *5.12*.

Table 5.4: C_{6v} Space Frame buckling values and buckling mode symmetries

Number	Buckling value	Buckling mode symmetry	Sway/ Non-sway mode
1	2.631	$C^{A}{}_{1v}$	Sway
2	2.631	$C^{3}{}_{1v}$	Sway
3	2.961	C_6	Twisting
4	4.003	C_2	Sway
5	4.003	C_2	Sway
6	4.775	C_{6v}	Non-sway
7	5.012	C_1	Sway
8	5.012	C_1	Sway
9	5.170	C_{3v}	Non sway
10	5.258	C_2	Sway
11	5.258	C_2	Sway
12	5.400	C_{3v}	Sway
13	5.464	C_2	Sway
14	5.464	C_2	Sway

Unlike the C_{3v} and C_{4v} space frames, the sequence of symmetries shown in Table *5.4* was found not to be repeating for all fifty buckling values produced. However, it was also observed that the buckling mode for the lowest buckling value was C_{1v} symmetric, in which the frame sways along one line of symmetry. The lowest buckling value for a non-sway mode produced a C_{6v} buckling mode. It was also observed that repeating buckling values produced buckling modes symmetric to the following subgroups: C_{1v} and C_2. On the other hand, non-repeating buckling values produced buckling modes with the following symmetries: C_{3v}, C_6, and C_{6v}.

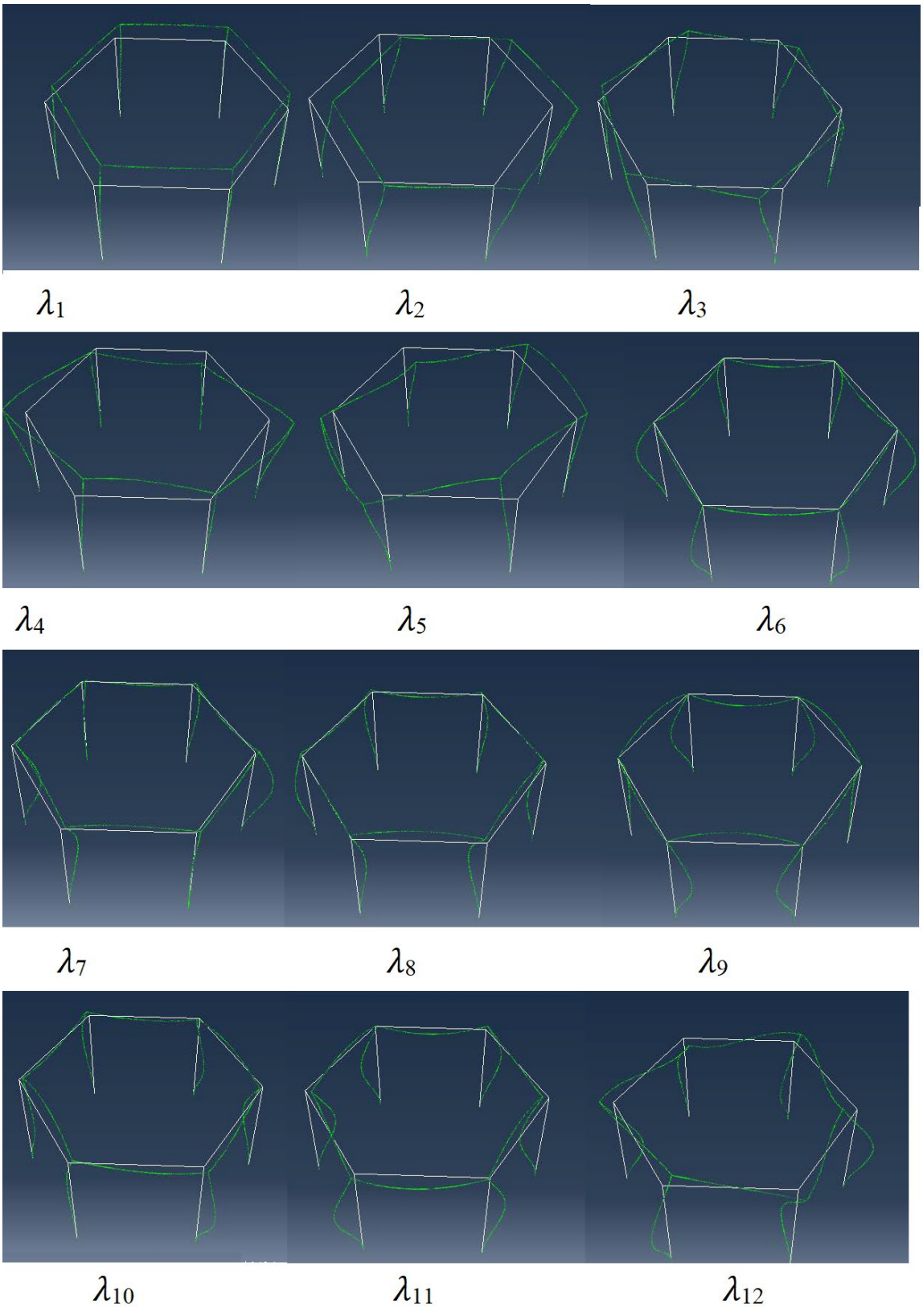

Figure 5.12: C_{6v} space frame buckling modes

5.6 Influence of symmetry on the stability behaviour of Space frames

From the results produced from the *FEMs* of the laterally unrestrained C_{nv} space frames studied, we can conclude the following about the buckling behaviour of such frames for $n>2$:

i. The buckling mode for the lowest buckling value is C_{1v} symmetric, and the frame sways along one line of symmetry; and
ii. the lowest buckling value is a repeating buckling value.

Further inferences on the buckling behaviour and symmetry could not be drawn based on the results obtained in this study.

5.7 Summary and concluding remarks

In this chapter, the analytical findings derived from the examination of plane frames in Chapter four were initially utilized to validate finite element models of C_{nv} space frames. Finite element models of space frames exhibiting symmetries such as C_{2v}, C_{3v}, C_{4v}, and C_{6v} were investigated. These models were then employed to analyse the impact of symmetry on the buckling behaviour of laterally unrestrained C_{nv} space frames. The buckling behaviour was characterised by the symmetries of buckling modes and the presence of repeating and non-repeating buckling values.

For the C_{2v} space frame, it was observed that the buckling mode with the lowest buckling value exhibited a C_{1v} symmetric sway mode. Subsequent higher buckling values displayed buckling modes with symmetry orders, n, progressing from lower to higher orders. The lowest buckling value for non-sway modes demonstrated C_{2v} symmetry. Moreover, no consistent sequence in the emergence of symmetries of buckling modes was observed within the initial fifty buckling values analysed, and no repeating buckling values were identified.

In contrast to the C_{2v} space frame, the C_{3v} space frame revealed a repeating sequence of buckling mode symmetries every six buckling values, starting from the fifth value. The lowest buckling value presented a C_{1v} symmetric sway buckling mode, while the lowest buckling value for non-sway modes displayed C_{3v} symmetry. Each C_{1v} buckling mode arose from a repeating buckling value, whereas every C_{3v} and C_3 buckling mode emerged from a non-repeating buckling value.

The lowest buckling value for the C_{4v} space frame manifested as a C_{1v} symmetric sway buckling mode, while for non-sway modes, it exhibited a C_{2v} symmetric buckling mode. Additionally, every

buckling value except those producing C_4 symmetric buckling modes was identified as a repeating buckling value. The pattern of buckling mode emergence from the fourth buckling value repeated every eight values.

In contrast to the C_{3v} and C_{4v} space frames, the sequence of symmetries in buckling modes for the C_{6v} space frame did not repeat for all fifty buckling values. However, it was observed that the buckling mode corresponding to the lowest buckling value displayed C_{1v} symmetry, with the frame swaying along one line of symmetry. The lowest buckling value for non-sway modes generated a C_{6v} buckling mode. Furthermore, repeating buckling values generated buckling modes symmetric to the following subgroups: C_{1v} and C_2, while non-repeating buckling values produced modes with symmetries such as C_{3v}, C_6, and C_{6v}.

Chapter 6

6. Influence of symmetry on the stability behaviour of D_{nh} space symmetric frames

6.1 Introduction

The stability behaviour of D_{nh} space frames symmetric to the following symmetry groups was studied: D_{2h}, D_{3h}, D_{4h}, D_{5h}, and D_{6h} (see Figure *1.3*) to establish the influence of symmetry on their stability behaviour. *FEM* models were made in Abaqus to study the buckling behaviour of each space frame under different load arrangements. The models created in Abaqus were made from a circular hollow section with an outer diameter of *52 mm and a* thickness of *6 mm* and a solid circular section with an equivalent radius of gyration. The material properties of the cross-section were as follows: *E=200 MPa* and Poisson's ratio *v=0.3*. The beam elements used for the model were *B31* two-node linear elements. Analytical results from Chapter Four on Plane Frames in this study were used to validate the *FEM*. The mesh refinement was carried out using results obtained from the analytical analysis. A linear eigenvalue analysis was carried out for the first fifty buckling values, and the buckling modes produced were categorised by symmetry.

The post-buckling behaviour of each frame was also investigated in Abaqus using the method of superimposed eigenmodes described in Section *3.3.2* of this study. Further, the influence of the ratio of the stiffness of the beams to columns on the post-buckling behaviour of the space frames was also investigated.

6.2 Space Frames with D_{2h} symmetry

The symmetry group D_{2h} is the symmetry of a prism with a rectangular base (see Figure *6.1*). It has a group order (n) of eight, and its subgroups are listed in Table *6.1* (Altmann & Herzig, 2011). The eight symmetry elements with respect to the coordinate directions $\{x, y, z\}$ and associated orthogonal planes $\{xy, xz, yz\}$ shown in Figure *6.1* are the following:

i. e is the identity element;

ii. C_2^z , C_2^x , C_2^y are rotations through an angle of π about the (*z, x, y*) axes, respectively;

iii. σ_{xy} , σ_{xz} , σ_{yz} are in the central (*xy, xz, yz*) planes, respectively. The σ_{xy} is conventionally denoted as the σ_h since it is a horizontal plane of reflection. The σ_{xz} and σ_{yz} are also conventionally denoted as σ_v and σ_d respectively; and

iv. *i* is an inversion, that is, a reflection through the centre of symmetry of the configuration. This is equivalent to a rotation of π about the z axis followed by a reflection in the central *xy* plane. This operation is also denoted by S_2.

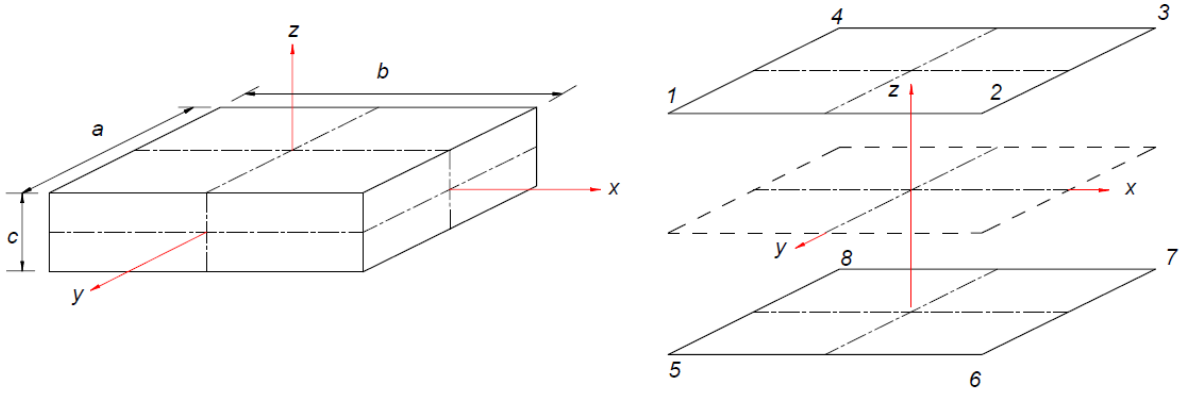

Figure 6.1: D_{2h} space frame

Table 6.1: Subgroups of D_{2h}

Group	order (*m*)	Group index (*n/m*)
C_i	2	4
C_s	2	4
C_2	2	4
C_{2v}	4	2
C_{2h}	4	2
D_2	4	2

6.2.1 Buckling Behaviour of a D_{2h} Symmetric Space Frame

The buckling behaviour of a D_{2h} symmetric space frame under three load arrangements was studied. The stiffness of the space frame was set as D_{2h} and the loading was arranged as follows: D_{2h}, D_{1h} or C_{2h}. These loading arrangements were as shown in Table *6.2*, with reference to Figure *6.1*. For each load arrangement shown in Table *6.2*, the ratio of beam to column stiffness ($\beta=I_b/I_c$)

was varied from *0.25* to *4* to investigate the effect of β on the post-buckling behaviour. The boundary conditions applied to the *FEM* are shown in Figure *6.2*. The boundary conditions at the base of the frame are labelled *BC-1* and those at the top *BC2-*. The dimensions of the space frame were $a=c=l=2\ m$ and $b=l/2$.

Table 6.2:D_{2h} space frame loading arrangements

Node	1	2	3	4	5	6	7	8
D_{2h} Loading P_z	P	P	P	P	-P	-P	-P	-P
D_{1h} Loading P_z	P	0	0	P	-P	0	0	-P
C_{2h} Loading P_z	2P	P	2P	P	-2P	-P	-2P	-P

P_z denotes a loading parallel to z-axis for each respective node in Figure 6.1.

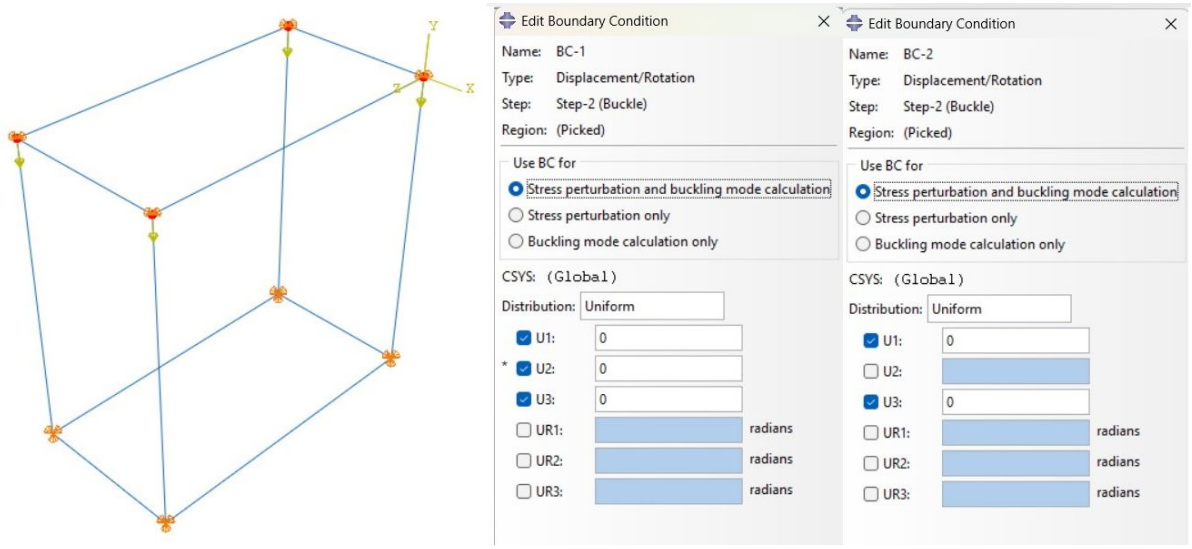

Figure 6.2:D_{2h} Boundary conditions.

A linear eigenvalue analysis was performed in Abaqus for the first fifty buckling values. The results of the convergence analysis used to select the mesh density are shown in Figure *6.3*. Sample sketches of the buckling modes produced are shown in Figure *6.4*.

The D_{2h} frame with $\beta=1$, was first analysed using the slope deflection method to determine the approximate buckling values with buckling modes that are D_{2h} symmetric. A typical example of the type of buckling mode considered here is the second buckling mode shown in Figure *6.4*. To analytically determine the buckling values with D_{2h} buckling modes, the D_{2h} frame was modelled as two separate frames. For the case where $a=c=l$ and $b=l/2$, the buckling loads previously

obtained using the slope deflection method for a C_{2v} symmetric frame were compared with the buckling loads from the finite element model of the D_{2h} frame for D_{2h} symmetric buckling modes, as shown in Figure *6.5*. As can be seen from Figure *6.5*, the results obtained from the finite element analysis were in close agreement with the results obtained from the analytical solution for C_{2v} symmetric modes. The minimum and maximum percent error relative to the result obtained from the analytical solution were 0.4% and 0.7%, respectively.

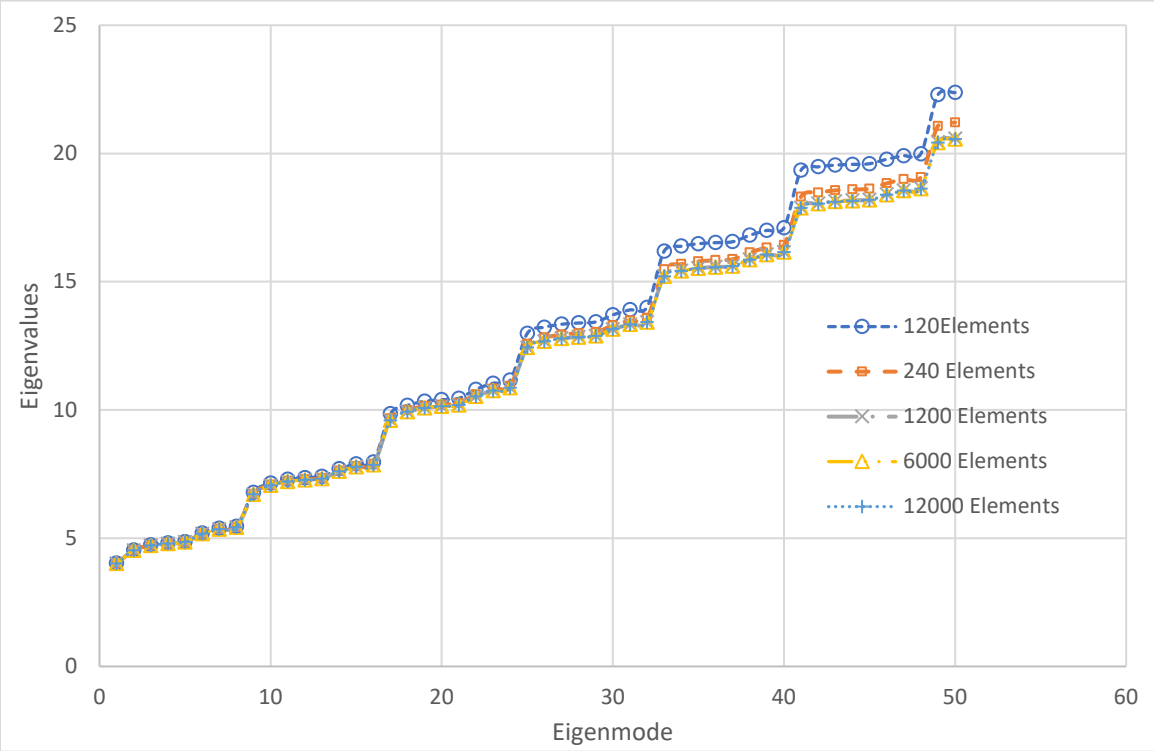

Figure 6.3: D_{2h} space frame convergence analysis

The symmetry of the buckling modes for each buckling value was also categorised, and these are shown for the first sixteen buckling values in Table *6.3* and plotted for all buckling values by buckling mode symmetry as shown in Figures *6.6*, *6.7,* and *6.8*. Samples of the buckling modes produced from Abaqus have already been presented in Figure *6.4* for the D_{2h} load arrangement with $\beta=1$. From Table *6.3*, we observe that the lowest buckling value for D_{2h} loading produced a D_{2h} buckling mode. Subsequent higher buckling values produced buckling modes of progressive lower order symmetry. It was also observed that the lowest buckling values for the D_{1h} and C_{2h} loading arrangements produced buckling modes that were D_{1h} and C_{2h} symmetric, respectively. Again, higher buckling values produced buckling modes with symmetries of lower order.

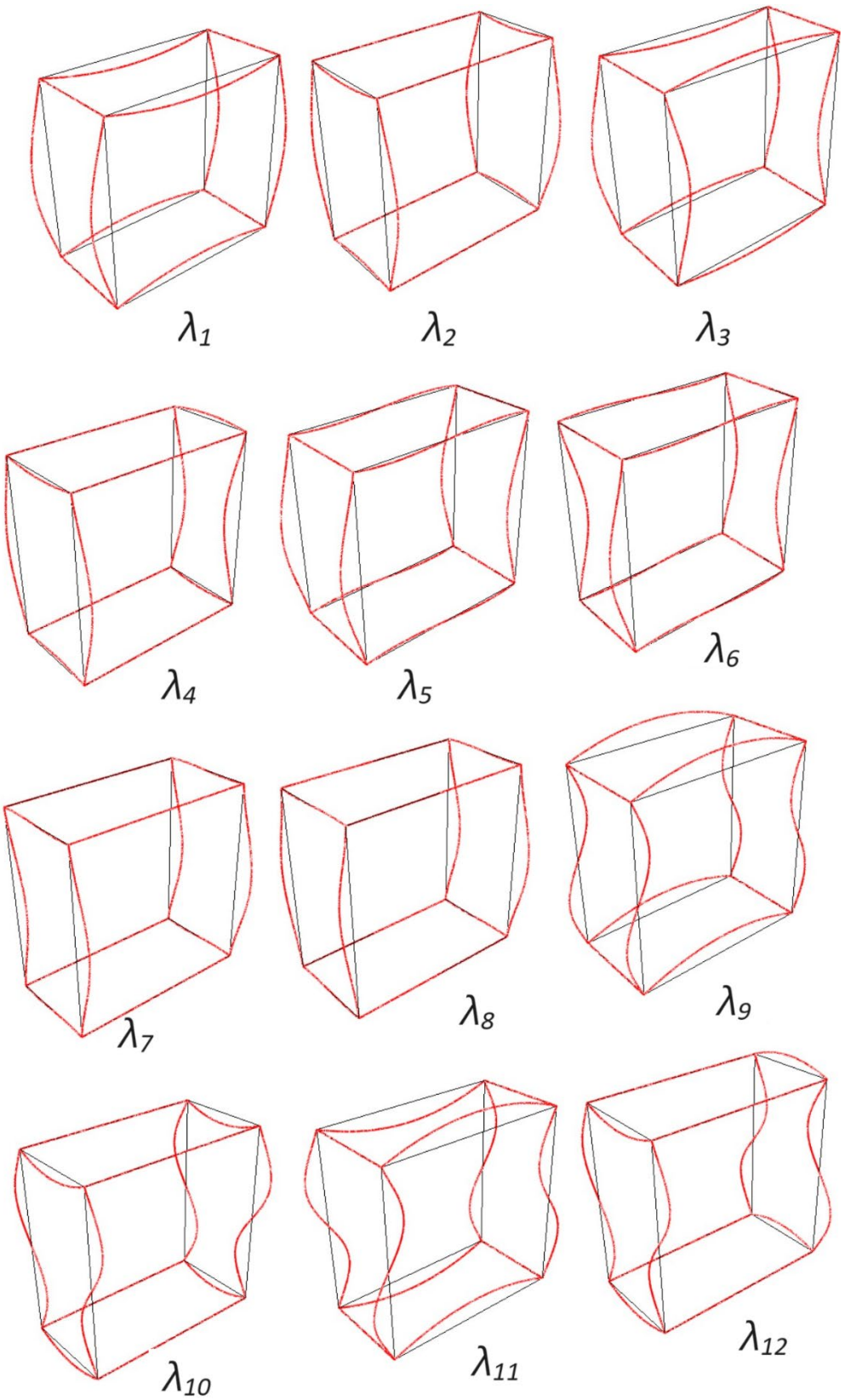

Figure 6.4: D_{2h} frame buckling modes

The pattern of the emergence of symmetries of buckling modes shown in Table *6.3* for D_{2h} and D_{1h} loading was repeating for all the buckling modes of the fifty buckling values produced from the finite element analysis. The pattern was repeating for every sixteen buckling values for the D_{2h} loading case and every eight buckling values for the D_{1h} loading case. This pattern was the same for all values of β investigated for the D_{2h} loading case. The reason for the clear repeating pattern can be seen from Figures *6.6* and *6.7* of plots of buckling values by buckling mode symmetry. It is observed that the curves for each plot have the same general trend, and thus the symmetries of the buckling modes emerge in a very clear and repeating pattern. For C_{2h} loading, no repeatable pattern in the symmetries of buckling modes was noted, and from Figure *6.8*, it can be observed that the curves of buckling values by symmetry of buckling mode do not share a common trend and intersect at several irregular points.

Lastly, there was no difference observed in the nature of the buckling behaviour with either the *FEM* created with either a circular hollow section or a solid circular section of equivalent radius of gyration.

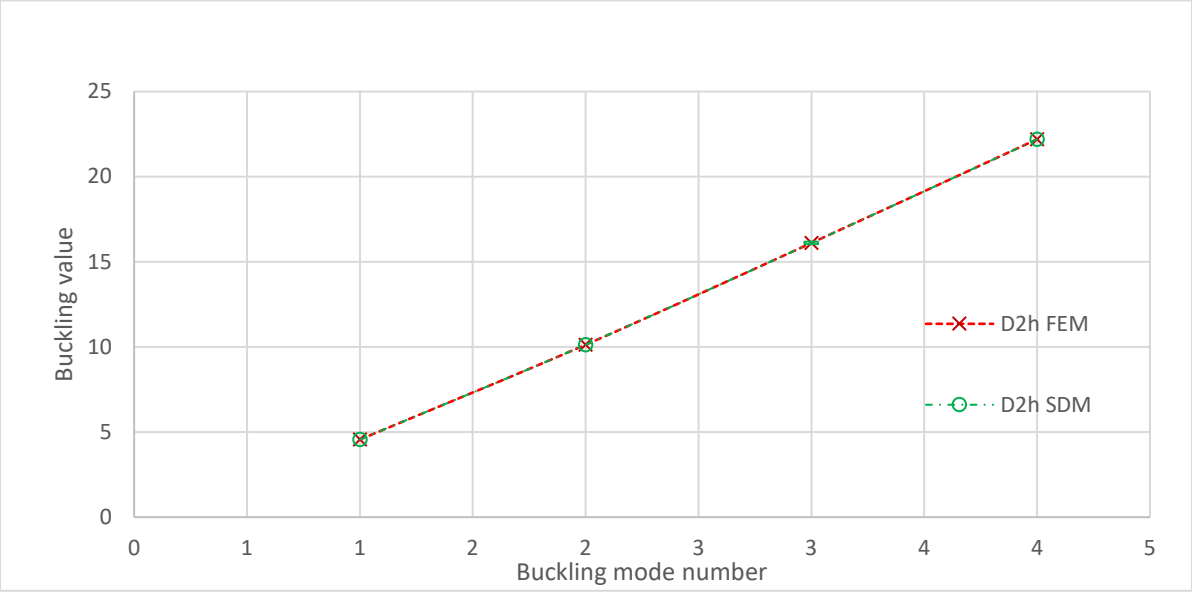

Figure 6.5: D_{2h} Space Frame (β=1), buckling values Abaqus and Analytical results

Table 6.3: D_{2h} Space Frame (β=1)buckling value and buckling mode symmetries

	D_{2h} loading		D_{1h} loading		C_{2h} loading	
No.	λ_{cr}	mode	λ_{cr}	mode	λ_{cr}	mode
1	4.041	D_{2h}	4.328	D_{1h}	3.124	C_{2h}
2	4.559	D_{2h}	4.863	D_{1h}	3.419	C_s
3	4.754	D_{1h}	4.974	C_s	3.469	C_{2h}
4	4.825	D_{1h}	5.048	C_s	3.593	Cs
5	4.890	D_{1h}	6.828	C_{1v}	4.780	C_{2h}
6	5.214	C_{2h}	7.224	C_{1v}	4.838	C_s
7	5.409	D_{1h}	7.285	C_2	5.072	C_2
8	5.486	C_{2h}	7.362	C_i	5.109	C_{2h}
9	6.782	C_{2v}	9.371	D_{1h}	5.159	C_s
10	7.150	C_{2v}	9.745	D_{1h}	5.218	C_i
11	7.305	C_{1v-}	9.842	C_2	5.315	C_2
12	7.364	C_{1v}	9.910	C_i	5.391	C_i
13	7.420	C_{1v}	11.669	C_{1v}	7.263	C_{2h}
14	7.714	C_2	11.931	C_{1v}	7.299	C_2
15	7.908	C_{1v}	11.976	C_2	7.327	C_s
16	7.989	C_2	12.037	C_i	7.377	C_i

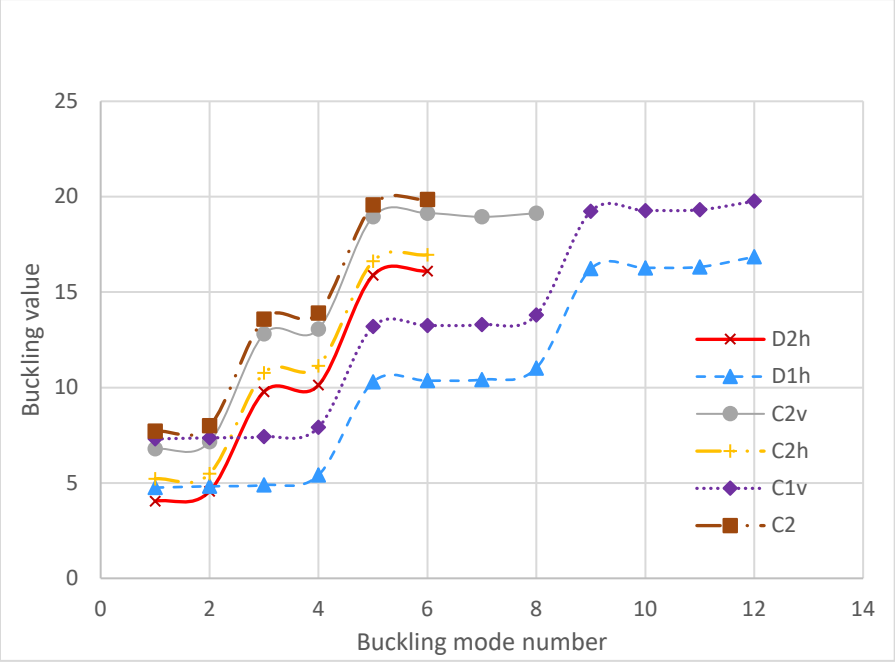

Figure 6.6: D_{2h} Space Frame buckling value versus mode symmetry, D_{2h} loading (β=1)

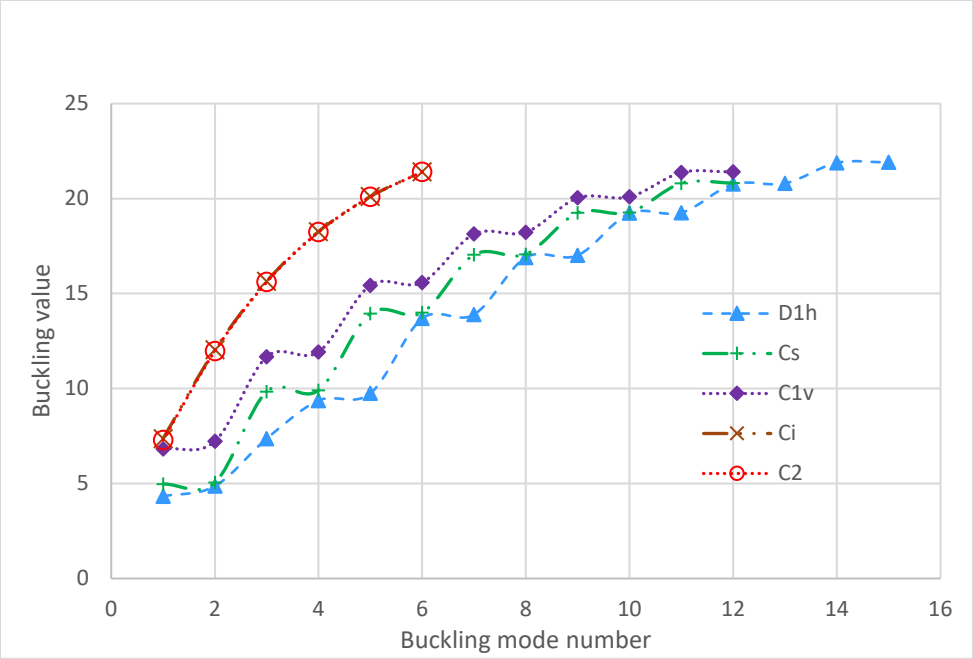

Figure 6.7: D_{2h} Space Frame Buckling value versus mode symmetry, D_{1h} loading (β=1)

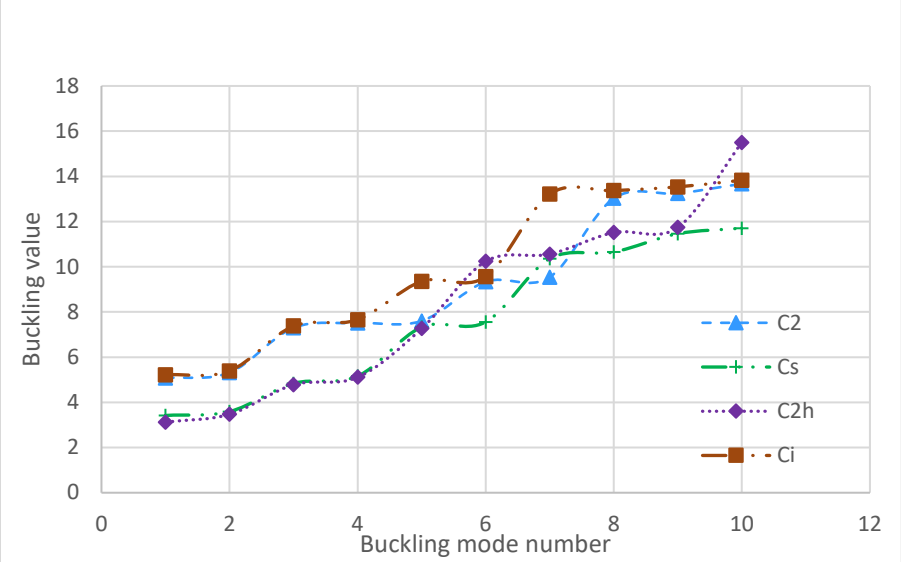

Figure 6.8: D_{2h} Space Frame Buckling value versus mode symmetry, C_{2h} loading (β=1)

6.2.2 Post-buckling Behaviour of a D_{2h} Symmetric Space Frames

The post-buckling behaviour of the space frame was investigated using a geometric nonlinear analysis in Abaqus by applying the method of superimposed eigenmodes described in Section *3.3.2* of this study. The Riks Arc method was used to trace the post-buckling equilibrium paths,

and it was found that all post-buckling equilibrium paths were symmetric stable bifurcation paths for the three load cases investigated. This is shown in Figure *6.9* for the case of D_{2h} loading. In Figure *6.9*, Δ represents the maximum lateral column displacement at mid-height, L the column length, $D_{1h\text{-}1}$ represents the post-buckling path for the first critical point, $D_{1h\text{-}2}$ for the second critical point and, C_{2h} represents the path for the sixth critical point. The values of the buckling loads obtained from the linear eigenvalue analysis for the first and second critical points are represented by P_{cr1} and P_{cr2}, respectively. In Figure *6.9,* on the primary equilibrium path, the deformation pattern of the space frame is D_{2h} symmetric; however, on the bifurcated paths, the deformation pattern of the space frame is a subgroup of the D_{2h} symmetry group shown in Table *6.3*. The equilibrium paths for deformation patterns of D_{1h}, and C_{2h} for the second and sixth bifurcation points are also shown in Figure *6.9* below. It was also observed that all bifurcation paths were symmetric and stable.

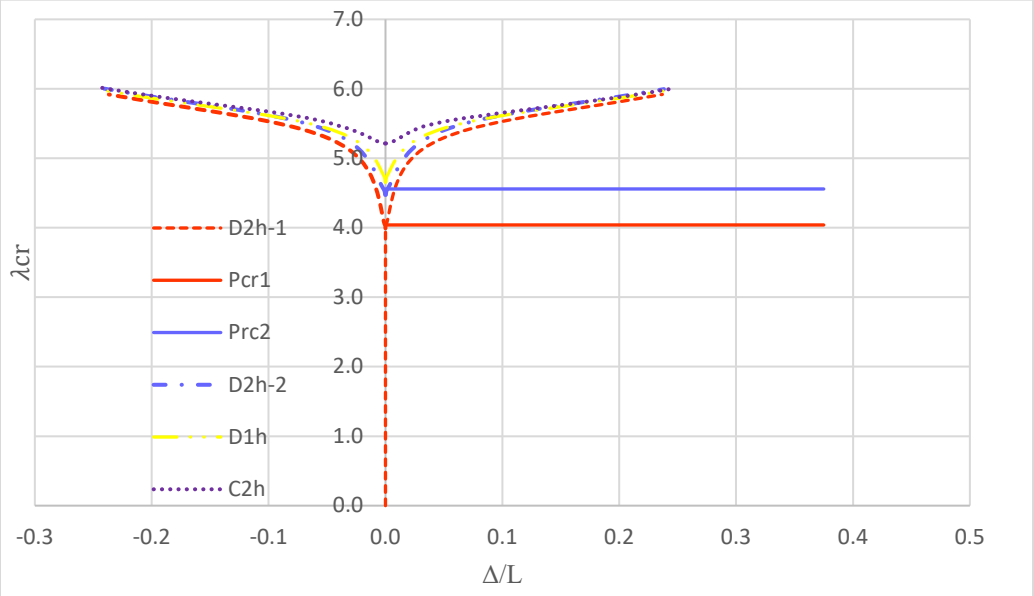

Figure 6.9: Equilibrium paths of D_{2h} symmetric Frame (β=1)

The nature of post-buckling behaviour shown in Figure *6.9* did not change when the ratio of beam to column stiffness (β) was varied from *0.25* to *4*. This is shown in Figure *6.10* for the first critical point in the case of D_{2h} symmetric loading. There was no difference observed in the nature of the stability behaviour with either the *FEM* created with a circular hollow section or a solid circular section of equivalent radius of gyration.

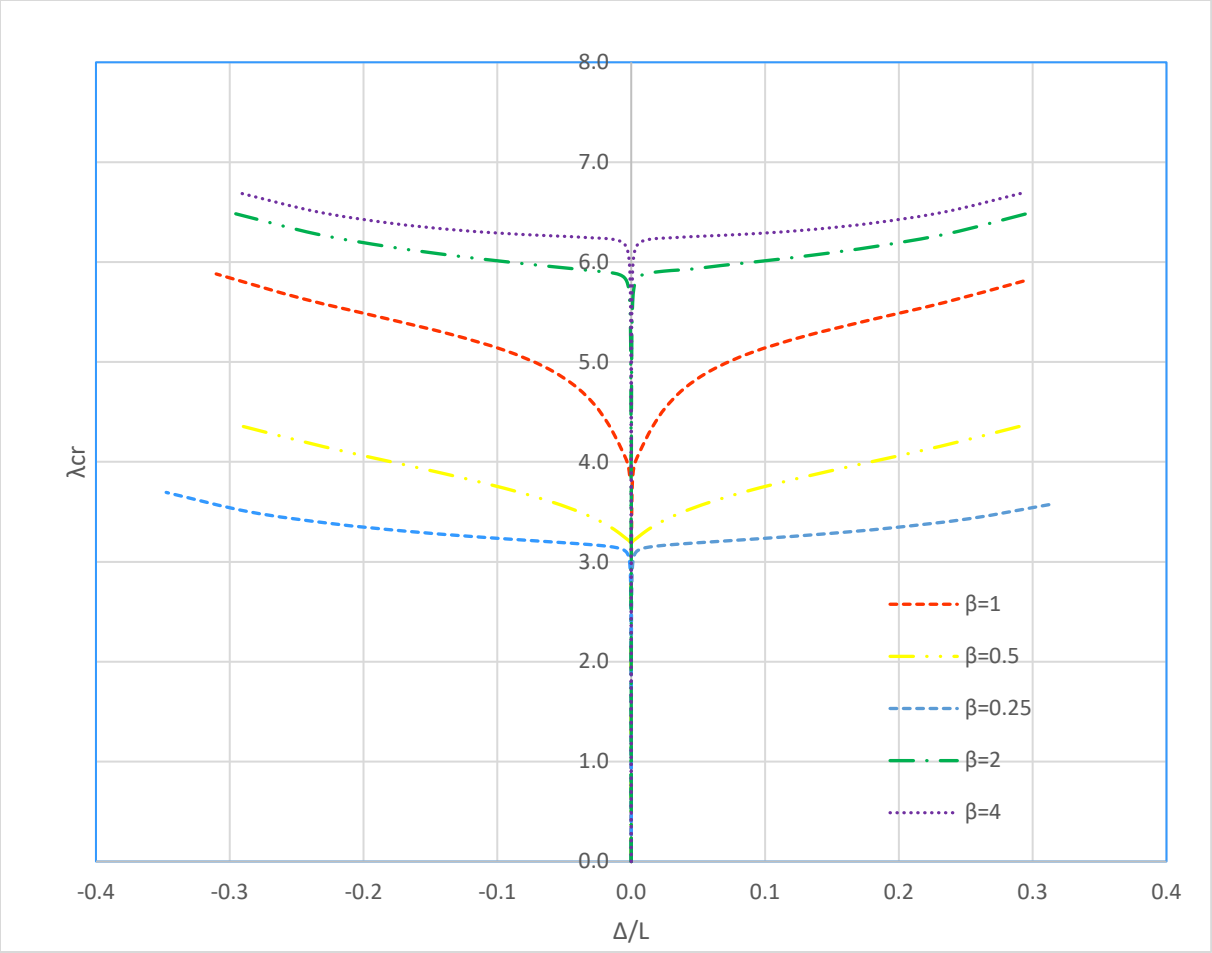

Figure 6.10: Effect of β ratio on equilibrium paths of D_{2h} frame for first D_{2h} critical point

6.3 Space Frames with D_{3h} symmetry

The symmetry group D_{3h} is the symmetry of a prism with a triangular base. It has the following twelve symmetry elements with respect to the coordinate directions and associated vertical planes shown in Figure *6.11*.

i. e is the identity element;

ii. C_3 , C_3^{-1} are rotations about the *z* axis through angles of *2π/3* and *-2π/3*, respectively;

iii. C_2^1, C_2^2, C_2^3 are rotations through an angle of π about the axes of symmetry *1*, *2,* and *3,* respectively;

iv. S_3, S_3^{-1} are rotary-reflections through angles of *2π/3* and *-2π/3*, respectively. The operations consist of a rotation about the *z* axis through angles of *2π/3* or *-2π/3*, followed by a refection σ_h in the middle horizontal plane;

v. σ_1, σ_2, σ_3 are reflections in the vertical planes containing axes *1* and *z*, *2* and *z*, *3* and *z* respectively; and

vi. σ_h is a reflection in the middle horizontal plane containing axes *1*, *2,* and *3*.

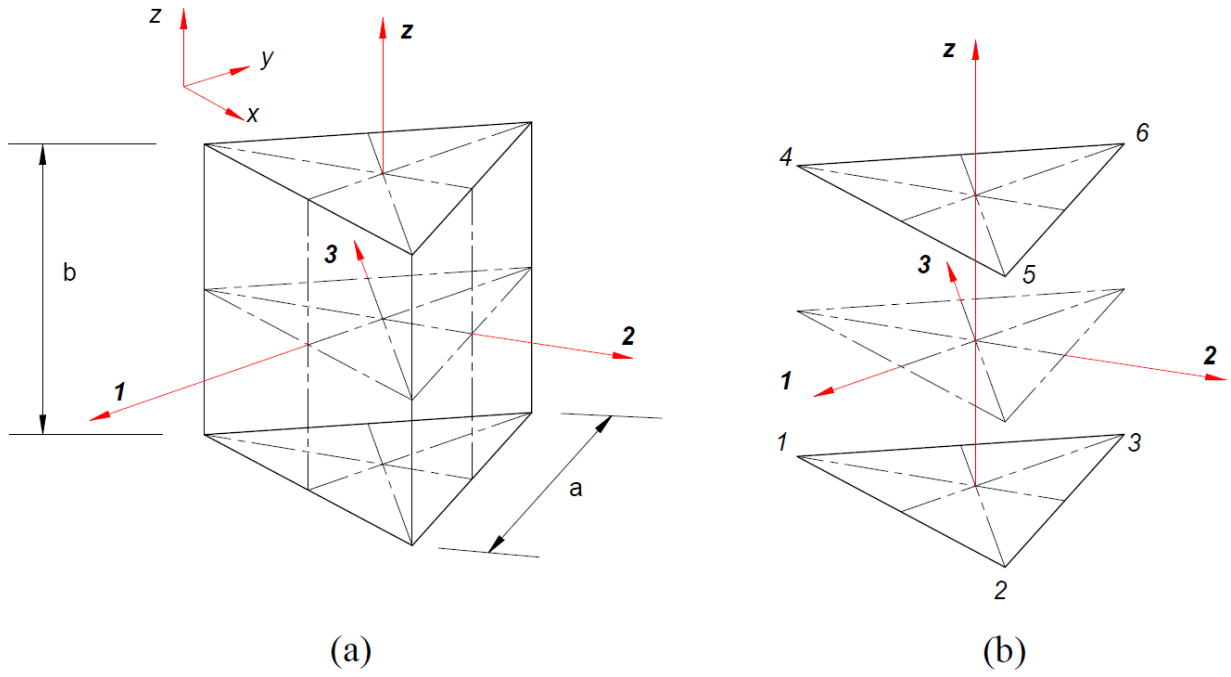

Figure 6.11: D_{3h} space frame

The D_{3h} symmetry group has the following subgroups (Altmann & Herzig, 2011) as shown in Table *6.4* below:

Table 6.4: Subgroups of D_{3h}

Group	*m*	*n/m*
C_s	2	6
C_2	2	6
C_3	3	4
C_{2v}	4	3
C_{3h}	6	2
C_{3v}	6	2
D_3	6	2

6.3.1 *Buckling Behaviour of a D_{3h} Symmetric Space Frame*

The space frame was modelled with D_{3h} stiffness and subjected to a loading arrangement that was either D_{3h} or D_{1h} symmetric, as shown in Table *6.5* with reference to Figure *6.11*. For the D_{3h} load configuration shown in Table *6.5*, the effect of β on stability behaviour was also investigated.

Table 6.5:D_{3h} space frame load arrangements

Node	1	2	3	4	5	6
D_{3h} Loading P_z	P	P	P	-P	-P	-P
D_{1h} Loading P_z	P	P	2P	-P	-P	-2P

P_z denotes a loading parallel to σ_z-axis for each respective node in Figure 8.

The dimensions of the space frame modelled in Abaqus were $a=l= 1\ m$ and $b=2l$. The boundary conditions applied to the model are shown in Figure *6.12*. Thus, the frame was effectively laterally restrained with pinned supports. The boundary conditions at the base of the frame are labelled *BC-4* and those at the base *BC-1*.

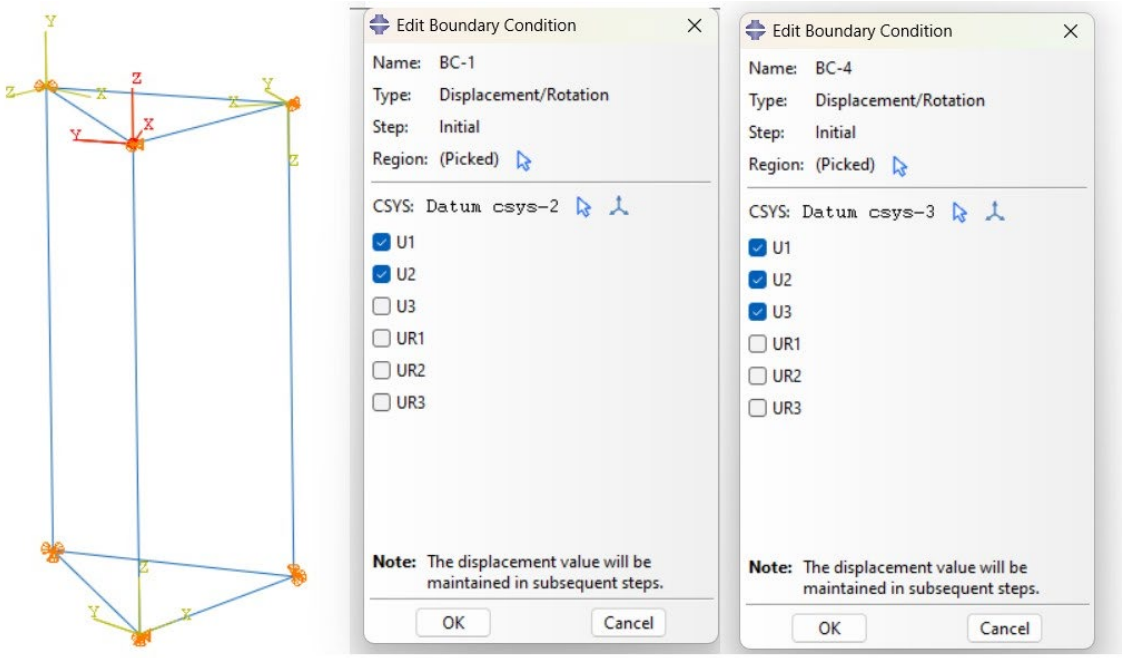

Figure 6.12: D_{3h} space frame boundary conditions

A linear eigenvalue analysis was performed in Abaqus for the first fifty buckling values, and the convergence analysis is shown in Figure *6.13*. A sample of the buckling modes produced is shown in Figure *6.14*.

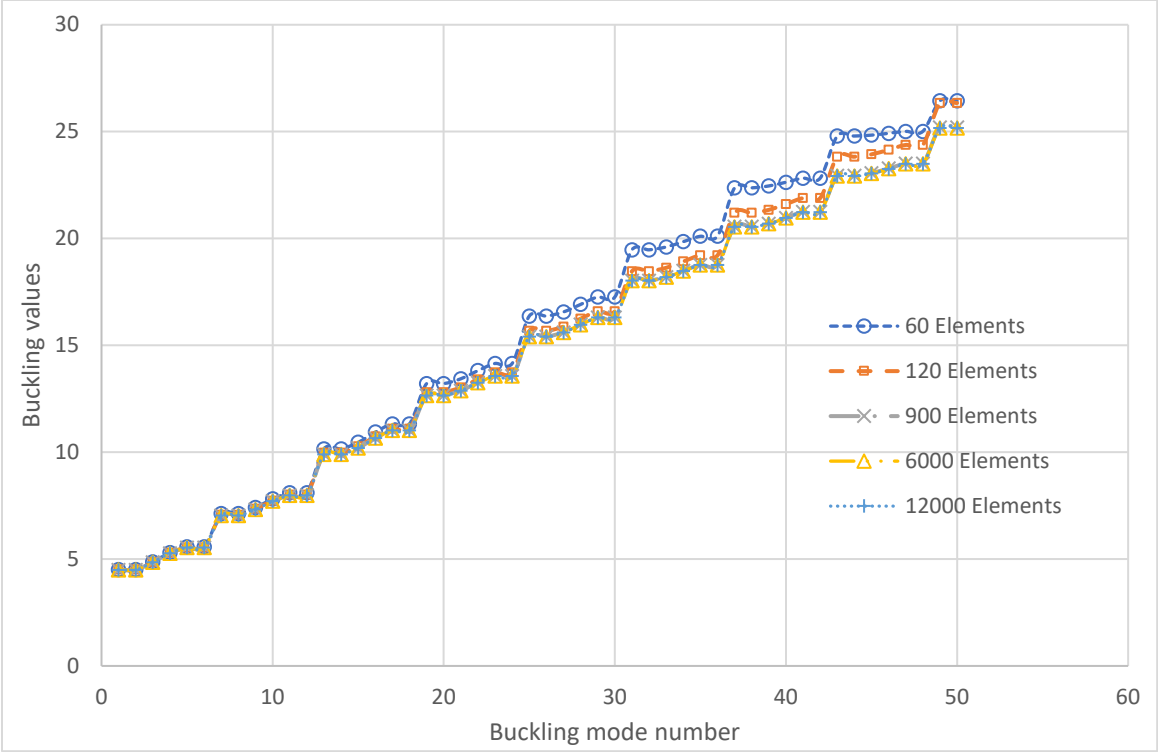

Figure 6.13: D_{3h} space frame convergence analysis

To validate the FEM results, the frame was first analysed using the slope deflection method to determine the approximate buckling values with buckling modes that are D_{3h} and C_{3v} symmetric for a D_{3h} symmetric frame in terms of loading and stiffness. Examples of these buckling modes are shown in Figure *6.14*: λ_3 for the D_{3h} symmetric buckling mode and λ_9 for the C_{3v} symmetric buckling mode. To analytically determine the buckling values, the frame was analysed as three independent frames. When this approach is taken, the buckling values obtained for D_{3h} and C_{3v} symmetric modes are approximately equal to the buckling values obtained from an equivalent C_{2v} frame for C_{2v} and C_{1v} symmetric buckling modes. Therefore, the buckling loads for C_{2v} and C_{1v} buckling modes previously obtained using the slope deflection method for a C_{2v} symmetric frame were compared with the buckling loads for D_{3h} and C_{3v} buckling modes from the finite element model of the D_{3h} frame, and this comparison is graphically shown in Figure *6.15*. The maximum percent error with reference to the analytical solution was *6.5%* and *4%* for the D_{3h} and C_{3v} symmetric modes, respectively. On the other hand, the minimum percent error with reference to the analytical solution was *0.9%* and *1.3%* for the D_{3h} and C_{3v} symmetric modes, respectively.

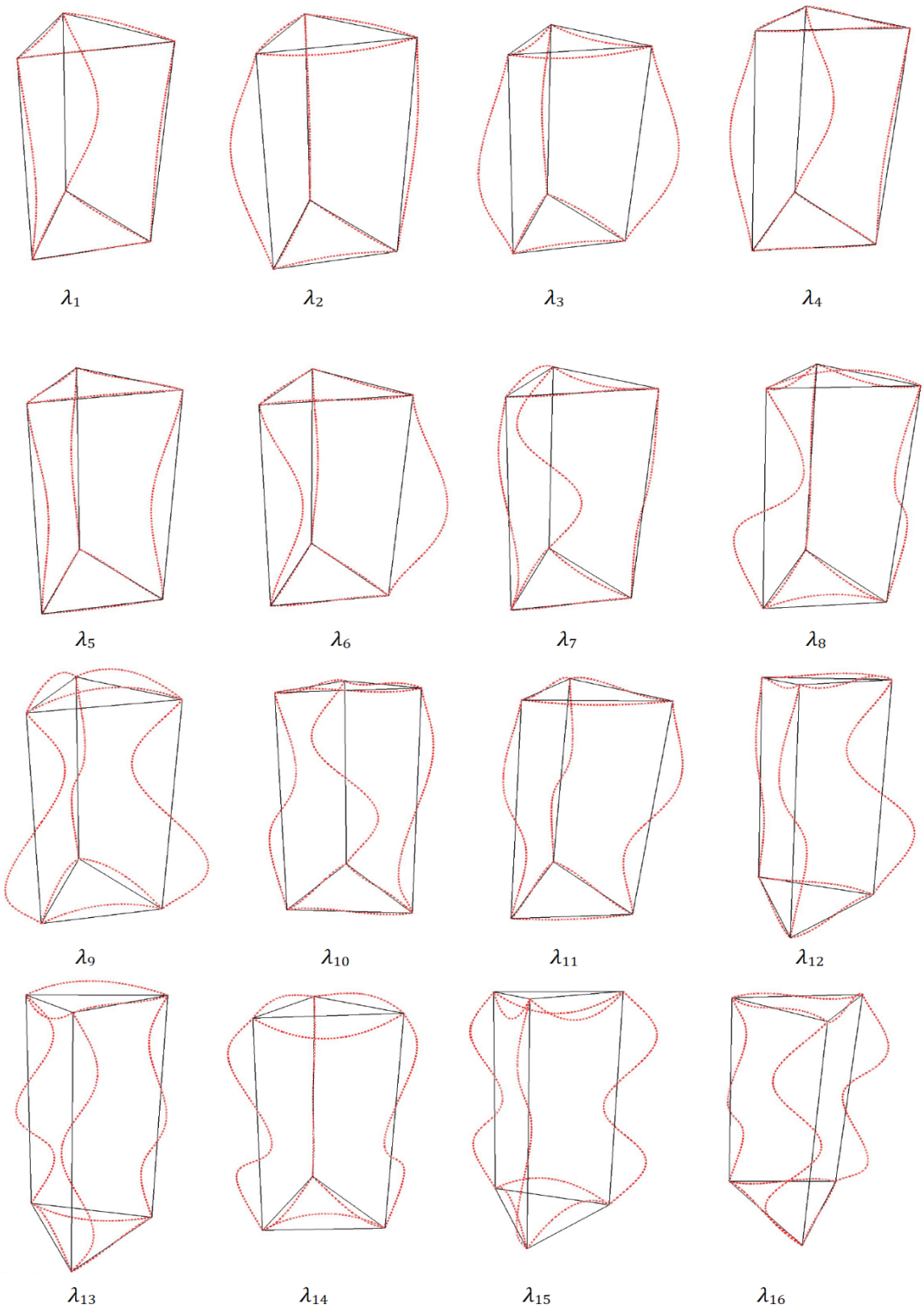

Figure 6.14: D_{3h} space frame buckling modes

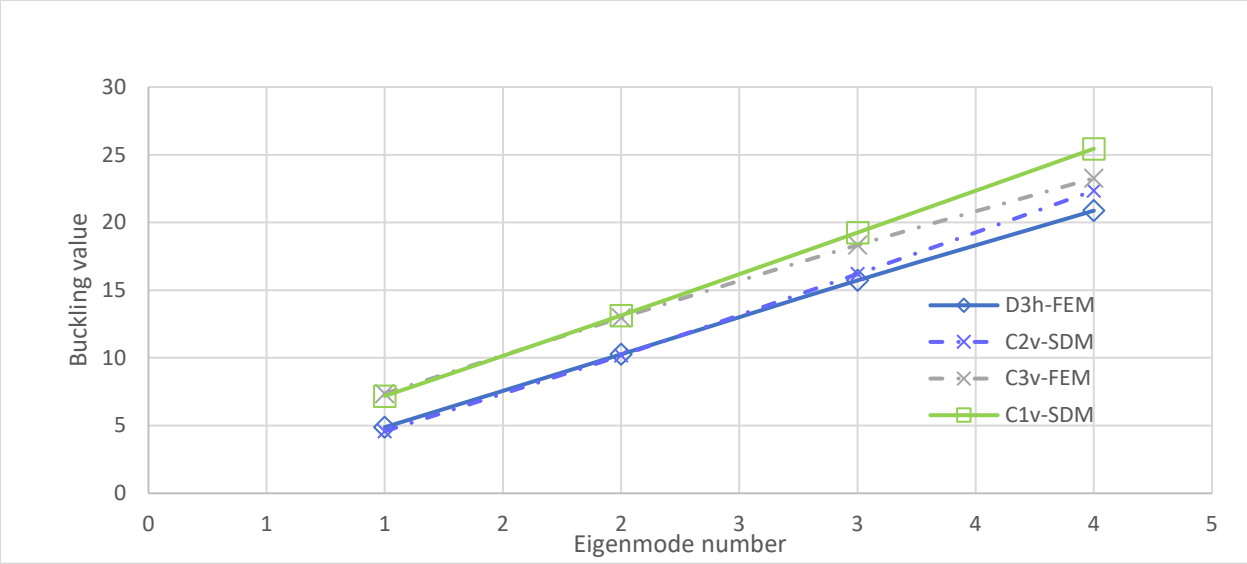

Figure 6.15: D_{3h} Space Frame FEM buckling values and Analytical buckling values (β=1)

As earlier stated, the first fifty buckling modes and buckling values were produced from the D_{3h} *FEM* model using a linear eigenvalue analysis. The symmetry of the buckling modes for each buckling value was also categorised, and these are shown for the first sixteen buckling values in Table *6.6* and plotted for all buckling values as shown in Figures *6.16* and *6.17*. Samples of the buckling modes produced from Abaqus have already been presented in Figure *6.14* for the case of D_{3h} stiffness and loading for the buckling values shown in Table *6.6*.

From Table *6.6,* we can observe that one of the repeating buckling values produces buckling modes that are either C_s or D_{1h} symmetric. The other set of repeating buckling values produces buckling modes that are either C_1 or C_{1v} symmetric. Non-repeating buckling values produced buckling modes that were D_{3h}, C_{3h}, and C_3 symmetric, respectively. Three subgroups shown in Table *6.4* were not produced from the linear eigenvalue analysis, and these are: D_3, C_{2v}, and C_2. The D_3 point group is isomorphic to the C_{3v} group; thus, it is indistinguishable from the C_{3v} from the linear eigenvalue analysis carried out. The C_2 point group is isomorphic to the C_s and C_i symmetry groups, thus its absence from Table *6.6*. It is not clear why the C_{2v} symmetry group is absent in Table *6.6*; however, the C_2 and C_{2v} symmetry groups both have the C_2 symmetry element, which is absent from any of the symmetry groups present in Table *6.6*.

From Table *6.6,* it is observed that they are cases of symmetry groups with an even index that are produced from either a repeating or non-repeating buckling value. No symmetry with a prime

index (3) is present in Table *6.6*. Therefore, a relationship could not be drawn between buckling behaviour and group index.

The pattern for the emergence of symmetries of buckling modes shown in Table *6.6* for D_{3h} loading was repeating for all the buckling modes of the fifty buckling values produced from the finite element analysis for every twelve buckling values for all values of β investigated. The reason for this clear repeating pattern can be seen in Figure *6.16*, of plots of buckling values by buckling mode symmetry. It is observed that the curves of the plots have the same general trend, and thus the symmetries of the buckling modes emerge in a very clear and repeating pattern. For D_{1h} loading, no repeatable pattern in the symmetries of buckling modes was noted, and from Figure *6.17*, it is clear that the plots for each symmetry group do not have the same general trend. Lastly, there was no difference observed in the nature of the buckling behaviour with either the *FEM* created with either a circular hollow section or a solid circular section of equivalent radius of gyration.

Table 6.6: D_{3h} Space Frame buckling values and buckling mode symmetries (β=1)

	D_{3h} loading		D_{1h} loading	
No.	λ_{cr}	mode	λ_{cr}	mode
1	4.545	C_s	3.352	C_s
2	4.545	D_{1h}	3.729	D_{1h}
3	4.904	D_{3h}	4.552	D_{1h}
4	5.341	C_{3h}	5.102	C_s
5	5.614	D_{1h}	5.176	D_{1h}
6	5.614	C_s	5.183	C_1
7	7.150	C_1	5.521	C_{1v}
8	7.150	C_{1v}	5.588	C_s
9	7.439	C_{3v}	7.130	C_{1v}
10	7.844	C_3	7.307	C_s
11	8.133	C_{1v}	7.579	C_1
12	8.133	C_1	7.647	C_{1v}
13	10.133	C_s	7.710	D_{1h}
14	10.133	D_{1h}	8.072	C_1
15	10.444	D_{3h}	9.306	C_1
16	10.939	C_{3h}	9.642	C_{1v}

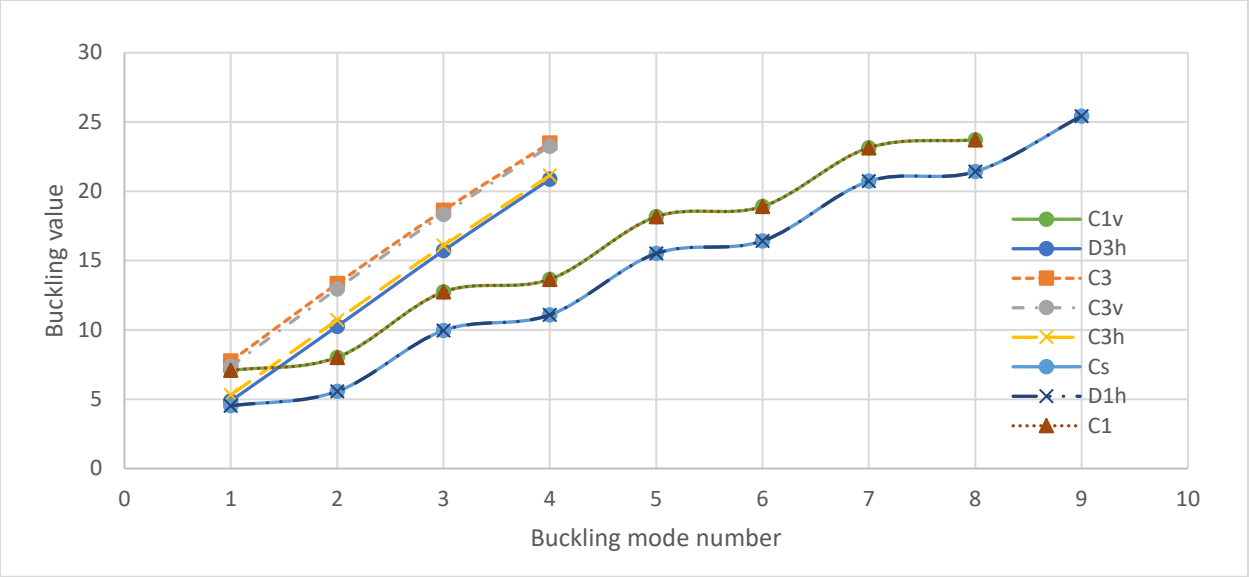

Figure 6.16:D_{3h} Space Frame buckling value versus buckling mode symmetry, D_{3h} loading (β=1)

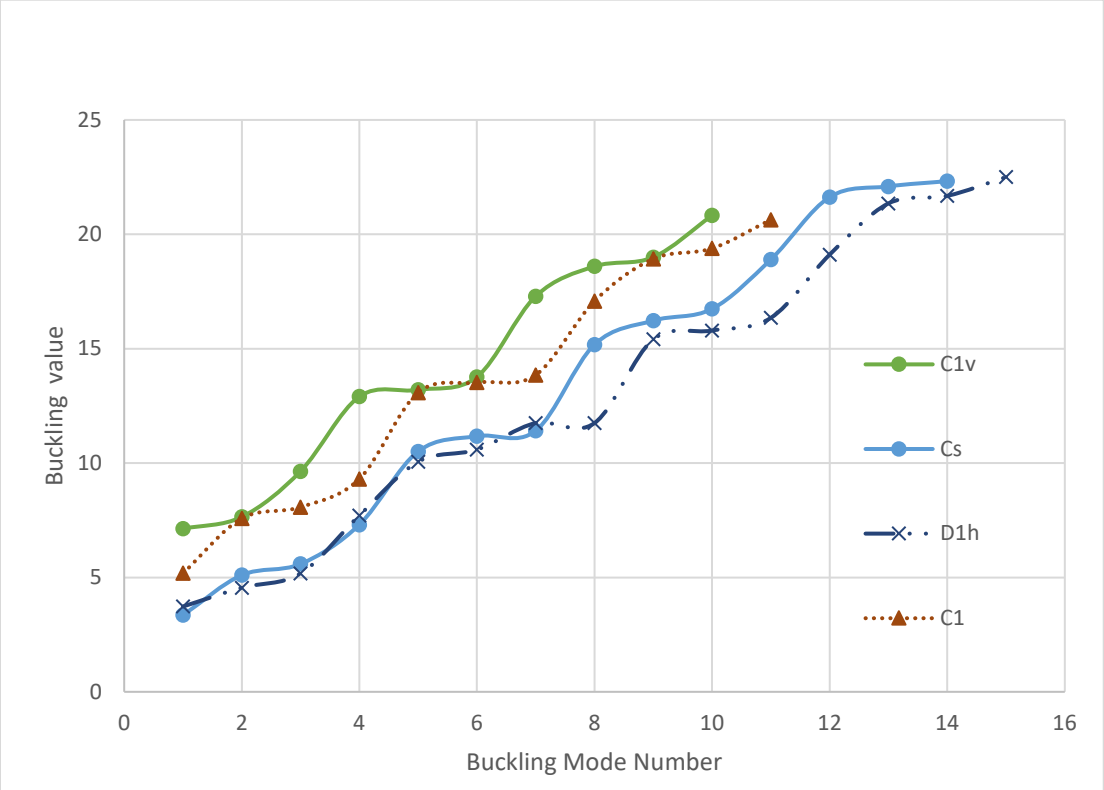

Figure 6.17: D_{3h} Space Frame buckling value versus buckling mode symmetry, D_{1h} loading (β=1)

6.3.2 Post-Buckling Behaviour of a D_{3h} Symmetric Space Frame

The post-buckling behaviour of the space frame was investigated using a geometric nonlinear analysis in Abaqus using the method of superimposed eigenmodes described in Section *3.3.2* of this study. It was found that all post-buckling equilibrium paths were stable bifurcation paths for the two load cases investigated. This is shown in Figure *6.18* for the first three critical points in the case of D_{3h} loading. In Figure *6.18*, Δ represents the maximum lateral column displacement at mid-height in the middle plane (Figure *6.11*) and L the column height. The symbols P_{cr1} and P_{cr3} represent the first and second buckling loads produced from the linear eigenvalue analysis. In Figure *6.18,* on the primary equilibrium path, the deformation pattern of the space frame is D_{3h} symmetric; however, on the bifurcated paths, the deformation pattern of the space frame is a subgroup of the D_{3h} symmetry group shown in Table *6.6*.

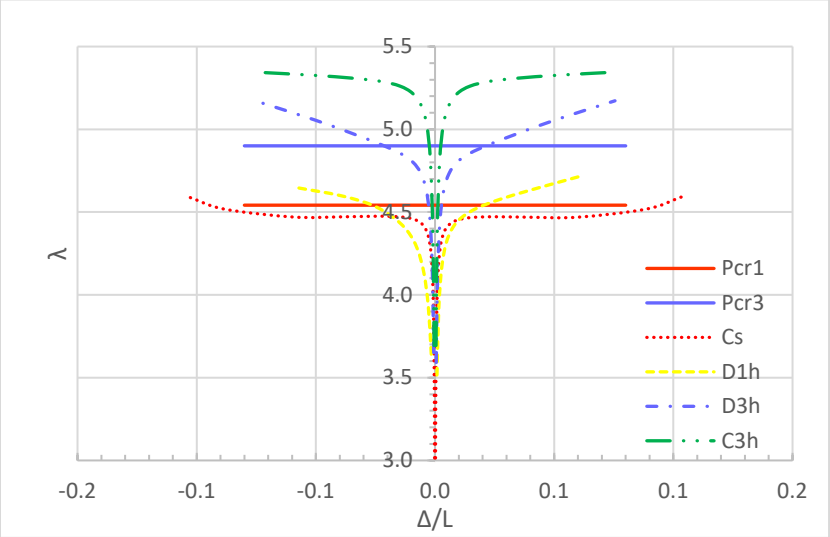

Figure 6.18: Equilibrium paths of D_{3h} symmetric Frame

The influence of β on the post-buckling behaviour was also investigated in the case of D_{3h} loading and stiffness at the first critical point. The value of β was varied from *0.25* to *3,* and the post-buckling behaviour of the equilibrium path that emerges at the first critical point was traced. This post-buckling behaviour is shown in Figure *6.19* for the case where the deformation pattern of the space frame is D_{1h} symmetric (Figure *6.20).* From Figure *6.19*, it can be observed that for the same critical point, the post-buckling behaviour is stable and unstable for cases where $\beta>1$. For cases where $\beta\leq1$, the post-buckling behaviour is stable. The deformation pattern of the space frame on the stable and unstable paths is shown in Figure *6.20 (a)* and *(b),* respectively, for D_{1h} space frame

deformation pattern. It was also observed that for the unstable path, the path became stable after a deformation of about *0.075L*.

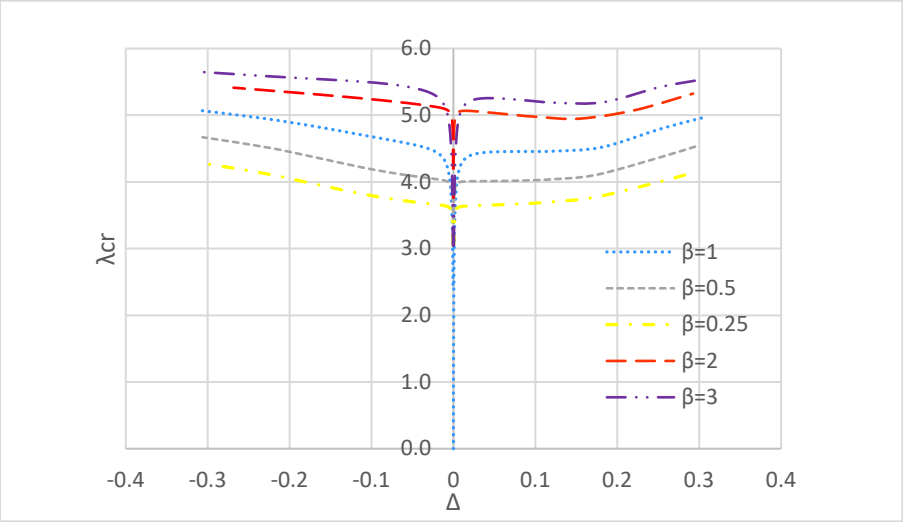

Figure 6.19: Effect of β on equilibrium paths of D_{3h} frame for D_{1h} deformation pattern

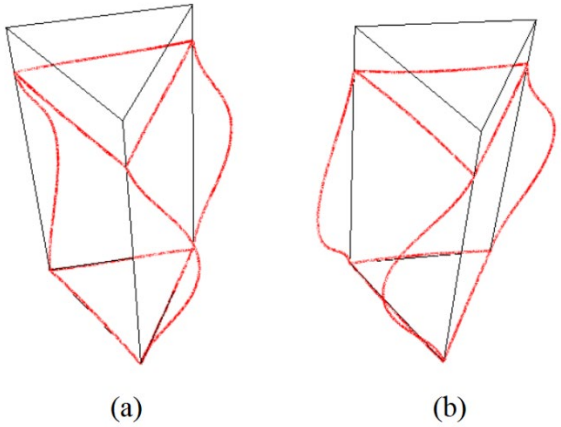

Figure 6.20: Deformation pattern (a) Stable path (b) Unstable path

When the deformation pattern of the space frame is C_s for equilibrium paths emanating from the first critical point, the paths are symmetric stable when $\beta \leq 1$ and symmetric unstable when $\beta > 1$ as shown in Figure *6.21*.

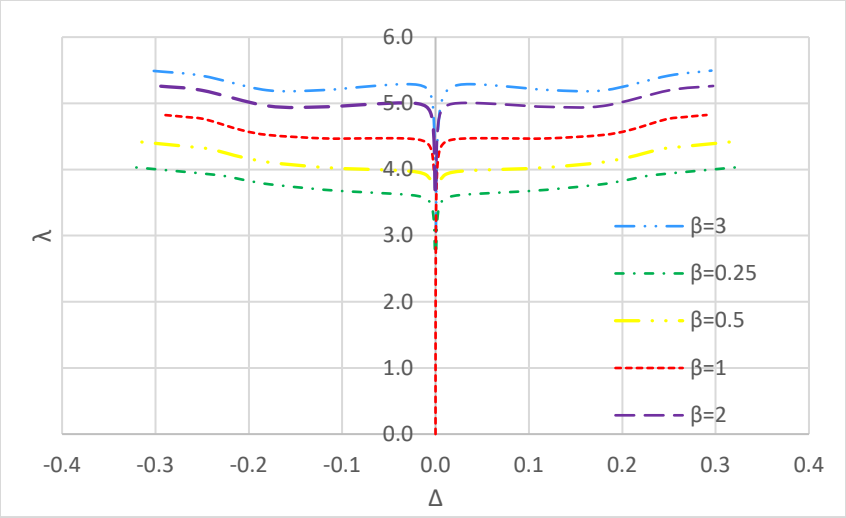

Figure 6.21:Effect of β on equilibrium paths of D_{3h} frame for C_s deformation pattern

6.4 Space Frames with D_{4h} symmetry

The symmetry group D_{4h} is the symmetry with a prism of square base. It has the following sixteen symmetry elements with respect to the coordinate directions $\{x, y, z\}$, associated orthogonal planes $\{xy, xz, yz\}$ and vertical diagonal planes containing the diagonal axes *d* 1 and *d* 2 (Figure *6.22*):

i. e is the identity element;

ii. C_2^z , C_2^x , C_2^y are rotations through an angle of π about the (*z, x, y*) axes, respectively;

iii. C_4 , C_4^{-1} are rotations about the z-axis through an angle of π/4 and - π/4 respectively;

iv. C_2^{d1} , C_2^{d2} are rotations of π about the *d1* and *d2* axes respectively;

v. σ_{xy} , σ_{xz} , σ_{yz} are reflections in the central (*xy, xz, yz*) planes, respectively;

vi. σ_{d1} and σ_{d2} are reflections in the vertical plane containing *d1* and *d2* axes respectively;

vii. *i* is an inversion, that is, a reflection through the centre of symmetry (*O*) of the configuration. This is equivalent to a rotation of π about the *z* axis followed by a reflection in the central *xy* plane; and

viii. S_4, S_4^{-1} are rotary-reflections through angles of $\pi/4$ and $-\pi/4$, respectively. The operations consist of a rotation about the z axis through angles of $\pi/4$ or $-\pi/4$, followed by a refection σ_{xy} in the middle horizontal plane.

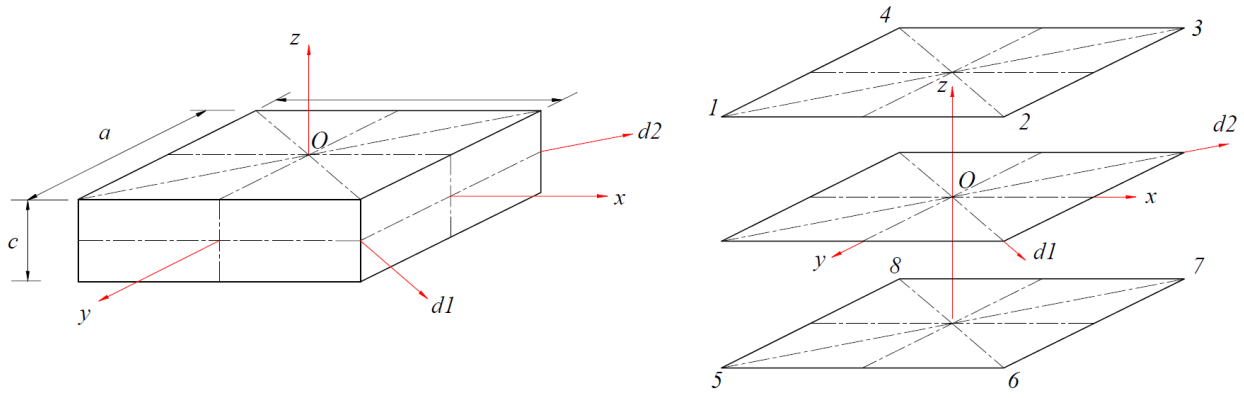

Figure 6.22: D_{4h} space frame

The D_{4h} group has twenty-five distinct nontrivial subgroups of thirteen different kinds as shown in Table *6.7* (Altmann & Herzig, 2011).

Table 6.7: Subgroups of D_{4h}

Group	*m*	*n/m*
C_i	2	8
C_s	2	8
C_2	2	8
C_{2v}	4	4
C_4	4	4
C_{2h}	4	4
D_2	4	4
S_4	4	4
D_{2h}	8	2
D_{2d}	8	2
C_{4v}	8	2
C_{4h}	8	2
D_4	8	2

6.4.1 Buckling Behaviour of a D_{4h} Symmetric Space Frame

The frame was modelled with D_{4h} stiffness and subjected to a loading arrangement that was either D_{4h}, D_{2h}, or D_{1h}, as shown in Table *6.8* with reference to Figure *6.22*.

Table 6.8:D_{4h} loading

Node	1	2	3	4	5	6	7	8
D_{4h} Loading P_z	P	P	P	P	-P	-P	-P	-P
D_{2h} Loading P_z	P	2P	P	2P	-P	-2P	-P	-2P
D_{1h} Loading P_z	P	P	2P	2P	-P	-P	-2P	-2P

P_z denotes a loading parallel to z-axis for each respective node in Figure 6.16.

For the D_{4h} load configuration shown in Table *6.8*, the effect of the ratio of beam to column stiffness ($\beta=I_b/I_c$) on the stability behaviour of the equilibrium paths emanating from the primary equilibrium path was investigated.

The dimensions of the space frame modelled in Abaqus were $a=l= 1\ m$ and $c=2l$. The boundary conditions applied to the model were as shown in Figure *6.23*. Thus, the frame was effectively laterally restrained with pinned supports. In Figure *6.23,* the boundary conditions at the base of the frame are labelled *BC1* and those at the top *BC2*.

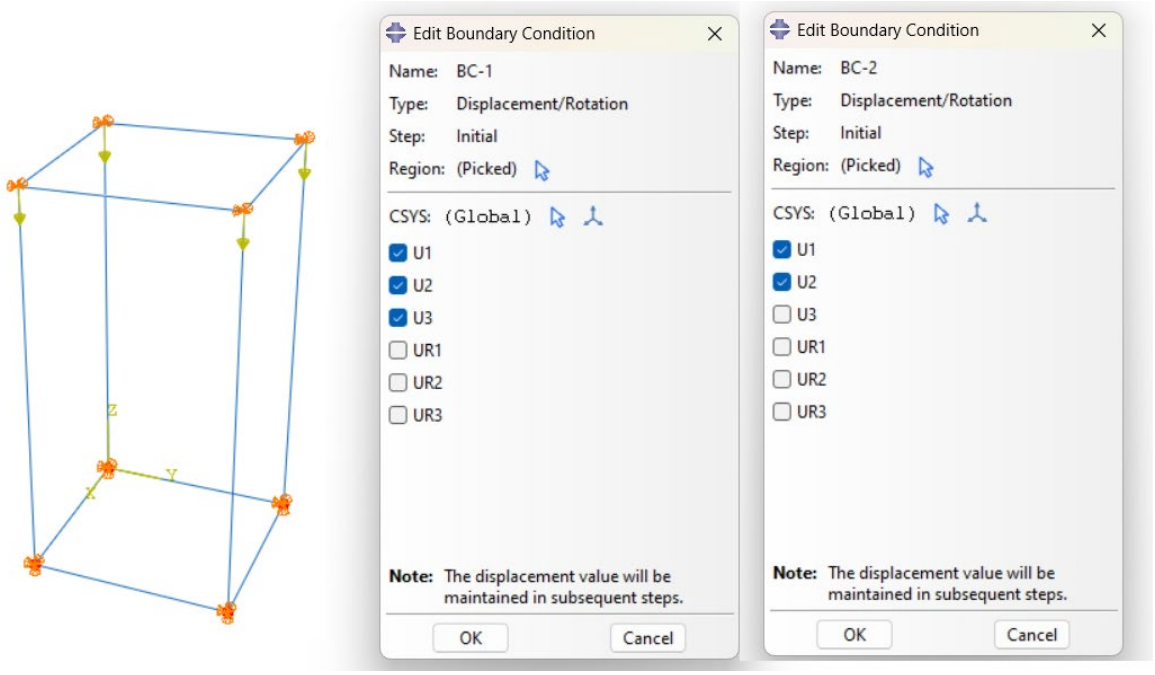

Figure 6.23: D_{4h} space frame boundary conditions

A linear buckling value analysis was performed in Abaqus for the first fifty buckling values, and the convergence analysis is shown in Figure *6.24*. Samples of buckling modes produced are shown in Figure *6.25*.

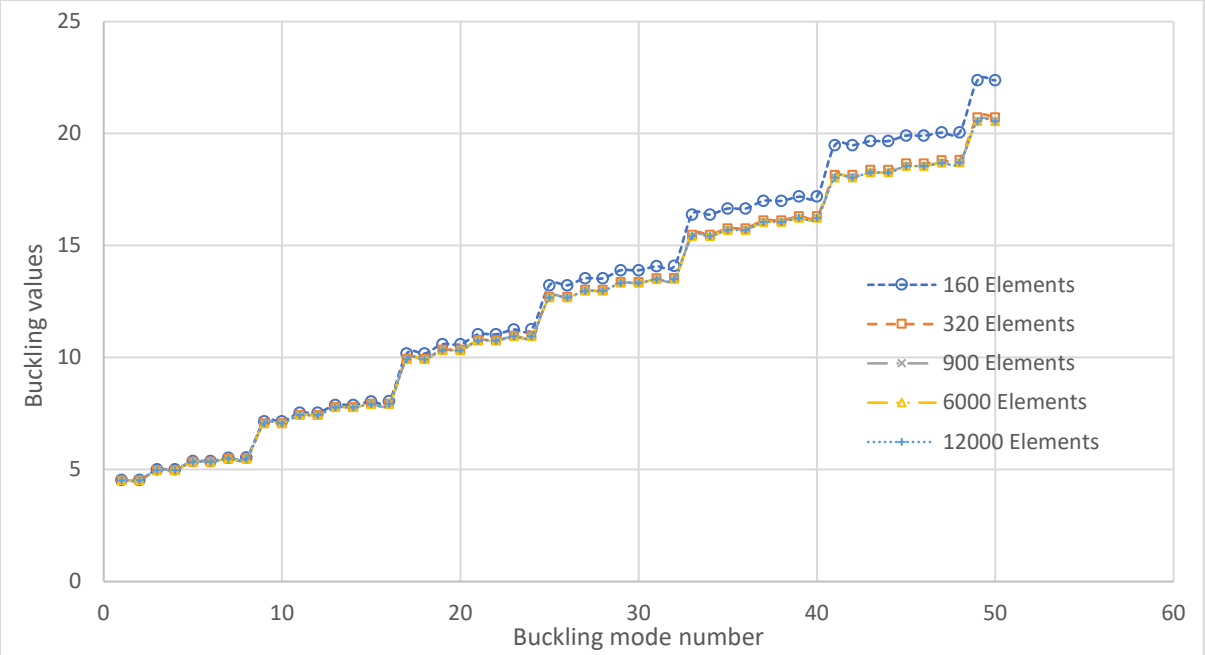

Figure 6.24:D_{4h} space frame convergence analysis

To validate the *FEM* results, the frame was also analysed using the *SDM* to determine the approximate buckling values with buckling modes that are D_{2h} and D_{1h} symmetric for a D_{4h} symmetric frame in terms of loading and stiffness. These are the buckling modes where the beams and columns deflect in the same vertical planes as the unbuckled frame. Samples of these buckling modes are shown in Figure *6.25,* and these are:

- λ_{cr1}- sample buckling mode for D_{2h}; and
- λ_{cr5}- sample buckling mode for D_{1h}.

To analytically determine the buckling values using the *SDM*, the frame was analysed as two independent frames. When this approach is taken, the buckling values obtained for D_{2h} and D_{1h} symmetric modes are approximately equal to the buckling values obtained for C_{2v} and C^{x}_{1v} symmetric buckling modes, respectively, obtained from an equivalent C_{2v} symmetric frame. Therefore, the buckling loads for C_{2v} and C^{x}_{1v} buckling modes previously obtained using the *SDM* were used to validate the D_{4h} space frame *FEM* model. The comparison of the analytical and *FEM* results is graphically shown in Figure *6.26*. The maximum percent error with reference to the analytical solution was *4.4%* and *4.6%* for the D_{2h} and D_{1h} symmetric modes, respectively. On the other hand, the minimum percent error with reference to the analytical solution was *0.2%* and *0.5%* for the D_{2h} and D_{1h} symmetric modes, respectively.

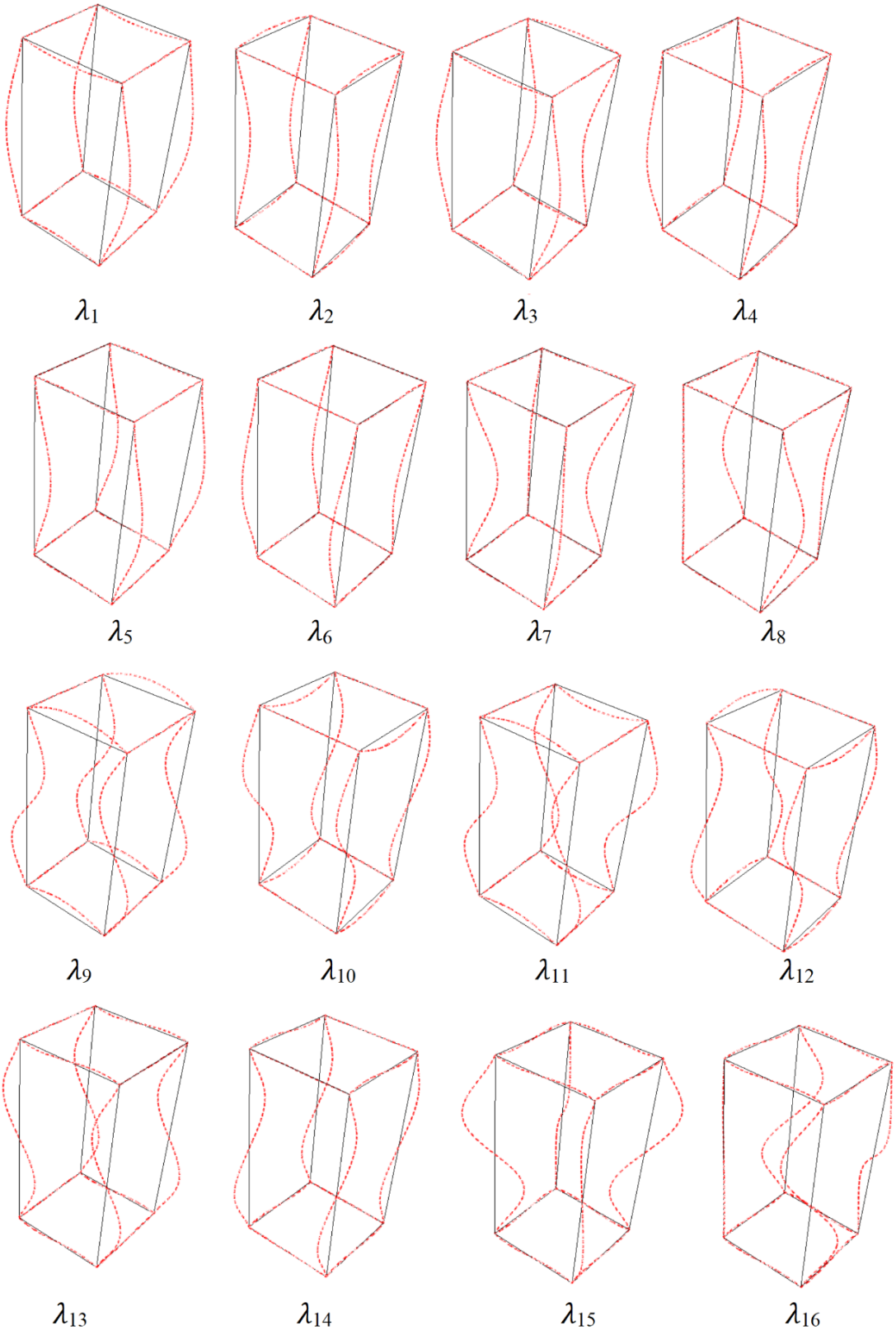

Figure 6.25:D_{4h} space frame buckling modes

To analytically determine the buckling values using the *SDM*, the frame was analysed as two independent frames. When this approach is taken, the buckling values obtained for D_{2h} and D_{1h} symmetric buckling modes are approximately equal to the buckling values obtained for C_{2v} and C^{x}_{1v} symmetric buckling modes, respectively, obtained from an equivalent C_{2v} symmetric frame. Therefore, the buckling loads for C_{2v} and C^{x}_{1v} buckling modes previously obtained using the *SDM* were used to validate the D_{4h} space frame *FEM* model. The comparison of the analytical and *FEM* results is graphically shown in Figure *6.26*. The maximum percent error with reference to the analytical solution was *4.4%* and *4.6%* for the D_{2h} and D_{1h} symmetric buckling modes, respectively. On the other hand, the minimum percent error with reference to the analytical solution was *0.2%* and *0.5%* for the D_{2h} and D_{1h} symmetric buckling modes, respectively.

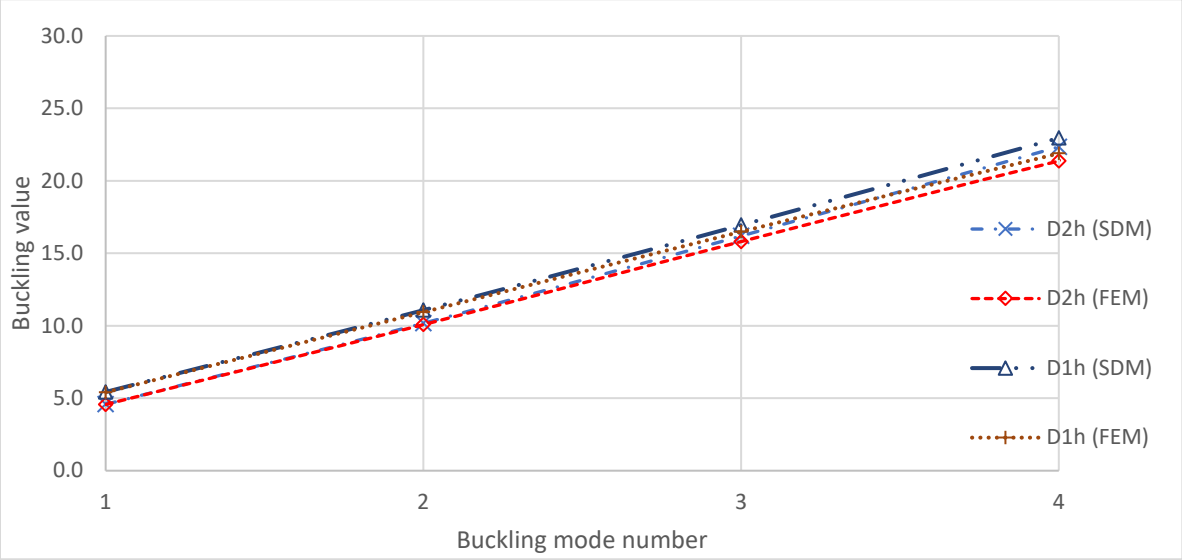

Figure 6.26: D_{4h} Space Frame FEM buckling values and Analytical buckling values

The first fifty buckling modes and buckling values were produced from the D_{4h} *FEM* model using a linear buckling value analysis. The symmetry of the buckling modes for each buckling value was categorised, and these are shown for the first sixteen buckling values in Table *6.9,* and samples of the buckling modes produced from Abaqus have previously been presented in Figure *6.26* for the case of D_{4h} stiffness and loading.

The pattern of the emergence of symmetries of buckling modes shown in Table *6.9* for D_{4h} loading was repeating for all the buckling modes of the fifty buckling values produced from the finite

element analysis for every sixteen buckling values. This pattern was the same regardless of whether a solid circular section or a hollow circular section was used in the model. The explanation for the clear repeating pattern is apparent when the buckling values for each type of symmetry are plotted, as shown in Figure *6.27*. For D_{2h} and D_{1h} loading, no repeatable pattern in the symmetries of buckling modes was noted.

Table 6.9: D_{4h} Space Frame buckling values and buckling mode symmetries

	D_{4h} loading		D_{2h} loading		D_{1h} loading	
No.	λ_{cr}	mode	λ_{cr}	mode	λ_{cr}	mode
1	4.569	D_{2h}	3.477	D_{2h}	3.370	D_{1h}
2	4.569	D_{2h}	3.478	C_{2h}	3.450	D_{1h}
3	5.033	D_{1h}	3.680	D_{1h}	3.715	Cs
4	5.033	D_{1h}	3.680	D_{1h}	3.874	Cs
5	5.408	D_{1h}	5.129	D_{2h}	4.820	D_{1h}
6	5.408	D_{1h}	5.132	C_{2h}	5.048	D_{1h}
7	5.549	D_{2h}	5.220	D_{1h}	5.179	D_{1h}
8	5.555	C_{4h}	5.220	D_{1h}	5.277	D_{1h}
9	7.146	C_{2v}	5.317	C_{2v}	5.308	C_s
10	7.146	C_{2v}	5.318	C_2	5.477	C_s
11	7.528	C_{1v}	5.446	C_{1v}	5.487	C_2
12	7.528	C_{1v}	5.446	C_{1v}	5.629	C_2
13	7.884	C_{1v}	7.494	D_{2h}	7.273	D_{1h}
14	7.884	C_{1v}	7.497	C_{2h}	7.337	C_{1v}
15	8.032	C_{2v}	7.582	D_{1h}	7.424	D_{1h}
16	8.038	C_4	7.582	D_{1h}	7.525	C_{1v}

From Table *6.9,* we can observe that every buckling value is a repeating buckling value for D_{4h} and D_{2h} loading arrangements. The case of D_{1h} loading did not display any repeating buckling values, however, the buckling values were closely spaced. Further, it was noted that for all load arrangements, the order of emergence of buckling modes was from those of a higher order of symmetry to those of a lower order of symmetry. The symmetry groups of the buckling modes were subgroups of the symmetry groups of the respective loadings. It was also observed that of the subgroups for D_{4h} symmetry shown in Table *6.7*, only the following subgroups are present in Table *6.9* for the case of D_{4h} loading: C_{2v}, C_4, D_{2h} and C_{4h}. The absence of some subgroups can be explained by the reference to isomorphisms in the subgroups. That is: C_{2h} is isomorphic to C_{2v}, D_2 is also isomorphic to C_{2v} and S_4 is isomorphic to C_4. The explanation for the absence of the other subgroups shown in Table *6.7* in Table *6.9* is not clear.

For the D_{2h} load arrangement, all subgroups of D_{2h} were present in Table *6.9*, except for the C_i and C_s symmetry groups. For the D_{1h} load arrangement, only the C_i subgroup was absent from the buckling behaviour shown in Table *6.9*.

Figure 6.27: D_{4h} loading buckling value versus buckling mode symmetry

6.4.2 Post-Buckling Behaviour of a D_{4h} Symmetric Space Frame

The post-buckling behaviour of the space frame with D_{4h} loading was investigated using a geometric nonlinear analysis in Abaqus for the first and second critical points. It was found that the post-buckling equilibrium paths were stable, as shown in Figure *6.28*. On the primary equilibrium path, the deformation pattern of the space frame is D_{4h} symmetric; however, on the bifurcated paths, the deformation pattern of the space frame is a subgroup of the D_{4h} symmetry group. In Figure *6.28*, Δ represents the maximum lateral column displacement at mid-height in the middle plane of the space frame (Figure *6.16*), and L is the column length. The symbol P_{cr1} represents the first buckling load from the linear eigenvalue analysis.

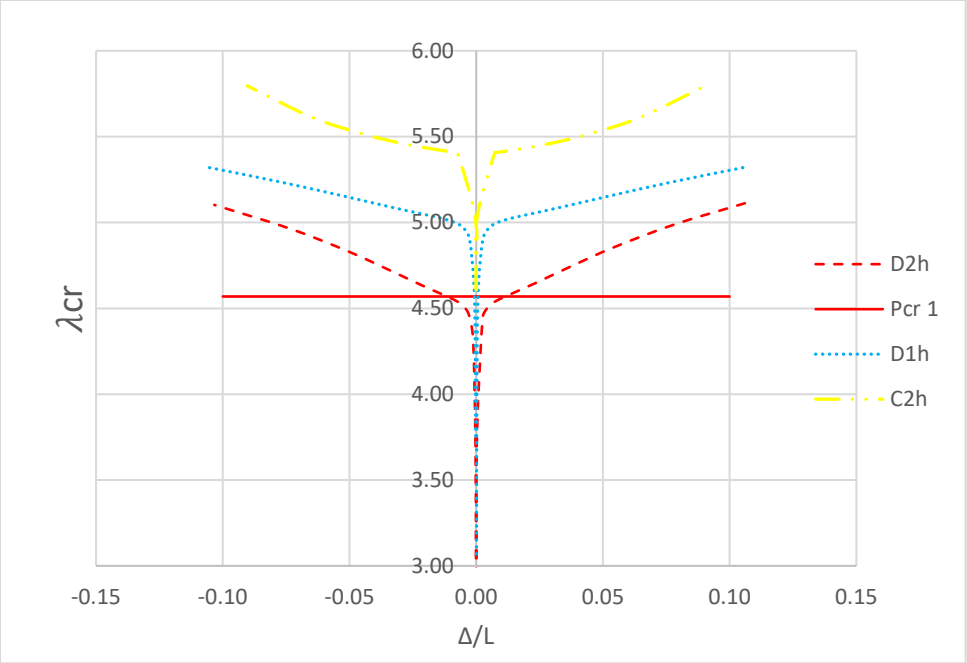

Figure 6.28:Equilibrium paths of D_{4h} symmetric Frame

6.5 Space Frames with D_{5h} symmetry

The symmetry group D_{5h} is the symmetry of a prism with a pentagonal base. It has the following twenty symmetry elements with respect to the *z*-direction associated with the horizontal middle plane and the vertical planes containing the median axes *1*, *2*, *3*, *4,* and *5* (Figure *6.29*):

i. *e* is the identity element

ii. C_2^1, C_2^2, C_2^3, C_2^4, C_2^5 are rotations through an angle of π about the *1*, *2*, *3*, *4* and *5* axes, respectively;

iii. C_5, C_5^{-1}, C_5^2, C_5^{-2} ,are rotations about the z-axis through an angle of *2π/5*, - *2π/5*, *4π/5*, - *4π*/5, respectively;

iv. σ_h is a reflection in the middle horizontal plane;

v. σ_1, σ_3, σ_4, σ_5 are reflections in the vertical plane containing median *1*, *2*, *3*, *4* and *5* axes respectively;

vi. S_5, S_5^{-1} are rotary-reflections through angles of *2π/5* and- *2π/5* respectively; and

vii. S_5^3 , S_5^{-3} are rotary-reflections through angles of 6π/5 and- 6π/5 respectively.

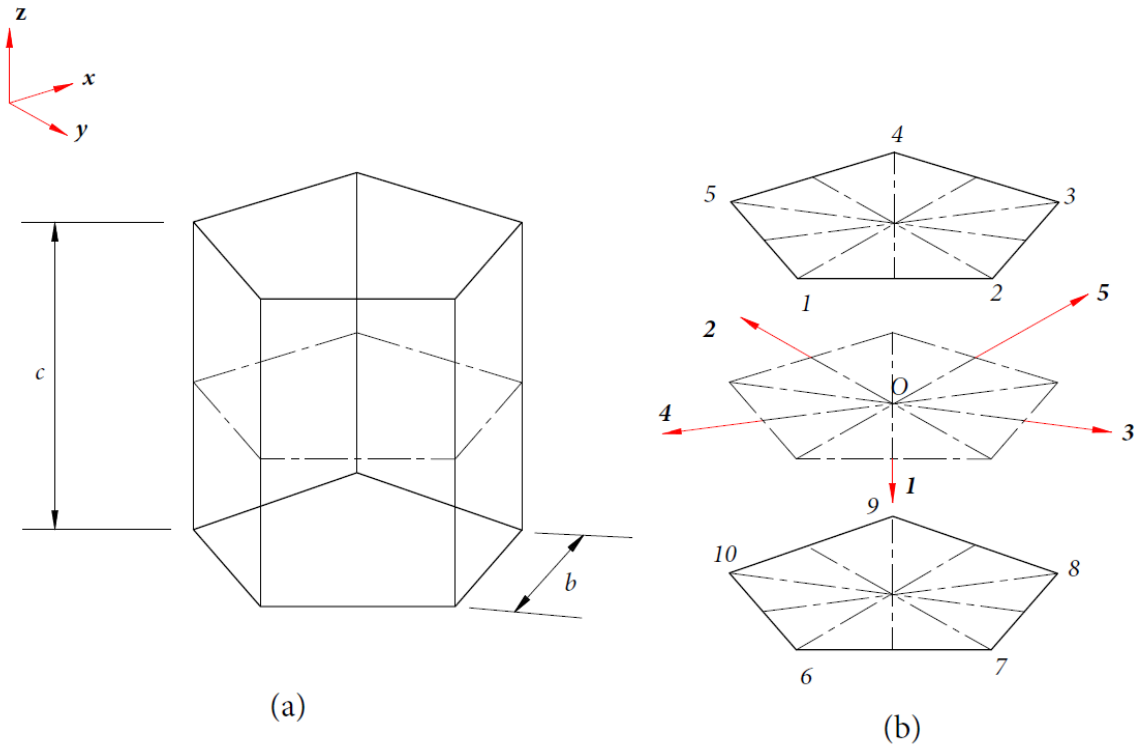

Figure 6.29: D_{5h} space frame

The D_{5h} group has seven distinct nontrivial subgroups as shown in Table *6.10* (Altmann & Herzig, 2011).

Table 6.10: Subgroups of D_{5h}

Group	*m*	*m/n*
C_s	2	10
C_2	2	10
C_{2v}	4	5
C_5	5	4
C_{5v}	10	2
C_{5h}	10	2
D_5	10	2

6.5.1 Buckling Behaviour of a D_{5h} Symmetric Space Frame

The frame was modelled with D_{5h} stiffness and loading arrangement as shown in Table *6.11* with reference to Figure *6.20*.

Table 6.11: D_{5h} loading

Node	1	2	3	4	5	6	7	8	9	10
D_{5h} Loading P_z	-P	-P	-P	-P	-P	P	P	P	P	P

P_z denotes a loading parallel to z-axis for each respective node in Figure 6.20.

The model created in Abaqus had the following dimensions: *b=1 m* and *c=2 m* (Figure *6.29*). This frame was modelled as a laterally restrained frame with pinned supports, and the boundary conditions that were applied in Abaqus are shown in Figure *6.30*. The boundary conditions at the base of the space frame are labelled *BC-1* and the base *BC-2* in Figure *6.30*.

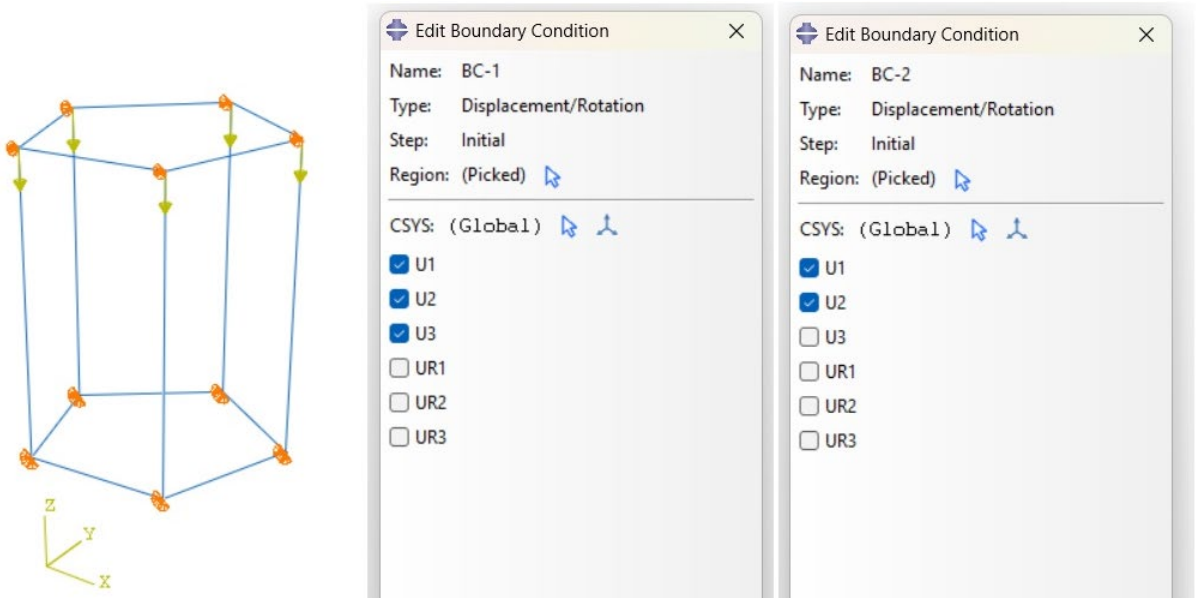

Figure 6.30: D_{5h} space frame boundary conditions

A linear eigenvalue analysis was performed in Abaqus for the first fifty buckling values, and the convergence analysis is shown in Figure *6.31*.

The symmetry of buckling modes for each buckling value produced from the linear eigenvalue analysis was categorised, and these are shown for the first twenty buckling values in Table *6.12*. Sample images of the buckling modes for the first sixteen buckling values are shown in Figure *6.32*. The pattern of emergence of symmetries shown in Table *6.12* was repeating for every twenty buckling values.

The lowest buckling value shown in Table *6.12*, had a D_{5h} symmetric buckling mode. The repeating buckling values had buckling modes that were C_1 or C_s symmetric. Nonrepeating

buckling values, on the other hand, had buckling modes that were C_5, C_{5h} or D_{5h} symmetric. Further from the buckling behaviour shown in Table *6.12*, it can be observed that two subgroups of the D_{5h} are absent: C_2 and C_{2v}.

If the buckling values are arranged by symmetry and plotted on the same graph as shown in Figure *6.33*, it is observed that the buckling values with C_s symmetric buckling modes form the lower bound values, while buckling values with C_5 symmetric buckling values form the upper bound values.

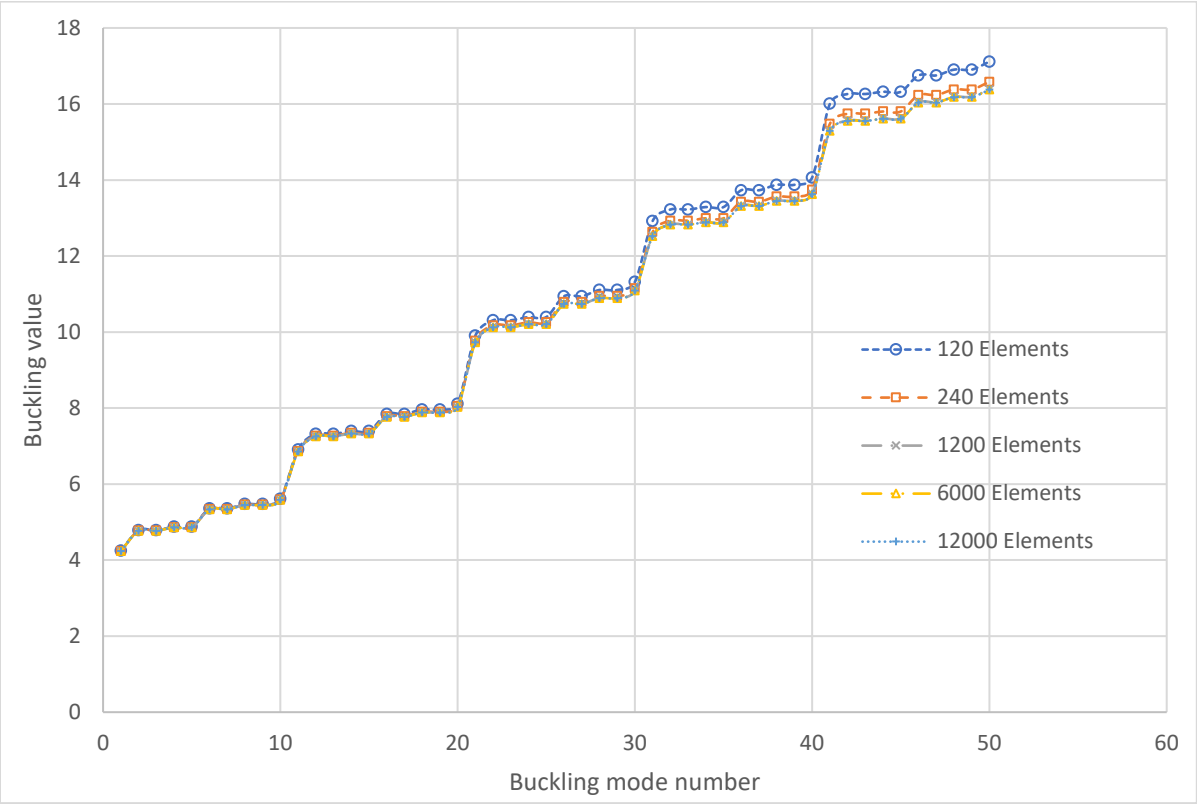

Figure 6.31: D_{5h} space frame convergence analysis

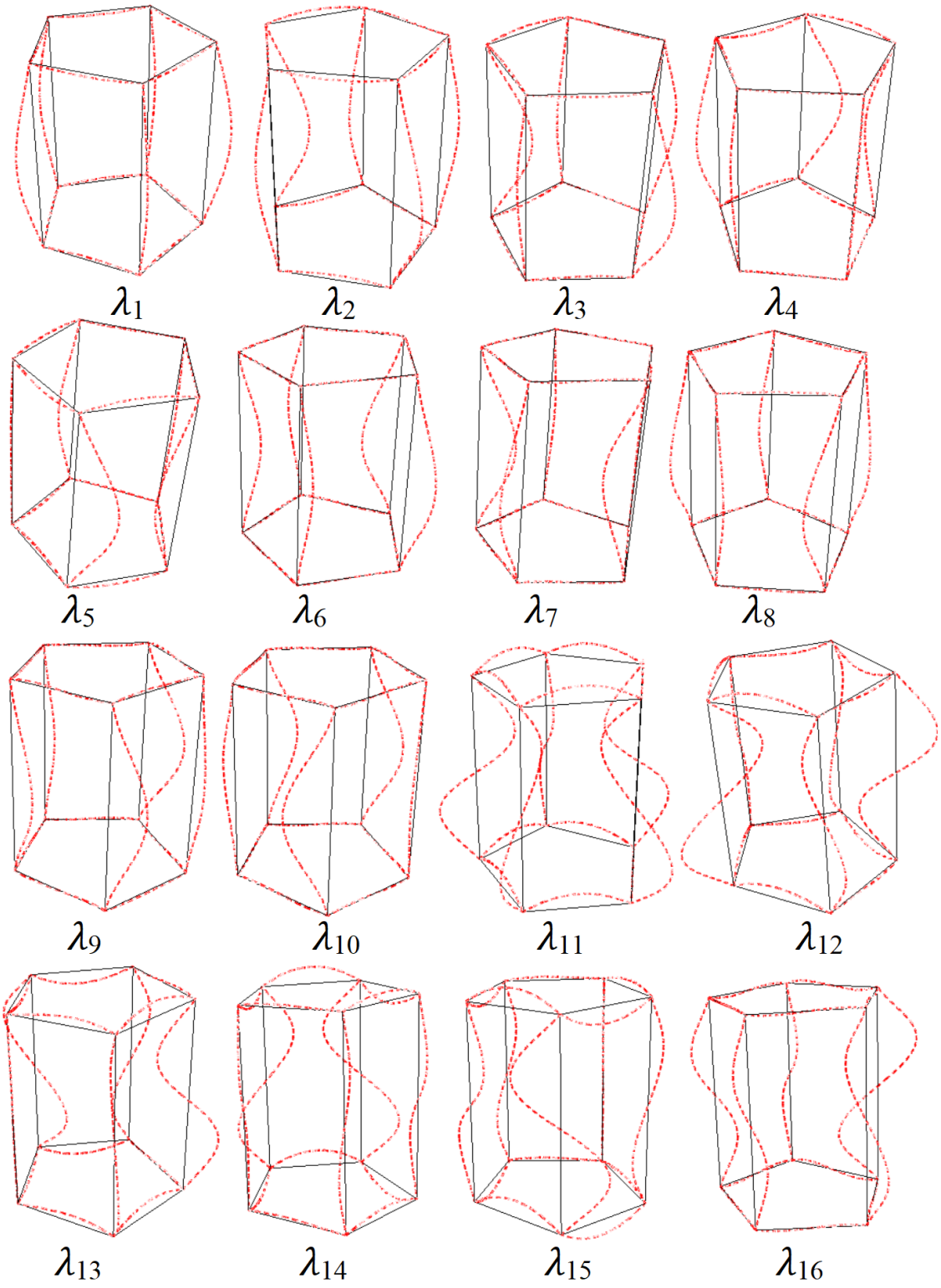

Figure 6.32: D_{5h} space frame buckling modes

Table 6.12:D_{5h} Space Frame buckling values and buckling mode symmetries

No.	λ_{cr}	mode
1	4.280	D_{5h}
2	4.820	C_s
3	4.820	C_s
4	4.911	C_s
5	4.911	C_s
6	5.395	C_s
7	5.395	C_s
8	5.512	C_s
9	5.512	C_s
10	5.647	C_{5h}
11	6.936	C_{5v}
12	7.346	C_1
13	7.346	C_1
14	7.422	C_1
15	7.422	C_1
16	7.871	C_1
17	7.871	C_1
18	7.993	C_1
19	7.993	C_1
20	8.139	C_5

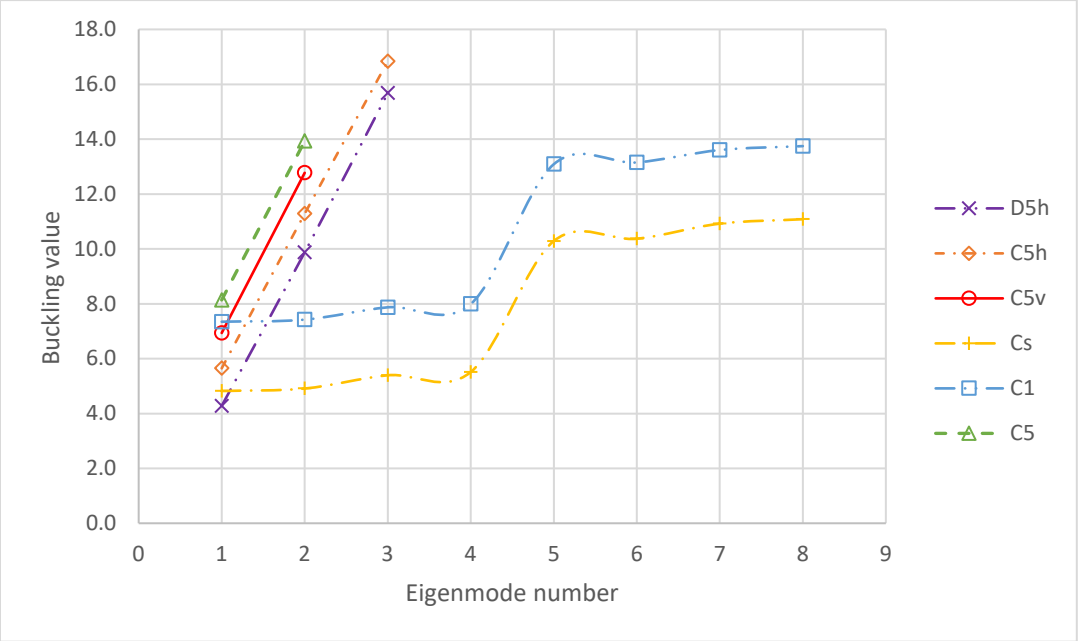

Figure 6.33: C_{5v} Buckling values versus buckling mode number

6.5.1 Post-Buckling Behaviour of a D_{5h} Symmetric Space Frame

The post-buckling behaviour of the space frame with D_{5h} loading was investigated using a geometric nonlinear analysis in Abaqus for the first and second critical points, and it was found

that the post-buckling equilibrium paths were stable, as shown in Figure *6.34*. On the primary equilibrium path in Figure *6.34*, the deformation pattern of the space frame is D_{5h} symmetric; however, on the bifurcated paths, the deformation pattern of the space frame is a subgroup of the D_{5h} symmetry group. The symbol Δ in Figure *6.34*, represents the maximum lateral column displacement at mid-height in the middle plane of Figure *6.29,* and *L* the column length. The labels P_{cr1} and P_{cr2} represent the first and second buckling loads from the linear eigenvalue analysis.

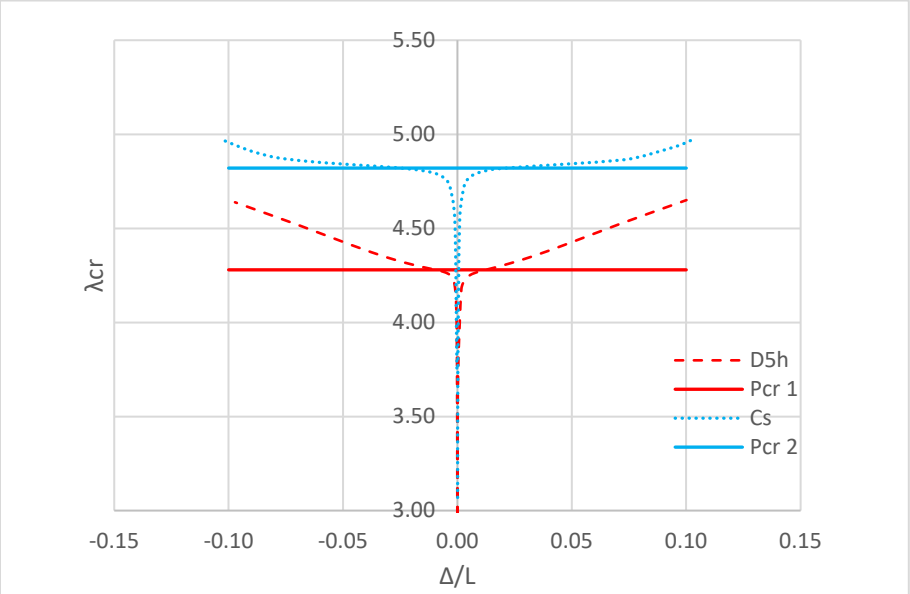

Figure 6.34:Equilibrium paths of D_{5h} symmetric Frame

6.6 Space Frames with D_{6h} symmetry

The symmetry group D_{6h} is the symmetry of a prism with a hexagonal base. It has the following twenty-four symmetry elements with respect to the coordinate directions $\{x, y, z\}$, associated middle horizontal plane, and vertical planes containing the diagonal axes *1*, *2*, *3*, and bisector axes *A, B, C* as shown in Figure *6.35*:

i. e is the identity element;

ii. C_6 , C_6^{-1} are rotations about the z-axis respectively through an angle of π/3, and - π/3;

iii. C_3 , C_3^{-1} are rotations about the z-axis respectively through an angle of 2π/3, and - 2π/3;

iv. C_2 is a rotation about the z-axis through an angle of π;

v. C_2^1, C_2^2, C_2^3 are rotations respectively through an angle of π about the *1*, *2*, and *3* axes;

vi. C_2^A, C_2^B, C_2^C are rotations respectively through an angle of π about the *A*, *B*, and *C* axes;

vii. *i* is an inversion, that is, a reflection through the centre of symmetry (*O*) of the configuration;

viii. σ_h is a reflection in the middle horizontal plane;

ix. σ_1, σ_2, and σ_3 are reflections in the vertical plane containing diagonals *1*, *2*, and *3* respectively;

x. σ_A, σ_B, and σ_C are reflections in the vertical plane containing bisectors *A*, *B*, and *C* respectively;

xi. S_3, S_3^{-1} are rotary-reflections through angles of 2π/3 and- 2π/3 respectively; and

xii. S_6, S_6^{-1} are rotary-reflections through angles of π/3 and -π/3 respectively.

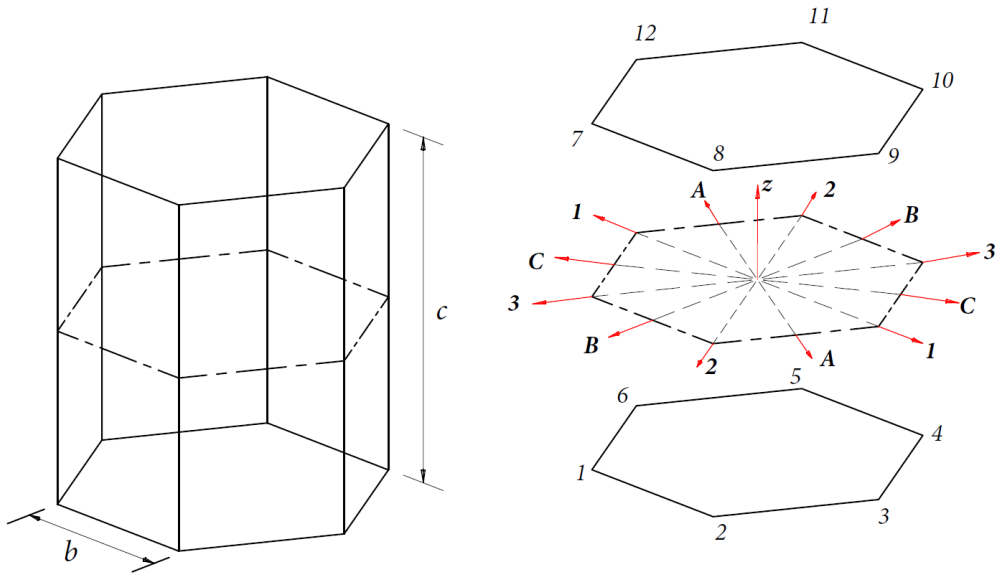

Figure 6.35: D_{6h} space frame

The D_{6h} group has eighteen distinct nontrivial subgroups, as shown in Table *6.13* (Altmann & Herzig, 2011).

Table 6.13: Subgroups of D_{6h}

Group	*m*	*n/m*
C_s	2	12
C_i	2	12
C_2	2	12
C_3	3	8
C_{2v}	4	6
C_{2h}	4	6
D_2	4	6
D_3	6	4
C_{3v}	6	4
C_6	6	4
C_{3h}	6	4
S_6	6	4
D_{2h}	8	3
C_{6v}	12	2
C_{6h}	12	2
D_{3h}	12	2
D_{3d}	12	2
D_6	12	2

6.6. 1 Buckling Behaviour of a D_{6h} Symmetric Space Frame

The frame was modelled with D_{6h} stiffness and D_{6h} or D_{3h} loading arrangements as shown in Table *6.14* with reference to Figure *6.35*.

Table 6.14:D_{6h} loading

Node	1	2	3	4	5	6	7	8	9	10	11	12
D_{6h} Loading P_z	P	P	P	P	P	P	-P	-P	-P	-P	-P	-P
D_{3h} Loading P_z	P	2P	P	2P	P	2P	-P	-2P	-P	-2P	-P	-2P

P_z denotes a loading parallel to z-axis for each respective node in Figure 6.23.

The dimensions of the space frame constructed in Abaqus were *b=l= 1 m* and *c=2l.* The boundary conditions applied to the model are shown in Figure *6.36*. The frame was effectively laterally restrained with pinned supports. In Figure *6.36*, the pin supports at the base are labelled *BC-1* and those at the top *BC-2*.

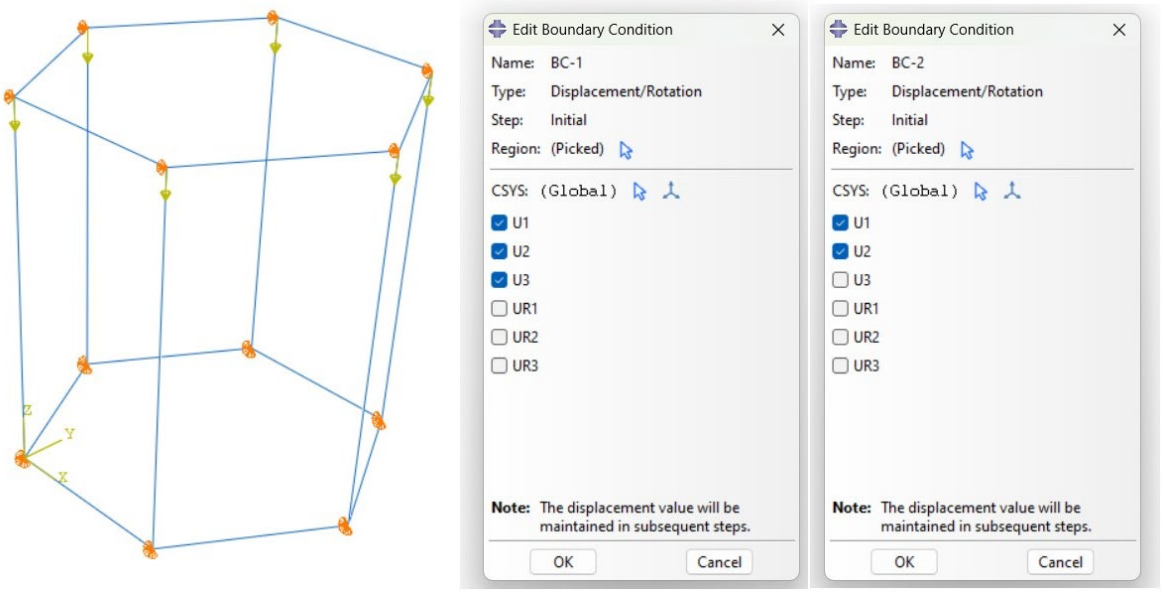

Figure 6.36: D_{6h} space frame boundary conditions

A linear buckling value analysis was performed in Abaqus for the first fifty buckling values, and the convergence analysis is shown in Figure *6.37*.

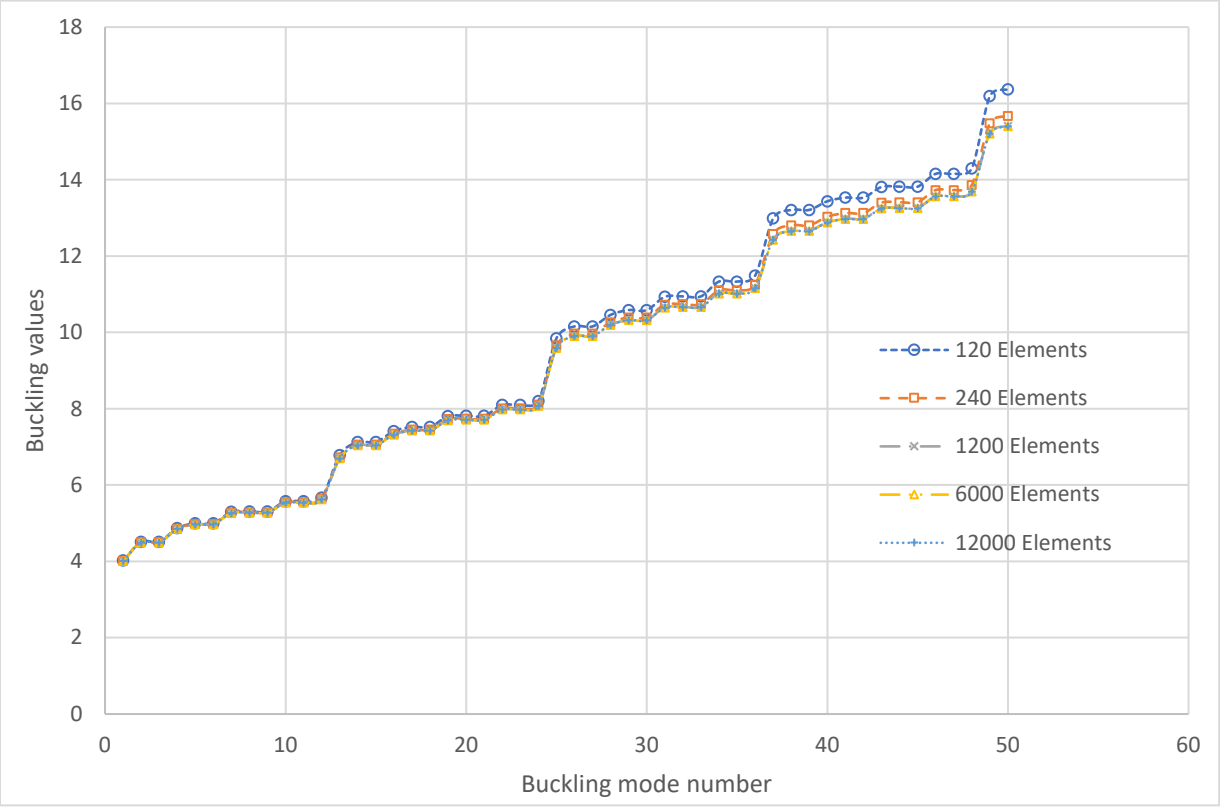

Figure 6.37: D_{6h} space frame convergence analysis

The symmetry of the buckling modes for each buckling value was categorised, and these are shown for the first fifty buckling values in Table *6.15*. Sample images of the buckling modes for D_{6h} loading are shown in Figure *6.38*. The sequence of symmetries shown in Table *6.15* was repeating every twenty-four buckling values for the model with D_{6h} loading. However, no repeatable pattern for the case of D_{3h} loading was observed.

Table 6.15:D_{6h} Space Frame buckling values and buckling mode symmetries

	D_{6h}		D_{3h}	
No.	λ_{cr}	mode	λ_{cr}	mode
1	4.051	D_{6h}	3.137	D_{3h}
2	4.542	C_s	3.390	C_s
3	4.542	C_s	3.390	C_s
4	4.900	D_{3h}	3.686	C_{3h}
5	5.026	C_{2h}	3.798	C_s
6	5.026	C_{2h}	3.798	C_s
7	5.327	D_{3h}	4.833	D_{3h}
8	5.339	C_{2h}	4.883	C_s
9	5.339	C_{2h}	4.883	C_s
10	5.601	C_s	5.087	C_{3v}
11	5.601	C_s	5.212	C_1
12	5.693	C_{6h}	5.212	C_1
13	6.781	C_{6v}	5.325	C_{3h}
14	7.126	C_1	5.396	C_s
15	7.126	C_1	5.396	C_s
16	7.413	C_{3v}	5.485	C_3
17	7.522	C_2	5.571	C_1
18	7.522	C_2	5.571	C_1
19	7.803	C_{3v}	7.272	D_{3h}
20	7.815	C_2	7.310	C_{3v}
21	7.815	C_2	7.328	C_s
22	8.089	C_1	7.328	C_s
23	8.089	C_1	7.376	C_1
24	8.191	C_6	7.376	C_{1v}

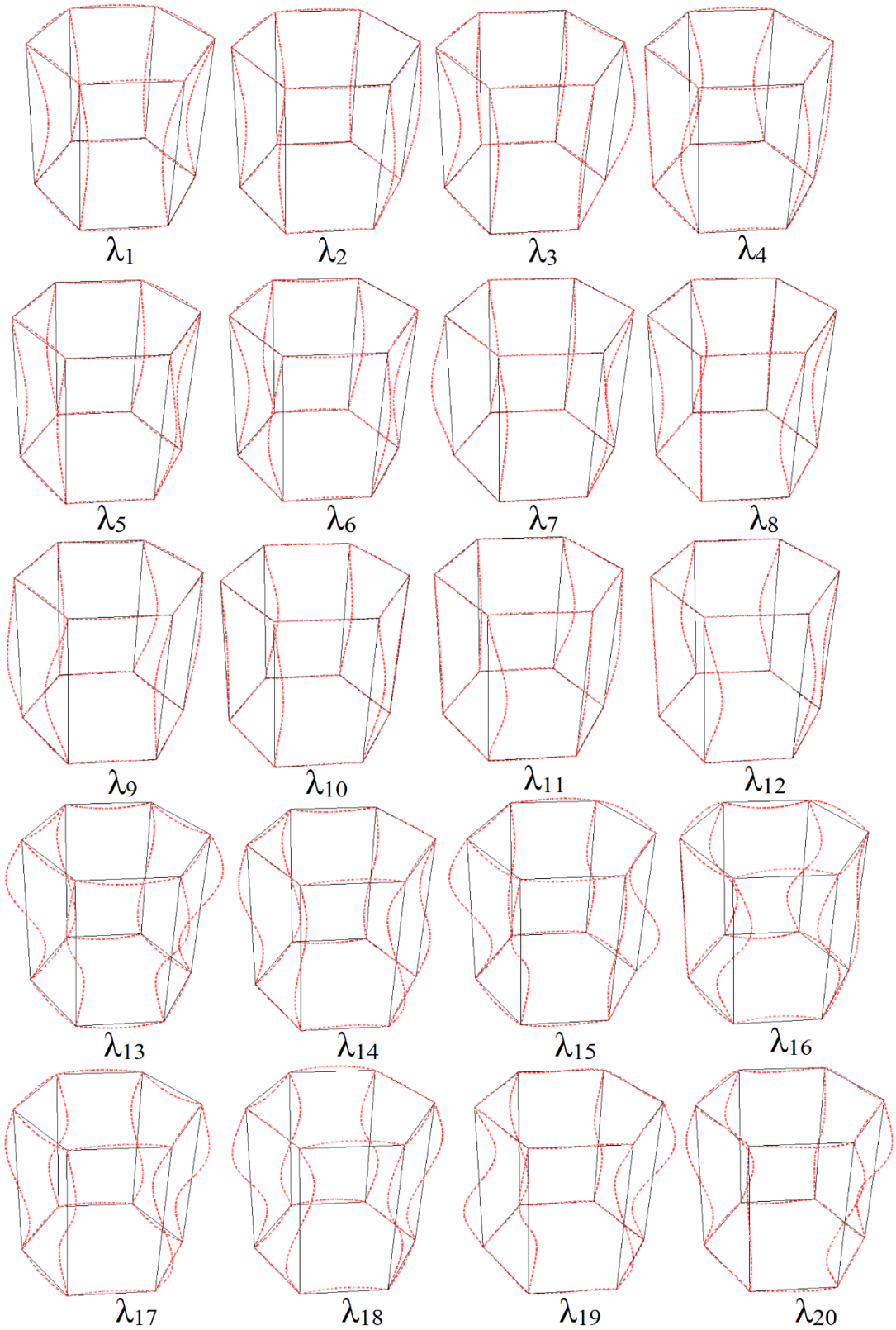

Figure 6.38: D_{6h} space frame buckling modes

For each load arrangement, it was observed that the buckling mode symmetries were subgroups of the symmetry group of the loading arrangement. However, not all symmetry subgroups were produced. For D_{6h} loading, it was observed that D_n and D_{nd} subgroups were absent, as shown in Table *6.15*. The C_i, C_3, C_{2v}, C_{3h}, S_6, and D_{2h} subgroups were also absent from the buckling behaviour displayed. Further C_s, C_{2h}, C_1, and C_2 symmetric buckling modes were produced from repeating buckling values. The D_{6h}, D_{3h}, C_{6v}, and C_{3v} symmetric buckling modes were produced by non-repeating buckling values. Lastly, it was observed that buckling modes produced from repeating and non-repeating buckling values both had a group index which is even.

The buckling modes for D_{6h} loading were grouped by symmetry and plotted on the same graph as shown in Figure *6.39* below. From Figure *6.39*, it is observed that the buckling values with C_1 symmetric buckling modes are very close to the buckling values with C_2 symmetric buckling modes. The buckling values with C_{2h}, C_s, and D_{3h} symmetric buckling modes are also observed to be very close.

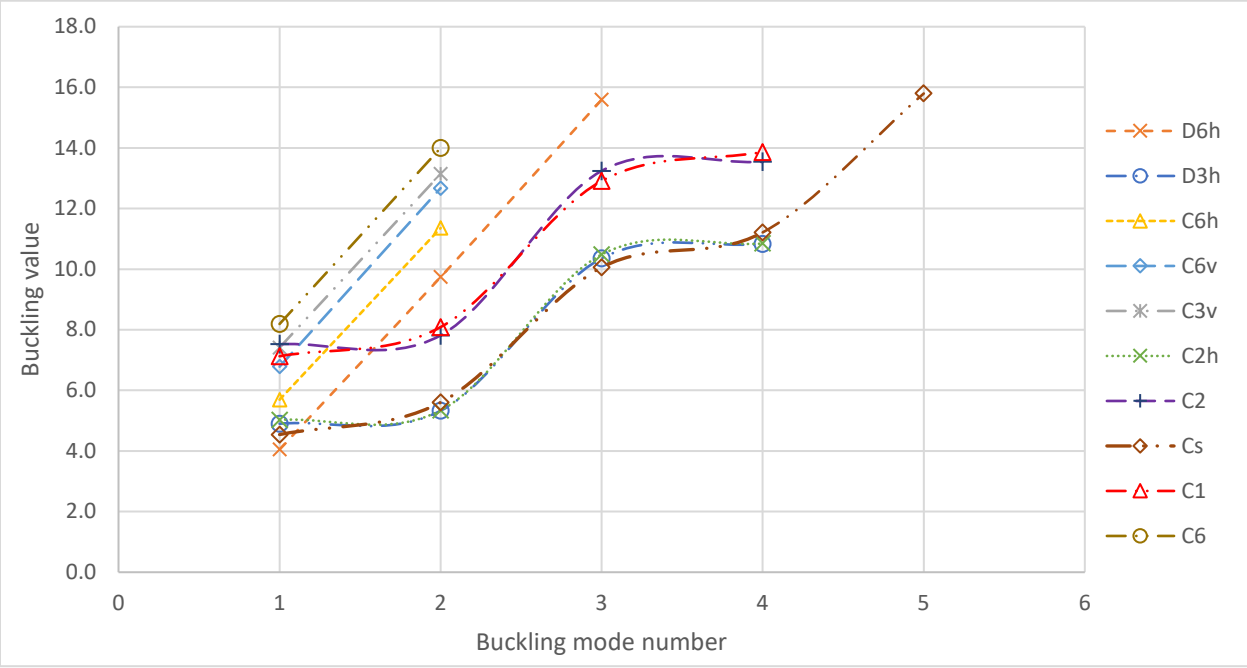

Figure 6.39: D_{6h} frame buckling values by symmetry versus mode number

6.6. 2 Post-Buckling Behaviour of a D_{6h} Symmetric Space Frame

The behaviour following buckling of the space frame under D_{6h} loading was examined through geometric nonlinear analysis conducted in Abaqus. Utilizing the Riks Arc method, the post-

buckling equilibrium paths for both the first and second critical points were traced. Results indicated the stability of the post-buckling equilibrium paths, depicted in Figure *6.40*. On the primary equilibrium path shown in Figure *6.40*, the deformation pattern of the space frame exhibited D_{6h} symmetry. However, on the bifurcated paths, the deformation pattern was a subgroup of the D_{6h} symmetry group. Additionally, in Figure *6.40*, Δ denotes the maximum lateral column displacement at mid-height in the middle plane depicted in Figure *6.35*, while L represents the column length. Furthermore, symbols P_{cr1} and P_{cr2} signify the first and second buckling loads obtained from the linear eigenvalue analysis.

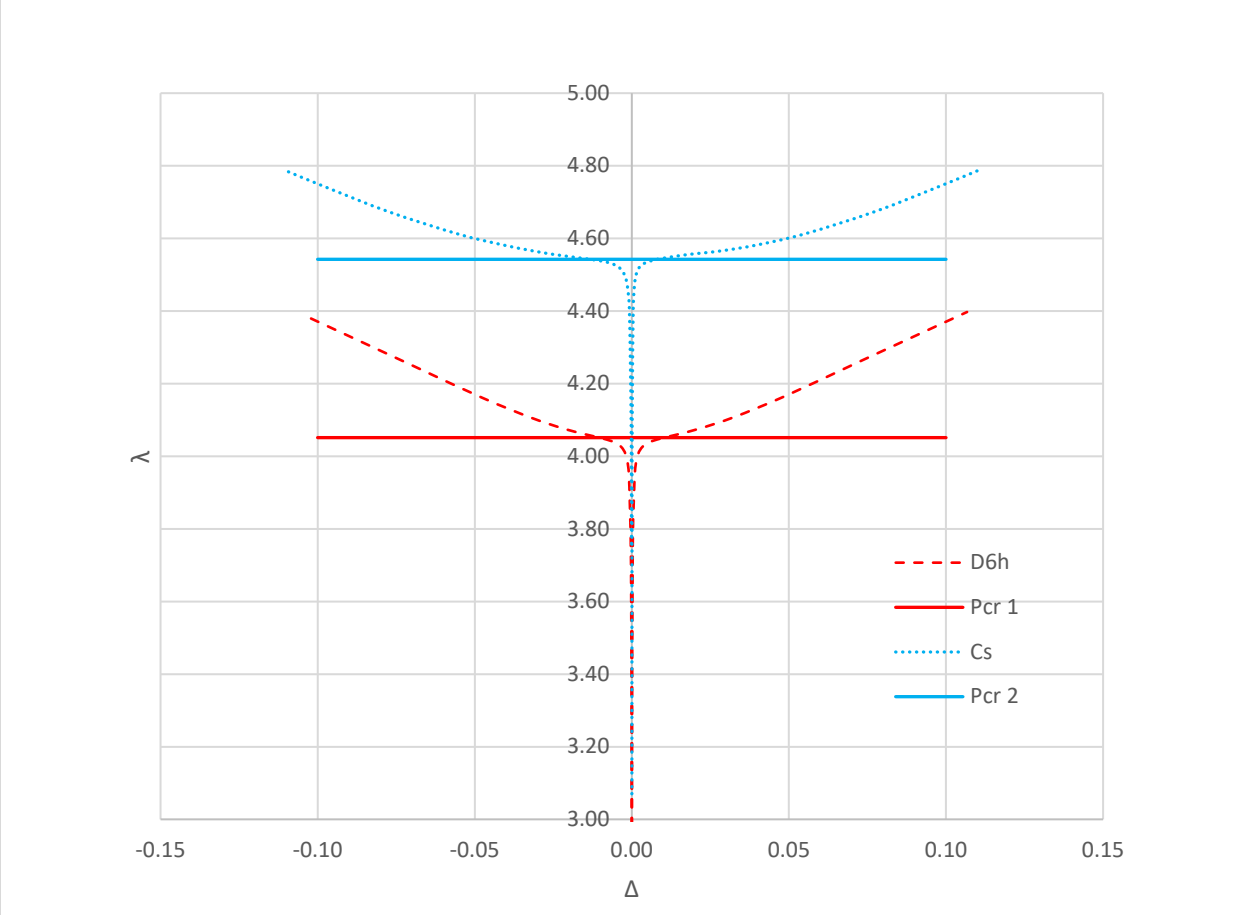

Figure 6.40:Equilibrium paths of D_{6h} symmetric Frame

6.7 Influence of Symmetry on the Stability Behaviour D_{nh} Space Frames

This part of the study sought to investigate the influence of symmetry on the stability behaviour of D_{nh} symmetric frames. Stability behaviour was studied in terms of symmetries of buckling

modes produced from a linear eigenvalue analysis and post buckling behaviour of the equilibrium path.

From all of the five D_{nh} symmetries considered in this study, we have seen that it is possible to deduce the possible symmetries of buckling modes produced from a linear eigenvalue analysis of D_{nh} symmetric frames by making reference to the known subgroups of the respective symmetry groups. However, from the results obtained from this study, the following subgroups were not observed from a linear eigenvalue analysis of D_{nh} space frames: D_n, D_{nd}, and S_n subgroups. D_n buckling modes can, however, be considered to be produced from a linear eigenvalue analysis since they are isomorphic to the C_{nv} and C_{nh} symmetry groups. The subgroups of a D_{nh} symmetry group that were produced from the linear eigenvalue analysis carried out in this study were of the following types: D_{nh}, C_{nh}, C_{nv}, C_n, C_i and C_s. Nonetheless, not all known D_{nh}, C_{nh}, C_{nv} and C_n were observed to be produced for any of the symmetry groups studied. Further, the study failed to find a method of predicting exactly which subgroups would be produced.

The order of emergence of symmetries of buckling modes produced from an eigenvalue analysis for a frame that is D_{nh} symmetric in terms of geometry, stiffness, and load arrangement was observed to be generally from the subgroup with the highest order of elements or group index. Thus, the concept of a hierarchy of bifurcations still applies for D_{nh} symmetric frames. It was also observed that, for each case of a D_{nh} symmetric frame in terms of loading and stiffness, the order of emergence of buckling modes was a pattern that was repeating for every $4n$ buckling value. The behaviour of the pattern repeating every $4n$ buckling value was not observed when a frame with D_{nh} stiffness was subjected to a loading of a lower order of symmetry.

The symmetries of the buckling modes for the lowest buckling value for a D_{nh} frame with D_{nh} loading and stiffness are summarised in Table *6.16*. As can be seen from Table *6.16*, unlike the case of C_{nv} plane frames, the symmetry of the buckling mode for the lowest buckling value is not always that of the subgroup with the highest order of elements.

Table 6.16: Buckling mode symmetry for lowest buckling value

Group	Buckling mode symmetry for lowest Buckling value
D_{2h}	D_{2h}
D_{3h}	D_{1h} *or* C_s
D_{4h}	D_{2h}
D_{5h}	D_{5h}
D_{6h}	D_{6h}

When the buckling values produced from the linear buckling value analysis were categorised by symmetry and plotted on the same graph for a D_{nh} frame in terms of stiffness and loading, no common pattern of behaviour was observed across the five D_{nh} space frames considered in this study. For the D_{6h}, D_{5h}, and D_{3h} symmetry groups, the buckling values with C_s symmetric buckling modes formed lower bound values. While for the D_{2h} and D_{4h} space frames, buckling values with D_{2h} symmetric buckling modes formed the lower bound values. However, for all D_{nh} frames, buckling values with C_n symmetric buckling modes formed higher bound values. This kind of behaviour can be noted in Figures *6.6*, *6.16*, *6.27*, *6.33,* and *6.39*.

When a space frame that is D_{nh} symmetric in terms of stiffness is subjected to a loading arrangement symmetric to a subgroup of D_{nh}, the buckling behaviour displayed by such a frame is that of a frame that is symmetric to that particular subgroup in terms of stiffness and loading. That is, the symmetries of the buckling modes produced are those of the applicable subgroup of D_{nh}. This kind of behaviour can be noted in Tables *6.3*, *6.6*, *6.9*, *6.12*, and *6.15*.

The post-buckling behaviour of space frames was investigated and found to be stable for all critical points investigated, except for a D_{3h} symmetric frame for the case where the deformation pattern is C_s on the post-buckling equilibrium path and $\beta>1$. This is a sharp contrast to C_{nv} symmetric lattice domes, which are known to display unstable post-buckling behaviour as shown in Figures *2.13* and *2.18*. Further, it was found that the ratio of beam to column stiffness did not alter the stable post-buckling behaviour of space frames for the vast majority of cases investigated.

When the group index was used to classify the symmetry of the buckling modes, this study failed to find any relation between the group index and whether a buckling value would be repeating or non-repeating.

From the foregoing discussion, we can conclude that for a space frame that is D_{nh} symmetric in terms of stiffness and loading, the following buckling and post-buckling behaviour will be displayed:

1. the symmetries of the buckling modes will be subgroups of D_{nh};
2. the order of emergence of symmetries of buckling modes will repeat every $4n$ buckling value;
3. the buckling values whose buckling modes have the C_n symmetries form the higher bound buckling values when all buckling values are arranged by buckling mode symmetry;
4. space frames that are D_{nh} symmetric in terms of stiffness and subjected to a loading arrangement symmetric to a subgroup of D_{nh}, display the buckling behaviour of a frame that is symmetric to that particular subgroup in terms of stiffness and loading;
5. the post-buckling behaviour of space frames is stable and is independent of the beam to column stiffness, with the exception of a D_{3h} symmetric frame for the case where the deformation pattern is C_s on the post-buckling equilibrium path and $\beta>1$.

6.8 Summary and concluding remarks

This study aimed to determine how symmetry impacts the stability of D_{nh} symmetric frames. Stability was assessed through the symmetries of buckling modes and post-buckling behaviour. It was observed that the symmetries of buckling modes could be inferred from linear eigenvalue analysis, referencing known subgroups of symmetry groups. However, certain subgroups like D_n, D_{nd}, and S_n were not detected in the analysis. The study found various subgroups generated from the linear eigenvalue analysis, such as D_{nh}, C_{nh}, C_{nv}, C_n, C_i, and C_s, though not all expected subgroups were observed.

In terms of emergence, symmetries of buckling modes generally followed a hierarchy based on group index for D_{nh} symmetric frames. A recurring pattern was noted in the order of buckling mode emergence, particularly every $4n$ buckling value. However, this pattern did not hold when frames with D_{nh} stiffness were subjected to lower order loading symmetry. The lowest buckling mode symmetry did not always correspond to the subgroup with the highest element order. No consistent pattern of behaviour in the emergence of buckling mode symmetries was observed

across the D_{nh} frames examined. When loading arrangements matched subgroups of D_{nh} symmetry, the buckling behaviour mirrored that subgroup's symmetry in stiffness and loading.

Post-buckling behaviour was generally stable across critical points, except for a D_{3h} symmetric frame exhibiting C_s deformation patterns on the equilibrium path with $\beta>1$. This contrasts with C_{nv} symmetric lattice domes, known for their unstable post-buckling behaviour. Moreover, the ratio of beam to column stiffness (β) showed minimal impact on post-buckling behaviour in most cases studied.

Chapter 7

7. Benefits of Study and Further Research

7.1 Benefits of study

The main objective of this study was to investigate the influence of symmetry on the global stability behaviour of space frames under static loading. To this end, this study developed two group theoretic approaches to determine the buckling loads of plane frames:

- Group theoretic formulation of buckling using the matrix stiffness method; and
- Group theoretic formulation of buckling using the slope deflection method.

Other researchers have also demonstrated how the group theoretic approach can be applied to the buckling analysis of plane frames using the matrix stiffness method (Kaveh & Nikbakht, 2006; Kaveh & Nikbakht, 2008; Kaveh & Nikbakht, 2010). However, these researchers applied transformation matrices to the conventional stiffness matrix to transform it into a symmetry-adapted stiffness matrix. The approach developed in this study obtains the symmetry-adapted stiffness matrices directly by simple superimposition of the appropriate values of the conventional stiffness coefficients in accordance with the coordinates of the basis vector causing the effect. This approach requires less computational effort since the symmetry adapted stiffness matrices are obtained by simple addition of matrix coefficients rather than by multiplication of transformation matrices.

The other group theoretic approach to buckling analysis developed in this study was based on the slope deflection method. As has been demonstrated in this study, this approach can be used to obtain analytical results that can be used to validate the *FEM* results for the buckling loads of plane and space frames. For plane frames, this study showed how the group-theoretic slope deflection method can be used to obtain useful insights on the character of the buckling modes (such as the symmetry properties of modes) before detailed computations have been carried out. This a priori

knowledge can be used to validate the results of the buckling of symmetric frames obtained from *FEM* results.

The buckling behaviour of C_{nv} plane frames, C_{nv} space frames, and D_{nh} space frames was studied using *FEM* results. These results can be used as a validation tool for *FEM* results on the symmetry of buckling modes produced by the lowest buckling values, the symmetry of the buckling modes produced by repeating buckling values, as well as non-repeating buckling values. Further, this study has shown that a linear eigenvalue analysis with only $2n$ *or* $4n$ buckling values (where $2n$ or $4n$ is the order of the group) is sufficient to determine all possible buckling mode symmetries, since the pattern of symmetries that emerge repeats every $2n$ or $4n$ buckling value for C_{nv} plane frames and D_{nh} space frames, respectively.

Symmetric structures are known to be highly sensitive to imperfections, and therefore, the tracing of the post-buckling path is important. This is because unstable post-buckling paths make the symmetric structures very sensitive to imperfections. Special path switching algorithms are required to trace the buckling paths of symmetric structures such as lattice domes. This study has shown how the Load excitation method can be used to trace the buckling paths of symmetric structures such as lattice domes without having to utilise special path switching algorithms.

Further, this study found that the post buckling behaviour of D_{nh} space frames is stable. This is unlike the known unstable post-buckling behaviour of C_{nv} symmetric lattice domes. Thus, D_{nh} space frames are not as sensitive to imperfections as C_{nv} symmetric lattice domes, and this knowledge can be applied in the analysis and design of D_{nh} space frames.

7.2 Future studies

This study investigated the stability behaviour of plane and space frames using *FEM* results. Analytical results were used to validate the *FEMs*. However, no experimental tests were conducted. Future studies can carry out experimental studies on the buckling and post-buckling behaviour of C_{nv} symmetric plane and space frames and D_{nh} space frames.

While two group theoretic approaches to buckling have been developed for plane frames in this study, the same has not been done for space frames. Future studies can demonstrate how the group theoretic approach can be applied to the buckling analysis of space frames.

Lastly, this study only considered frames constructed using circular section members. Future studies can consider other types of cross-sections that are singly or doubly symmetric. The buckling and post-buckling behaviour of such frames can then be studied, and similar questions answered in this study can be explored.

References

Altmann, S.L. & Herzig, P. 1994. *Point-group theory tables.* First ed. Oxford; New York: Clarendon Press; Oxford University Press.

Altmann, S.L. & Herzig, P. 2011. *Point group theory tables.* 2nd ed. Vienna: University of Vienna.

Aristizabal, O.J.D. 1997. Amplification Factor for Three-Dimensional Reinforced Concrete Framed Structures: A Nonparadoxical Approach. *ACI Structural Journal.* 94(5):538-548.

Aristizábal-Ochoa, J.D. 2002. Classic Buckling of Three-Dimensional Multicolumn Systems under Gravity Loads. *Journal of Engineering Mechanics.* 128(6):613-624. DOI:6(613) Available: http://ascelibrary.org/doi/abs/10.1061/(ASCE)0733-9399(2002)128:6(613)

Aristizábal-Ochoa, J.D. 2003. Elastic Stability and Second-Order Analysis of Three-Dimensional Frames: Effects of Column Orientation. *Journal of Engineering Mechanics.* 129(11):1254-1267. DOI:11(1254) Available: http://ascelibrary.org/doi/abs/10.1061/(ASCE)0733-9399(2003)129:11(1254)

Aslam, K. & Reza, A. 1991. Large Deformation Analysis of Elastic Space Frames. *Journal of Structural Engineering.* 117(7):2069-2087. DOI:10.1061/(ASCE)0733-9445(1991)117:7(2069) Available: https://doi.org/10.1061/(ASCE)0733-9445(1991)117:7(2069)

Attard, M.M. 1986. Nonlinear theory of non-uniform torsion of thin-walled open beams. *Thin-Walled Structures.* 4(2):101-134. DOI://doi.org/10.1016/0263-8231(86)90019-4 Available: http://www.sciencedirect.com/science/article/pii/0263823186900194

Axler, S.J. 1997. *Linear Algebra Done Right.* Second ed. Secaucus, USA: Springer.

Barsoum, R.S. & Gallagher, R.H. 1970. Finite element analysis of torsional and torsional–flexural stability problems. *International Journal for Numerical Methods in Engineering.* 2(3):335-352. DOI:10.1002/nme.1620020304 Available: https://doi.org/10.1002/nme.1620020304

Bathe, K. & Bolourchi, S. 1979. Large displacement analysis of three-dimensional beam structures. *International Journal for Numerical Methods in Engineering.* 14(7):961-986. DOI:10.1002/nme.1620140703 Available: https://doi.org/10.1002/nme.1620140703

Bathe, K. & Dvorkin, E.N. 1983. On the automatic solution of nonlinear finite element equations. *Computers & Structures.* 17(5):871-879. DOI://doi.org/10.1016/0045-7949(83)90101-3 Available: http://www.sciencedirect.com/science/article/pii/0045794983901013

Bažant, Z.P. 2000. Structural stability. *International Journal of Solids and Structures.* 37(1):55-67. DOI://doi.org/10.1016/S0020-7683(99)00078-5 Available: http://www.sciencedirect.com/science/article/pii/S0020768399000785

Belytschko, T., Schwer, L. & Klein, M.J. 1977. Large displacement, transient analysis of space frames. *International Journal for Numerical Methods in Engineering.* 11(1):65-84. DOI:10.1002/nme.1620110108 Available: https://doi.org/10.1002/nme.1620110108

Belytschko, T. & Glaum, L.W. 1979. *Applications of higher order corotational stretch theories to nonlinear finite element analysis.* Available: http://www.sciencedirect.com/science/article/pii/0045794979900853

Berry, A. 1919. Calculation of Stresses in Aeroplane Wing Spars. *Transactions of the Royal Aeronautical Society.* 1:3-33. DOI:10.1017/S2398188100000079 Available: https://www.cambridge.org/core/article/calculation-of-stresses-in-aeroplane-wing-spars/CE5B19D20DB4067B4047697271E79C35 [2019/02/13]

Biezeno, C.B. & Hencky, H. 1928. On the general theory of elastic stability. *Proceedings of the Section of Sciences,''Koninklijke Akademie Van Wettenschappen Te Amsterdam.* 31:569-592.

Biot, M.A. 1938. Theory of elasticity with large displacements and rotations. *Proceedings of the Fifth International Congress of Applied Mechanics.* September 12–16, 1938. Cambridge, United States: Wiley and Sons. 117-122.

Bleich, F. 1952. *Buckling strength of metal structures.* New York: McGraw-Hill.

Britvec, S.J. 1960. *The post-buckling behaviour of frames.* Cambridge.

Bryan, G.H. 1888. On the stability of elastic systems ... *Proceedings of the Cambridge Philosophical Society, Mathematical and Physical Science.* 1888. [Cambridge]: Cambridge. 199-210.

Budiansky, B. 1974. *Theory of Buckling and Post-Buckling Behavior of Elastic Structures.* Available: http://www.sciencedirect.com/science/article/pii/S0065215608700309

Carter, W.O. 1963. *Stability analysis of rigid-jointed plane frames by matrix methods.* Stanford University.

Castellani, E. 2003. On the meaning of symmetry breaking. *Symmetries in Physics: Philosophical Reflections.* :321-334.

Chajes, A. 1974. *Principles of structural stability theory.* 2. print. ed. Englewood Cliffs, NJ: Prentice-Hall.

Chan, S.L. 1988. Geometric and material non-linear analysis of beam-columns and frames using the minimum residual displacement method. *International Journal for Numerical Methods in Engineering.* 26(12):2657-2669.

Chan, S.L. & Zhou, Z.H. 1994. Pointwise Equilibrating Polynomial Element for Nonlinear Analysis of Frames. *Journal of Structural Engineering.* 120(6):1703-1717. DOI:6(1703) Available: https://doi.org/10.1061/(ASCE)0733-9445(1994)120:6(1703)

Chen, Y. & Feng, J. 2015. Group-theoretic method for efficient buckling analysis of prestressed space structures. *Acta Mechanica.* 226(3):957-973. DOI:10.1007/s00707-014-1234-x Available: https://search.proquest.com/docview/1658648484

Chen, Y. & Feng, J. 2018. Group-Theoretic Exploitations of Symmetry in Novel Prestressed Structures. *Symmetry.* 10(6):229. DOI:10.3390/sym10060229 Available: https://doaj.org/article/a0b1fb3a60cf49838e1c4e536ac12ec7

Chen, Y., Fan, L. & Feng, J. 2018. Automatic and Exact Symmetry Recognition of Structures Exhibiting High-Order Symmetries. *Journal of Computing in Civil Engineering.* 32(2) DOI:10.1061/(ASCE)CP.1943-5487.0000743 Available: http://ascelibrary.org/doi/abs/10.1061/(ASCE)CP.1943-5487.0000743

Zhang, P., Fan, W., Chen, Y., Feng, J. & Sareh, P. 2022. Structural symmetry recognition in planar structures using Convolutional Neural Networks. *Engineering Structures.* 260:114227. DOI:10.1016/j.engstruct.2022.114227 Available: https://dx.doi.org/10.1016/j.engstruct.2022.114227

Chiba, T. & Nagahama, H. 2001. Curie Symmetry Principle in Nonlinear Functional Systems. *Forma-Tokyo-.* 16(3):225-231.

Chilver, A.H. 1956. Buckling of a simple portal frame. *Journal of the Mechanics and Physics of Solids.* 5(1):18-25. DOI://doi.org/10.1016/0022-5096(56)90004-7 Available: http://www.sciencedirect.com/science/article/pii/0022509656900047

Chwalla, E. 1928. Die Stabilität zentrisch und exzentrisch gedrückter Stäbe aus Baustahl. Sitz. *Ber.D.Wiener Ak.D.Wiss.* :21-23.

Chwalla, E. 1938. Die Stabilität lotrecht belasteter Rechteckrahmen. *Der Bauingerieur.*

Chwalla, E. & Jokisch, F. 1941. Ueber Das Ebene Knickproblem Des Stockwerkrahmens. *Stahlbau.* :33-40.

Citipitioglu, E. 1965. *Stability of Rigid-Jointed Space Frames.* Oklahoma State University.

Clarke, M.J. & Hancock, G.J. 1990. A study of incremental-iterative strategies for non-linear analyses. *International Journal for Numerical Methods in Engineering.* 29(7):1365-1391. DOI:10.1002/nme.1620290702 Available: https://doi.org/10.1002/nme.1620290702

Connor, J.J., Logcher, R.D. & Chan, S. 1968. Nonlinear analysis of elastic framed structures. *Journal of the Structural Division.* 94(6):1525-1548.

Crisfield, M.A. 1997. *Non linear finite element analysis of solids and structures.* Vol. 2 ed. Wiley.

Crisfield, M.A. 1981. A fast incremental/iterative solution procedure that handles "snap-through". *Computational Methods in Nonlinear Structural and Solid Mechanics.* :55-62. DOI://doi.org/10.1016/B978-0-08-027299-3.50009-1 Available: http://www.sciencedirect.com/science/article/pii/B9780080272993500091

Crisfield, M.A. 1983. An arc-length method including line searches and accelerations. *International Journal for Numerical Methods in Engineering.* 19(9):1269-1289. DOI:10.1002/nme.1620190902 Available: https://doi.org/10.1002/nme.1620190902

Crisfield, M.A. 1990. A consistent co-rotational formulation for non-linear, three-dimensional, beam-elements. *Computer Methods in Applied Mechanics and Engineering.* 81(2):131-150. DOI://doi.org/10.1016/0045-7825(90)90106-V Available: http://www.sciencedirect.com/science/article/pii/004578259090106V

Douglas, J.M. 1964. *Buckling strength of frames under primary bending.* M.A.Sc. University of Windsor.

Ekhande, S.G., Mohan, S. & Madugula, M.K. 1989. Stability Functions for Three-Dimensional Beam-Columns. *Journal of Structural Engineering.* 115(2):467-479. DOI:2(467) Available: https://doi.org/10.1061/(ASCE)0733-9445(1989)115:2(467)

El-Zanaty, M.H. & Murray, D.W. 1983. Nonlinear finite element analysis of steel frames. *Journal of Structural Engineering.* 109(2):353-368.

Engesser, F. 1889. Die Knickfestigkeit Gerader Stäbe. *Zeitschrift Des Architekten Und Ingenieure Vereines Zu Hannover.* 35:455.

Ettouney, M.M. & Kirby, J.B. 1981. Warping restraint in three-dimensional frames. *Journal of the Structural Division.* 107(8):1643-1656.

Euler, L. 1744. *Methodus inveniendi lineas curvas maximi minimive proprietate gaudentes, sive Solutio problematis isoperimetrici latissimo sensu accepti.* Lausannae et Genevae.

Farshad, M. 1994. *Stability of structures.* Amsterdam u.a: Elsevier.

Fujii, F. & Ramm, E. 1997. Computational bifurcation theory: path-tracing, pinpointing and path-switching. *Engineering Structures.* 19(5):385-392. DOI:10.1016/S0141-0296(96)00094-6 Available: https://dx.doi.org/10.1016/S0141-0296(96)00094-6

Fujii, F. & Choong, K.K. 1992. Branch Switching in Bifurcation of Structures. *Journal of Engineering Mechanics.* 118(8):1578-1596. DOI:10.1061/(ASCE)0733-9399(1992)118:8(1578) Available: http://ascelibrary.org/doi/abs/10.1061/(ASCE)0733-9399(1992)118:8(1578)

Gioncu, V. 1995. Buckling of Reticulated Shells: State-of-the-Art. *International Journal of Space Structures.* 10(1):1-46. DOI:10.1177/026635119501000101 Available: https://journals.sagepub.com/doi/full/10.1177/026635119501000101

Golubitsky, M. & Schaeffer, D.G. 1985. *Singularities and Groups in Bifurcation Theory.* New York, NY: Springer New York. DOI:10.1007/978-1-4612-5034-0.

Goto, Y. & Chen, W. 1987. Second-order elastic analysis for frame design. *Journal of Structural Engineering.* 113(7):1501-1519.

Haisler, W.E., Stricklin, J.A. & Key, J.E. 1977. Displacement incrementation in non-linear structural analysis by the self-correcting method. *International Journal for Numerical Methods in Engineering.* 11(1):3-10.

Hamermesh, M. 1962. *Group Theory and Its Application to Physical Problems.* New York: Dover Publications.

Hangai, Y. & Kawamata, S. 1972. Perturbation method in the analysis of geometrically nonlinear and stability problems. *Advances in Computational Methods in Structural Mechanics and Design.* :473-489.

Harrison, H.B. 1965. *The application of the principles of plastic analysis of three dimensional steel structures.* University of Sydney.

Hartz, B.J. 1965. Matrix formulation of structural stability problems. *Journal of the Structural Division.* 91(6):141-158.

Healey, T.J. 1985. *Symmetry, Bifurcation, and Computational Methods in Nonlinear Structural Mechanics* . University of Illinois at Urbana-Champaign.

Healey, T.J. 1988. A group-theoretic approach to computational bifurcation problems with symmetry. *Computer Methods in Applied Mechanics and Engineering.* 67(3):257-295. DOI:10.1016/0045-7825(88)90049-7 Available: https://www.sciencedirect.com/science/article/pii/0045782588900497

Hoff, H.J. 1941. Stable and Unstable Equilibrium of Plane Frameworks. *Journal of the Aeronautical Sciences.* 8(3):115-119. DOI:10.2514/8.10659 Available: http://arc.aiaa.org/doi/full/10.2514/8.10659

Hoff, N.J. 1966. The perplexing behavior of thin circular cylindrical shells in axial compression. *Israel Journal of Technology.* 4(1):1-28. Available: http://www.dtic.mil/docs/citations/AD0631508

Holzer, S.M., Watson, L.T. & Vu, P. 1981. Stability analyses of lamella domes. *Long Span Roof Structures.* October 26-30, 1981. ASCE. 179-209.

Horne, M.R. 1961. The stability of elastic-plastic structures. *Progress in Solid Mechanics.* 2:277-322.

Horne, M.R. 1963. Elastic-plastic failure loads of plane frames. *Proceedings of the Royal Society of London.Series A.Mathematical and Physical Sciences.* 274(1358):343-364.

Hsiao, K.M., Yang, R.T. & Lin, W.Y. 1998a. *A consistent finite element formulation for linear buckling analysis of spatial beams.* Available: http://www.sciencedirect.com/science/article/pii/S0045782597002107

Hsiao, K.M., Yang, R.T. & Lin, W.Y. 1998b. *A consistent finite element formulation for linear buckling analysis of spatial beams.* Available: http://www.sciencedirect.com/science/article/pii/S0045782597002107

Hsiao, K.M. 1992. Corotational total Lagrangian formulation for three-dimensional beamelement. *AIAA Journal.* 30(3):797-804.

Hsiao, K.M. & Lin, W.Y. 2000. *A co-rotational finite element formulation for buckling and postbuckling analyses of spatial beams.* Available: http://www.sciencedirect.com/science/article/pii/S0045782599002844

Hussey, M.J.L. 1967. General theory of cyclically symmetric frames. *Journal of the Structural Division.* 93(2):163-176.

Hutchinson, J.W. & Koiter, W.T. 1970. Postbuckling theory. *Applied Mechanics Review.* (23 Vol 12):1353-1366.

Ikeda, K. & Torii, K. 1987a. Group theoretic description of bifurcation behavior of axisymmetric regular-polygonal truss domes. October 1987. Japan Society of Civil Engineers. 21-31.10.2208/jscej.1987.386_21.

Ikeda, K. & Torii, K. 1987b. Group theoretic study of bifurcation points of truss dome structures. October 1987. Japan Society of Civil Engineers. 33-42.10.2208/jscej.1987.386_33.

Ikeda, K., Torii, K. & Matsushita, S. 1986a. Group theoretic categorization of bifurcation modes of truss dome structures. October 1986. Japan Society of Civil Engineers. 89-98.

Ikeda, K., Matsushita, S. & Torri, K. 1986b. Symmetry breaking bifurcation behavior of dome structures and group theory. April 1986. Japan Society of Civil Engineers. 125-134.10.2208/jscej.1986.368_125.

Ikeda, K. & Murota, K. 1991. Bifurcation analysis of symmetric structures using block-diagonalization. *Computer Methods in Applied Mechanics and Engineering.* 86(2):215-243. DOI://doi.org/10.1016/0045-7825(91)90128-S Available: http://www.sciencedirect.com/science/article/pii/004578259190128S

Ikeda, K. & Murota, K. 2010. *Imperfect bifurcation in structures and materials.* 2. ed. ed. New York [u.a.]: Springer.

Ikeda, K., Murota, K. & Fujii, H. 1991. Bifurcation hierarchy of symmetric structures. *International Journal of Solids and Structures.* 27(12):1551-1573. DOI:10.1016/0020-7683(91)90077-S.

Izzuddin, B.A. & Lloyd, S.D. 1996. Large-Displacement Analysis of Elastoplastic Thin-Walled Frames. I: Formulation and Implementation. *Journal of Structural Engineering.* 122(8):905-914. DOI:8(905) Available: https://doi.org/10.1061/(ASCE)0733-9445(1996)122:8(905)

James, B.W. 1935. *Principal effects of axial load on moment-distribution analysis of rigid structures.* Washington, D.C.: National Advisory Committee for Aeronautics.

Johnson, D.E. 1961. Lateral stability of frames by energy method. *Journal of the Engineering Mechanics Division.* 86(4):23-42.

Kaluba, C. & Zingoni, A. 2022. Influence of symmetry on the buckling behaviour of plane frames. In *Current Perspectives and New Directions in Mechanics, Modelling and Design of Structural Systems.* 1st ed. CRC Press. 249-250. Available: https://www.taylorfrancis.com/books/9781003348450/chapters/10.1201/9781003348450-117

Kaluba, C. & Zingoni, A. 2021. Group-Theoretic Buckling Analysis of Symmetric Plane Frames. *Journal of Structural Engineering.* 147(10):04021153. DOI:10.1061/(ASCE)ST.1943-541X.0003131 Available: https://doi.org/10.1061/(ASCE)ST.1943-541X.0003131

Kangwai, R.D., Guest, S.D. & Pellegrino, S. 1999. An introduction to the analysis of symmetric structures. *Computers and Structures.* 71(6):671-688. DOI:10.1016/S0045-7949(98)00234-X Available: https://www.sciencedirect.com/science/article/pii/S004579499800234X

Kaveh, A. & Nikbakht, M. 2006. Buckling load of symmetric plane frames using canonical forms and group theory. *Acta Mechanica.* 185(1-2):89-128.

Kaveh, A. & Nikbakht, M. 2008. Stability analysis of hyper symmetric skeletal structures using group theory. *Acta Mechanica.* 200(3-4):177-197.

Kaveh, A. & Nikbakht, M. 2010. Improved group-theoretical method for eigenvalue problems of special symmetric structures, using graph theory. *Advances in Engineering Software.* 41(1):22-31. DOI:10.1016/j.advengsoft.2008.12.003 Available: https://www.sciencedirect.com/science/article/pii/S0965997808002093

Kaveh, A., Nikbakht, M. & Rahami, H. 2010. Improved group theoretic method using graph products for the analysis of symmetric-regular structures. *Acta Mechanica.* 210(3-4):265-289.

Kerr, A.D. 1977. On the adjacent equilibrium method in the stability theory of conservative elastic continua. *International Journal of Non-Linear Mechanics.* 12(5):269-283. DOI:10.1016/0020-7462(77)90002-6.

Kim, S., Lee, J. & Park, J. 2002. 3-D second-order plastic-hinge analysis accounting for lateral torsional buckling. *International Journal of Solids and Structures.* 39(8):2109-2128. DOI:10.1016/S0020-7683(02)00082-3 Available: https://www.sciencedirect.com/science/article/pii/S0020768302000823

Koiter, W.T. 1970. *A translation of the Stability of elastic equilibrium.* Detroit: Management Information Services.

Kounadis, A.N., Giri, J. & Simitses, G.J. 1977. Nonlinear stability analysis of an eccentrically loaded two-bar frame. *Journal of Applied Mechanics.* 44(4):701-706.

Lee, K.S. & Han, S.E. 2012. A bifurcation analysis of space structures by using 3d beam-column element considering finite deformations and bowing effect. *Advanced Steel Construction.* 8(3):256-281.

LeRoy, G.B. 1961. *Stability of space frames, triangular in plan.* Buffalo: University of New York at Buffalo.

Le-Wu, L. 1963. Stability of Frames under primary bending moment. *Proc.ASCE, ST.* 3.

Livesley, R. K., Chandler,D.B. 1968. *Stability Functions for Structural Frameworks.* [S.l.]: Manchester University Press.

Lu, L.W. 1963. *Stability of frames under initial bending moments.* Fritz Laboratory Reports.

Lundquist, E.E. 1937. *Stability of structural members under axial load.*

Maewal, A. & Nachbar, W. 1977. Stable postbuckling equilibria of axially compressed, elastic circular cylindrical shells: a finite-element analysis and comparison with experiments. *Journal of Applied Mechanics.* 44(3):475-481.

Mallett, R.H. & Marcal, P.V. 1968. Finite element analysis of nonlinear structures. *Journal of the Structural Division.* 94(9):2081-2106.

Masur, E.F. & Cukurs, A. 1957. Lateral buckling of plane frameworks. *Journal of the Engineering Mechanics Division.* 83(1) Available: https://doi.org/10.1061/JMCEA3.000001

Masur, E.F. 1954. Lower and upper bounds to the ultimate loads of buckled redundant trusses. *Quarterly of Applied Mathematics.* 11(4):385-392.

Masur, E.F. 1955. On the lateral stability of multi-story bents. *Proceedings of the American Society of Civil Engineers.* ASCE. 1-13.

Masur, E.F., Chang, I.C. & Donnell, L.H. 1962. Stability of Frames in the Presence of Primary Bending Moments. *Transactions of the American Society of Civil Engineers.* 127(1):736-751.

Meek, J.L. & Hoon Swee Tan,. 1984. *Geometrically nonlinear analysis of space frames by an incremental iterative technique.* Available: http://www.sciencedirect.com/science/article/pii/0045782584900793

Meek, J.L. & Xue, Q. 1998. *A study on the instability problem for 3D frames.* Available: http://www.sciencedirect.com/science/article/pii/S0045782598002540

Mises, R.V. & Ratzersdorfer, J. 1926. Hauptaufsätze: Die Knicksicherheit von Rahmentragwerken. *ZAMM - Journal of Applied Mathematics and Mechanics / Zeitschrift Für Angewandte Mathematik Und Mechanik.* 6(3):181-199. DOI:10.1002/zamm.19260060302 Available: https://doi.org/10.1002/zamm.19260060302

Nishino, F., Ikeda, K., Sakurai, T. & Hasegawa, A. 1984. A total Lagrangian nonlinear analysis of elastic trusses. April 1984. Japan Society of Civil Engineers. 39-53.10.2208/jscej.1984.39.

Oran, C. 1973. Tangent stiffness in space frames. *Journal of the Structural Division.* 99(6):987-1001.

Orlando, D., Gonçalves, P.B., Rega, G. & Lenci, S. 2013. Influence of symmetries and imperfections on the non-linear vibration modes of archetypal structural systems. *International Journal of Non-Linear Mechanics.* 49:175-195. DOI:10.1016/j.ijnonlinmec.2012.10.004.

Papadrakakis, M. & Ghionis, P. 1986. Conjugate gradient algorithms in nonlinear structural analysis problems. *Computer Methods in Applied Mechanics and Engineering.* 59(1):11-27. DOI:10.1016/0045-7825(86)90021-6 Available: https://www.sciencedirect.com/science/article/pii/0045782586900216

Pecknold, D.A., Ghaboussi, J. & Healey, T.J. 1985. Snap-through and bifurcation in a simple structure. *Journal of Engineering Mechanics.* 111(7):909-922.

R. V. Southwell. 1914. On the General Theory of Elastic Stability. *Philosophical Transactions of the Royal Society of London. Series A, Containing Papers of a Mathematical Or Physical Character.* 213:187-244. Available: https://www.jstor.org/stable/91065

Ramm, E. . 1981. Strategies for tracing the nonlinear response near limit points. In *Nonlinear finite element analysis in structural mechanics.* Springer. 63-89.

Renton, J.D. 1964. On The Stability Analysis Of Symmetrical Frameworks. *The Quarterly Journal of Mechanics and Applied Mathematics.* 17(2):175-195. DOI:10.1093/qjmam/17.2.175.

Riks, E. 1979. *An incremental approach to the solution of snapping and buckling problems.* Available: http://www.sciencedirect.com/science/article/pii/0020768379900817

Rothert, H., Renner, D. & Dickel, T. 1981. Snap-through buckling of reticulated space trusses. *Journal of the Structural Division.* 107(1):129-143.

Sattinger, D.H. 1979. *Group theoretic methods in bifurcation theory.* Berlin [u.a.]: Springer.

Schweizerhof, K.H. & Wriggers, P. 1986. Consistent linearization for path following methods in nonlinear fe analysis. *Computer Methods in Applied Mechanics and Engineering.* 59(3):261-279. DOI://doi.org/10.1016/0045-7825(86)90001-0 Available: http://www.sciencedirect.com/science/article/pii/0045782586900010

Shi, G. & Atluri, S.N. 1988. Elasto-plastic large deformation analysis of space-frames: A plastic-hinge and stress-based explicit derivation of tangent stiffnesses. *International Journal for Numerical Methods in Engineering.* 26(3):589-615. DOI:10.1002/nme.1620260306 Available: https://doi.org/10.1002/nme.1620260306

Shosuke, M. 1970. *Analysis of space frames.* Lehigh University.

Stevens, L.K. 1967. Elastic Stability of Practical Multi - Storey Frames. *Proceedings of the Institution of Civil Engineers.* 36(1):99-117. DOI:10.1680/iicep.1967.8592.

Stewart, I. 1999. Symmetry-breaking cascades and the dynamics of morphogenesis and behaviour. *Science Progress (1933-).* 82(1):9-48. Available: http://www.jstor.org/stable/43424050

Stewart, I. & Golubitsky, M. 1992. *Fearful symmetry: is God a geometer?* First Edition ed. Oxford, UK; Cambridge, Mass., USA: Blackwell.

Teh, L.H. & Clarke, M.J. 1998. *Co-rotational and Lagrangian formulations for elastic three-dimensional beam finite elements.*

Thomas, D.L. 1979. Dynamics of rotationally periodic structures. *International Journal for Numerical Methods in Engineering.* 14(1):81-102. DOI:10.1002/nme.1620140107 Available: https://doi.org/10.1002/nme.1620140107

Thompson, J.M.T. 1963. Basic principles in the general theory of elastic stability. *Journal of the Mechanics and Physics of Solids.* 11(1):13-20. DOI://doi.org/10.1016/0022-5096(63)90003-6 Available: http://www.sciencedirect.com/science/article/pii/0022509663900036

Thompson, J.M.T. & Hunt, G.W. 1973. *A General Theory of Elastic Stability.* London [u.a.]: Wiley.

Timošenko, S.P. & Gere, J.M. 1963. *Theory of elastic stability.* 2. ed. ed. New York <>: McGraw Hill. Available: .

Timoshenko, S. 1983. *History of strength of materials: with a brief account of the history of theory of elasticity and theory of structures.* Courier Corporation. Available: .

Trahair, N.S. & Teh, L.H. 2001. *Second order moments in torsion members.* Available: http://www.sciencedirect.com/science/article/pii/S0141029600000833

Vaart, A. 1965. *Elastic stability of space frameworks.* New. York University,.

Vannucci, P., Cochelin, B., Damil, N. & Potier-Ferry, M. 1998. An asymptotic-numerical method to compute bifurcating branches. *International Journal for Numerical Methods in Engineering.* 41(8):1365-1389. DOI:AID-NME332>3.0.CO;2-Y Available: https://doi.org/10.1002/(SICI)1097-0207(19980430)41:83.0.CO;2-Y.

W. A. Oldfather, C. A. Ellis & Donald M. Brown. 1933. Leonhard Euler's Elastic Curves. *Isis.* 20(1):72-160. DOI:10.1086/346767 Available: https://www.jstor.org/stable/224885

Weinberg, S. 2009. *Lake views.* Cambridge, Mass.; London: Belknap Pr. of Harvard Univ. Pr. Available: .

Wempner, G. 1972. *Energy Criteria for Stability of Structures.*

Wempner, G.A. 1971. Discrete approximations related to nonlinear theories of solids. *International Journal of Solids and Structures.* 7(11):1581-1599. DOI://doi.org/10.1016/0020-7683(71)90038-2 Available: http://www.sciencedirect.com/science/article/pii/0020768371900382

Wen, R.K. & Jalil, R. 1983. Nonlinear Elastic Frame Analysis by Finite Element. *Journal of Structural Engineering.* 109(8):1952-1971. DOI:8(1952) Available: https://doi.org/10.1061/(ASCE)0733-9445(1983)109:8(1952)

Williams, F.W. 1964. An approach to the non-linear behaviour of the members of a rigid jointed plane framework with finite deflections. *The Quarterly Journal of Mechanics and Applied Mathematics.* 17(4):451-469.

Wohlever, J.C. 1996. *Symmetry, Nonlinear Bifurcation Analysis, and Parallel Computation.* Cornell University.

Wohlever, J.C. & Healey, T.J. 1995. *A group theoretic approach to the global bifurcation analysis of an axially compressed cylindrical shell.* Available: http://www.sciencedirect.com/science/article/pii/0045782594007345

Yang, Y. & Kuo, S. 1991a. Buckling of frames under various torsional loadings. *Journal of Engineering Mechanics.* 117(8):1681-1697.

Yang, Y. & Kuo, S. 1991b. Consistent frame buckling analysis by finite element method. *Journal of Structural Engineering.* 117(4):1053-1069.

Yang, Y. & McGuire, W. 1984. A procedure for analysing space frames with partial warping restraint. *International Journal for Numerical Methods in Engineering.* 20(8):1377-1398. DOI:10.1002/nme.1620200803 Available: https://doi.org/10.1002/nme.1620200803

Yang, Y. & McGuire, W. 1986. Stiffness matrix for geometric nonlinear analysis. *Journal of Structural Engineering.* 112(4):853-877.

Young, T. 1807. *A course of lectures on natural philosophy and the mechanical arts.* London: Johnson.

Zalka, K.A. 2002. Buckling analysis of buildings braced by frameworks, shear walls and cores. *The Structural Design of Tall Buildings.* 11(3):197-219. DOI:10.1002/tal.194 Available: https://onlinelibrary.wiley.com/doi/abs/10.1002/tal.194

Zalka, K.A. 2012. *Structural Analysis of Regular Multi-Storey Buildings.* CRC Press. Available: http://www.crcnetbase.com/isbn/9781136895128

Zienkiewicz, O.C. 1971. Incremental displacement in non-linear analysis. *International Journal for Numerical Methods in Engineering.* 3(4):587-588.

Zingoni, A. 1996. An efficient computational scheme for the vibration analysis of high tension cable nets. *Journal of Sound and Vibration.* 189(1):55-79. DOI:10.1006/jsvi.1996.0005 Available: https://www.sciencedirect.com/science/article/pii/S0022460X9690005X

Zingoni, A. 2001a. Group-theoretic computation of matrices for rectangular hexahedral finite elements. Oxford: Elsevier Science. 1683-1685.

Zingoni, A. 2005a. A group-theoretic formulation for symmetric finite elements. *Finite Elements in Analysis and Design.* 41(6):615-635. DOI://doi.org/10.1016/j.finel.2004.10.004 Available: http://www.sciencedirect.com/science/article/pii/S0168874X04001581

Zingoni, A. 2005b. On the symmetries and vibration modes of layered space grids. *Engineering Structures.* 27(4):629-638. DOI:10.1016/j.engstruct.2004.12.004 Available: https://www.sciencedirect.com/science/article/pii/S0141029605000118

Zingoni, A. 2008. On group-theoretic computation of natural frequencies for spring–mass dynamic systems with rectilinear motion. *Communications in Numerical Methods in Engineering.* 24(11):973-987. DOI:10.1002/cnm.1003 Available: https://onlinelibrary.wiley.com/doi/abs/10.1002/cnm.1003

Zingoni, A. 2009. Group-theoretic exploitations of symmetry in computational solid and structural mechanics. *International Journal for Numerical Methods in Engineering.* 79(3):253-289. DOI:10.1002/nme.2576 Available: https://doi.org/10.1002/nme.2576

Zingoni, A. 2012a. A group-theoretic finite-difference formulation for plate eigenvalue problems. *Computers & Structures.* 112-113:266-282. DOI://doi.org/10.1016/j.compstruc.2012.08.009 Available: http://www.sciencedirect.com/science/article/pii/S004579491200209X

Zingoni, A. 2012b. Symmetry recognition in group-theoretic computational schemes for complex structural systems. *Computers and Structures.* 94-95:34-44. DOI:10.1016/j.compstruc.2011.12.004 Available: https://www.sciencedirect.com/science/article/pii/S0045794911003026

Zingoni, A. 2014. Group-theoretic insights on the vibration of symmetric structures in engineering. *Philosophical Transactions of the Royal Society A: Mathematical, Physical and Engineering Sciences.* 372(2008):20120037.

Zingoni, A. 2015. *Vibration analysis and structural dynamics for civil engineers: essentials and group-theoretic formulations.* Boca Raton, FL: Taylor & Francis.

Zingoni, A. 2018. Insights on the vibration characteristics of double-layer cable nets of D4h symmetry. *International Journal of Solids and Structures.* 135:261-273. DOI://doi.org/10.1016/j.ijsolstr.2017.11.025 Available: http://www.sciencedirect.com/science/article/pii/S0020768317305280

Zingoni, A. 2019. Group-theoretic vibration analysis of double-layer cable nets of D4h symmetry. *International Journal of Solids and Structures.* 176-177:68-85. DOI:10.1016/j.ijsolstr.2019.05.020 Available: https://www.sciencedirect.com/science/article/pii/S0020768319302549

Zingoni, A. 2001b. Subspace Formulation for Symmetric Finite Elements. *Structural Engineering, Mechanics and Computation.* :663-673. DOI://doi.org/10.1016/B978-

008043948-8/50072-2 Available: http://www.sciencedirect.com/science/article/pii/B9780080439488500722

Zingoni, A. & Pavlovic, M.N. 1994. On natural-frequency determination of symmetric grid-mass systems. *Structural Dynamics: Recent Advances, Institute of Sound and Vibration Research, Southampton.* :151-163.

Zingoni, A., Pavlovic, M.N. & Zlokovic, G.M. 1994. Symmetry and the direct stiffness method in structural analysis: A formulation based on group theory. Southampton: Institute of Sound and Vibration Research. 151-163.

Zingoni, A., Pavlovic, M.N., Lloyd-Smith, D. & Zlokovic, G. 1993. Application of group theory to the analysis of space frames. *Space Structures 4.* 1334-1347.

Zloković, G.M. 1989. *Group theory and G-vector spaces in structural analysis: vibration, stability, and statics.* Chichester, West Sussex, England; New York: E. Horwood; Halsted Press.

Zweig, A. 1984. Force Method for Frame Buckling Analysis. *Journal of Structural Engineering.* 110(8):1893-1912. DOI:8(1893) Available: http://ascelibrary.org/doi/abs/10.1061/(ASCE)0733-9445(1984)110:8(1893)